MOTION SENSATION DEPENDENCE ON VISUAL AND VESTIBULAR CUES

by

GREG L. ZACHARIAS

S.B. MASSACHUSETTS INSTITUTE OF TECHNOLOGY, 1967

S.M. MASSACHUSETTS INSTITUTE OF TECHNOLOGY, 1974

SUBMITTED IN PARTIAL FULFILLMENT OF THE

REQUIREMENTS FOR THE DEGREE OF

DOCTOR OF PHILOSOPHY

IN INSTRUMENTATION

at the

MASSACHUSETTS INSTITUTE OF TECHNOLOGY

SEPTEMBER, 1977

Signature of Author _____
Department of Aeronautics and Astronautics, August 1977

Certified by _____
Thesis Committee Chairman, Laurence R. Young

Certified by _____
Charles M. Oman

Certified by _____
Richard M. Held

Accepted by _____
Chairman, Instrumentation Doctoral Program

MOTION SENSATION DEPENDENCE ON VISUAL AND VESTIBULAR CUES

by

GREG L. ZACHARIAS

Submitted to the Department of Aeronautics and Astronautics
on August 8, 1977 in partial fulfillment of the requirements
for the degree of Doctor of Philosophy in Instrumentation.

ABSTRACT

Measurements are made of human control performance in the closed-loop task of nulling perceived self-velocity about an earth vertical rotation axis. Self-velocity estimation is modelled as a function of the simultaneous presentation of vestibular and peripheral visual field motion cues. Based on measured low-frequency operator behavior in three visual field environments, a parallel channel linear model is proposed which has separate visual and vestibular pathways summing in a complementary manner. To look more closely at the dynamic interaction involved, a correction to the data is provided by a separate measurement of manual control performance in an analogous visual pursuit nulling task. The resulting dual-input describing-function for motion perception dependence on combined cue presentation qualitatively supports the complementary model, in that vestibular cues dominate sensation at frequencies above 0.05 Hz, while visual cues dominate low-frequency sensation. The dual channel model, however, is shown to be inconsistent with the results of single cue studies, and forces a reexamination of linearity assumptions. An alternative non-linear model is proposed, which incorporates selective cue weighting based on an internally-generated measure of intercue conflict. Simulation of the model demonstrates its ability to fit the experimentally derived data, and response trends observed in single cue studies. Modifications are proposed and evaluated to extend the model's applicability to large amplitude stimulus situations.

Thesis Supervisors:

Laurence R. Young
Professor of Aeronautics and Astronautics

Charles M. Oman
Associate Professor of Aeronautics
and Astronautics

Richard M. Held
Professor of Experimental Psychology

ACKNOWLEDGEMENTS

I wish to express my gratitude to my thesis advisors, Professors Laurence R. Young, Charles M. Oman, and Richard M. Held, for their guidance through the course of the research and their comments regarding the thesis document itself. Professor Young provided considerable insight into the basic perceptual mechanisms involved, and suggested innovative experimental approaches for the research. Professor Oman's suggestions regarding model simulation are also appreciated, as is Professor Held's advice regarding the fundamentals of psychophysical experimentation.

Many people at the Man Vehicle Laboratory were very helpful to me during my stay, and I appreciate both their assistance and their time spent as subjects. In particular, I thank Dr. John R. Tole for his introduction to and assistance with the various pieces of hardware involved with the experiment, and his help in using the software associated with the hybrid computer. Mr. William A. Morrison was especially helpful with his introduction to the Link trainer, and provided me with unfailing support of the equipment, for which I am very grateful; during his temporary absence, Mr. Robert L. Renshaw helped in equipment maintenance, and his support is also gratefully acknowledged. Finally, I should like to thank Dr. Lindesay I.K. Harkness for her many hours spent discussing different cue models and their behavioral implications, and also for her slightly less than accurate rendition of the experimental equipment used in my research.

The creation of the final manuscript is due to the efforts of Ms. Sherry A. Modestino, with assistance from Ms. Kerry M. Campbell, and I thank them both for their typing and editing expertise, and their continued patience with my requests for text and equation revisions.

This research was conducted as part of NASA Grant NSG 2032. I received support from the National Institutes of Health, under a National Research Service Award, and wish to acknowledge their assistance and thank them for the opportunity they have given me. In addition, the Research Laboratory of Electronics provided me with an account at the Information Processing Center (MIT), which I used for off-line data processing, and I am grateful for their support.

Finally, I wish to give special thanks to my wife, Susan, for her patience with my absence from home during the course of the research, for her moral support at times of stress, and for her continued unselfish dedication to the furtherance of my education.

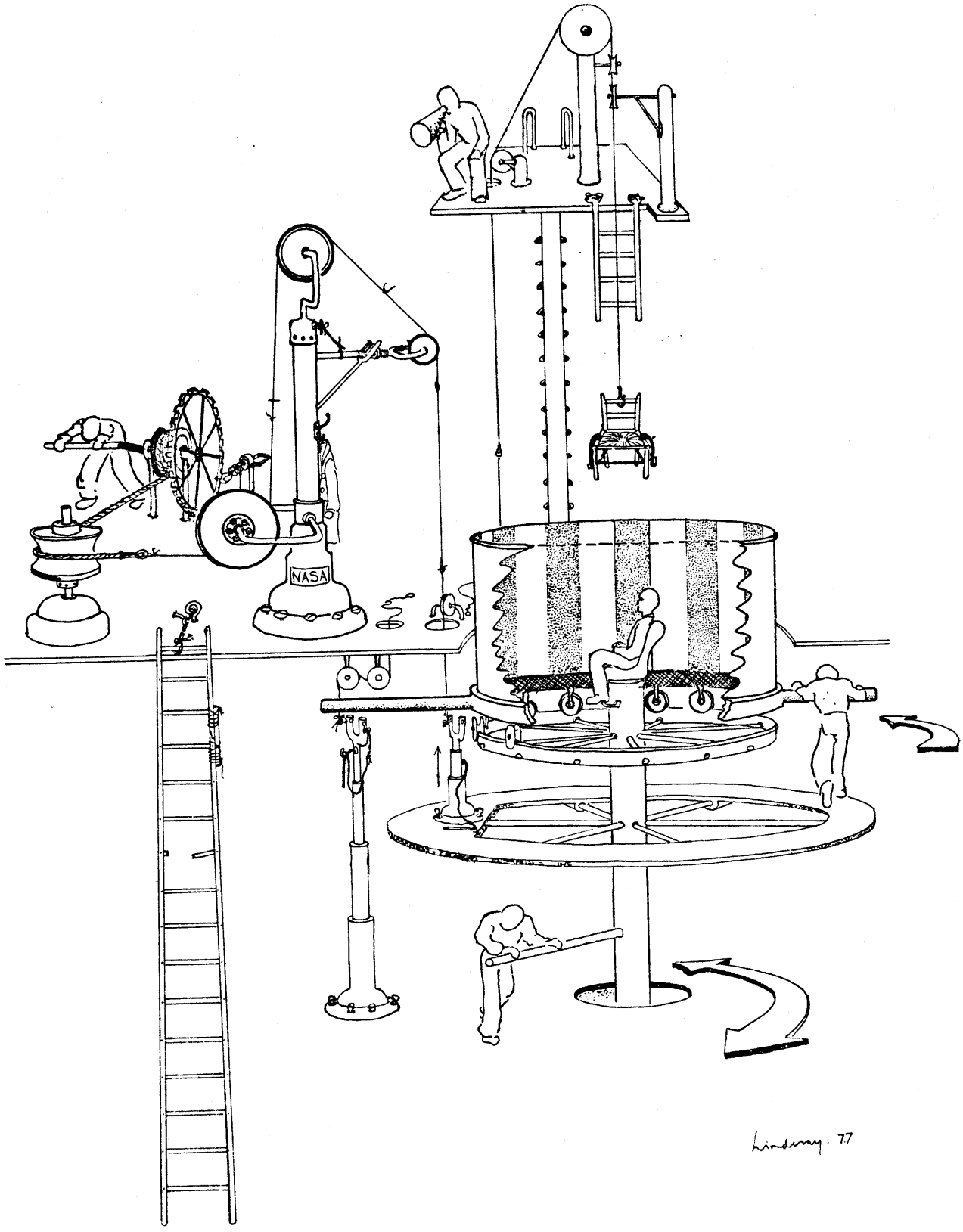
NASA
Lindsay. 77

TABLE OF CONTENTS

CHAPTER I

INTRODUCTION

The objective of this research is to develop a functional model of how vestibular cues and moving peripheral visual fields act in concert to produce a sensation of self-motion in humans. Modelling of vestibularly induced motion sensation has been the subject of considerable research effort for many years, and the functional approach of describing input-output relations has met with a fair degree of success in predicting human subjective response to various rotational and tilt stimuli, in the absence of other cues. A concomitant effort directed toward understanding how visual cues influence motion sensation has a more recent history, and models describing subjective response induced solely by moving visual fields are of a more qualitative nature, with the emphasis on identifying the visual field qualities most important in inducing motion sensation. This characterization of field properties is a prerequisite for the functional modelling of subjective response to one or a few quantified attributes of the moving visual field; some work is thus currently directed toward developing an input-output model of subjective response due solely to visual cues, using techniques similar to those used in past vestibular modelling. The natural extension of both the vestibular and visual studies is an effort directed toward understanding how simultaneous cues interact and contribute to motion sensation, and initial research in this area has already begun to uncover subjective

response patterns not apparent in the separate vestibular and visual studies conducted in the past. It is the object of this research effort to extend these efforts with more quantitative measurements of subjective response to combined visual and vestibular cues, and to integrate these results with those of past and current research in a functional model, one which relates the dynamics of motion sensation to the sensory inputs of vestibular stimuli and moving peripheral visual fields.

It is anticipated that such a functional model would be a significant contribution in both the basic research area of understanding the properties of motion perception and the applications areas which rely on human motion perception models. In the research areas, considerable effort has been devoted toward neurophysiological studies of cells along the vestibular pathway , and work has begun on recording single unit responses to combined visual and vestibular stimuli. Because of the past success in correlating subjective response characteristics with single cell activity, it is anticipated that a dual-input functional model at the subjective level can complement neural response studies using the same visual and vestibular cues. In particular, it is felt that a functional model of sensation can not only suggest appropriate stimulus sequences to be used in single unit experiments, but can also provide a mathematical framework for modelling the dynamics of the observed single unit responses.

A second application of a functional model describing motion sensation is in the development of realistic moving base simulators, where it is desired to maintain a maximum of realism within the constraints imposed

by the mechanical travel limitations and the sophistication of the projection system. In this instance, it is anticipated that a functional model could be used in an inverse sense, so that given a desired motion sensation to be simulated, the appropriate visual and vestibular cues to be supplied by the simulator could be backed out of the model. Such an approach may not only minimize the current trial-and-error procedures used in simulator design, but may also indicate how simultaneous presentation of fairly simple visual and vestibular cues may be used to induce a relatively complex sensation of motion, one which is not particularly amenable to simulation by conventional moving base simulators.

Finally, an extension of the dual-input functional model of subjective sensation may prove to be a tool reasonably well-suited for the continuing effort directed at elucidating the causes of disorientation and motion sickness. Specifically, a functional model could be modified to generate, in response to a fixed visual and vestibular input stimulus pair, a spectrum of possible motion sensations, each assigned a particular probability consistent with its prevalence in a test subject population. Such a measure could be used in conjunction with the current "conflict theory" which suggests that an inconsistent set of sensory inputs (e.g., vestibular inputs with no corresponding changes in the peripheral visual field) can result in an internal conflict of how to process the sensory data in a physically meaningful way, which, in turn, can lead to disorientation and malaise. Thus, a probabilistic dual-input functional model could be used to determine various combinations of visual and vestibular inputs which lead to motion sensations characterized by consistently

low probabilities, and hence, presumably are associated with a low probability of inferring correct orientation. Clearly, such a model could be used to test the conflict theory of disorientation and motion sickness.

This chapter is organized into four sections. Section 1.1 provides a brief review of neurophysiological and psychophysical studies of responses to various vestibular and peripheral visual field stimuli, with the objective of providing a general introduction to the subject of separate and combined cue stimulus studies. This section draws on the obvious parallels seen between transducer dynamics and the time course of subjective sensation, and proceeds to a discussion of the current theory of visual-vestibular interaction, a theory which has been proposed to explain the observed sensory mixing. It is at this point that some of the discrepancies between theory and fact are discussed and the point made that, to date, no functional model has been proposed to explain the dynamics of sensation dependence on combined visual cue presentation. Section 1.2 then proceeds to define the objective and scope of the research reported on here: that of developing a dual-input functional dynamic model of motion sensation, one which is restricted to rotational motion about earth-vertical. Section 1.3 then outlines the research approach used here: the proposing of differently structured functional models and an experimental investigation of their appropriateness in mimicking measured sensory dependence on visual and vestibular motion cues. Finally, Section 1.4 provides a brief chapter-by-chapter outline.

1.1 Background

As noted above, research directed toward understanding the influence of combined visual and vestibular cues on motion sensation and attitude perception can be separated into three functional areas: experimental work involving only vestibular stimulation; similar studies utilizing only peripheral visual field stimuli; and research into the effects of simultaneous presentation of visual and vestibular cues. A summary of the relevant results of these efforts is given in the following three subsections. The last subsection then relates these results to current ideas of how these cues are combined to provide the sensation of motion, both at the neurophysiological level and at the functional modelling level.

1.1.1 Vestibularly Induced Motion Sensation

Models of vestibularly-induced motion sensation and attitude perception rest heavily on an understanding of the static and dynamic characteristics of the vestibular organ components: the semicircular canals and the otolith organs.

1.1.1.1 Semi-circular Canal Function

Perhaps the most influential model of end-organ dynamics was produced by Steinhausen (1933), who developed a linear second-order model of canal cupula dynamics to explain the observed characteristics of vestibularly induced eye movements in the pike. Neurophysiological support for this second-order model was subsequently provided by the work of Lowenstein and Sand (1936, 1940) who , by means of ampullar nerve and

single unit recordings on the dogfish, showed that the primary afferent response to mechanical inputs also followed Steinhausen's model. The simplest interpretation of these observations assumed the hair cells to be approximately linear transducers of cupula motion, so that the basic characteristics of the afferent response are dictated by the dynamics of cupula deflection, and not the dynamics of neural transduction. It should be noted that Lowenstein and Sand also made clear the bidirectional response capabilities of the canals, and suggested the possibility of a push-pull interaction between contralateral canals. The canal model became more formalized with the introduction of the "torsion pendulum" model of Van Egmond et al (1949), who showed how the physical characteristics of the canal could be used to infer one of its time constants and, further, how subjective cupulometry could also be utilized to infer the model's parameters. In particular, by monitoring motion sensation in response to a rotational stimulus, using a variety of experimental approaches, they were able to infer both a threshold and both time constants associated with subjective sensation; the implication was that rotational sensation is dictated almost entirely by the physical properties of the canals.

Further development of a functional model describing motion sensation has been motivated on two fronts: the use of other measures of behavioral response to rotational stimuli, particularly the vestibulo-ocular reflex and the oculogyral illusion; and an expansion of the types of vestibular stimuli used in testing, specifically off-vertical rotation and linear acceleration. Some of these research results are discussed below.

1.1.1.2 Rotational Time Constants

A better understanding of the vestibulo-ocular reflex was made possible by quantitative cupulometry based on vestibular nystagmus experiments (see, for instance, Robinson (1968) and Sugie and Melvill Jones (1971)). However, as shown in a study by Melvill Jones et al (1964), the long time constant of the torsion pendulum model takes on different values, depending on whether subjective response or nystagmus records are used for its calculation. This study also demonstrated that subjective and nystagmus time constants varied with the subject's rotation axis (yaw, pitch, or roll, always about the earth vertical), further complicating the one-dimensional simplicity of the torsion pendulum model. Of course, this observation can be explained by associating different physical properties with each of the three synergistic canal pairs, but Melvill Jones et al (1964) point out that standard body-axis yaw, pitch and roll rotations excite all six canals to some extent, so that ascribing an axis time constant to one canal pair's physical properties may be entirely inappropriate. They also note that Ledoux (1958) found no significant differences in time constants when cupulometry was performed about three rotation axes, each (approximately) perpendicular to one of the three canal planes, and thus suggested a more central origin for the subjective dynamics observed during standard body-axis rotation tests.

1.1.1.3 Rotational Thresholds

Similar differences are seen in threshold studies, both in terms of axis-by-axis dependence and in terms of dependence on the type of beha-

vioral response measure used. Meiry (1965) showed yaw-axis thresholds to be on the order of $0.1^{o}/s^{2}$, with roll axis thresholds approximately five times larger. The idea of different "cupular" thresholds provides a possible explanation, as does the idea of a more centrally located processor working with body-axis coordinates and associating different thresholds to each axis. However, neither of these explanations appears necessary, in light of Clark and Stewart's (1968) more extensive study of subjective thresholds about all three axes: they showed mean roll and yaw thresholds to be equal ($0.4^{o}/s^{2}$) and although the mean pitch threshold was slightly greater ($0.6^{o}/s^{2}$), the difference was barely significant. The suggestion is that all three subjective thresholds are approximately the same, across the test population, and might thus be ascribed to similar end-organ characteristics.

In contrast, however, single-axis studies using different response measures suggest a more central location for the factors influencing threshold behavior. For instance, in yaw rotation about the vertical, Clark and Stewart (1969) show a mean subjective threshold of $0.4^{o}/s^{2}$, and yet with the same test population, shown a mean threshold for the oculogyral illusion (Howard and Templeton, 1966) to be approximately four times smaller, or $0.1^{o}/s^{2}$. Similar results were discussed by Oosterveld (1970), who noted that all three measures of vestibular function (subjective, oculogyral, and nystagmoid) demonstrate differing threshold values, thus compounding the problem of attempting to fit the data with a simple torsion pendulum model.

1.1.1.4 Otolith Function

Another development which has led to a less simplistic view of vestibular function has been the increasing interest in response to vestibular stimuli which consist of either linear accelerations or rotatory motion about non-vertical axes (the majority of the early studies were concerned with rotary motion about earth-vertical).

As discussed by Henn and Young (1975), Ernst Mach was perhaps the earliest investigator to study what is now generally considered to be otolith function, but approximately a century passed before quantitative studies of subjective responses to linear acceleration led to the functional models proposed by Meiry (1965) and Young and Meiry (1966). Here the subjective response is modelled by a second order transfer function with lead compensation, acting on specific force, so that static tilts away from the vertical and linear accelerations are equivalent stimuli.

This model of subjective response was motivated by the known physical properties of the otolith organs, specifically the inertial reaction mass of the otoconia and the shear force input (Schöne, 1964) due to head motions and/or gravity. The static characteristics of this model are consistent with the single unit recordings of otolith afferents conducted by Fernandez et al (1972), who found a linear relationship between tilt angle (i.e. specific force) and steady state firing rate. However, the dynamics of the model disagree with the functional model proposed by Fernandez and Goldberg (1976), whose single unit recording results imply acceleration transduction characteristics which are relatively independent of frequency, over the physiological range of interest. Presumably, the

dynamics of tilt sensation are more centrally mediated.

1.1.1.5 Off-vertical Rotation

Studies involving off-vertical rotation stimulation have yet to result in the proposal of definitive functional models, probably because of the complexity of higher-level processing involved in combining canal and otolith signals. As an example, Benson and Bodin (1966) argue for the notion of an additional mechanical influence of gravity on the canals (for example, the "roller-pump" theory of Steer (1967)), motivated by their nystagmus records taken during experiments. Specifically, they show barbecue-axis rotation to result in nystagmus patterns characterized by a sinusoidal oscillation in slow phase eye velocity superimposed on a bias velocity. As argued by Young and Henn (1975), who conducted similar testing with monkeys, the sinusoidal component is consistent with studies on linear nystagmus (Steer, 1967; Young, 1972), that is, compensatory eye movement mediated by otolith transduction of linear acceleration, but the bias term is still not understood.

1.1.1.6 Development of Transducer Models

As just described, model development of vestibular function has received impetus from both the use of more complicated stimulus patterns and the investigation of different response modalities (subjective sensation, eye movement, and visual perception illusions). The net result has been a better understanding of function both at the transducer level and at the systems level. In the former case, the torsion pendulum

model of canal dynamics has been coupled to an adaptation operator , proposed by Young and Oman (1969), to account for the above-noted discrepancies between parameter values calculated from subjective and nystagmus cupulograms. Such an operator also helps explain response reversals in experimental situations in which the torsion pendulum model predicts no such reversal (Young and Oman, 1969). Although the adaptation function can be thought of as being central in origin, Fernandez and Goldberg (1971) adduce neurophysiologic evidence to support the notion of peripheral adapation for some of the primary canal afferents, although at higher rates than seen in cupulograms. The other basic components of the vestibular organ, utricle and sacculus, have received less attention, although functional modelling efforts are continuing along the lines proposed by Meiry (1965). By using the results of past studies in perceived static orientation, Ormsby (1974, 1975) has proposed a functional model of tilt perception which attributes non-linear processing of specific force information to the sacculus, which, when combined with the presumed linear output of the utricle, result in a subjective perception of down consistent with the results of earlier psychophysical experiments.

1.1.1.7 Development of Systems Models

On the systems level of model development, there has been a trend toward integrating the results of vestibular experimentation, with the goal of developing a unified functional model which is an appropriate descriptor of the physical components of the system (i.e., semi-circular canals, otoliths, neural pathways and signal processing centers), and

which can also serve as a model of motion sensation dynamics. This parallel between the detailed physical structure of the system and the gross behavioral measure of subjective sensation has its roots in the close correspondence seen between simple rotatory sensation and dynamics of primary canal afferents. As vestibular testing has expanded in scope, other parallels have been drawn, supporting this notion. Several workers have proposed various functional models (Steer, 1967; Young, 1969, 1970, 1974; Young and Oman, 1969; Robinson, 1968, 1972; Schmid , 1973; Sugie and Melvill Jones, 1971; Melvill Jones and Milsum, 1965), models which, in one way or another, have attempted to correlate the transducer/neural dynamics with measurable behavioral variables; such models thus serve the dual function of providing some understanding of the neural integration which must be taking place and of providing a descriptive functional model of sensation dynamics. It is appropriate at this point to discuss some of the salient features, so as to summarize some of the points made earlier, and to provide a structure for later discussion.

1.1.1.8 Rotatory Dynamic Model

Shown in fugure 1.1 is a functional block diagram which models the transduction dynamics of the horizontal canals; by extension to higher behavioral levels, it also serves as the basis for predicting rotatory motion sensation dynamics. The input is the head's angular velocity component normal to the canal planes, and the output represents an ensemble average firing rate of some central cell population (or, again by extension, subjective sensation). Several points should be made regarding this model, and are noted in the following paragraphs.

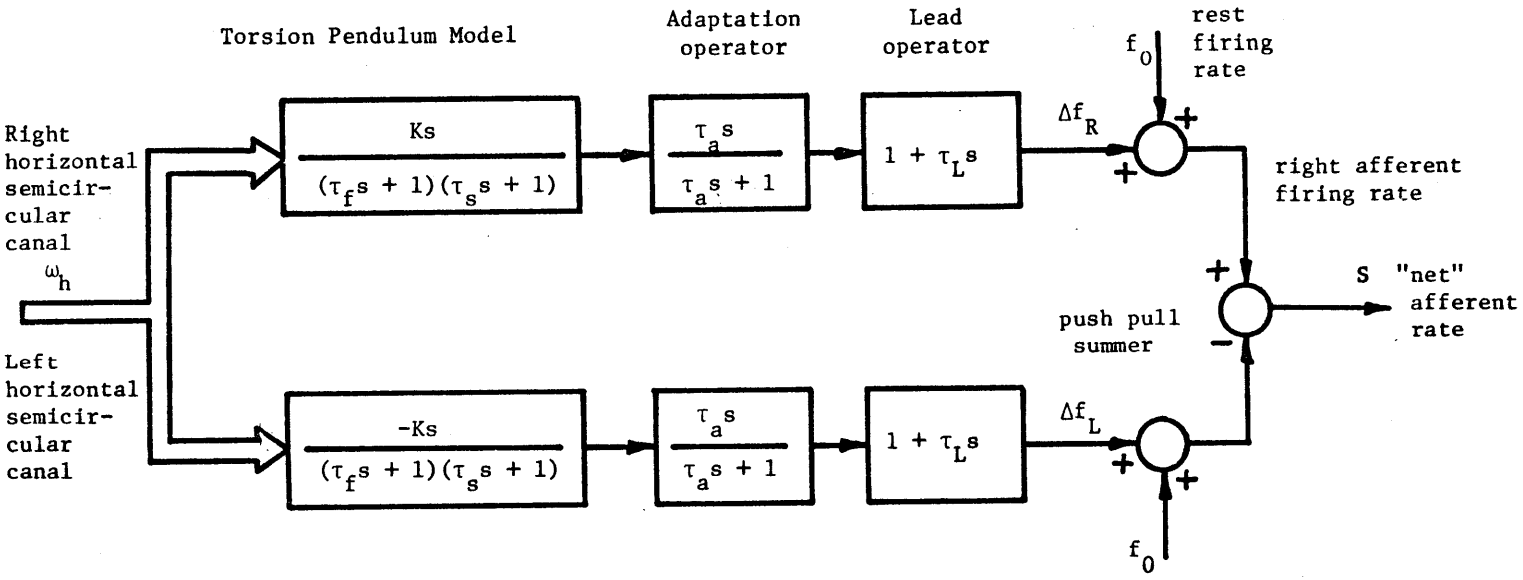

ω_h: horizontal canal component of head angular velocity (right ≡ positive)

Figure 1.1: Bilateral functional model of canal afferents

The two canals are modelled with opposite sign gains, in line with the observed excitatory response with ipsilateral rotations, and inhibitory response with contralateral rotations. The summer at the other end of the path complements this push-pull synergism of opposing canals, and provides for a single output whose sign indicates stimulus direction. Perhaps more significantly, it also provides for a linearization of canal-pair output in the face of individual canal saturation (observed in the inhibitory direction by Fernandez and Goldberg (1971)), and thus allows the canal dynamics to be approximated with a linear constant gain K as shown.

The adaptation and lead operators (the latter indirectly proposed by Nashner (1970) to explain observed postural compensation and more recently by Fernandez and Goldberg (1971) to better fit the frequency response curves calculated from primary afferent recordings) represent average behavior over the primary afferent population, as does the non-zero resting firing rate. As has been pointed out by several researchers, the torsion pendulum dynamics provide for a relatively flat frequency response over the range of 0.01 to 1.0 Hz, thus acting as a velocity transducer for normal physiologic head motions; the adaptation operator is effective at only very low frequencies, while the lead term effects are seen at the other end of the frequency range.

The model has identical parameter values for each path, an obviously unrealistic situation. It is presumed that any differences can be compensated for by more central processing and thus, the model is in some sense an equivalent of a more complicated peripheral model followed by a

central compensatory logic. The simplest example would involve a difference in rest firing rates, f_0, so that the net output would be non-zero for a null input; clearly this firing rate asymmetry could be subtracted off at some later stage to allow for a more accurate measure of a null input.

This model makes no provision for threshold phenomena. The conventional approach is to simply apply a deadband non-linearity to the output, motivated by the functional threshold characterizing subjective response (Young and Oman, 1969). Ormsby (1974) argues that this is too simplistic a view, and proposes a signal-in-noise model which attributes threshold behavior to signal detection confidence. This is supported by the results of single unit studies, which show no evidence of discrete threshold behavior at the periphery, mechanical or otherwise (Goldberg and Fernandez, 1971).

It is generally accepted that such a model can be extended to the other canal pairs, where pairing is done on the basis of canal planes (Ormsby, 1974) (e.g., right superior with left posterior) and thus a three-axis model consisting of three similar channels can be used to represent the transduction of an arbitrary angular velocity vector into a three-dimensional sensor signal.

The two channel model of figure 1.1 can be reduced to a single channel equivalent simply by lumping the two canals together; shown in Figure 1.2 is the equivalent "cyclopean" functional model which not only is simpler, but avoids the problems introduced when one considers the question of left-right parameter mismatches. What is important to note is that we have labelled Figure 1.2 a functional model of subjective sensation, not afferent firing rate; the assumed interchangeability of

the two measures of vestibular function should be obvious from the functional equivalence of their models.

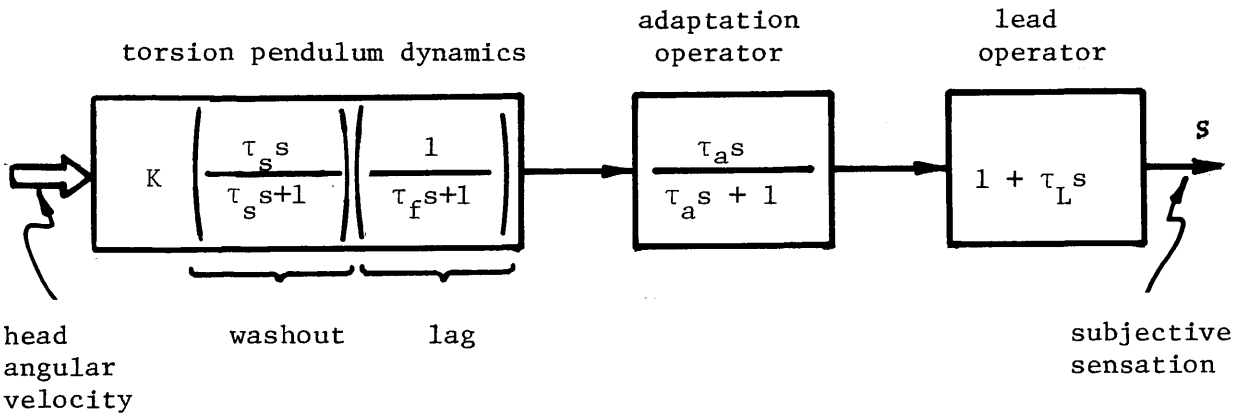

Figure 1.2: Functional model of rotatory sensation

1.1.1.9 Tilt/Acceleration Dynamic Model

As noted earlier, less effort has been devoted toward modelling otolith function via subjective sensation measurements, primarily because of the difficulty of assuring canal non-involvement in the measured response. Further, the situation contrasts with that seen in rotatory studies, in that there is not as clear a correspondence between the measured otolith dynamics and the dynamics of subjective tilt and/or acceleration. However, a functional model of sensation has been proposed by Ormsby (1974), an adapted portion of which is sketched in Figure 1.3, incorporating individual "accelerometer" blocks taken from the work of Young and Meiry (1966).

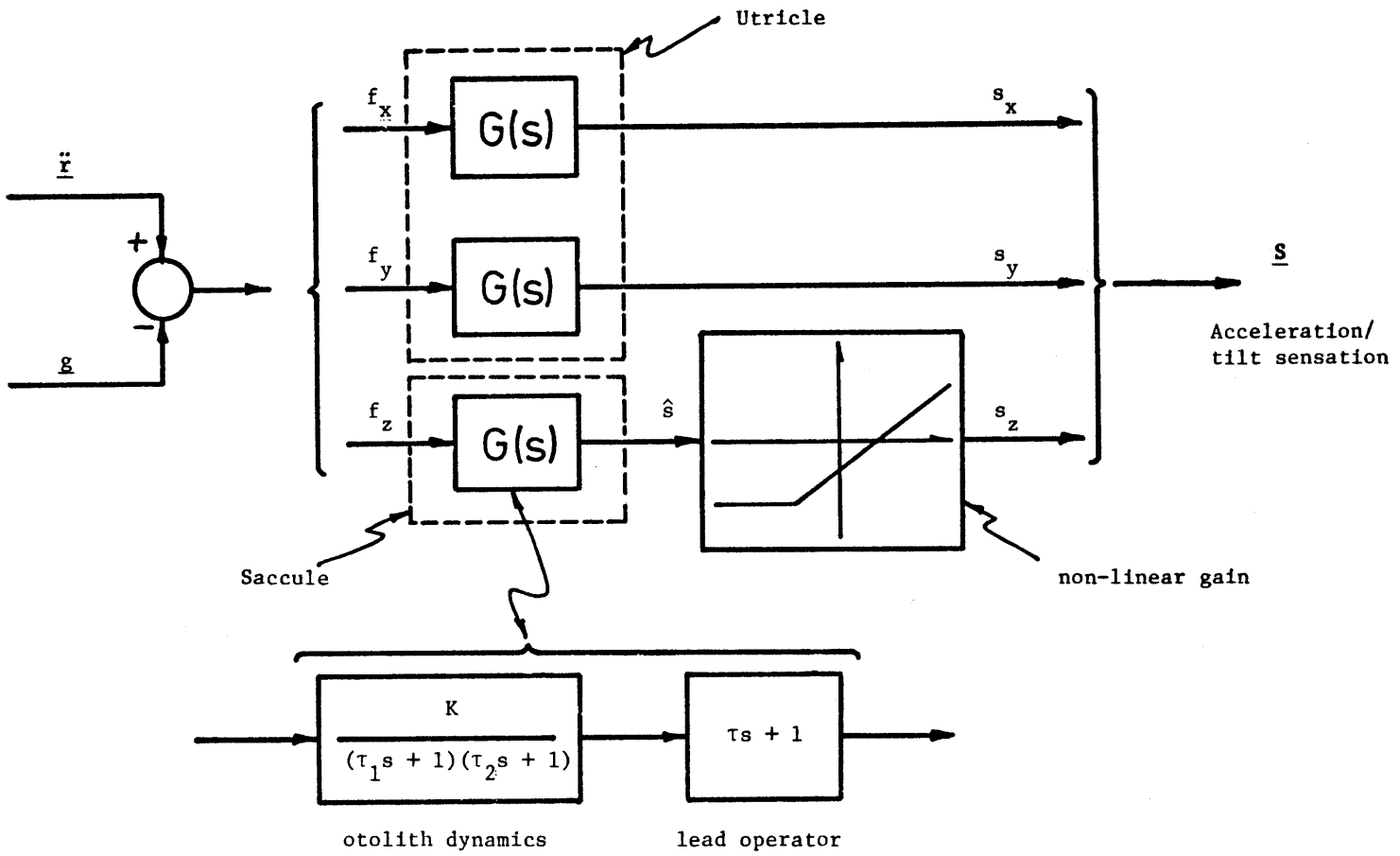

Figure 1.3: Functional model of linear acceleration/tilt sensation

The functional form of the blocks themselves are, of course, motivated by the shear dynamics of the otolith otoconia discussed earlier.

The model's input is specific force (linear head acceleration minus gravity) and the output is a vector signal, $\underline{s}$, which can be used to infer linear acceleration and/or tilt from the vertical. The saccular non-linearity shown is a particularly efficient means of modelling the results of past experiments involving illusions of determining the vertical (particularly the Aubert and Muller phenomena as described in Howard and Templeton (1966)), and is not inconsistent with the results of recordings at the single unit level (Fernandez et al, 1972). The actual utilization of the output of such a model in further sensory processing is an open question. Clearly, for the static situation, a simple vector normalization could provide an estimate of the "down" direction with respect to some body reference frame, and thus a measure of body attitude with respect to the vertical.

What is not apparent is how the sensory information is interpreted in the dynamic situation of rotation in the presence of gravity. One approach to this question is given by Ormsby (1974), and is based on the different dynamic characteristics of the canals and otoliths, relying on frequency separation effects to differentiate between changes in body attitude and changes in the specific force vector. The model appears to fit the data well in certain instances, although it is far from the point of having been exhaustively tested.

1.1.2 Visually-Induced Motion Sensation

Functional modelling of visually-induced motion sensation and attitude perception is not nearly as well-developed as in the vestibular studies, nor does it have the relatively sound basis of extensive neurophysiological studies on which to base a relevant functional structure. For this reason, this section will briefly describe some of the findings of various visual motion studies on an axis-by-axis basis, and defer the discussion of possible models to section 1.1.4.

Both rotatory and linear moving visual fields have been used to induce motion sensations (referred to as circularvection (CV) and linearvection (LV), respectively), with the greatest concentration of effort being in yaw circularvection about an earth-vertical axis. The general aspects of the motion illusion have been known for some time (Henn and Young , 1975): initially the subject feels himself fixed and the visual field to be moving; gradually, a transfer of differential velocity occurs so that the steady-state condition is reached in which the field appears stationary in space and the subject perceives himself to be moving in the direction opposite to the initially perceived direction of field motion.

1.1.2.1 Yaw Circularvection

A quantitative measure of this illusion was undertaken by Brandt, el al (1973), who showed that the most important visual stimulus quality is its location within the subject's visual field, peripheral stimulation being a necessary and sufficient condition for eliciting CV. In terms of subjective response characteristics, they found the following: CV latencies are slow compared to equivalent vestibular inputs, being on the

order of one to five seconds, and are essentially independent of stimulus velocity or acceleration (over the range of 10 to 90 °/s. CV rise times, in response to velocity steps of the visual field, are also relatively slow, being on the order of ten seconds, and display a slight tendency to increase with stimulus velocity. Finally, subjective velocity was found to be linearly related to stimulus velocity over a wide range, with saturation occurring only at the highest velocities used (~120°/sec). Subsequent tests reported by Young and Oman (1974) showed a latency dependence on stimulus velocity at very low stimulus velocities, below those used by Brandt et al (1973).

The illusion is quite convincing, and given adequate attention to the elimination of other motion cues, cannot, in the steady-state, be subjectively differentiated from true self-rotation. This suggests an intimate dependence of motion sensation on visual cues, with the mixing of sensory cues occurring at perhaps relatively low levels, possibly within the "vestibular" system. Evidence for this is given in the next section; it suffices at this point to note two other studies which support the equivalence of visually-induced yaw CV to the sensation associated with real rotation with an earth-fixed visual surround.

In a study by Dichgans and Brandt (1973), it was shown that motion sickness could be induced by a CV-inducing field and an appropriate head motion to the side, in a manner similar to the method of inducing motion sickness with an actual body rotation and subsequent head tilt. The implication is that the illusion is convincing enough to elicit symptoms indistinguishable from those of "real" motion sickness.

A second study by Young and Henn (1974) demonstrated the presence of a cross-modality habituation, in which vestibularly-induced nystagmus was reduced by preconditioning with a CV-inducing visual field. They argue that a necessary condition for a stimulus to be habituating is that it provide the same subjective sensation which will be encountered in the actual test for measuring habituation effects. Thus, the results support the conclusion that the habituating stimulus (the moving visual field) produces a sensation of motion equivalent to what would be experienced under true rotation, again lending credence to the realism of the illusion.

1.1.2.2 Roll Vection

A moving peripheral visual field whose rotation axis is in the horizontal plane produces a qualitatively different response from the one just described. As discussed in a paper by Dichgans et al (1972), when the field rotation axis is along the observer's line of sight, the apparent vertical assumes a steady-state offset from the true vertical, in the direction of field rotation; the illusion is called roll vection. Since the subjective tilt was measured by requiring the subject to adjust a reference line to the apparent vertical (thus depending on his visual system for indicator feedback), it was necessary to determine if the effect was entirely within the visual modality, or actually involved a change in the subject's internal representation of the down direction. A postural control experiment reported on in the same paper (Dichgans et al, 1972), confirmed the latter hypothesis, as it was shown that the "postural" up-

right also tended toward a steady-state offset from true vertical, again in the direction of field rotation.

A quantitative study of the stimulus and response parameters was made by Held et al (1974) who again asserted the importance of peripheral field stimulation on illusion strength. They noted latencies on the order of a few seconds, followed by a counterrolling sensation, which led to a steady-state perceived tilt approximately 30 seconds after stimulus onset. Latency dependence on stimulus velocity and acceleration was not reported on, but perceived tilt angle dependence on stimulus velocity was shown to be approximately linear, with saturation occurring at stimulus velocities near $40^{o}/s$.

An interesting aspect of the roll vection illusion is the demonstrated dependence of subjective tilt magnitude on head position with respect to the true vertical. One study by Young et al (1975) showed that, with a fixed visual field velocity, the induced subjective tilt was greater as the head was moved from its normal upright position to positions farther from the vertical. A parallel study was run by Dichgans et al (1974), using less tilt variation, but finding the same qualitative behavior. To ensure this was not due simply to the well-known Aubert or Muller phenomena (Howard and Templeton, 1966), control studies were run so as to correct for false vertical perception due to head tilt alone. The results show that the toll vection tilt remains an increasing function of head tilt, and, further, that the variance in response measures also increases.

These results were extended by Young et al (1975) who investigated response at various stimulus speeds and with a larger range of head tilts,

to find that tilt response sensitivity to stimulus speed was a minimum with the head pitched 25^{o} forward (so that the utricles are approximately normal to gravity) and increased signigicantly as the head approached the inverted position. As in the earlier studies, response saturation occurred with large stimulus speeds; the results show the induced tilt at saturation also to be an increasing function of head tilt.

1.1.2.3 Pitch Vection

Pitch vection, an illusion induced by a rotating visual field whose spin axis is perpendicular to the saggital plane, has received less attention than roll vection, perhaps because of the response ambiguities encountered during testing. As reported by Young et al (1975), there is an induced pitch tilt illusion which shows a similarity to roll vection in terms of its dependence on stimulus speed and head position. It differs, however, in that there exists a marked directional asymmetry: for the same stimulus speed, the pitch down sensation is stronger than the pitch up sensation. No corresponding left-right asymmetry is seen in the population responses in the roll vection experiments, although small individual asymmetries were noted by Tang (1974). Although originally argued by Dolezal and Held (1975) that this could be due to ocular torsion asymmetries, more recent roll vection studies suggest a more complex interaction of stimuli (Held, personal communication).

The pitch vection experiments resulted in a substantial amount of vertical linearvection (Young and Oman, 1974), a qualitatively different subjective response to be discussed shortly. Whether or not such a sensation

contaminates the subjective indication of pitch tilt is unclear at this time.

1.1.2.4 Linearvection

Linearvection (LV) or the sensation of linear motion induced by a moving visual field, has received less study than the rotary analogs, and only a brief review of the results of two studies will be given here.

By the use of a peripheral visual field moving in the fore-aft direction, Berthoz et al (1975) were able to induce a sensation of linear motion oppositely directed to field velocity, a linear analog to yaw circularvection. They found latencies on the order of one second, independent of stimulus velocity, and demonstrated a non-linear saturating relationship between stimulus velocity and LV magnitude. It was also shown that considerable adaptation occurs over the course of a few minutes, so that greater stimulus velocities are required to maintain the same level of LV. Finally, the use of sinusoidal velocity profiles allowed for a describing function description of the response: the results show a gain roll-off at about 0.02 Hz, and a 90^{o} phase lag at about 0.2 Hz.

A second study, conducted by Chu (1976), investigated some of the properties of up-down LV induced by vertical peripheral visual field motion. Using a pseudo-random velocity profile to avoid subject prediction, and applying a small correction for manual control dynamics, he found the describing function gain-phase characteristics to be similar to the above, with slightly less gain at the low frequencies and more phase lag at the higher frequencies.

A discussion of current theory which attempts to unify and account for some of the observations made in CV and LV studies will be deferred to section 1.1.4; a brief review now follows of studies using combined cue presentations.

1.1.3 Visual-Vestibular Interactions in Motion Sensation

The studies just described have been primarily concerned with motion and tilt sensations induced by separate application of vestibular and visual motion stimuli; those to be discussed here have begun to answer the question of what happens with combined stimulation. It should be realized that any of the CV or LV experiments are fundamentally dual-input, because of the constant presence of gravity (assuming normal vestibular fucntion in the subjects); thus many of the previously-described observations should directly support any dual-input modelling effort. This section will briefly describe some additional studies using both cues, and their implications for functional modelling of subjective response will be discussed in section 1.1.4.

1.1.3.1 Neurophysiological Studies

Both psychophysical and neurophysiological studies support the theory that visual and vestibular cues are jointly processed to provide for a perceived sense of motion and/or body orientation. Support for such a convergence of sensory inputs comes from the identification of one possible interaction site: the vestibular nucleus complex.

Single unit recordings from the vestibular nuclei of goldfish, as reported by Dichgans et al (1973), indicate that the majority of cells respond to both vestibular and moving visual field inputs. Their results may be briefly summarized in schematic form as shown in Figure 1.4. With the goldfish in the dark and using a yaw rotation stimulus consisting of a ramp to a constant velocity, a unit's response was seen to be consistent with that predicted by the torsion pendulum model, returning to its rest firing rate after an excitatory period during the acceleration pulse. For the same unit, an oppositely-directed rotation of the visual surround, with no vestibular input, resulted in a slight increase in the firing rate, which held constant during the constant velocity portion of the stimulus.

When both stimuli were presented, in opposing directions consistent with rotation in the presence of a physically stationary visual surround, the firing rate was characterized by the faster response and greater sensitivity of vestibular stimulation, combined with the non-adapting behavior of visual stimulation. The result is a signal which accurately indicates true body angular velocity.

Although it is clear that the two individual cue responses are roughly complements of one another, the study points out that simple linear summation of the two responses fails to predict the response when both cues are simultaneously presented. The suggestion is that there is a non-linear mixing of the two cues which elicits a response larger than what would be expected from a linear system.

Similar results were found by Henn et al (1974), recording from vestibular nucleus units of the monkey responding to visual and vestibular

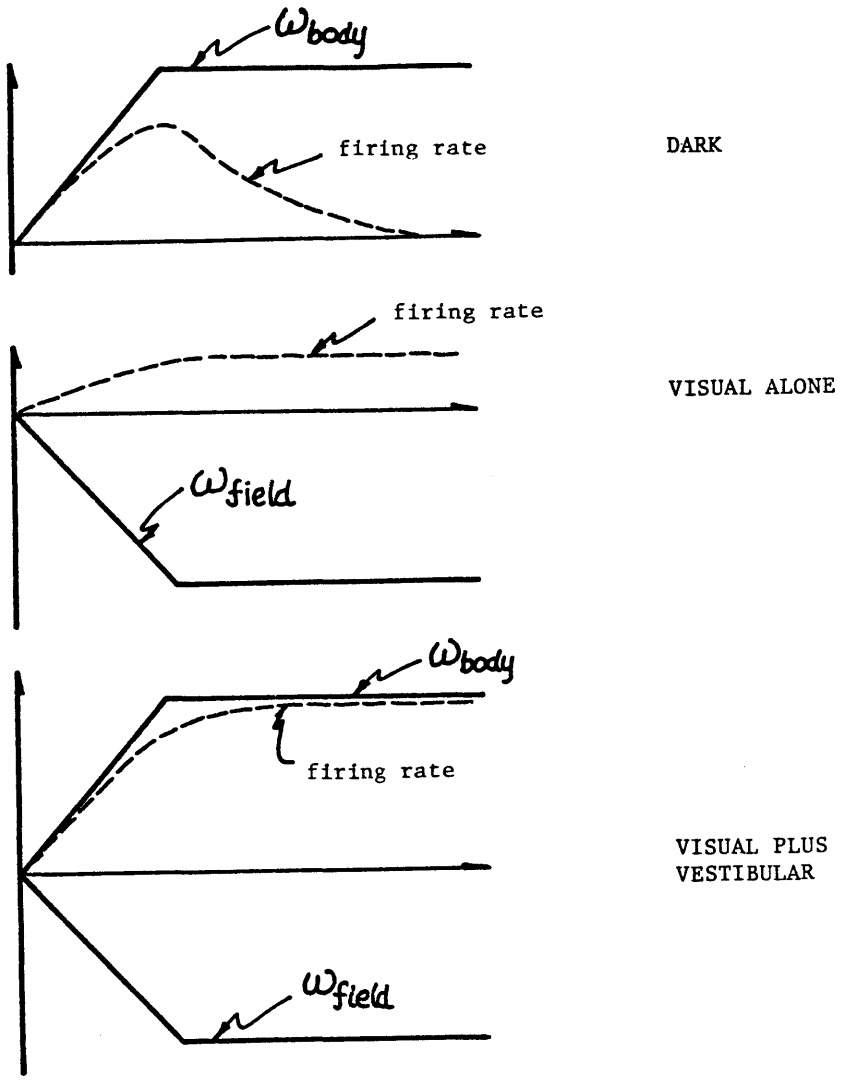

Figure 1.4: Vestibular nucleus recordings in the goldfish (after Dichgans, et al, 1973)

cues. Using sinusoidal stimulation, they noted the familiar low frequency phase lead in the response due to a vestibular input alone; the addition of a confirming visual input abolished the lead, resulting in an accurate transduction of true velocity. A modulation effect due to visual inputs was demonstrated by simultaneous application of sinusoidal rotation and constant visual field velocity. The unit response was seen to be basically sinusoidal, following the vestibular stimulus, but its amplitude was modulated by the visual input. That is, if the field were moving in a direction which normally resulted in an excitatory response, the amplitude was increased over that observed during fixed-field rotation; the converse was also noted, decreased amplitude with inhibitory field motion. Figure 1.5a schematically illustrates such behavior for a unit which responds in an excitatory manner to left head motion and right field motion. Also shown is the observed change in mean firing rate, a bias attributable to the steady visual motion stimulus.

Although it is tempting to label such behavior as simple amplitude modulation of the vestibular signal by visual input, the response dynamics are compounded by the observation of a non-linear response asymmetry observed during a step change from one visual field direction to the other. For the same type of unit just discussed, Figure 1.5b shows how, in going from an inhibitory to an excitatory visual field motion, response amplitude rises slowly. The converse transition, however, results in a rapid drop in amplitude, implying a response asymmetry in visual cue modulation.

Figure 1.5a: Single unit response to sinusoidal head rotation plus a constant visual-field velocity (unit responds to left head motion, right field motion; after Henn, et al, 1974)

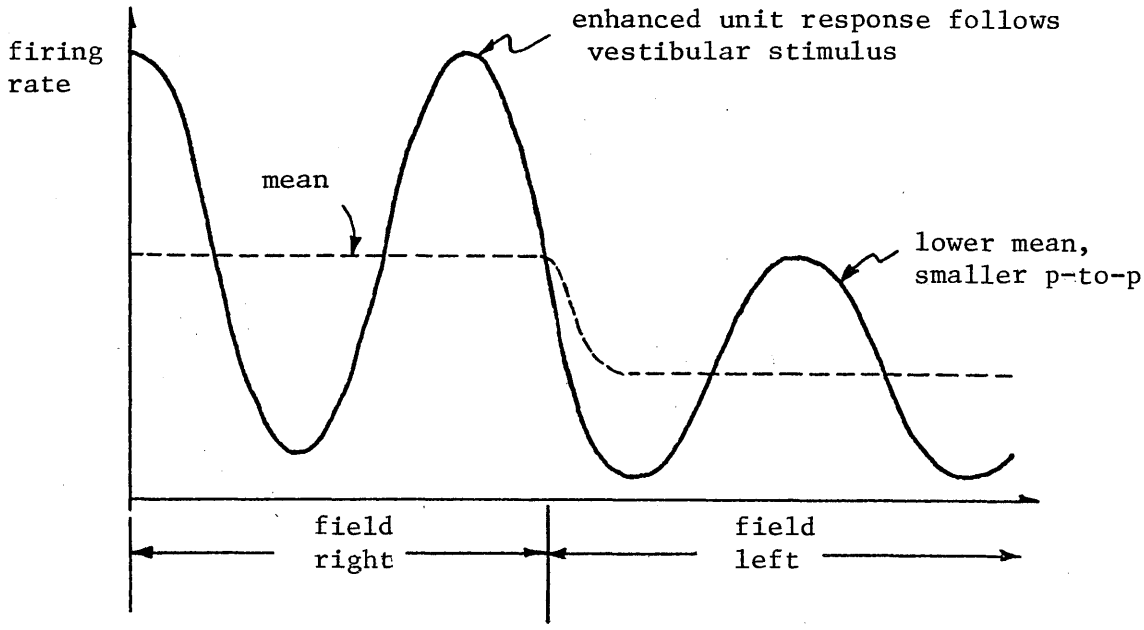

Figure 1.5b: Single unit response to step changes in visual field velocity (unit responds to left head motion, right field motion; after Henn, et al, 1974)

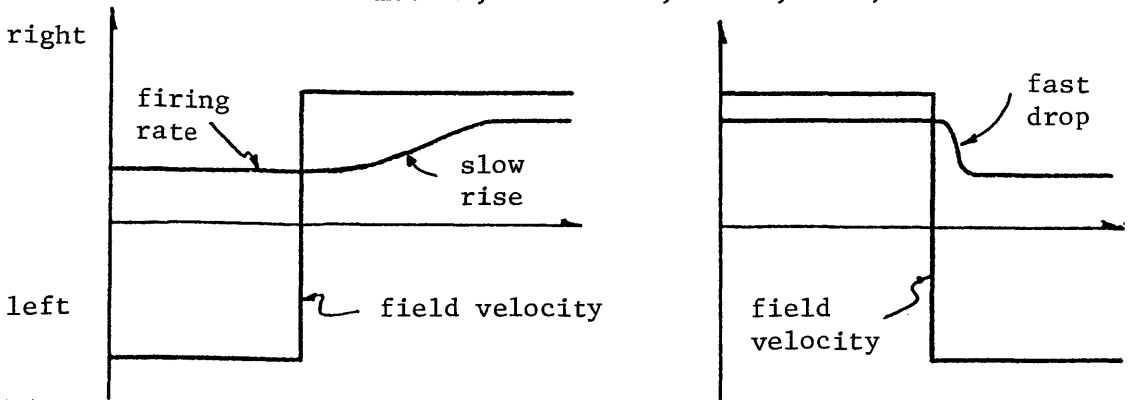

1.1.3.2 Psychophysical Studies

Psychophysical studies of subjective response to simultaneous cues have also demonstrated the presence of interesting interaction dynamics. In one study by Young et al (1973), subjective velocity and acceleration detection indications were made by subjects in response to combined earth-vertical yaw-axis rotational cues. These consisted of angular acceleration pulses in conjunction with the presentation of a visual field moving at constant angular velocity. A pulse was considered "confirming" when it was in the direction of the induced circularvection and "conflicting" when in the opposite direction. The study showed the following. First, subjective velocity was found to be biased in the direction of the induced CV, but not to the extent of a simple summation of CV and expected vestibular response. Second, the detection of a confirming pulse was characterized by a lower threshold and shorter detection time compared to the detection of a conflicting pulse. Finally, the detection of a confirming pulse generally led to a moderate increase in subjective velocity, whereas a conflicting pulse, if detected, resulted in a marked decrease in subjective velocity. These results are schematically summarized in Figure 1.6.

A similar study was conducted by Berthoz et al (1975) in which linear fore-aft acceleration pulses were combined with linear field motion. They found qualitatively the same subjective velocity dependence on combined cue presentation. Pulse detection was also similar, the study showing detection to be degraded when the pulse conflicted with the induced linearvection sensation.

Figure 1.6: Subjective response in humans (after Young, et al, 1973)

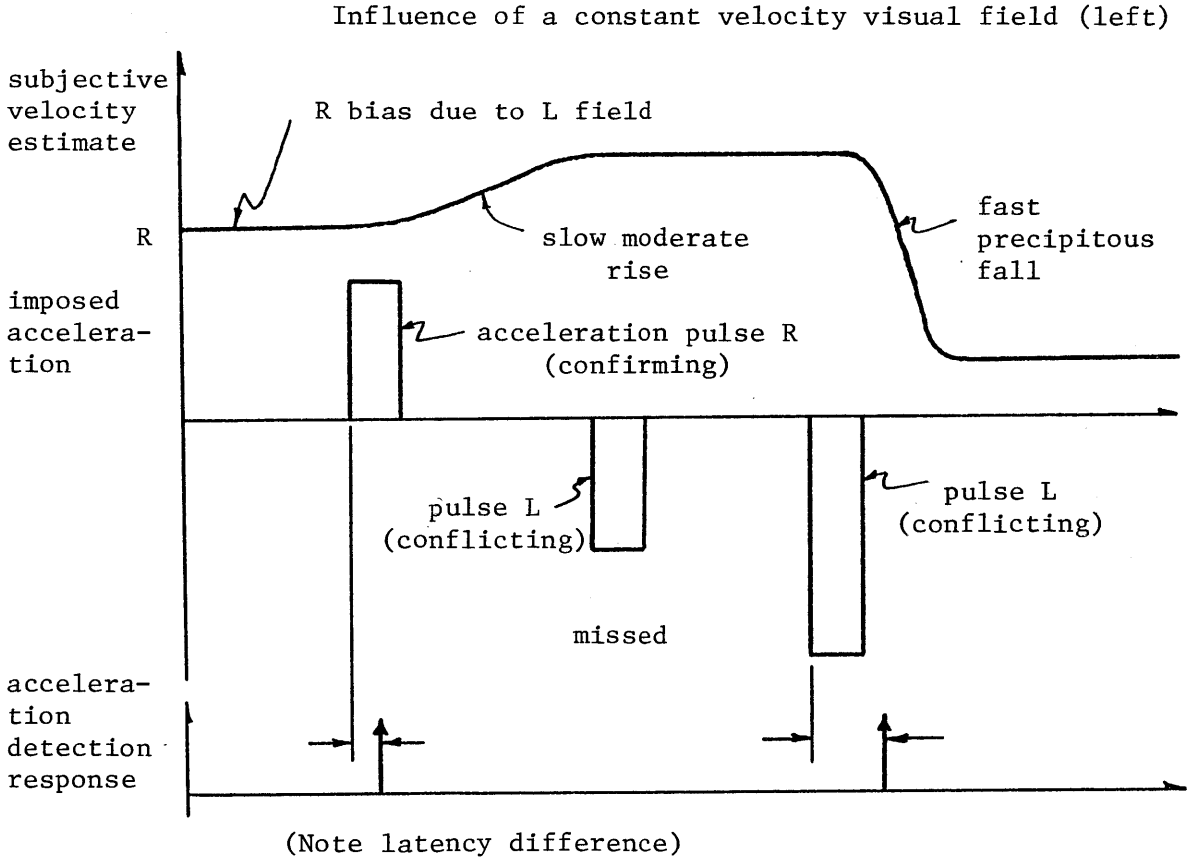

1.1.4 Theories of Visual-Vestibular Interaction

As noted earlier, functional modelling of combined visual and vestibular stimulation is at a very early stage of development, with only qualitative theories to explain some of the experimental results; certainly there exist no detailed dynamic models comparable to those describing pure vestibular stimulation. What will be attempted here is a brief discussion of some of these ideas and how they relate to the research just described.

1.1.4.1 Visual-Vestibular Cue Convergence

Basic to the study of visually induced motion sensation is the concept of convergence of both visual and vestibular information at some point which is relatively low in the central nervous system; and further, that the convergence site is responsible for generating a neural signal which is intimately related to the sensation of self motion. As noted earlier, this idea is motivated both by the identification of vestibular nuclei units whose responses parallel subjective circular-vection sensations, and by the realism of visually induced motion illusions. This correspondence between vestibular nuclei unit activity and subjective sensation was emphasized by Henn et al (1974):

> *"The slow gain of activity when visual and vestibular responses agree in direction, the sudden drop in activity when they disagree, the delay in onset of activity following opto-kinetic stimulation, and the outlasting of activity after the*

end of a moving visual stimulus are all qualitatively similar to the pattern of circularvection sensation in equivalent psychophysical experiments in humans."

One is clearly tempted to suggest that not only is the vestibular nucleus a prime candidate as a convergence site, but that it codes motion sensation, a function significantly different from simply relaying primary vestibular afferent information. Although speculative, such an idea has support on two fronts. First, Henn et al (1975) showed that their recorded unit activity was only loosely correlated with nystagmoid eye movements, and was present even when animal drowsiness precluded nystagmus. This observation is consistent with the notion that the unit output is not merely a signal in the vestibulo-ocular reflex arc (Robinson, 1968), although more recent findings have indicated a higher degree of correlation between unit activity and nystagmus than originally reported (Henn, 1976).

Additional evidence was provided by Henn and Young (1975) in an extension of the study above, by investigating the time course of reflexive head torques during cue presentation: they were unable to find a consistent relationship between intended head movements (signalled by torque changes) and vestibular nuclei unit activity, thus suggesting that neither is unit output merely a signal in the vestibulo-colic reflex arc. It should be noted that obvious counter-arguments can be made against the conclusion that vestibular nucleus activity in this experimental situation is the neural equivalent of motion sensation, but they will not be pursued here, as the question is still open.

1.1.4.2 Functional Modelling of Cue Convergence

Turning to the functional modelling of this convergence process, one proposal by Young (1970) suggests that the resolution of sensory cue conflicts is fundamental to the understanding of multiple cue interaction dynamics. Specifically, it is proposed that visual and vestibular motion cues are independently processed to infer two estimates of body "state" (e.g., angular velocity) and then compared with one another to provide some measure of cue conflict. Should the conflict be low, that is, the cues consistent with one another, then perceived body state is calculated from the weighted sum of the two estimates. The weighting is, in turn, dependent on the a priori knowledge of sensory cue noise characteristics in the given situation and presumably would be chosen to minimize the error in the combined cue estimate. Should the conflict be high, that is, the cues failing to confirm one another, then the weighting is shifted to emphasize one cue over another, according to a predetermined schema based on cue reliability and the subject's set.

Although this model has yet to be formalized in a mathematical framework, it has served, with various extensions, as the basis for qualitative explanations of some of the observed sensory cue interactions. Two extensions are worth briefly noting here: frequency dependent weighting, and the introduction of additional conflict measures.

The idea of frequency dependence proposes that both the conflict measure and the weighting scheme depend on the frequency characteristics of each sensory system. Thus, any conflict measure must take into account

differences in sensory channel response if a true measure of cue consistency is to be obtained. Basically, this requires an internal model of sensory channel dynamics. Response differences also motivate the introduction of a more selective weighting approach. In particular, it has been proposed (Young, 1970) that the high-frequency components of a vestibular cue are weighted more heavily than those of a visual cue, with the reverse holding true for low-frequency components. The motivation for such a weighting scheme, and its implications, will be discussed below.

The second extension of the conflict model concerns the introduction of additional measures of conflict. For instance, instead of simply comparing each cue with the other to check on consistency, one might propose comparing each cue with the current estimate of the body state, to provide a measure of how well each cue confirms the current state. This feedback of estimator output is not only appealing because of its potential for explaining the results of certain combined cue studies (e.g. the variable "vestibular" thresholds found by Young et al (1973)), but also has a clear parallel in Kalman filtering applications (Kleinman, et al, 1969), suggesting the possible applicability of optimal estimator techniques to the problem. Conclict measures can obviously be extended by proposing that the cues also be compared with a predicted sensation, as one more check on consistency. Thus by monitoring motor commands and processing them through internal models of motor response and sensor response, a prediction can be made regarding the expected sensory channel signals, which can then be compared directly with the actual sensory signals. Although such internal models were originally

proposed to help explain adaptation behavior (Knoop and Fu, 1964), their utility here is suggested when one compares differences in response behavior (and presumably sensation) observed during passive movement of a subject to response observed when a subject actively controls his own movement (Young, 1973; Fukuda, 1976). This active-versus-passive influence on perceived motion suggests the possibility of one more means of validation of cue consistency.

The next four subsections will discuss some of these ideas in more detail, on an axis by axis basis, and relate them specifically to some of the experimental results described earlier.

1.1.4.3 Yaw-Axis Circularvection

Figure 1.7 is a block diagram of a sensory conflict model of the type just discussed, applicable to the case of yaw-axis rotation about earth-vertical. The canals provide a vestibular estimate of velocity, which is compared with the visual estimate to generate a conflict signal. This conflict measure is then used by the weighting logic to mix the two cues appropriately to provide the estimate of the perceived velocity. Although the diagram is quite general as it stands, it provides a framework for interpreting the results discussed earlier concerning circularvection.

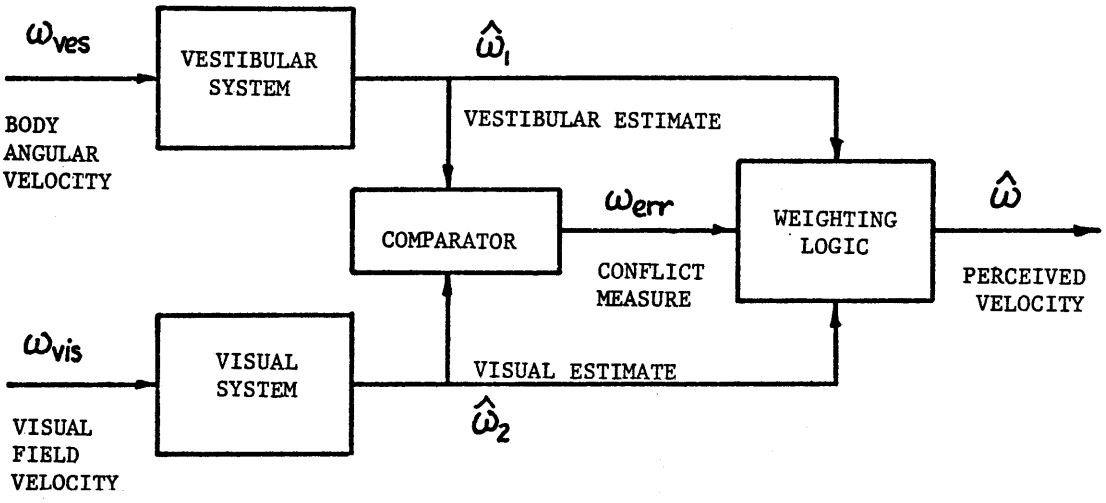

Figure 1.7: Sensory conflict model (after Young, 1970)

Vestibular response to a velocity step exhibits an approximate exponential decay to zero (with slight overshoot due to adaptation) with a time constant on the order of 10 seconds (Clark and Stewart, 1962); thus, in the face of constant velocity rotation we can expect no steady state vestibular contribution to subjective velocity sensation. In the yaw CV illusion experiments, we observe a very slow build-up of subjective sensation (10 to 20 seconds), until the sensation is indistinguishable from true rotation in the presence of a fixed visual field. The conflict theory argues that the steady-state sensation of CV is the result of no visual-vestibular conflicts, since the null vestibular signal is entirely consistent with what would be expected a few time constants after the

start of a velocity step. Since the visual information also implies rotation at constant velocity, the two cues agree and it is merely a question of combining them to get a good estimate of velocity in the steady state. Obviously, this calls for heavy weighting of the visual cue. In the diagram, the steady state conflict measure, ω_{err}, is zero, and the weighting logic essentially gates out the null vestibular signal.

The initial response during the CV illusion can be explained similarly. Here there is clearly a conflict between the two cues, since the visual information indicates a step change in velocity while the null vestibular cue denies the presence of any acceleration. If we presume heavy weighting of high-frequency vestibular information, then we should expect the visual information to be initially discounted, resulting in a null subjective response following stimulus onset. As time from stimulus onset increases, the conflict lessens since the expected vestibular step response decays to zero, approaching the actual null vestibular signal. If we propose a weighting logic which begins to emphasize visual information once conflict is below some level, then we might expect to see CV latency times on the order of the vestibular long time constant. As noted earlier, this is what is observed, with CV latencies of one to five seconds, at least an order of magnitude larger than individual visual or vestibular response latencies. In the diagram, we are simply suggesting that ω_{err} is initially large due to the visual step failing to be confirmed vestibularly; and that this conflict gates out the visual signal for the time it takes ω_{err} to become small.

In explaining the growth of CV to its steady-state value following onset, it might be assumed that the visual information is weighted by

some parameter inversely proportional to the visual-vestibular conflict signal, and added to the actual vestibular signal, which is zero in the CV experiments. Thus, as the conflict disappears in the course of a run, the visual information predominates and the illusion grows stronger. Since the time course of this conflict is determined by the vestibular system's long time constant, this model is consistent with the observed slow rise in motion sensation.

1.1.4.4 Roll Vection

The results of studies of motion and tilt sensation about the roll axis can be similarly explained in terms of the conflict model, by the additional consideration of otolith involvement. The steady-state tilt illusion experienced in roll vection is explained as a compromise between conflicting visual and otolith cues, the canals not being involved because their null signal is in agreement with what an internal model would predict in the face of constant velocity rolling. An internal model of the otoliths, however, would predict an approximately sinusoidal response with a period equal to the rotation period of the visual field. Since the actual otolith signal indicates the presence of a non-rotating gravity vector, the conflict is never resolved, even in the steady state. What results is a compromise, in which the perceived gravity vector is shifted in the direction of the visual field rotation, so that the DC quality of the otolith sensation is preserved, and the visually-induced motion sensation is in some sense satisfied by a perceived tilt displacement. It should be noted that although the perceived tilt has been shown to be an

approximately linear function of field velocity, for low field speeds, (Dichgans, et al , 1972), it is unlikely that a simple linear relation exists at the more basic functional levels.

The dynamics of roll vection build-up are explained in a fashion similar to that for yaw CV development. Specifically, it is proposed that the lack of confirming roll acceleration sensation from the vertical canals, during the start of visual field rotation, results in an initial conflict resolved in favor of the canals, in turn resulting in the relatively long latencies seen. As the expected canal output dies out, the conflict lessens and the tilt sensation slowly grows to its steady-state value. Of course, otolith conflict is also present during this time, and it seems reasonable to assume additional response lags from this quarter.

As noted earlier, estimates of the apparent vertical exhibit larger errors and increasing variance as the head is tilted from the vertical; the conflict model interpretation is that the otoliths become less reliable indicators of the vertical. If it is assumed that this information is weighted according to its reliability, then the visual-vestibular conflict should result in a compromise perceived tilt which is more heavily influenced by the visual cue (whose variance should be unaffected by head tilt because of symmetry about the line of sight). Of course, this is precisely what Dichgans et al (1974) observed; the finding by Young et al (1975) that induced tilt was at a minimum when the utricular plane was normal to the earth-vertical is also consistent with this explanation, if it is assumed that the head attitude for maximum transduction accuracy

corresponds to that for maximum tilt sensitivity. Also noted in roll vection experiments (Dichgans et al, 1974) is an increased variance of the subjective tilt indications with increased head tilt, a finding consistent with increased variance of the otolith component of tilt sensation.

1.1.4.5 Pitch Vection

As noted earlier, the qualitative findings for pitch vection resemble those of roll, with two notable exceptions: up-down asymmetry and LV involvement. Young and Oman (1974) propose the possibility of a visual origin for the former, and advance a plausible explanation for the observed dependence of LV on visual field placement. Modelling the subjective response is also complicated by the lack of knowledge concerning saccular otolith function, a peripheral organ which may prove to be intimately involved in the visual-vestibular processing. It may eventually prove possible to apply the same basic functional model used to describe roll vection, but it should be clear that the additional features of pitch vection serve only to complicate an already difficult task.

1.1.4.6 Fore-Aft Linearvection

One final note should be made regarding the application of the conflict model to the results of the fore-aft LV study (Berthoz et al, 1975) discussed earlier. It should be apparent that this illusion is the linear

analog of yaw CV, with the linear accelerometers of the otoliths replacing the canal angular accelerometers. Thus, a step input in field speed initially conflicts with an otolith signal which denies the presence of an acceleration impulse, resulting in a conflict resolved by accepting the (null) high-frequency vestibular information, and manifested by relatively long latencies to onset. The slow acceptance of the visual information is consistent with the long subjective response time to acceleration, as the internal model of the expected acceleration signal gradually decays to the actual null signal. Finally, the steady-state sensation of constant linear velocity is a no conflict situation in view of the otoliths signalling the absence of any acceleration.

1.2 Research Scope and Objectives

As noted at the beginning of this chapter, the basic objective of this research is to develop a functional model of motion sensation dependence on combined visual and vestibular motion cues. Although qualitative theories have been proposed to explain the various experimental results obtained from motion sensation research, there has been a dearth of quantitative descriptive models, models which can be tested in different experimental situations and which can provide us with a better understanding of some of the apparently diverse results reported on in the literature. Thus, rather than extend the current base of the research in terms of discovering and describing new modes of visual-vestibular interaction, it is felt that a greater current need exists for a more quantitative functional model of interaction dynamics in a stimulus situation which has already been investigated.

To take advantage of previous work in this area, the scope of the research is restricted to yaw-axis earth-vertical rotation sensations. Clearly, most of the research effort in single and combined cue presentations has been in this area, and it is felt that any initial modelling effort should build on the current qualitative understanding of the interaction dynamics described in the literature. Furthermore, this type of motion is perhaps the simplest to investigate, because of the lack of otolith involvement. It should be recognized that any motion which involves a change in the specific force vector immediately brings up the question of

how canal and otolith signals are combined to provide a vestibular sensation. Although the vestibular processing model proposed by Ormsby (1974) has met with some success in modelling combined vestibular cue response, the base is not sufficiently well established to extend the modelling effort by including visual motion cues. Restricting the research to earth-vertical rotation thus avoids this problem.

Any modelling effort in this one type of motion should be cognizant of the results of motion studies in other axes. Thus, although much of the literature just reviewed does not bear directly on the problem of earth-vertical rotation, it is felt that the fundamental ideas contained within an earth-vertical rotation model should be consistent with many of the qualitative aspects of off-vertical rotation and linear translation. By formulating the model in a generalizable framework (e.g., the conflict model) and by verifying some of its more fundamental properties, a single axis earth-vertical rotation model may prove to be a solid base on which to extend functional modelling to combined visual-vestibular cues applied about other axes.

The specific questions we wish to answer in this research are consequently basic to any visual-vestibular modelling effort. We would like to verify the notion of frequency separation in cue emphasis: is low-frequency sensation determined by the visual input, and do high-frequency vestibular inputs complement this information? Can the mixing of cues be adequately modelled with a simple linear complementary filter, or are there fundamental non-linear mechanisms involved, such as a direct influence of visual cues on "vestibular" dynamic response? Is any linear filter

appropriate in a combined cue situation, or must recourse be made to a non-linear mixing of cues? If the latter is the case, does the conflict model hypothesis then provide an adequate framework for quantitative functional modelling? Clearly, answers to these questions for the case of earth-vertical rotation can provide a base for later multi-axis modelling.

1.3 Research Approach

The research approach to answering the questions above consists of experimental measures of subjective response, in combination with functional model building and parameter identification. Since non-linear systems identification has no theoretical base, much less a set of well developed techniques for application purposes, the initial modelling effort presumes a linear system structure; in this way, standard systems identification techniques may be brought to bear on the combined cue problem. Non-linear modelling can then proceed with the linear system data base, by matching simulated system response with the experimental results. This approach is discussed in slightly more detail below, with particular reference to the research questions posed above.

1.3.1 Frequency Separation

Basic to the question of cue mixing is the frequency dependence of sensation on combined cues. A simple experimental approach directed towards answering this question is illustrated in Figure 1-8. It is proposed that a subject be presented with low-frequency visual motion cues in conjunction with wide-band vestibular rotatory cues, and that some measure be made of his resultant perceived angular velocity. A correlation of the low-frequency portion of his response with visual field velocity then allows some conclusions to be drawn regarding sensation dependence on low-frequency visual cues. In particular, one might expect the visual cues to dominate, even in the presence of conflicting

low frequency vestibular information; the experimental approach provides a means of verifying this idea.

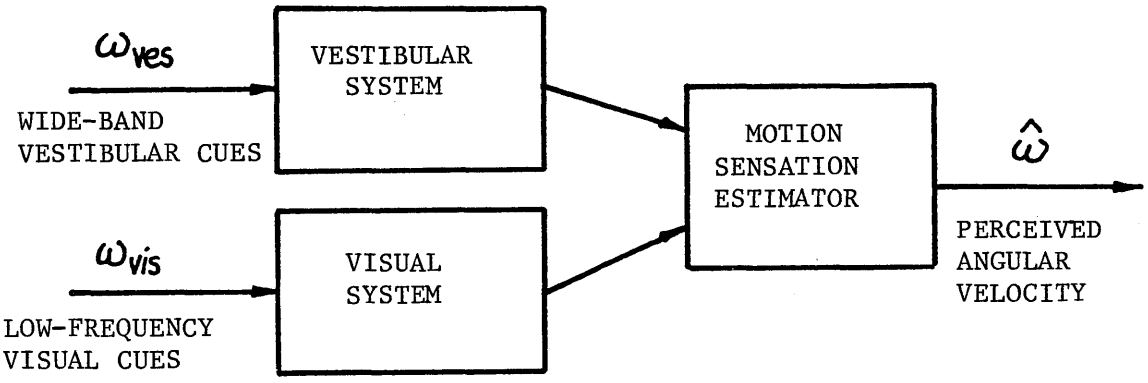

Figure 1.8: Frequency separation measurement

It should be recognized that this is an extension of the combined cue work done by Murphy (1972), in which vestibular pulses and constant velocity field motion were simultaneously presented to the subject. Although quantitative results were found for vestibular detection threshold variation, perceived velocity dependence on visual cues was only qualitatively described. It is proposed that this dependence be more firmly specified by a combined cue experiment and a quantitative dual-channel functional model.

1.3.2 Dependence of Vestibular Response on Visual Input

Simultaneous cue presentation also allows for an investigation into

the possible effects of visual input on vestibular dynamic response. In particular, a describing-function approach may be used to linearly model subjective dynamic response to vestibular cues, for a given type of visual field motion. The resulting quasi-linear vestibular transfer function can then be examined for sensitivity to visual cues, and thus provide a means for assessing the importance of visual cue impact on the dynamics of vestibularly-induced sensations. In essence, this approach complements the low-frequency modelling effort just described, in that the objective here is to determine if visual inputs significantly affect transient vestibular sensations.

One way of modelling sensation dependence on the two cues is shown in figure 1.9. The vestibular describing function, $E(s,\underline{p})$ specifies perceived velocity as a dynamic function of vestibular input, and has a parameter vector $\underline{p}$ which depends on the type of visual motion we present. By examining the dependence of $\underline{p}$ on visual motion cue type, a direct statement can be made regarding whether or not low-frequency visual inputs affect high-frequency vestibular response, and if so, in what manner.

Figure 1.9: Quasi-linear Vestibular Response Model

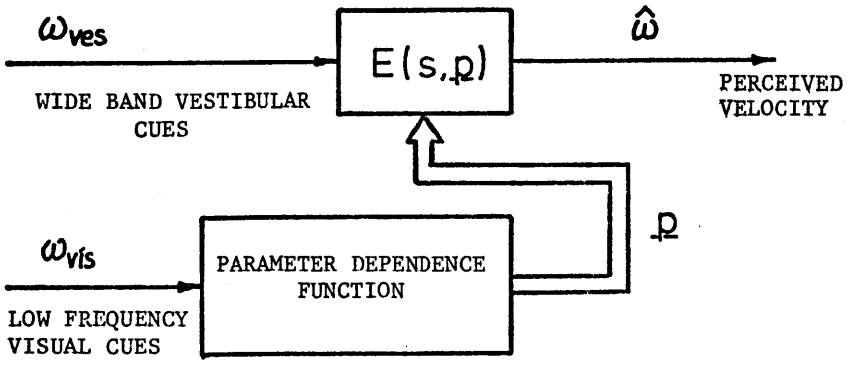

1.3.3 Parallel Channel Dynamic Modelling

To this point, the discussion has been concerned with motion sensation dependence on low-frequency visual cues; the logical next step in functional modelling is an investigation of the dynamic response to visual cue presentation. Although some work has been done in defining latencies and rise times in response to a simple circularvection stimulus (Brandt et al, 1973), a closer look at visual dynamic response in a combined cue situation is clearly called for.

An extension of single-channel describing function techniques can be applied to the dynamic identification problem by assuming a linear parallel channel model of sensation as shown in Figure 1.10. As with the previously described conflict model, it is presumed that each pathway provides its own motion sensation signal, both being combined linearly to provide a motion estimate. The particular choice of the identification technique need not be discussed here, since a detailed discussion will be given later. What should be noted, however, is that the main objective of this modelling effort will be to determine if a linear parallel channel model provides an adequate functional description of combined cue response, and if so, how it can be used to integrate the results obtained from earlier single stimulus studies. Even though we anticipate non-linear cue interactions, this type of linear modelling effort can provide a data base for subsequent attempts at non-linear identification.

Figure 1.10: Linear Parallel Channel Model

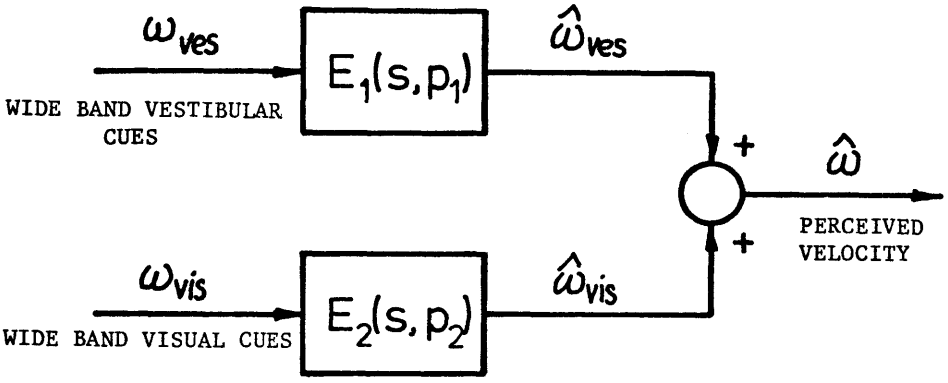

1.3.4 Non-Linear Dynamic Modelling

Once the limitations of the linear model are identified, the research effort can be directed toward non-linear model development, based on the framework provided for by the conflict model (recall figure 1.7). Since no analytic techniques are available for this situation, dynamic simulation of any proposed non-linear estimator is called for. A non-linear model can be constructed to match known single channel response behavior, and then matched to the measured time and frequency response characteristics observed under simultaneous cue presentation conditions. A simulation capability allows for an evaluation of model behavior, and for the validation of proposed functional relations contained within the model.

Clearly, one of the major objectives here will be to assess the utility of the conflict hypothesis in quantitatively explaining subjective response to combined cue stimulation.

1.4 Outline

This thesis is organized into six chapters which interleave experimental descriptions, data analysis, and modelling, so as to parallel the functional model development just described.

Chapter 2 describes an experiment directed at verifying the apparent frequency separation properties of combined cue processing. By presenting subjects with low-frequency visual motion cues in conjunction with wide-band vestibular cues, a time domain analysis of subject response demonstrates how the visual cues dominate low-frequency motion perception. This provides a justification for the complementary filter model proposed in this chapter, and it is shown how such a model is consistent with observed response under the tested experimental conditions.

Chapter 3 continues the analysis of the experimental data, by using describing functions to specify a subject's frequency response to vestibular motion cues. Since various visual motion cues are considered, a quasi-linear, variable parameter model (see figure 1.9) is proposed to help explain combined cue processing. This model also supports the complementary filter model, since it is shown how subject response at high frequencies remains basically unaffected by concurrent presentation of visual motion cues.

This modelling effort is extended by the experiment described in Chapter 4, in which response to wide-band vestibular and visual motion cues is investigated. Analysis is predicated on a linear parallel channel model of combined cue processing (see figure 1.10), and describing functions for both channels are derived from the experimental data. A linear fit to the

derived data then allows for a direct comparison of model predictions for response to single cue presentations. It is shown here how the predictions are inconsistent with known single cue response patterns, and suggests that the validity of the linearity assumptions be re-examined.

Chapter 5 proposes an alternative to the linear model, by presuming a conflict model structure (see figure 1.7) for combined cue processing. A detailed functional non-linear model is proposed, and its behavior under various cue presentation situations is simulated, for direct comparison with the experimental results presented in the earlier chapters. It is shown how this model is capable of fitting the data under simultaneous cue presentation conditions, and also of following the response trends found by other researchers in single cue studies. The results support the notion that cue conflict is central to the integration of motion information derived from different sensory modalities.

Chaper 6 summarizes the major findings of this research, presents the conclusions to be inferred from the analysis and modelling effort, and suggests avenues of continuing research, based on the results presented here.

CHAPTER II

VELOCITY DRIFT MODELLING: LOW-FREQUENCY RESPONSE

As discussed in the introduction, our initial objective is to verify the hypothesis of frequency separation during sensory processing of simultaneous visual and vestibular motion cues. Specifically, we wish to demonstrate how low-frequency visual cues dominate low-frequency sensation, and how they can be used to augment the AC transduction characteristics of the vestibular system. This chapter will concentrate on visually-induced motion sensation and models appropriate thereto, while the next chapter will discuss sensation dynamics at the other end of the frequency spectrum, concentrating on vestibular modelling.

This chapter is organized into five section. Section 2.1 discusses the basic problem of sensation measurement and motivates the choice of monitoring subject performance in a closed-loop velocity-nulling task. Section 2.2 then provides a brief description of the experimental hardware and protocol, while section 2.3 details the low-frequency trends seen in operator behavior, when presented with different visual motion cue stimuli. This section also provides a comparison of RMS tracking errors. Fairly simple velocity bias models are then presented in section 2.4, in an attempt to explain functionally the observed behavior in terms of our current knowledge of motion sensation dependence on the two cues. Finally, section 2.5 summarizes the results, and briefly notes how models fall within the complementary filter hypothesis framework.

2.1 General Experimental Approach

One of the primary concerns of any experimental procedure directed at modelling sensation is the choice of behavioral response measurement to use. Although there are clearly many possibilities to be considered, most protocols would appear to fall into either one of two categories (Chapanis, 1959): open-loop magnitude estimation or closed-loop nulling of sensation.

2.1.1 Open-loop Magnitude Estimation

In its most general form, magnitude estimation requires a subject to associate his sensation with a response measurable by the experimenter (Stevens, 1968), the stimulus-to-response mapping being determined by the response options allowed the subject and an initial "calibration" protocol. In the velocity magnitude estimation experiments conducted by Young et al (1973), for instance, the response modality was a linear, continuous, bidirectional, numerical scale, so that a directionally sensitive scalar magnitude could be associated with the subject's velocity sensation, under differing experimental conditions.

As discussed at length by Poulton (1968), the problem of obtaining meaningful magnitude estimates, estimates which somehow truly correspond to the subject's sensation, is a far from trivial exercise. Among other things, magnitude estimates are corrupted by the range of stimuli used, their distance from threshold, the size of the modulus and the position of the associated stimulus within the overall range, and the type of

numerical scale available to the subject. In addition, vestibular experimentation is complicated by the fact that response calibration to a pretest velocity modulus must be a dynamic process because of equipment acceleration limits (necessitating a truncated ramp velocity profile rather than simple steps). Finally, habituation is a well-recognized characteristic of vestibular testing, and it might be expected that stimulus ordering artifacts would play a significant role in shaping a subject's response over the span of a test session.

In spite of these possible pitfalls, a pilot study was initiated to assess the applicability of velocity magnitude estimation to dual-input sensory modelling.* Shown in Figure 2.1 is a time history of actual subject velocity and the corresponding magnitude estimation for rotation in the absence of any visual motion cues. The AC characteristics of the canals make themselves clearly evident; what is also evident, however, is the instance of an incorrect direction indication, and later, the spontaneous increase in indicated velocity when no stimulus was present. Although this type of response "noise" was minimized with extended training at the task, response inconsistencies showed a sharp increase when the subject was simultaneously presented with non-corroborating visual motion cues, an experimental condition critical to the dual-input sensory modelling effort.

For these reasons, it was decided not to use subjective velocity magnitude estimation as a behavioral measure of rotational sensation. The alternative is discussed below.

---

*A description of the experimental equipment is given in section 2.2.1.

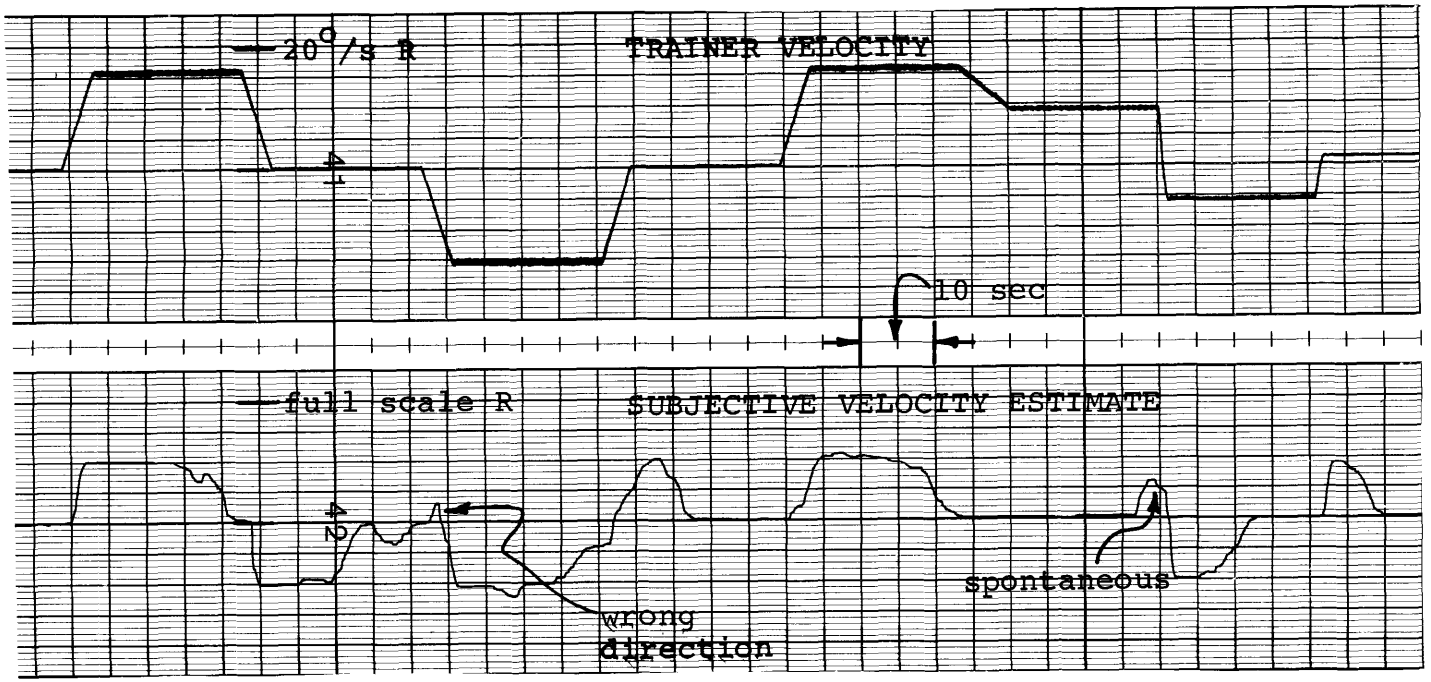

Figure 2.1: Open-loop Subjective Velocity Estimate

2.1.2 Closed-loop Velocity-Nulling

A less direct method avoids many of the problems just discussed, and involves giving the subject the task of closed-loop control over his own (sensed) velocity. One approach is to require the subject to maintain at zero the yaw velocity of a platform on which he is seated, by use of a velocity control stick which commands the platform drive. The task requires no magnitude estimation as such, since the basic objective is one of simply matching sensation with the sensation of sitting still. Furthermore, the task is closed-loop, since the closure is provided by the subject's own sensation of velocity, which, in turn, is derived from visual and vestibular motion cues. To avoid a null response from the subject, a non-predictable disturbance signal can be added to the platform drive, so that disturbance compensation must be performed throughout the course of the run. The overall scheme is illustrated in block diagram form in Figure 2.2. The subject is presented in a similar block diagram format, the estimator structure motivated by the modelling discussion given in Chapter 1, and the control structure patterned after the functional modelling used in conventional human operator studies (McRuer and Krendel, 1957).

Since we are interested in subjective response to low-frequency visual motion cues, the most obvious candidate for a test stimulus is one of zero frequency; i.e., a constant velocity field motion. A second choice can be motivated by a desire to observe operator response in a purely "vestibular" situation, that is, when deprived of visual motion cues. A field fixed with respect to the subject is thus called for. Finally, it is of interest to observe response when visual field motions exactly confirm vestibular sensations, obtainable by rotating the visual

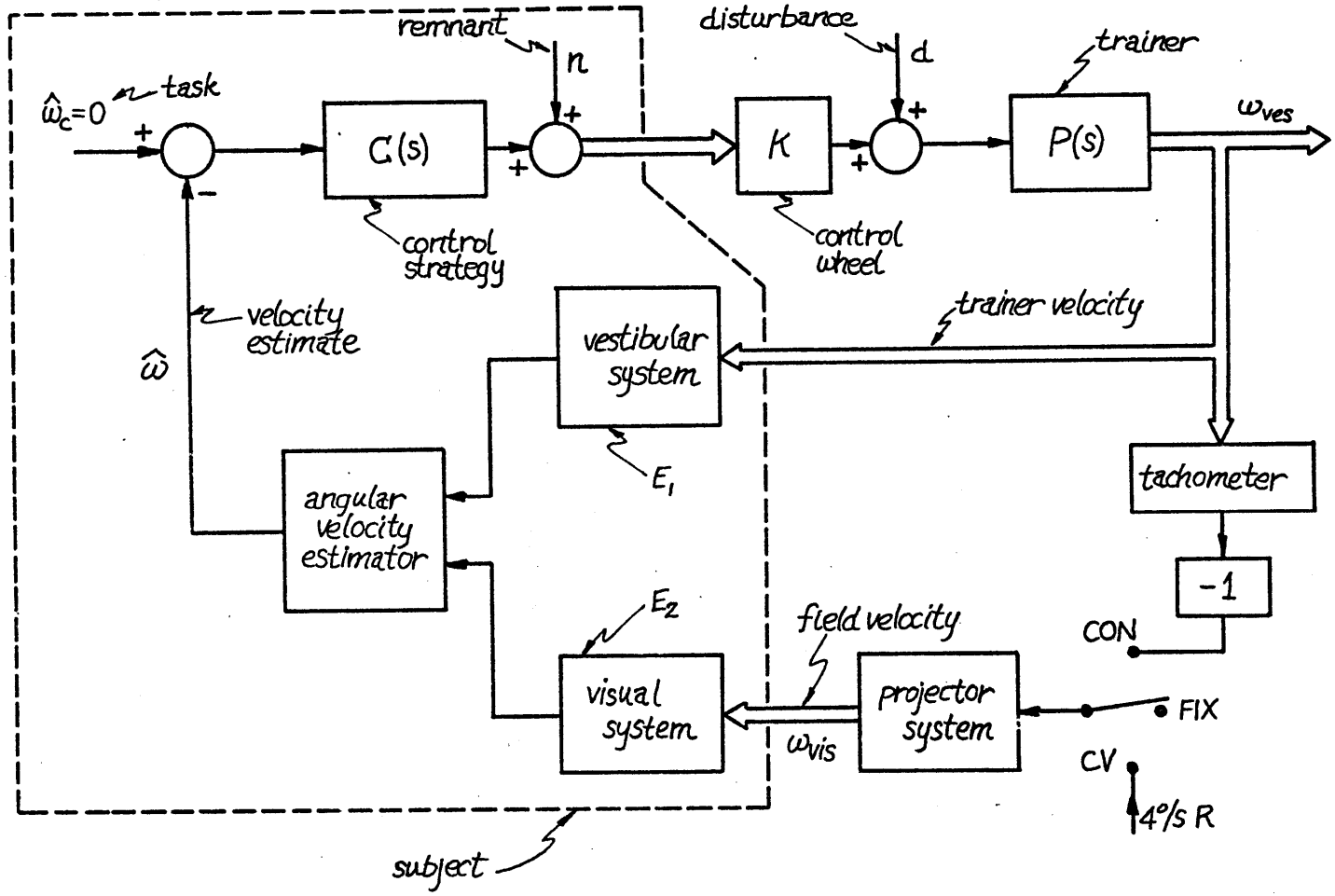

Figure 2.2: Closed-Loop Velocity Nulling Task

field with respect to the subject, in exact negative correspondence with actual platform motion.

These choices motivate the visual motion stimuli illustrated in the preceding block diagram, and are labelled as follows:

1. CON: A counterrotating field, which moves left with respect to the subject when the platform moves right, mimicking the everyday correspondence between visual and vestibular cues.
2. FIX: A field fixed with respect to the subject, so that reliance is entirely on vestibular cues.
3. CV: A field moving at constant velocity with respect to the subject, independent of actual platform velocity, and of the type shown to induce a circularvection sensation.

By measuring subject responses during the nulling task, in particular, his control of platform velocity, it will be possible to compare differences due to operation in three different visual field environments. How field type can be correlated with subject response to infer a functional model of low-frequency parallel channel processing will be obvious once the typical response histories are presented in section 2.3. For now, however, it is appropriate to describe some of the specifics of the velocity-nulling experiment.

2.2 Experimental Description

This section gives a brief description of the hardware implementing the loop of Figure 2.2, and the protocol used in the experimental runs.

2.2.1 Hardware Description

2.2.1.1 Platform

The enclosed platform used to rotate the subject is a modified small aircraft trainer, the Link GAT-1 Trainer, driven in yaw rotation only, as a velocity servo. Loop closure is provided by tachometer feedback implemented on a GPS 290T analog computer, which also provides command signal prefiltering to avoid resonance in the trainer drive at high frequencies. Details of the analog circuitry are given in Appendix A, as are the results of input-output testing of the servo loop. It suffices to note here that the overall closed-loop velocity transfer function associated with the platform, P(s), can be approximated by a simple second-order system:

$$P(s) \equiv \omega/\omega_c = \omega_n^2/(s^2 + 2\zeta_n\omega_n s + \omega_n^2) \qquad (2.1)$$

where the break frequency is 0.90 Hz and the damping ratio is 0.7.

2.2.1.2 Projector System

A peripheral visual field motion cue is provided to the subject via

the two translucent side windows of the trainer, upon each of which is projected a vertical stripe pattern via a trainer-mounted slide projector, lens, mirror, and servo-drive system (Murphy, 1972; Morrison, 1975). The drive allows velocity control of a film loop passing through the projector and containing the stripe pattern, and thus, velocity control of the projected images on the side windows. The mirror arrangement is configured so that when the image on one window moves forward, the other window's image moves aft.

When the subject is seated in the trainer looking forward, with his head supported by the headrest, the side windows subtend approximately 64^{o} in the vertical direction, measured from subject eye position. They subtend approximately 52^{o} in the forward direction and 12^{o} aft, resulting in a projected image exceeding normal peripheral field limits. The alternating black and white vertical stripes projected on these windows subtend angles of approximately 12°, and when moving differentially as just described, result in a quite compelling yaw circularvection illusion.

Scaling of the projector drive signal is implemented with analog computer circuitry (described in Appendix A) so that commanded visual field velocity can be given in angular units, a measure consistent with actual trainer velocity. This allows for tachometer crossfeed from the trainer to the projector, and the projection of a realistically counter-rotating visual field which corroborates trainer motions. It is appropriate to note that the projector drive dynamics are considerably faster than the filtered trainer response dynamics noted in the previous section, so that field motion faithfully follows trainer motion when the counter-rotating mode is utilized.

2.2.1.3 Control Stick/Wheel

As will be noted in section 2.2.2, two experimental series were conducted, duplicates of one another except for the trainer velocity controller used by the subject. In the first series, a control stick was used. Full lateral deflection of approximately 30° results in a trainer velocity command of 20°/s, with right stick giving right trainer motion. The stick is center-loaded with a light spring, and investigation of the results of the first experimental series suggested that some of the subjects were using this center-loaded property as a cue to nulling trainer velocity (this is discussed at greater length in section 2.3). To eliminate this type of cue, the stick was replaced in the second series of experiments by a control wheel mounted in the horizontal plane directly in front of the subject. The wheel is not spring loaded, thus avoiding force centering cues. Further, the top of the control wheel is effectively featureless, providing neither visual nor tactile cues as to true center, although mechanical stops limit the total travel to a half-turn in either direction. As with the stick, full deflection results in a trainer velocity of 20°/s, trainer direction corresponding to the direction of wheel rotation.

2.2.1.4 Disturbance Generator

The disturbance signal injected into the trainer drive loop is generated by the real-time operation of a PDP-8 digital computer,

which creates the signal by summing 15 sinusoids and providing timed digital-to-analog conversion for subsequent analog computer scaling and summation with the subject's stick signal (see Figure 2.2). Details of the analog circuitry are given in Appendix A, as is a listing of the digital program.

The disturbance signal is characterized by a "shelf" line amplitude spectrum, illustrated in Appendix A, where each spectral component is a prime multiple of a base frequency of 1/128 Hz so that the signal is periodic with a period of 128 seconds. Because of this long period, the signal is not predictable by the subject, and thus may be termed pseudo-random. The time history is shown in Figure 2-3a of section 2.3.

2.2.1.5 Supplementary Equipment

Additional equipment used in the experimental design included a four-channel FM tape deck and four-channel strip chart recorder to record the basic variables of the closed-loop task: disturbance input, trainer velocity, visual field velocity, and subject stick deflection. In addition, a headphone/microphone set allowed for communication with the subject prior to the experimental run, and for audio cue elimination during a run, by providing background music supplied by an FM broadcast band tuner.

2.2.2 Protocol and Experiment Design

Six subjects participated in the experiment, five males and one

female, age 24 to 34, in normal health with normal peripheral vision, and having no known vestibular dysfunction. Each subject was instructed as to the nature of the velocity-nulling task and specifically told to keep the trainer as motionless as possible, by concentrating on his own sensation of motion and by providing the appropriate compensatory control stick deflections.

Prior to an actual run, each subject was given the opportunity to control trainer motion, with the door open, to observe how much control power was available to him, and to get an approximate idea of the trainer's response dynamics. Then, with no stick input, the disturbance signal was injected into the trainer drive so that the subject could obtain some estimate of the amplitude and frequency content of the signal he would be asked to null. Finally, with his head supported by a headrest and looking forward, he was given a practice session of two minutes with the trainer door closed and with a counterrotating visual field motion providing confirming visual motion cues. During this time, the subject wore the headphones, and the background music volume was adjusted to ensure that any mechanical sounds from the trainer were inaudible, but remaining at a comfort level acceptable to the subject.

A typical run lasted for approximately 12 minutes, during which time the subject was required to provide continuous velocity-nulling compensation against the disturbance signal. During this period, each of the three visual field conditions (CON, FIX and CV) was repeatedly presented to the subject in random order, the start of each presentation synchronized with the start of a new period of the disturbance signal.

Each field presentation lasted for 128 seconds, unless stick saturation necessitated early termination of the stimulus. Because operator drift occurred during FIX and CV presentations (see below), a short counter-rotating field presentation followed each FIX and CV presentation, of a duration sufficiently long to ensure nominal subject velocity-nulling performance prior to the next field presentation.

Shown in Table 2.1 is the design matrix specifying field presentation order for each subject. It may be noted that each subject received two presentations in each of two of the field types, and three presentations of the remaining field type, for a total of seven presentations. The matrix was designed to provide some control for both order of presentation and stimulus precedence effects. As just noted, implicit in the table is a short CON presentation following each FIX and CV presentation, and preceeding the next tabulated field presentation.

At the end of a run, each subject was questioned as to whether he may have been consciously using other cues besides motion sensation to null trainer velocity. Two of the subjects felt that they might have used the stick-centering property as a nulling cue, but no subjects felt that any other cues were available for inferring trainer motion.

As noted in section 2.2.1, the entire experiment was repeated, using the same subjects and the same protocol, for the purpose of assessing the effectiveness of the stick-centering cue. Thus, a complete duplicate series was run with the control stick replaced by the previously-described control wheel. Post-test questioning revealed no awareness by any of the subjects of any extraneous cue which might have aided the nulling task.

TABLE 2.1 DESIGN MATRIX FOR VISUAL FIELD PRESENTATION

PRESENTATION ORDER	SUBJECT NUMBER 1	2	3	4	5	6
1	CON	CON	FIX	FIX	CV	CV
2	FIX	CV	CON	CV	CON	FIX
3	CV	FIX	CV	CON	FIX	CON
4	CON	CON	FIX	FIX	CV	CV
5	CV	FIX	CV	CON	FIX	CON
6	FIX	CV	CON	CV	CON	FIX
7	CON	CON	FIX	FIX	CV	CV

CON: Counterrotating

FIX: Fixed

CV: Constant velocity ($4^{o}/s$)

2.3 Experimental Results

As mentioned at the beginning of this chapter, the major objective here is to correlate low-frequency subject performance with type of visual field presentation. To this end, section 2.3.1 will briefly discuss three sample strip chart histories, one for each field type, and motivate a closer look at velocity drift rates. Sections 2.2.3 and 2.3.3 will then look at drift rates under FIX and CV presentations, while section 2.3.4 will conclude the discussion with a comparison of RMS tracking errors.

2.3.1 Time Histories of Subject Response

Figure 2.3a shows a set of typical histories of the disturbance signal sent to the trainer drive, the trainer velocity, the subject's compensatory control stick deflection, and the visual field velocity. Since the visual field is counterrotating (CON), it is the exact negative of trainer velocity, and thus visual and vestibular cues complement one another. As might be expected, operator performance in this "normal" situation results in a well-met task objective, with the trainer being maintained at a zero-mean velocity throughout the run.

In contrast, Figure 2.3b illustrates performance in the absence of visual motion cues, where the visual field is held stationary with respect to the subject (FIX). It can be seen that after the visual field stops moving, the subject begins to lose his zero reference and gradually moves the control stick to the left, resulting in a leftward drift of

Figure 2.3a: Counterrotating Visual Field (CON)

- Visual Field Velocity Confirms Vestibular Inputs
- Zero Mean Trainer Velocity

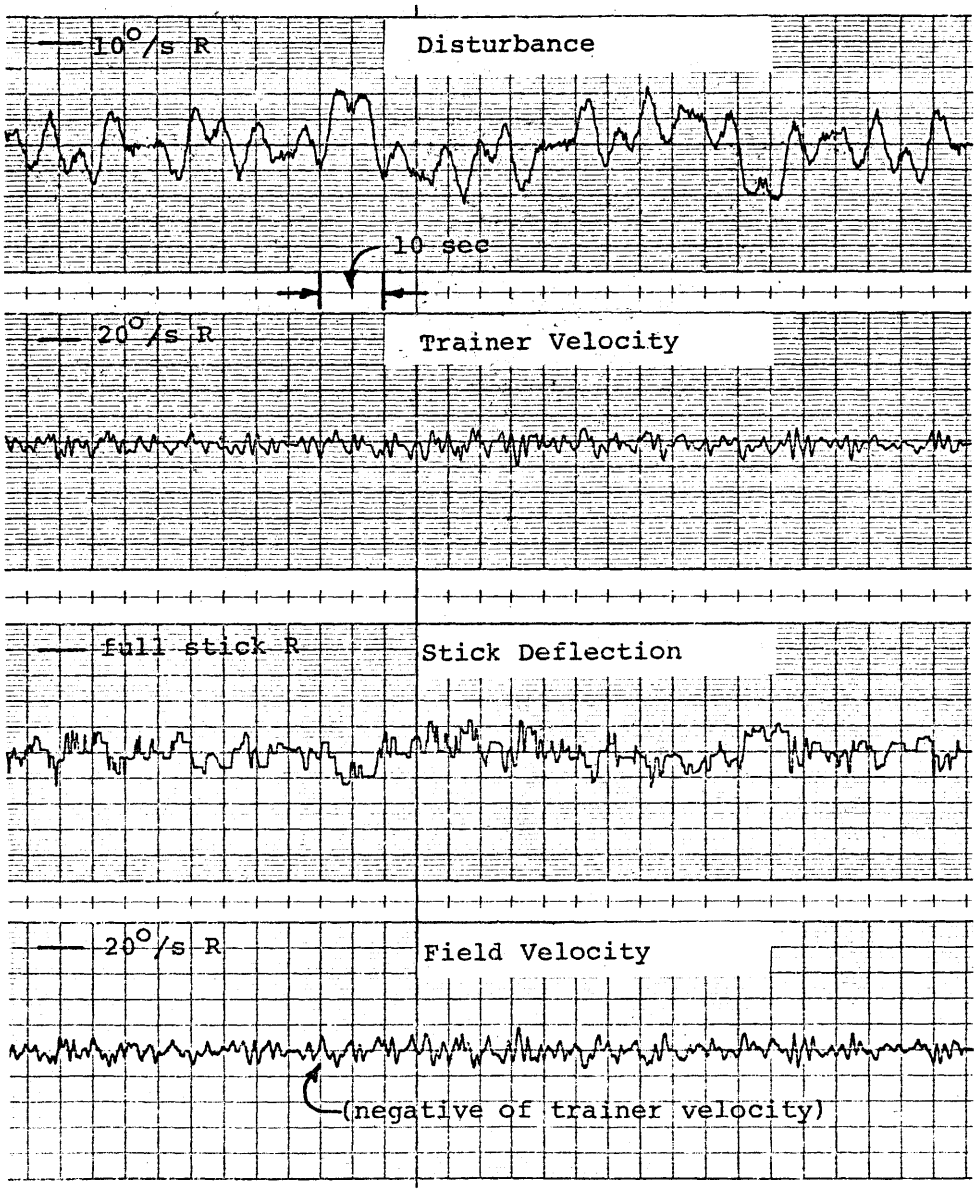

Figure 2.3b: Stationary Visual Field (FIX)

- No Visual Motion Cues
- Left Drift Acceleration of 0.05 Deg/s^2

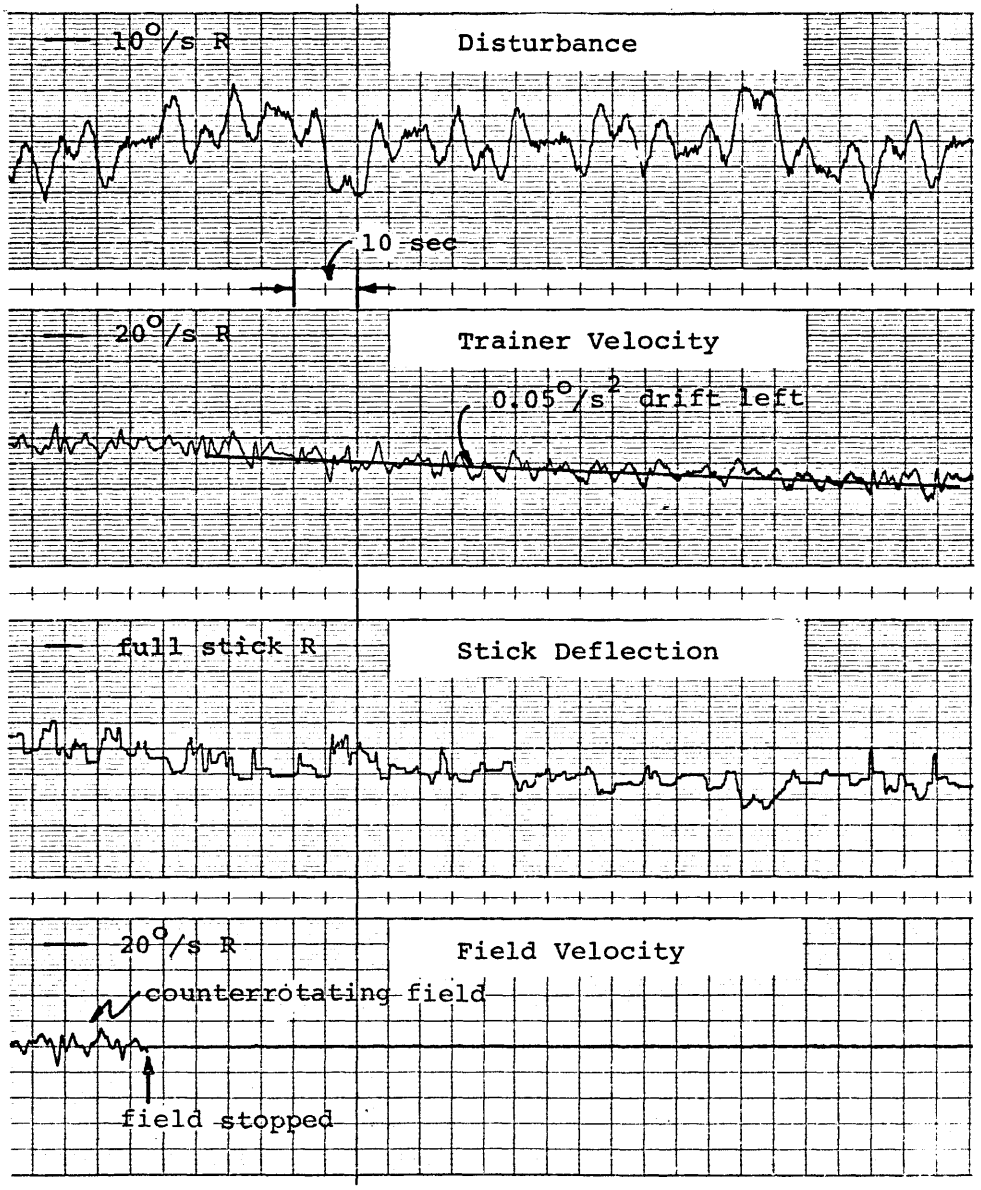

trainer velocity of approximately $0.05^{o}/s^{2}$. Since the subject feels that he is successfully performing the assigned nulling task, either his effective threshold must be greater than this value, or he must be operating with a vestibular "bias", or both. A threshold which is larger than the observed drift rate fails to explain why the subject undergoes a steady-state constant acceleration, however. The concept of a vestibular bias will be explored in more detail in section 2.4.

Figure 2.3c illustrates performance in the third type of visual field presentation, a constant velocity field rotating at $4^{o}/s$ to the right with respect to the subject (CV). Following a counterrotating presentation and good nulling performance by the subject, the field undergoes a step change in velocity. It is seen that the subject continues to maintain a zero mean trainer velocity for 15 or 20 seconds, and then begins to accelerate the trainer to the right, in effect "chasing" the visual field at ever-increasing trainer velocities.

Although operator performance is functionally similar to that just seen in the fixed field case, the two are distinguished by the order-of-magnitude increase in drift rate seen with a CV stimulus. The implication is that a circularvection illusion is influencing operator behavior. Presumably, after the 15 or 20 second latency period, the CV illusion takes hold, causing the subject to feel himself drifting to the left. To null out this illusory motion, he compensates with a right stick deflection, and begins to drift in that direction. In a normal situation with an earth-fixed visual reference, such compensation would result in a lessening of the visual field velocity, and, in turn, a return of

Figure 2.3c: Constant Velocity Visual Field (CV)

- Right Moving Visual Field Results in Left CV
- Left CV Results in Compensatory Right Stick
- Result is Right Drift Acceleration of 0.45 Deg/s^2

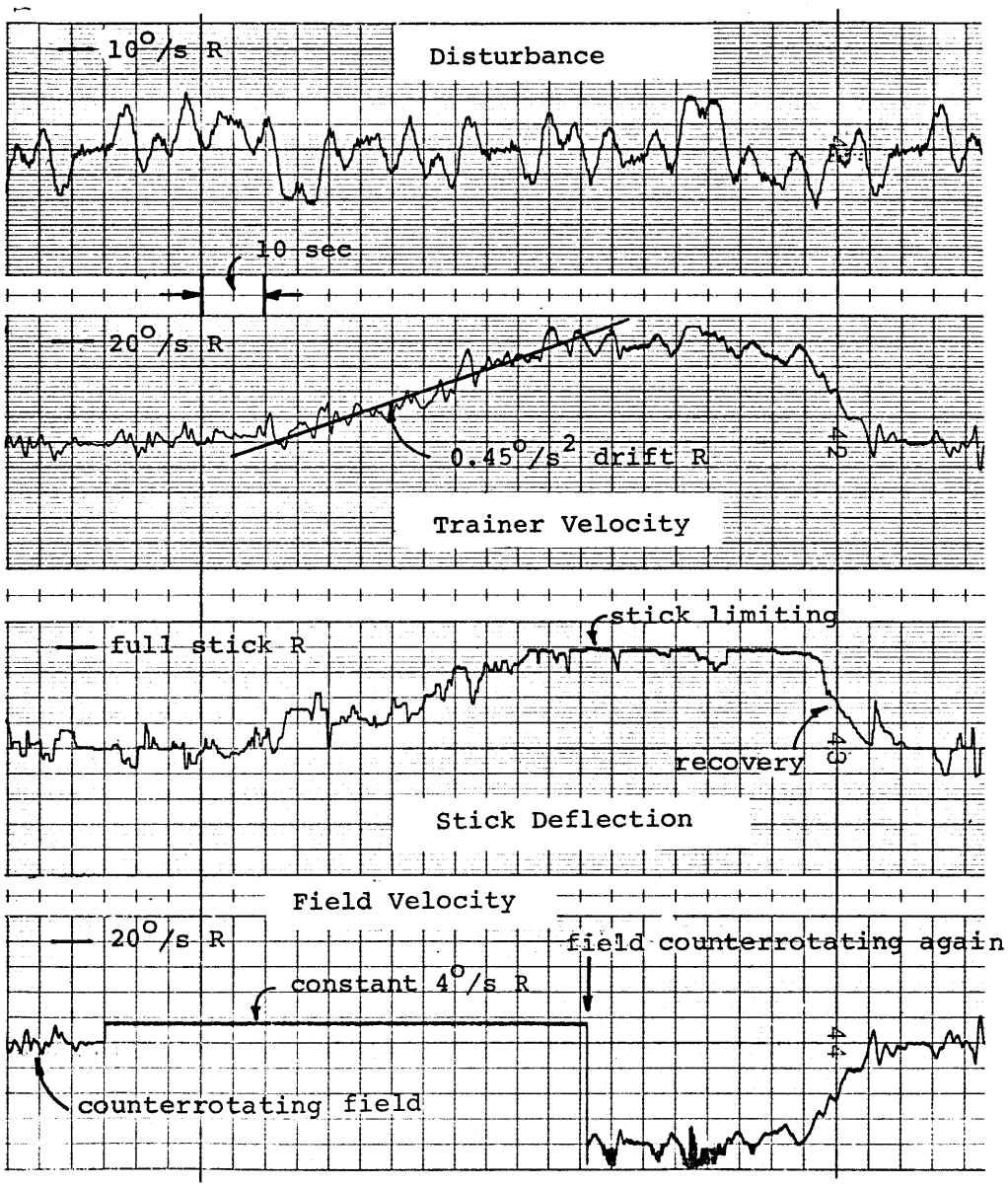

the stick to its zero position. Here, however, the subject's visual field motion is unaffected by actual trainer velocity, so that the strength of the visual stimulus is unchanged. With such a constant stimulus being presented it is not unexpected that the subject continues to "compensate" with more and more right stick deflection, until the limits are reached.

As in the preceeding fixed-field case, the subject presumably feels he is successfully performing the assigned nulling task, so that one would be inclined to hypothesize that the two motion cues are, on the average, exactly cancelling one another, to result in a zero sense of motion. This idea will be discussed in more detail in section 2.4, where it will be shown how such cancellation is consistent with the observed constant trainer acceleration.

Also shown in Figure 2.3c is the subject's recovery of zero mean velocity after the CV presentation. Following stick saturation, the visual field was switched to the counterrotating mode, presenting the subject with a high-velocity left-moving field, which, in the subject's approximately stationary frame of reference, is analogous to a left-moving CV stimulus. Approximately 30 seconds pass before the subject feels himself moving to the right, and then a rapid deceleration (approximately $2^{o}/s^{2}$) brings him back to an average zero velocity. Presumably, the subject decelerates rapidly because both cues are confirming this transition phase, leading him to accept the visual cue as a true velocity reference; this is to be contrasted with the lower acceleration rate seen when the CV cue is not vestibularly confirmed.

This completes the qualitative discussion of subject operation under

the three visual field presentation conditions. The next two sections look more closely at the drift rate statistics for the test population, for the FIX and CV field presentations.

2.3.2 Velocity Drift with a Fixed Visual Field (FIX)

From the design matrix of Table 2.1, it is seen that four subjects received two FIX presentations, and two subjects received three FIX presentations, resulting in 14 opportunities to observe possible velocity drift in the subject responses. Since the experiment was run twice, first with stick control, then with wheel control, we can see if there are any effects due to cue centering.

2.3.2.1 Control Stick Responses

In the first series using the control stick, there were 8 instances of observed drift and 6 no responses (NR) observed, (i.e., no drift), within the accuracy afforded by the strip chart recording. Counting each NR as a $0.0^{o}/s^{2}$ drift rate, the population statistics are given by:

$$\text{stick control:}\quad \mu_1 = 0.004^{o}/s^{2} \qquad \sigma_1 = 0.041^{o}/s^{2} \qquad N_1 = 14 \tag{2.2a}$$

A t-test shows that the mean μ_1 is not significantly different from zero ($P > 0.2$), which is what would be hoped for, since a significant non-zero mean would suggest a directional bias in the experimental equipment, procedure, and/or subject population.

It should be noted that two subjects did not exhibit any drift when the visual field motion was stopped, suggesting either the presence of

exceptionally low thresholds, or, more likely, the use of the center-loaded stick as a cue in maintaining zero mean velocity. This latter explanation is consistent with behavior seen in other subjects, in which drift was sporadically nulled by the strategy of spontaneously returning the stick to its zero position, an action presumably motivated by the subject's knowledge that a non-zero constant stick deflection results in a steady trainer velocity. As noted earlier, this suspicion motivated the second experimental series using the effectively cueless control wheel.

2.3.2.2 Control Wheel Responses

With the experimental series repeated, there were again 14 opportunities to observe velocity drift. Actually observed were 13 cases of drift and one no response (NR). Again, counting the NR as a $0.0^{o}/s^{2}$ drift rate, the population statistics are given by:

$$\text{wheel control:} \quad \mu_2 = 0.015^{o}/s^{2} \qquad \sigma_2 = 0.050^{o}/s^{2} \qquad N_2 = 14 \tag{2.2b}$$

As with stick control, a t-test shows that the mean drift rate is not significantly different from zero, suggesting the absence of a directional bias.

2.3.2.3 Stick versus Wheel Control

We now address the question of whether or not the population responses are significantly affected by the substitution of wheel for stick

control. Comparing the statistics of (2.2a) with those of (2.2b), we find that an F-test on the variances shows them not to be significantly different ($P > 0.2$), so that we can pool them ($\sigma_p = 0.046^o/s^2$) and use a t-test on the means. We find that the means are also not significantly different ($P > 0.2$), so that this statistical measure shows no difference between wheel and stick control.

Perhaps, however, this conclusion is biased by the fact that the NR's of each series were included to arrive at the means and variances of (2.2) By excluding them, and simply looking at the drift statistics of the responding population, we find the following:

stick control: $\mu_1 = 0.016$ $\sigma_1 = 0.052$ $N_1 = 8$ (2.3a)

wheel control: $\mu_2 = 0.006$ $\sigma_2 = 0.056$ $N_2 = 13$ (2.3b)

An F-test shows the variances to be not significantly different ($P > 0.2$), so that we can pool them ($\sigma_p = 0.054^o/s^2$) and use a t-test on the means. Again, we find that the means are also not significantly different ($P > 0.2$), so that even excluding the NR's from the data, we find no significant difference between stick and wheel control, by these measures.

What should be obvious at this point, however, is that the number of NR's observed with wheel control (1) is quite a bit smaller than the number observed with stick control (6). To test the significance of this observation, we use a contingency table and the χ_0^2-test:

	stick	wheel
drift occurred	8	13
no drift occurred	6	1

$\chi_0^2 = 4.76$

$\nu = 1$

$P < 0.05$

Thus, there is a significant difference between stick and wheel control, in terms of the number of times zero drift (NR) was observed. The suggestion is that the stick provides centering information which completely suppresses drift in some cases, although the average drift rate is independent of the type of controller used.

2.3.2.4 Pooled Drift Rate Statistics

Since the statistical tests done above on the means and variances of the drift rates showed no significant differences between the stick and wheel control, it seems reasonable to pool the data. Of interest, then, is the manner in which the NR's are handled. If we assume the one NR observed with wheel control is a legitimate case of zero drift, uncorrupted by a controller centering cue, then we are obliged to include it in the population results. This is not unreasonable, since it seems safe to assume that no controller centering cues were possible with the wheel control.

Turning now to the NR's observed with stick control, one approach is to simply exclude them all, on the basis of possible response corruption due to centering cues. The corresponding contingency table test results in a χ_0^2 value of 0.39, a considerable reduction from the 4.76 value obtained above, and suggests that this is the proper direction in which to proceed. Including only one of the NR's observed during stick control results in a χ_0^2 value of 0.11, and including two NR's results in a value of 0.88. Including additional NR's only increases the χ_0^2 value; thus, the minimum χ_0^2 value is obtained with one NR included in the stick

responses.

For the results of the two experimental series to be most congruent, in terms of NR occurences, it is clear that a contingency table test should result in a minimum χ_0^2 value. Thus, the decision may be made to eliminate five of the six NR's obtained under stick control. When the data is so edited, keeping one NR from each series, the following statistics result:

$$\text{drift rate:} \quad \mu = 0.011^o/s^2 \qquad \sigma = 0.050^o/s^2 \qquad N = 23 \tag{2.4}$$

A t-test shows the mean to be not significantly different from zero ($P > 0.2$), as expected.

To gain an appreciation for the magnitude of the drift rates observed under fixed-field presentations, we can look at the statistics of the absolute values of the pooled stick/wheel data:

$$\text{drift rate (magnitude):} \quad \mu = 0.043^o/s^2 \qquad \sigma = 0.027^o/s^2 \qquad N = 23 \tag{2.5}$$

These drift rate magnitudes are well below accepted threshold values for yaw axis earth-vertical rotation ($\simeq 0.10^o/s^2$) and thus are consistent with the notion that the subject is completely unaware of his drift acceleration when deprived of visual motion cues. A summary of the above results is presented in Figure 2.4.

2.3.2.5 Normality of Drift Rates

A final note concerning the statistical characteristics of the velocity drift rates concerns the normality of the pooled data. Shown

Figure 2.4: Velocity Drift With No Visual Cues (FIX)

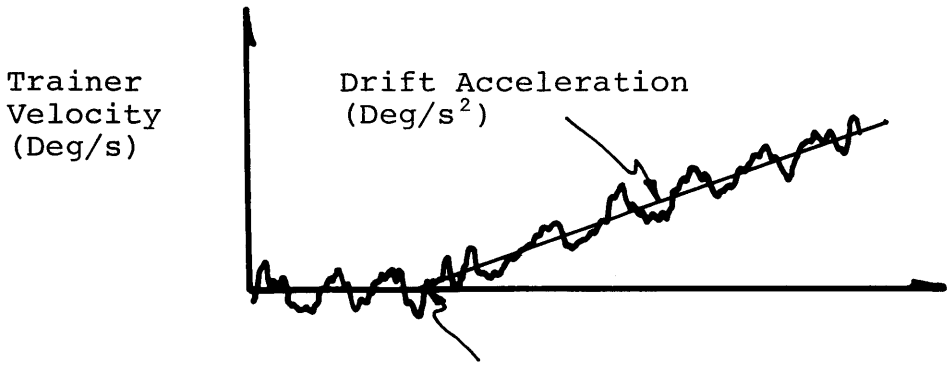

- Six Subjects, 14 Fixed Field Presentations Overall, Two Control Methods

CONTROL METHOD	DRIFT OCCURANCES	μ ($^o/s^2$)	σ ($^o/s^2$)
Stick	8	.016	.052
Wheel	13	.006	.056

- Only significant difference between methods is in number of drift occurances. Stick provides a centering Cue

- Pooled Data:

$\mu = .011\ ^o/s^2$ $\sigma = .050\ ^o/s^2$ N = 23

Not significantly different from zero. Balanced.

- Drift Magnitudes:

$|\mu| = .043\ ^o/s^2$ $\sigma = .027\ ^o/s^2$ N = 23

in Figure 2.5 is the cumulative distribution function (CDF) of the drift rates normalized with respect to the mean and variance of (2.5); superimposed on this experimentally derived curve is the CDF for the unit normal distribution, N(0,1). Use of the Kolmogorov-Smirnov test for normality (Afifi and Azen, 1972) strongly rejects non-normality, so that it is not unreasonable to conclude that velocity drift rates, caused by visual motion cue deprivation, are normally distributed. This will be contrasted to the results presented below, concerning drift rate distribution observed with subject performance during presentation of a constant velocity (CV) visual field.

A functional model of angular velocity perception incorporating the above-discussed drift characteristics will be presented in section 2.4 after a discussion of the CV drift results.

2.3.3 Velocity Drift with a Constant Velocity Visual Field (CV)

As with the fixed field presentations just described, there were 14 opportunities for CV-induced drift in each of the experimental series (recall Table 2.1). Out of this total of 28 possible drift instances, there were observed 27, with one case of severe disorientation and subsequent inconsistent and task-unrelated response. This case has been eliminated from the data base whose statistics are given below:

stick control: $\mu_1 = 0.261^o/s^2$ $\sigma_1 = 0.141^o/s^2$ $N_1 = 14$ (2.6a)

wheel control: $\mu_2 = 0.328^o/s^2$ $\sigma_2 = 0.265^o/s^2$ $N_2 = 13$ (2.6b)

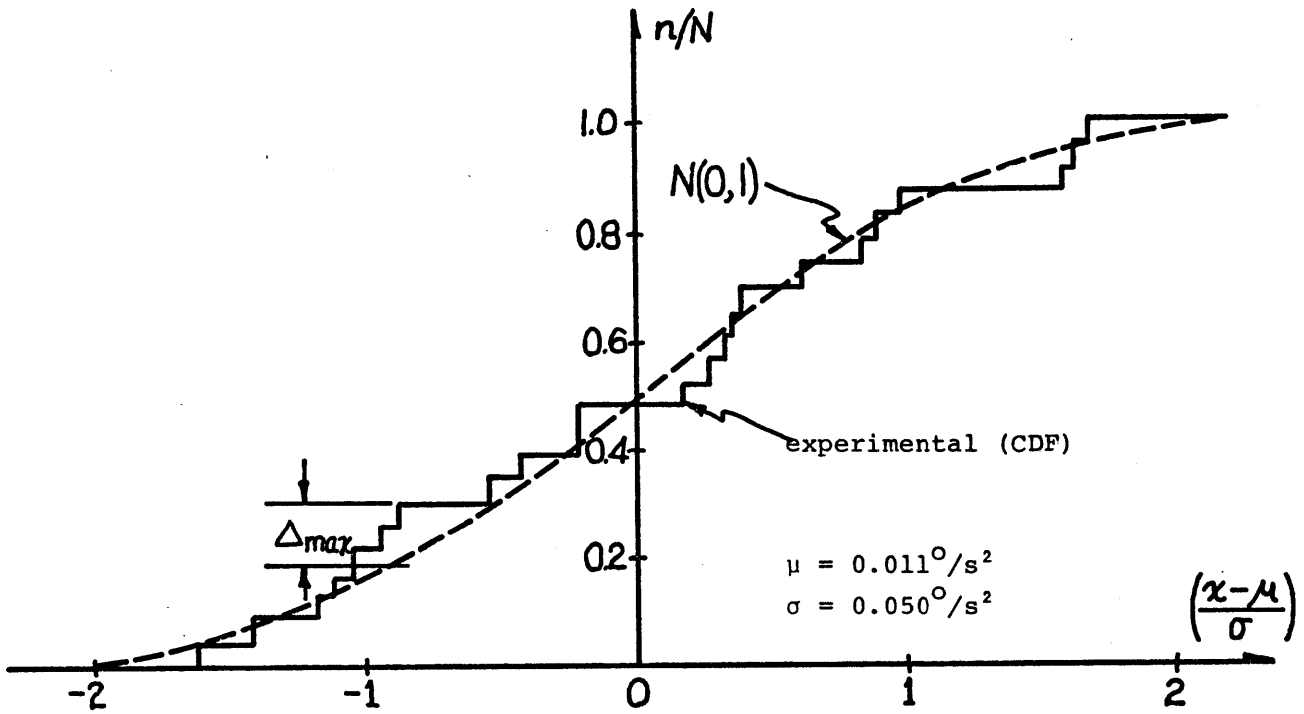

Visual Field: FIX
Control: Stick/Wheel

$\Delta_{max} = 0.11$
$N = 23$
$\Rightarrow P > 0.20 \Rightarrow$ Reject non-normality

Figure 2.5: Cumulative Distribution Function for Velocity Drift Rates (FIX)

2.3.3.1 Stick versus Wheel Control

As in the preceeding section, we can ask if stick control results in significantly different subject responses from those seen with wheel control. It should be clear that they are equivalent in terms of not suppressing drift responses; this in contrast to the large numbers of NR's seen with stick control and a fixed visual field presentation as noted earlier. What remains then is to compare the statistical measures just given.

Comparing the statistics of (2.6a) with (2.6b), an F-test on the variances shows them to be statistically different ($P < 0.05$). A Welch t-test, however, shows that the means are not significantly different ($P > 0.2$), and one is thus motivated to pool the data for the two control methods, in spite of the variance differences. The pooled data for CV presentation velocity drift rates are then characterized by the following statistics:

$$\text{drift rate: } \mu = 0.293^{o}/s^{2} \qquad \sigma = 0.209^{o}/s^{2} \qquad N = 27 \qquad (2.7)$$

It should be recalled that since all of the observed drift rates were in the same direction (following the direction of the visual field motion), these statistics also apply to the drift rate magnitudes. It is also appropriate to recall that these statistics apply to the single stimulus magnitude of a $4^{o}/s$ right-moving visual field.

2.3.3.2 FIX versus CV Drift Rates

A simple t-test on the pooled statistics of (2.7) show the mean

drift rate to be significantly different from zero ($P < 0.005$); this is to be contrasted to the approximately zero drift rate seen across the population in response to a fixed-field presentation. Further contrast between the responses to the two visual field environments is provided by comparing the drift rate magnitudes. From (2.5) of the previous section, fixed-field drift was characterized by:

$$\text{drift rate magnitude (FIX):} \quad \mu = 0.043^{o}/s^{2} \qquad \sigma = 0.027^{o}/s^{2} \qquad N = 23 \tag{2.8}$$

An F-test on the variances of (2.7) and (2.8) above shows a highly significant difference ($P < 0.001$), as does a Welch t-test on the means ($P < 0.005$). Thus we are led to conclude that drift rate magnitudes resulting from a CV visual field presentation are significantly different from those seen during a FIX presentation.

Also of interest is the fact that the mean CV drift rate of approximately $0.3^{o}/sec^{2}$ is near three times the accepted yaw axis earth-vertical rotational acceleration threshold. This might suggest a strong modulation of the vestibularly-sensed acceleration by the CV illusion of motion in the opposite direction. This will be discussed further in section 2.4.

A summary of the above findings concerning CV drift is presented in Figure 2.6.

2.3.3.3 Log-normality of Drift Rates

A final note concerning the statistical characteristics of the velocity drift rates concerns the normality of the pooled data. Shown in Figure 2.7a is the cumulative distribution function (CDF) of the drift

Figure 2.6: Velocity Drift With Constant Velocity Visual Field (CV)

- Six subjects, 14 CV field presentations overall, two control methods

CONTROL METHOD	DRIFT OCCURANCES	μ ($^{o}/s^{2}$)	σ ($^{o}/s^{2}$)
Stick	13 *	.261	.141
Wheel	14	.328	.265

*one severe disorientation eliminated from talley

- Significant difference between two methods in variance, not means

- Pooled data:

$\mu = 0.293\ ^{o}/s^{2}$ $\sigma = 0.209\ ^{o}/s^{2}$ $N = 27$

- Mean significantly different from zero ($P < .005$), and above threshold ($\sim 0.1\ ^{o}/s^{2}$)

- Results significantly different from FIX presentations.

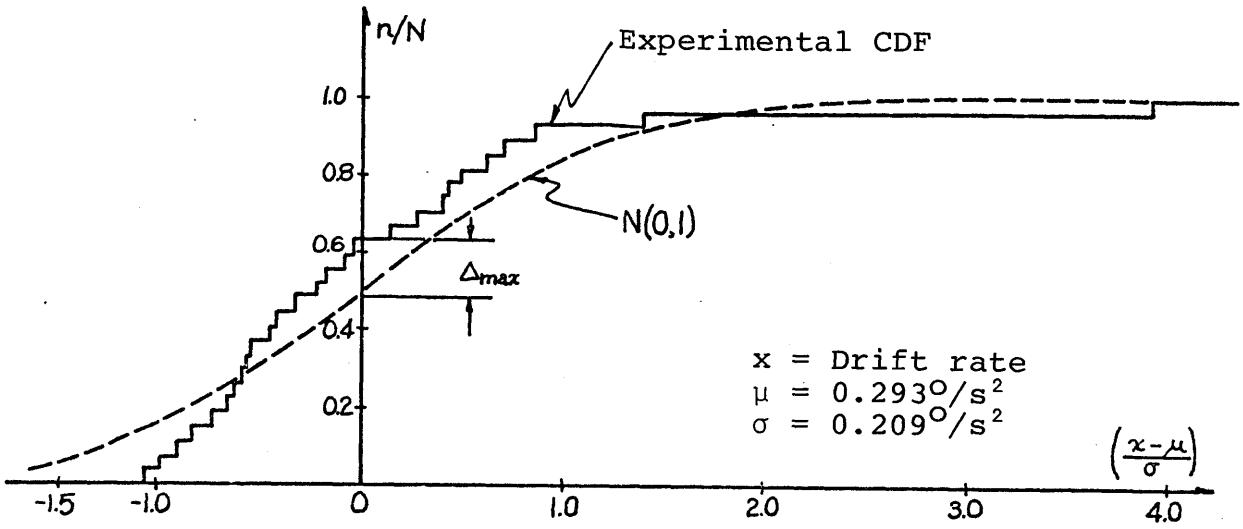

Visual Field: CV
Control: Stick/Wheel

$\Delta_{max} = 0.15$, $N = 27$ $\Rightarrow$ $P > 0.20$ $\Rightarrow$ Reject non-normality

Figure 2.7a: Cumulative Distribution Function for Velocity Drift Rates (CV)

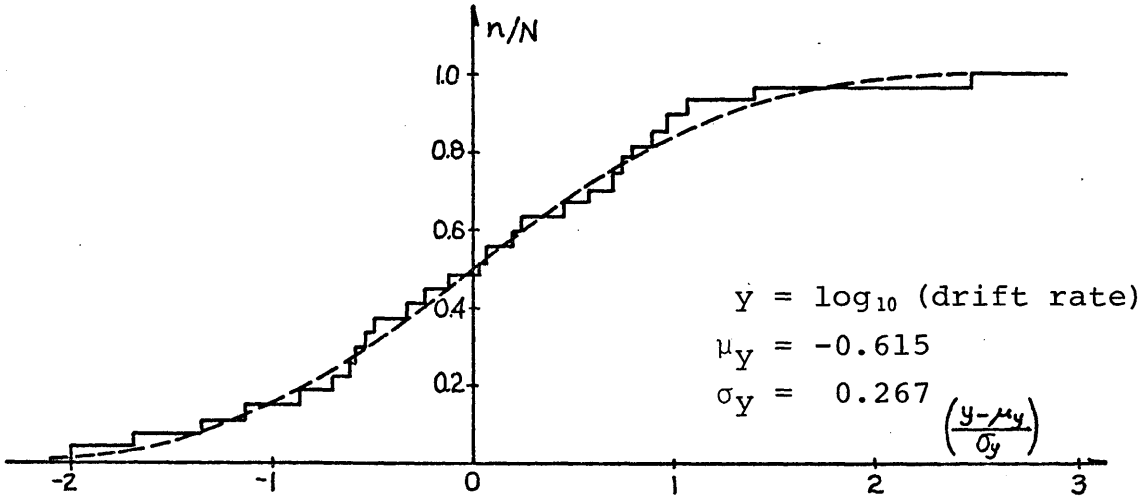

Visual Field: CV
Control: Stick/Wheel

Figure 2.7B: Cumulative Distribution Function for Log (Velocity Drift Rate) (CV)

rates normalized with respect to the mean and variance of (2.7), presented in the same format used previously for the FIX drift rates. As before, use of the Kolmogorov-Smirnov test for normality requires us to reject non-normality ($P > 0.2$). Comparing this figure with the one drawn for the FIX drift rates (Figure 2.5 of the last section), however, suggests that the CV drift data is "less normal", because of the late rise and slow tail off of the CDF. We are thus motivated to look at the log of the data, and the associated normalized CDF is plotted in Figure 2.7b. Comparing this with Figure 2.7a shows that the CV drift rate is more accurately described as a log-normal variable, rather than a normal random variable.

This type of behavior suggests that some portion of the human controller/estimator is behaving nonlinearly, either in the mixing of visual velocity information with vestibularly-sensed accelerations to produce a velocity estimate, or in the use of this estimate to produce the appropriate compensatory stick deflection. If the control portion of the loop were behaving non-linearly, we might expect to see the same log-normal distribution under fixed conditions, which we do not. If the visual channel itself were non-linear, we would expect to see a non-linear relation between subective magnitude estimates of CV and visual stimulus speed; however, Brandt et al (1973) showed both estimated field velocity and self-velocity to be linear functions of stimulus speed, at least for the range $10^{o}/s$ to $90^{o}/s$. Finally, the vestibular channel has been shown to be reasonably linear, in both neurophysiological studies (Fernandez and Goldberg, 1971) and psychophysical studies (Clark and Stewart,

1962, 1968; Guedry, et al, 1971). One is thus directed toward the mixing function of visual and vestibular information as the source of the apparent non-linearity.

It should be recognized, however, that this line of inference, based on a slight deviation from normality in the CV drift rates, should not preclude an attempt at linearly modelling the observed behavior. In fact, linear models will be developed in section 2.4 to explain the drift behavior just described, and will form the basis for the functional analysis of both Chapters 3 and 4. The question of the applicability of non-linear models will be readdressed in Chapter 5.

2.3.4 RMS Tracking Error

To gain some measure of subject performance at the velocity-nulling task, the RMS error in trainer velocity may be computed for each set of trials associated with the three visual field presentations. Since the drift associated with FIX and CV presentations will obviously lead to large RMS error figures, it is more appropriate to consider the velocity error measured from the mean drift rate; it is also more meaningful, since these deviations from the mean rate are clearly more closely related to the error signal which the subject is attempting to minimize in the nulling task.

Drift can be eliminated from the trainer histories during FIX and CV presentations by the simple expedient of high-pass filtering the signal through a washout filter, implemented on the analog computer. The filter used has the following form:

$$\frac{s}{s+1}$$

$$F(s) = \tau s/(\tau s + 1)$$

where the time constant τ is chosen to ensure that most of the drift is eliminated without much attenuation of the lower frequencies of interest. A time constant of 4 seconds was settled on to process all subject histories (the corresponding break frequency is 0.04 Hz); this allows for a relative comparison of RMS error, while avoiding the problem of variations in low frequency power contributions associated with an individual time constant for each trainer history. The particular choice of a four second time constant is short enought to affect the true estimate of RMS error, but its effect is small, as will be seen shortly.

Table 2.2 gives average RMS figures obtained for the test population, using the control stick in the nulling task, for each type of visual field presentation. All but the last were obtained by passing an individual recorded trainer history through the 4-second washout, sampling the signal at 8 Hz for the duration of the presentation (128 seconds, or less if stick saturation occurred, as in several CV presentations), and then performing the RMS calculation digitally, to obtain an RMS error for each presentation. The summary statistics for all presentations (mean and standard deviation) were then used to construct the table shown.

The last set of figures associated with the CON presentation were obtained similarly, except that the washout filter was not used. This allows for a check on how much influence the washout has on the absolute accuracy of the RMS calculation. By comparing the statistics of the two CON RMS figures, with and without filtering, it is seen that the washout

results in an RMS error which is 7.5% low, a computational error which is not too excessive, in light of the comparisons to be made.

TABLE 2.2 RMS VELOCITY NULLING ERRORS (Stick Control, N = 14)

FIELD PRESENTATION	RMS ERROR (^{o}/sec)	RMS ERROR S.D. (^{o}/sec)
CON	1.33	0.11
	1.34**	0.10**
FIX	1.35	0.10
CV	1.81	0.38
CON*	1.44	0.11

*Calculated without high-pass signal conditioning
**Pooled

It should be clear from the table that there is no signficant difference between the RMS error incurred under counterrotating field conditions and that incurred under fixed field conditions. A t-test verifies this ($P > 0.2$), so that the CON and FIX data may be pooled, resulting in the pooled statistics given in the table. The functional significance of this similarity in tracking performance would appear to be that the subject's dynamic response above approximately 0.05 Hz is little affected by the absence of visual cues: the primary effect is seen in the incurred drift.

Chapter 3 will discuss the subject's dynamic response in considerably more detail; for now, however, it is of interest to compare the RMS error associated with CV presentations to the pooled error associated with CON and FIX presentations. An F-test comparing the variances shows a significant difference ($F_{13,27} = 13.4$, $P < 0.001$), and a Welch t-test (Afifi and Azen, 1972) results in a similar conclusion regarding the RMS error figures themselves ($t = 4.42$, $\nu = 15$, $P < 0.005$). Thus, one is lead to conclude that a significantly higher RMS error is incurred under CV conditions, one which is approximately 25% larger than that seen during either FIX or CON presentations. This obviously suggests that the change in subject response due to a CV field presentation is not limited to the previously described drift rates; the dynamic changes which must be occurring will be discussed in the next chapter.

2.4 Velocity Drift Models

The previous section has just described the statistical properties of velocity drift incurred by subjects during the task of velocity-nulling when presented with fixed and counterrotating visual fields. This section will now present very simple models of the human operator's estimation function which are consistent with the drift observed with FIX and CV presentations (sections 2.4.1 and 2.4.2, respectively) and with the zero mean performance with CON presentations (section 2.4.3).

2.4.1 Fixed Visual Field Model

Since no visual cues were available during FIX presentations, it would be functionally appealing to attribute the observed drift behavior entirely to the vestibular sensory pathways. Similar velocity-nulling experiments (Young, 1970), conducted in the absence of visual cues, have indicated a correlation between a subject's preferred drift direction and a measure of directional preponderance obtained by caloric stimulation of the canals, thus suggesting that the source of the drift is an imbalance between left and right vestibular paths. No caloric tests were made during this experimental series, however, so that the presence of a physiological imbalance is not directly verifiable. It is, nonetheless, instructive to see how a very simple model can be constructed which is consistent with the observed drift and with the generally accepted dynamic properties of the semicircular canals.

2.4.1.1 Biased-output Model

Shown in Figure 2.8 is such a model: a bilateral model of the two horizontal semicircular canals, whose outputs are differenced to provide an estimate of head angular velocity. Note that both the canals are characterized as identical linear bandpass filters on velocity, but differing in DC gain and output bias.

Shortly it will be shown that a simple constant offset in the estimate $\hat{\omega}$ is sufficient to give rise to the drift behavior seen in the experiments. In particular, if a non-zero estimate $\hat{\omega}$ can be generated by the model of Figure 2.8, in the face of an angular velocity ω which is actually zero, then it is a fairly direct matter to predict velocity drift in the closed-loop velocity nulling task.

Of interest now is to see how an offset can arise from a model parameter imbalance. From the figure, the angular velocity estimate is given by:

$$\hat{\omega}(s) = (b_R - b_L) + \frac{(K_R - K_L)\, s}{(\tau_1 s + 1)(\tau_2 s + 1)}\, \omega(s) \qquad (2.9)$$

It should be clear that if the bias terms are equal ($b_R = b_L$), then a gain imbalance ($K_R \neq -K_L$) is not sufficient to provide a non-zero $\hat{\omega}$ when ω is actually zero*. Neither is it necessary, since a non-zero ω can be simply obtained when ω is zero by having the biases unequal ($b_R \neq b_L$). Thus a gain imbalance is irrelevant to a discussion of a steady offset in the velocity estimate, and for simplicity we can assume a gain balance:

* The same conclusion holds true for unequal left-right pairing of the time constants, τ_1 and τ_2.

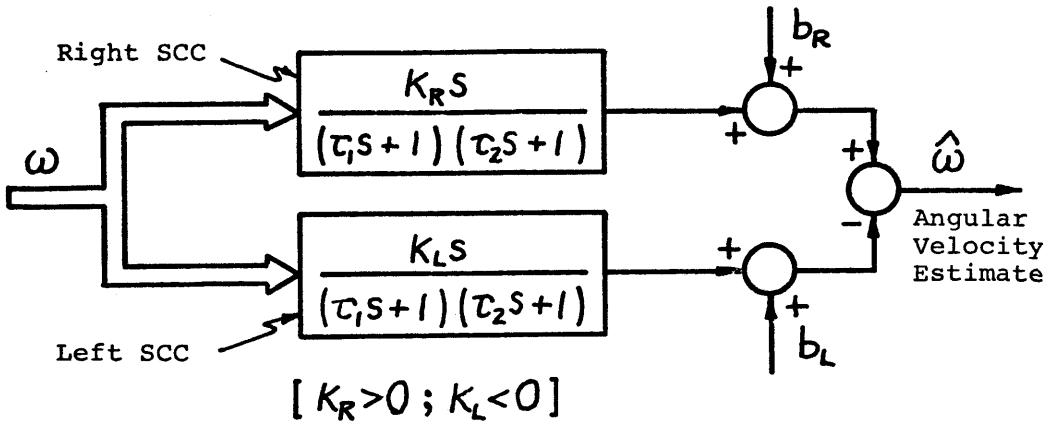

Figure 2.8: Bilateral Vestibular Model, with Output Biases

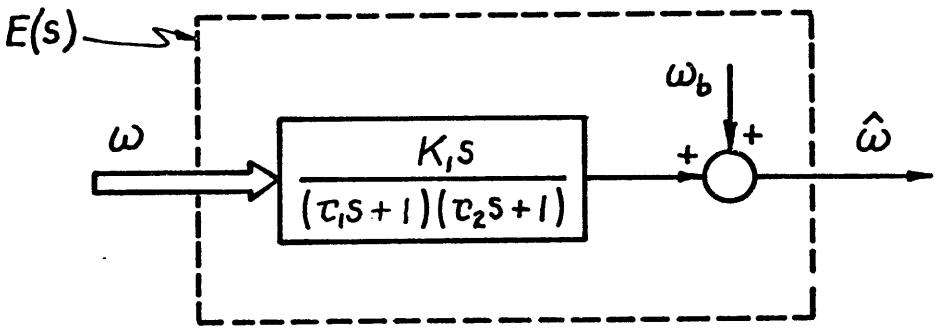

Figure 2.9: Cyclopean Vestibular Model, with Output Bias

$$K_R = -K_L \equiv K_1/2 \tag{2.10}$$

so that (2.9) simplifies to the standard "cyclopean" canal model, with bias:

$$\hat{\omega}(s) = \omega_b(s) + \frac{K_1 s}{(\tau_1 s + 1)(\tau_2 s + 1)} \omega(s) \tag{2.11}$$

where the bias velocity is defined by:

$$\omega_b \equiv b_R - b_L \tag{2.12}$$

The functional model corresponding to (2.11) and (2.12) is sketched in Figure 2.9, and will be used in the sequel.

2.4.1.2 Vestibular Bias and FIX Drift Rates

Now, to show how an angular velocity bias, ω_b, can give rise to the drift velocity observed in the nulling task, it is necessary to recall the functional loop diagram presented earlier (Figure 2.2), in which the subject is acting as a feedback compensator. Figure 2.10 shows a simplified linearized version of this loop. It assumes that the subject's control strategy C(s) is linear and works on the perceived rate error, ω_e, which is simply the difference between the task objective set point ($\hat{\omega}_c = 0$) and his perceived velocity $\hat{\omega}$. The latter is, in turn, assumed to be generated by a linear estimator block E(s), representing the function of motion perception.

Following the lead of many investigators of manual control performance (see for example, McRuer and Krendel, 1959, 1962), the subject's

output is modelled as a combination of the linear output of the C(s) block, and a remnant portion n(t), which is defined to be uncorrelated with the input disturbance signal d(t). The stick (wheel) transduces the operator output to a commanded trainer velocity, and is modelled as a pure gain, K. Stick output is summed with the loop disturbance signal d(t), and this summed command is passed through the trainer dynamics, represented by P(s), to result in the trainer velocity ω.

Figure 2.10: Linearized Model of Closed-Loop Velocity Nulling

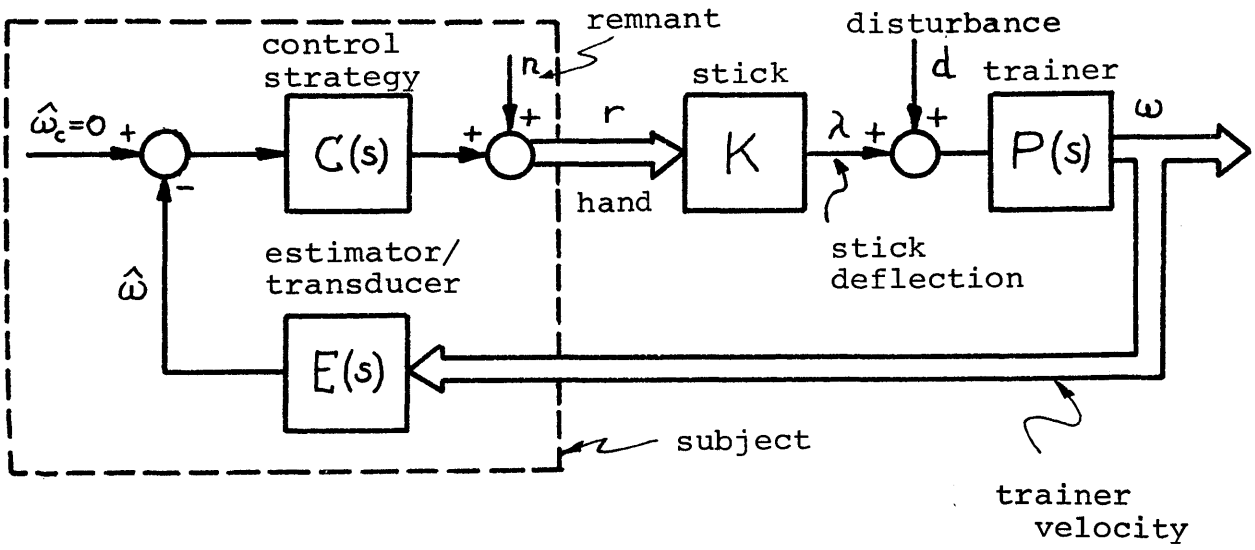

For the present objective of predicting drift rates, the control strategy C(s) can be approximated as an integator with gain, or:

$$C(s) = K_c/s \qquad (2.13)$$

The justification for this assignment will be discussed at greater length in section 4.4.4, in which it is shown that the operator's behavior at low frequencies is reasonably well-modelled by this approximation. Further, the estimator block E(s) can be replaced by the cyclopean

vestibular model of Figure 2.9. Simple block diagram arithmetic then yields the following expression for the angular velocity, ω, resulting from the subject's remnant, n, his vestibular bias, ω_b, and the input loop disturbance, d:

$$\omega(s) = \frac{P}{1 + KPCE'}\{Kn - KC\omega_b + d\} \tag{2.14}$$

where E' is the linear portion of the vestibular estimator (taken from Figure 2.9):

$$E'(s) \equiv K_1 s/\{(\tau_1 s + 1)(\tau_2 s + 1)\} \tag{2.15}$$

Since we are interested in low-frequency behavior (specifically, steady drift), we note that:

$$\lim_{s\to 0} E'(s) = K_1 s \tag{2.16a}$$

Further, the trainer transfer function is unity at DC (recall (2.1) of section 2.2), so that

$$\lim_{s\to 0} P(s) = 1 \tag{2.16b}$$

As described in section 2.2.2, the loop disturbance d(t) consists of a sum of sinusoids, so that

$$\lim_{s\to 0} d(s) = 0 \tag{2.16c}$$

Finally, if we assume the remnant to have no power at zero frequency, then

$$\lim_{s\to 0} n(s) = 0 \tag{2.16d}$$

Substituting (2.13) and (2.16) into (2.14), we find the low frequency portion of the angular velocity signal to be given by:

$$\lim_{s\to 0} \omega(s) = \lim_{s\to 0} \left\{ \frac{-KK_c}{1 + KK_cK_1} \right\} \frac{\omega_b}{s^2} \qquad (2.17)$$

where we have used the fact that the bias ω_b is a constant over time, so that

$$\omega_b(s) = \omega_b/s \qquad (2.16e)$$

In the time domain, then, (2.17) implies that, due to the velocity estimate bias ω_b, the subject will continue to accelerate at a constant rate, his angular velocity being given by:

$$\omega(t) = -\left\{ \frac{KK_c}{1 + KK_cK_1} \right\} \omega_b t \qquad \text{(FIX drift)} \qquad (2.18)$$

assuming zero initial conditions. The minus sign, of course, implies that a positive (rightward) bias will give rise to a negative (leftward) drift.

Thus, the simple cyclopean vestibular model, modified with the addition of a bias on the output, appears to be an adequate descriptor of subject performance when one is deprived of visual motion cues in the velocity nulling task.

2.4.1.3 Estimate of Bias Velocity

Presumably, the estimator bias ω_b for an individual could be inferred from (2.18) by measuring the drift acceleration and by estimating the individual transfer function gains K, K_c and K_1. The same could be done for the entire population, but it is simpler to recognize from (2.4)

of section 2.3.2 that the average drift rate $\bar{\omega}$ over the population is zero. Thus, from (2.18), the average velocity bias over the population must also be zero:

$$\bar{\omega}_b = 0 \tag{2.19}$$

Estimation of the variance of ω_b from drift rate measurement is, of course, complicated by the variance of the gains in (2.18), but a rough estimate can be made by treating them as simple constants across the population. That is, if we treat κ as a constant, where

$$\kappa \equiv KK_c/(1 + KK_cK_1) \tag{2.20}$$

then, from (2.18), we can relate the observed acceleration α to the velocity bias ω_b according to:

$$\alpha = -\kappa\omega_b \tag{2.21}$$

so that, from (2.19) and (2.21)

$$\sigma_b = \sigma_\alpha/\kappa \tag{2.22}$$

where σ_α and σ_b are the variances in observed acceleration and inferred bias, respectively. It is now only necessary to estimate κ from (2.20).

To obtain a value for K_1, the estimator gain, we assume that the vestibular transfer function has unity gain between break frequencies associated with the time constants τ_1 and τ_2 (Young, 1969). From the definition of E'(s) given in (2.15), this implies that

$$K_1 = \tau_1 \tag{2.23}$$

if we arbitrarily assign τ_1 to be the "slow" vestibular time constant. Its value is generally taken to be between 10 and 15 seconds (Melvill Jones,

1964); here, however, we will use the value of 13.8 seconds inferred from the analysis of the next section.

The open loop gain product, KK_c, can be computed from a dynamic analysis of human operator performance in a closely-related compensatory visual tracking task. As this is the subject of section 4.4.4, we may simply anticipate the result, and need only note here that a six-subject average value for KK_c is 1.8 s^{-1}.

From (2.20), then, the gain factor κ is found to be 0.069 s^{-1}. Furthermore, from (2.4) of section 2.3.2, we have the variance of the drift rate σ_α already calculated as $0.050^o/s^2$. Thus, from (2.22), the variance in the velocity bias is given by:

$$\sigma_b = 0.72^o/s \qquad (2.24)$$

2.4.1.4 Perceived Velocity During Drift

One final qualitative aspect of the above bias model is worth noting, and concerns the subject's perceived velocity while engaged in the velocity nulling task. If we presume that the subject is succeeding at the task objective, that is, maintaining himself apparently fixed with respect to the lab reference frame, then, on the average, his perceived velocity, $\hat{\omega}$, should be zero.

To see if the bias model is consistent with this interpretation of the results, we can substitute the transform of (2.18), which specifies the expected drift as a function of the bias, into (2.11), which defines the cyclopean model of perceived velocity. The resulting low-frequency sensation is given by:

$$\hat{\omega}_{LF}(s) = \lim_{s\to 0} \frac{\omega_b}{s} \left\{ 1 + \frac{K_1 s}{(\tau_1 s + 1)(\tau_2 s + 1)} \left\{ \frac{-KK_c}{1 + KK_c K_1} \right\} \right. \frac{1}{s} \left. \right\}$$

where the subscript LF emphasizes that we are interested in the low frequency portion of perceived velocity. The above expression simplifies to yield the following relation between bias velocity and perceived velocity:

$$\hat{\omega}_{LF} = \frac{1}{1 + KK_c K_1} \omega_b \tag{2.25}$$

Thus, the subject's estimated velocity, as predicted by the bias model, is simply the bias velocity attenuated by the closed loop gain. Since the bias average for the test population is zero, then the estimated drift velocity, averaged over the population, must also be zero:

$$\bar{\hat{\omega}}_{LF} = 0 \tag{2.26}$$

The above conclusion is based on a population average; it is of interest to see that the same conclusion effectively holds true for each individual. From the discussion of the preceeding subsection, the closed-loop gain is given approximately as 25.8, and from (2.24), a one-sigma value for the bias velocity is $0.72^o/s$. A subject with a three-sigma bias will then have, from (2.25), perceived velocity of less than $0.09^o/s$, a value well below normal thresholds. Thus, due to the subject's loop gain in the velocity-nulling task, the bias model predicts an average zero sensation of velocity, even in the face of a three-sigma bias. This, of course, is consistent with the subject feeling that he is successfully performing the nulling task, even while drifting.

2.4.2 Constant Velocity Visual Field Model

To this point, we have been concerned with the drift incurred with a fixed visual field (FIX); a similar argument can be made to help understand the cause of drift under constant velocity visual field presentation (CV).

2.4.2.1 Visual Field Velocity and CV Drift Rates

Shown in Figure 2.11 is perhaps the simplest possible parallel channel visual-vestibular model, in which it is presumed that the visual surround velocity contributes only to the low frequency portion of the angular velocity estimate, in a linear manner. Some justification for this model has already been given in the introduction; more will be given in Chapter 4 describing an experiment whose goal is to determine the dynamic characteristics of such a parallel channel model. For now, it suffices to note that the velocity estimate from this model is given by:

$$\hat{\omega}(s) = \omega_b(s) + K_2 L(s)\omega_2(s) + \frac{K_1 s}{(\tau_1 s + 1)(\tau_2 s + 1)}\omega_1(s) \qquad (2.27)$$

where ω_1 and ω_2 refer to vestibular and visual field velocities respectively. Note that by defining

$$\omega_b' \equiv \omega_b + K_2 L \omega_2 \qquad (2.28)$$

the equation is identical to (2.11), the biased estimator for the purely vestibular situation. Thus, the same low-frequency derivation is applicable and (2.18) can be used to describe the CV-induced drift rates seen

Figure 2.11: Parallel Channel Visual-Vestibular Velocity Estimator

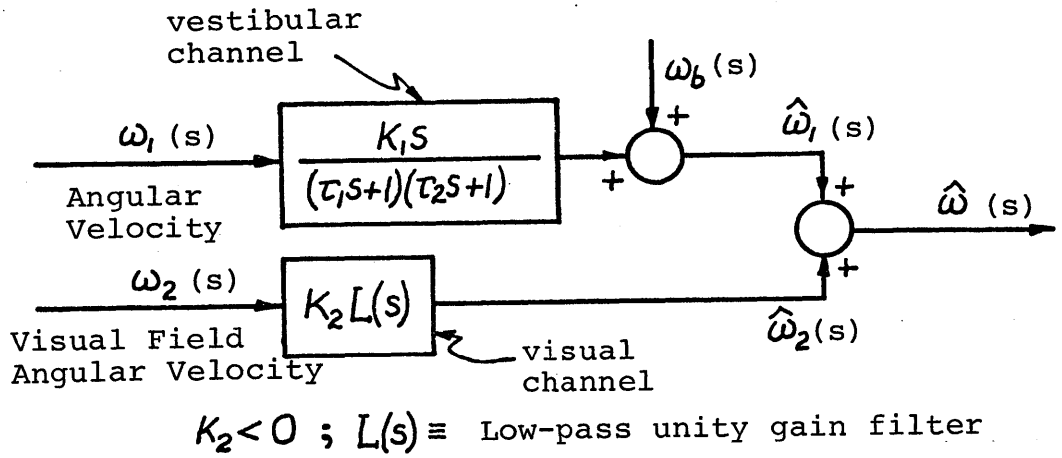

experimentally, with ω_b in the equation replaced by ω_b' above, so that:

$$\omega(t) = -\frac{KK_c}{1 + KK_cK_1}(\omega_b + K_2\omega_2)t \qquad \text{(CV drift)} \qquad (2.29)$$

The parallel channel model and the above equation thus show how visual field velocity, ω_2, acts effectively as a sensory bias in the vestibular channel, resulting in the observed drift rates.

2.4.2.2 Visual Velocity Bias Compared to Vestibular Output Bias

In section 2.3.3, it was noted that all CV-induced drifts were observed to be in the same direction as the stimulus visual field velocity. What this suggests is that the moving visual field effect is large with respect to the (bilateral) vestibular bias term. This is seen fairly directly by recasting (2.18) and (2.29) in terms of drift acceleration levels ($\alpha \equiv \dot{\omega}$):

$$\alpha_{FIX} = -\kappa\omega_b \tag{2.30a}$$

$$\alpha_{CV} = -\kappa(\omega_b + K_2\omega_2) = \alpha_{FIX} - \kappa K_2\omega_2 \tag{2.30b}$$

where κ is a function of the loop gain and was previously defined by (2.20). From section 2.3, however, the average drift acceleration magnitudes were

$$\begin{aligned} \alpha_{FIX} &\simeq 0.04^{\circ}/\,s^2 \\ \alpha_{CV} &\simeq 0.29^{\circ}/\,s^2 \end{aligned} \tag{2.31}$$

so that inspection of (2.30b) would lead one to conclude that, over the population,

$$\omega_b << K_2\omega_2 \tag{2.32}$$

That is, the vestibular bias velocity is small with respect to the visually induced sensation. It should, of course, be recognized that this conclusion is applicable to the particular visual field speed used in this experiment ($4^{\circ}/\,s$) and lower field velocities may not allow similar conclusions to be made.

2.4.2.3 Vestibular Time Constant

Additional support for the parallel channel model just proposed comes from an investigation of the vestibular time constant value predicted by the model. Success at the velocity nulling task, even in the face of a constant velocity visual motion cue, implies that the subject has, on the average, a perception of zero angular velocity ($\hat{\omega} = 0$). From the model's prediction of angular velocity given by (2.27) and the approximation afforded by (2.32), this implies that

$$\hat{\omega}(s) \simeq K_2\left(\frac{c}{s}\right) + \frac{K_1 s}{(\tau_1 s + 1)(\tau_2 s + 1)}\,\frac{\alpha}{s^2} \simeq 0$$

where we have recognized the fact that the visual field velocity ω_2 is a constant, C, and the average trainer velocity ω_1 is observed to be a ramp of constant acceleration α. Thus,

$$K_2C + \frac{K_1\alpha}{(\tau_1 s + 1)(\tau_2 s + 1)} \simeq 0$$

Since we are interested in low-frequency behavior, we let $s \to 0$, so that

$$K_2C + K_1\alpha \simeq 0$$

However, we have argued earlier in section 2.4.1.3 that K_1 can be replaced by the "slow" vestibular time constant τ_1. Furthermore, reference to the model diagram of Figure 2.11 suggests that the visual channel gain K_2 should be chosen to be -1, for consistency with the results of pure circularvection studies (e.g., Brandt et al, 1973); i.e., the model should predict a steady-state sensation of motion equal and opposite to the visual field motion. With these substitutions for K_1 and K_2, the above relation results in the following simple relation:

$$\tau_1 \simeq C/\alpha \qquad (2.33)$$

where it is recalled that the approximation is due to the neglect of the vestibular bias term, motivated by (2.32). Thus, the model predicts a vestibular time constant from the visual field velocity C and the observed trainer acceleration α. Using $C = 4^{\circ}/s$ and $\alpha = 0.29^{\circ}/s^2$ (from (2.31)), (2.33) predicts the time constant to be 13.8 seconds, a value in excellent agreement with that obtained from past research (Melvill Jones, 1964). Thus, this linear implementation of the previously-mentioned concept of cue cancellation (during a CV presentation) provides a simple explanation of the observed behavior, one which is consistent with our knowledge of vestibular dynamics and our knowledge of steady-state CV illusions.

2.4.3 Confirming Visual Field Model (CON)

At this point, it is appropriate to comment briefly on how well this parallel channel model predicts the observed behavior in the case when the subject is provided with confirming visual information by a counter-rotating visual field. As noted earlier, no drift was observed in any of the CON presentations. To see what the model predicts, we again assume that the subject is successful at the task of nulling apparent velocity, so that, from (2.27), we have:

$$\hat{\omega}(s) = 0 = \omega_b(s) + \omega_1(s) + \frac{K_1 s}{(\tau_1 s + 1)(\tau_2 s + 1)}\omega_1(s)$$

where we have made use of the fact that $\omega_2 = -\omega_1$ during this type of presentation, and have replaced K_2 by -1 as in the previous section. With a constant bias ω_b, the above relation predicts that, at low frequency,

$$\omega_1^{LF}(s) = \lim_{s\to 0} (-\frac{\omega_b}{s})/\{1 + \frac{K_1 s}{(\tau_1 s + 1)(\tau_2 s + 1)}\} = \lim_{s\to 0} (-\frac{\omega_b}{s})$$

or

$$\omega_1^{LF}(t) = -\omega_b \qquad (2.34)$$

so that the parallel channel model predicts a trainer velocity bias equal to and opposite to the subject's vestibular bias, during a CON field presentation. No velocity drift (i.e., acceleration) is predicted.

This is consistent with what is observed experimentally, since the model's prediction of no drift agrees with the drift-free records seen in

all trainer velocity histories associated with counterrotating field presentations. Further verification of the model could be provided if the predicted constant bias were observable in the records; unfortunately, it is too small for the measurement and recording measures used. That is, the model predicts a fairly small one-sigma trainer velocity: from (2.24) and (2.34) we might expect to see trainer velocity offsets on the order of $0.5^{o}/s$. However, this is on the order of uncalibrated DC offsets introduced by the analog computer, FM tape deck, and strip chart recorder, offsets which were normally zeroed out prior to replay of the recordings and subsequent processing. Thus, a more detailed verification of the model prediction of (2.34) is not supportable by this experiment; however, the observed drift-free performance is certainly in agreement with the model's prediction.

2.5 Summary

Subjects were given active control over their own rotational velocity while seated in a modified aircraft trainer, with a task objective of maintaining themselves stationary in space. A disturbance input required each subject to continuously provide compensatory control, via either a self-centering control stick or a control wheel. Visual motion cues, presented in the subject's peripheral visual field, were of three types: (a) counterrotating with respect to the actual rotation of the subject, providing a good measure of true velocity; (b) fixed with respect to the subject, depriving the subject of visual motion cues; and (c) moving at a constant speed with respect to the subject, providing a circularvection illusion stimulus. Six subjects participated in the velocity-nulling task, resulting in a total of 42 visual field presentations for stick control and the same number for wheel control.

This chapter has concentrated on analyzing and modelling the subject's low-frequency response in this task, primarily by detailing the low-frequency characteristics of trainer motion. When the field was counter-rotating, all subjects maintained the trainer at a zero mean velocity (within the resolution of the measurements), with an RMS error of approximately $1.3^{o}/s$. Performing in the absence of visual motion cues, most subjects drove the trainer at a constant low acceleration: the population average was zero indicating bilateral balance across subjects, with a standard deviation of $0.050^{o}/s^{2}$. A significant difference was found between stick and wheel control, the former providing an extraneous centering cue apparently used by some subjects to infer zero mean trainer

velocity; the pooled data from both control methods was corrected for this equipment artifact. With the drift rate eliminated from the trainer velocity record, RMS tracking errors were shown to be the same as those incurred under counterrotating field conditions. When presented with a visual field which moved at a constant velocity with respect to him, each subject drove the trainer at a constant acceleration in the direction of field motion, with an average acceleration of $0.3^{o}/s^{2}$. Under these conditions, the average RMS tracking error of approximately $1.8^{o}/s$ was shown to be significantly higher than that associated with either of the other two types of visual field presentation, even with the removal of the low frequency velocity drift component.

As noted in the introduction, the objective of this low-frequency analysis is to demonstrate how visual cues dominate subjective motion sensation at low frequencies, and how simple functional models may be used to explain the visual-vestibular interactions demonstrated in this closed-loop velocity nulling task. Section 2.4 presented two simplified models consistent with the observed behavior: the "cyclopean" vestibular model incorporating an output bias and sketched in Figure 2.9, and the parallel channel visual-vestibular model sketched in Figure 2.11. The former was used to explain behavior seen under fixed field conditions, while the latter was used in conjunction with the results obtained from constant velocity and counterrotating field presentations. The two are not mutually exclusive, however, and can be readily combined into one comprehensive dual-input model, as illustrated in Figure 2.12.

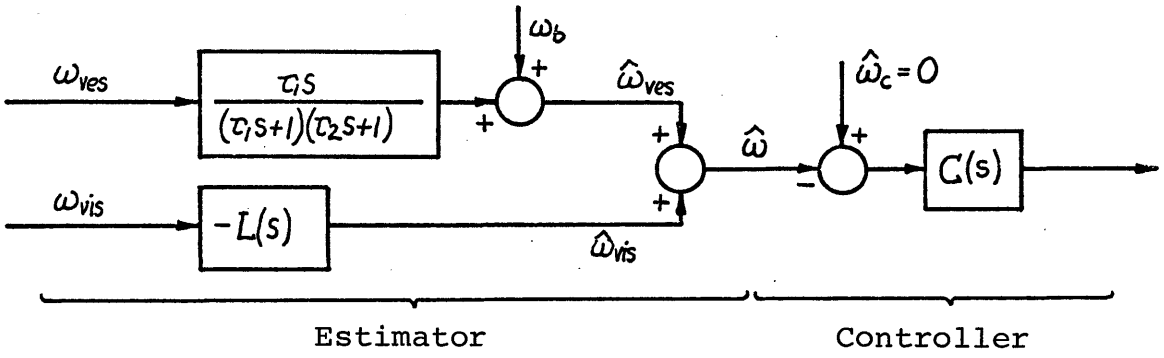

$L(s) \equiv$ low-pass unity gain filter

Figure 2.12: Low-frequency Visual-vestibular Model

As described earlier, the model provides a velocity estimate by summing the separate visual and vestibular estimates, each, in turn, dependent on the actual visual and vestibular stimuli and the transducer/processing dynamics along each pathway. The visual path dynamics are modelled with a simple unity gain low-pass filter, L(s), while the vestibular path is characterized by a biased-output high-pass filter: a washout with a high-frequency roll-off. Although the dynamics of the visual path have not been considered here, it should be clear that this model is entirely within the framework of the complementary filtering hypothesis, specifying that low-frequency visual information is combined with high-frequency vestibular information, to effect a wide bandwidth motion sensation estimator. What is not clear, of course, is whether or not the two pathways

are truly complements of one another, throughout the frequency range of interest, or whether they only provide complementary information in the most qualitative sense. Answering this question requires a closer look at the dynamics of each channel.

CHAPTER III

SINGLE CHANNEL DYNAMIC MODEL

The analysis and modelling of the previous chapter concentrated on the low frequency aspects of motion perception dependence on visual and vestibular cues. The complementary problem, that of dynamic modelling of high-frequency sensation, is the subject of the present chapter. In particular, we wish to propose a human operator describing function (DF) which adequately models the subject's dynamic behavior observed during the course of the assigned velocity-nulling task just described.

As discussed in the introduction, the basic motivation for this approach stems from the complementary filter notion of low-frequency visual motion cue dominance of sensation combined with high-frequency vestibular cue dominance. This chapter will attempt to model the latter, by subtracting out the low-frequency data trends (investigated in the previous chapter), and then performing a fairly conventional transfer function calculation with the resulting high-passed stimulus/response histories. The result, of course, will be a linear transfer function relating vestibular input to subject response output; as such, this transfer function can be viewed as a "vestibular" model, since the complementary filter notion assigns most of the dynamic perceptual response to the vestibular channel.

Because the velocity-nulling task described earlier provided the subject with three types of visual motion cues (FIX, CON, CV), a describing function analysis should uncover any functional dependence

on visual cue type. That is, if a single transfer function can be found which adequately fits the observed data for all three visual presentations, then the function's parameter dependence on cue type can be directly investigated.

These ideas are summarized in Figure 3.1, which is a modified version of the "vestibular" dynamic model sketched earlier in Figure 1.9b. The primary purpose of the linear transfer function $E(s,\underline{p})$ is to relate vestibular input to perceived velocity; the parameter vector $\underline{p}$ is presumed to be dependent on what type of visual cue is being presented. As before (recall Figure 2.10), the subject model is structured as a linear feedback model, consisting of a linear control strategy C(s) operating on perceived error; the resulting linear response is summed with a remnant component n to model total operator response as measured at the control wheel, λ.

Two points should be noted regarding this model. First, by eliminating low-frequency data trends in the generation of a linear describing function, the model will naturally fail to describe low-frequency sensations induced by visual cues. Thus, it is worth restating the fact that this model is a complement to the drift model of the previous chapter, and a complete description of operator behavior necessitates a merging of the two. The second point concerns the presence of the operator control strategy C(s). It should be clear that any input-output testing will result in a describing function in which C(s) is imbedded with and inseparable from the estimator E(s): control and estimation functions cannot be separated without additional information

on subject response. Thus, the allocation of parameter vector changes to only E(s, $\underline{p}$) in Figure 3.1 presumes control strategy constancy in the face of changes in visual input and/or changes in perceived velocity. This will be a subject of further discussion in section 3.4.

This chapter is organized into four sections: Section 3.1 describes the basic frequency domain identification method, and section 3.2 presents the resulting describing function data for the three visual field conditions tested. Section 3.3 then proposes a simple functional model to fit the data, and discusses the model dependence on field type. Finally, section 3.4 summarizes the results and motivates the need for a closer look at visual channel dynamics and human operator characteristics.

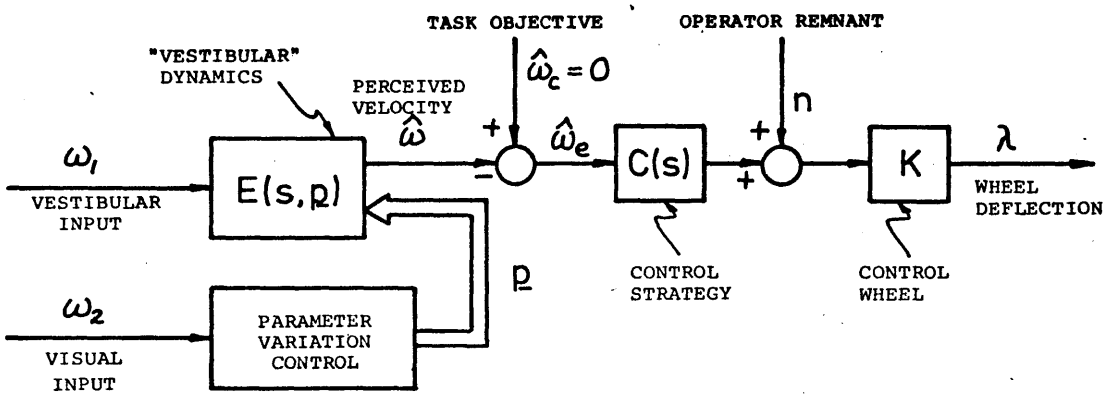

Figure 3.1: Single Channel Dynamic Model

3.1 Analytic Approach

The approach to constructing the model of Figure 3.1 is fairly straightforward: simply derive three human operator describing functions from the data, one function for each visual field presentation (CON, FIX, CV). This, in turn, is accomplished in the classic manner of input-output linear systems identification using frequency domain information.

3.1.1 Identification Method

The overall loop model of the velocity-nulling task has already been given in Figure 2.10; here we assume it to apply separately to each of the three types of visual motion cue presentations. Our objective here is to show how the operator transfer function can be solved for in terms of the two loop inputs, the disturbance d and the remnant n, and the two measurable loop outputs, trainer velocity ω_1, and stick deflection, λ. From block diagram algebra, the two outputs are related to the two inputs in the following manner:

$$\begin{aligned} \lambda(s) &= \frac{1}{\Delta}\left[\, n(s) - PCEd(s) \,\right] \qquad (a) \\ \omega_1(s) &= \frac{P}{\Delta}\left[\, n(s) + d(s) \,\right] \qquad (b) \end{aligned} \tag{3.1}$$

where

$$\Delta \equiv 1 + PCE \tag{3.2}$$

and where we have tacitly assumed wheel gain to be unity, thus effectively

measuring operator output in terms of commanded velocity (deg/s) rather than wheel deflection (deg).

Using auto- and cross-power spectral density functions, we can correlate d with λ and ω_1, so that, from (3.1), we have:

$$\begin{aligned} \Phi_{d\lambda} &= (-PCE/\Delta)\Phi_{dd} \qquad \text{(a)} \\ \Phi_{d\omega_1} &= (P/\Delta)\Phi_{dd} \qquad \text{(b)} \end{aligned} \tag{3.3}$$

where we have taken advantage of the fact that the remnant is defined to be uncorrelated with the loop disturbance:

$$\Phi_{nd} = \Phi_{dn} = 0 \tag{3.4}$$

Thus, division of (3.3a) by (3.3b) yields an expression for CE:

$$CE = - \Phi_{d\lambda}/\Phi_{d\omega_1} \tag{3.5}$$

which is the conventional input-output relation defining the operator describing function.

Rather than work with cross-power spectral densities, it was found computationally more convenient to use the more traditional input-output calculations based on Fourier transforms of the signals themselves. Appendix B presents a derivation showing that if the operator's remnant is small with respect to the disturbance signal injected into the loop, then his describing function can be defined by the following:

$$CE(f_i) = -\lambda(f_i)/\omega_1(f_i) \qquad (3.6)$$

where we are working with Fourier transforms evaluated at $f = f_i$, where f_i is one particular frequency contained in the disturbance input. As described in Appendix A, the disturbance signal used is composed of a sum of 15 sinusoids, so that the above relation holds at 15 different frequencies, spanning the spectrum of interest. Thus, for each visual field presentation, Fourier transforms may be taken of control stick deflection and trainer velocity, and the formal complex arithmetic of (3.6) performed, to define the operator describing function, CE(s), in the frequency domain.

3.1.2 Implementation of Identification Method

The operational details of implementing this calculation are worth commenting on briefly. To obtain the Fourier transforms of the stick and trainer signals, a digital program written for the PDP-8 was used (Van Houtte, 1970), which sampled both signals at 8 Hz for 128 seconds, calculated the Fourier coefficients with a standard FFT algorithm (IEEE, 1967; Brigham and Morrow, 1967), and then calculated each signal's amplitude and phase from the coefficients. The sample length was chosen to match the 128-second period of the disturbance input (see Appendix A), and the sample rate was chosen as a compromise between constraints imposed by program buffer size and the desire to have a high sample rate with respect to the highest frequency of interest (approximately 1 Hz).

As discussed at length in the previous chapter, FIX and CV visual field presentations were accompanied by considerable drift in the re-

sponse histories, which, in the frequency domain, translates to a large concentration of power at zero frequency. Since the FFT algorithm uses fixed point arithmetic and scales all coefficients with respect to the largest present, a considerable loss in precision would have resulted had transforms been taken directly on the raw data. For this reason, the recorded stick and trainer signals were passed through identical first order washout filters to eliminate any drift present during FIX and CV presentations. The filters were implemented on the analog computer and were of the following form:

$$F(s) = \tau s/(\tau s + 1) \tag{3.7}$$

where the time contant τ was chosen to yield a break frequency in the range of 0.02 Hz to 0.04 Hz, the particular value chosen being dependent on the drift rate present in each individual record. It may be recalled that this is the same signal processing approach used to obtain the RMS figures of section 2.3.4.

Program output was a teletype listing of all frequency components detected in each signal, specifying amplitude and phase. Manual calculation of gain and phase according to (3.6) was then performed at each frequency contained in the disturbance signal. The data was then used in generating Bode plots for individual subject describing functions, and/or further data processing via the UCLA BMD statistical software package (Dixon, 1973).

Figure 3.2 summarizes the data processing flow used in determining the operator describing functions.

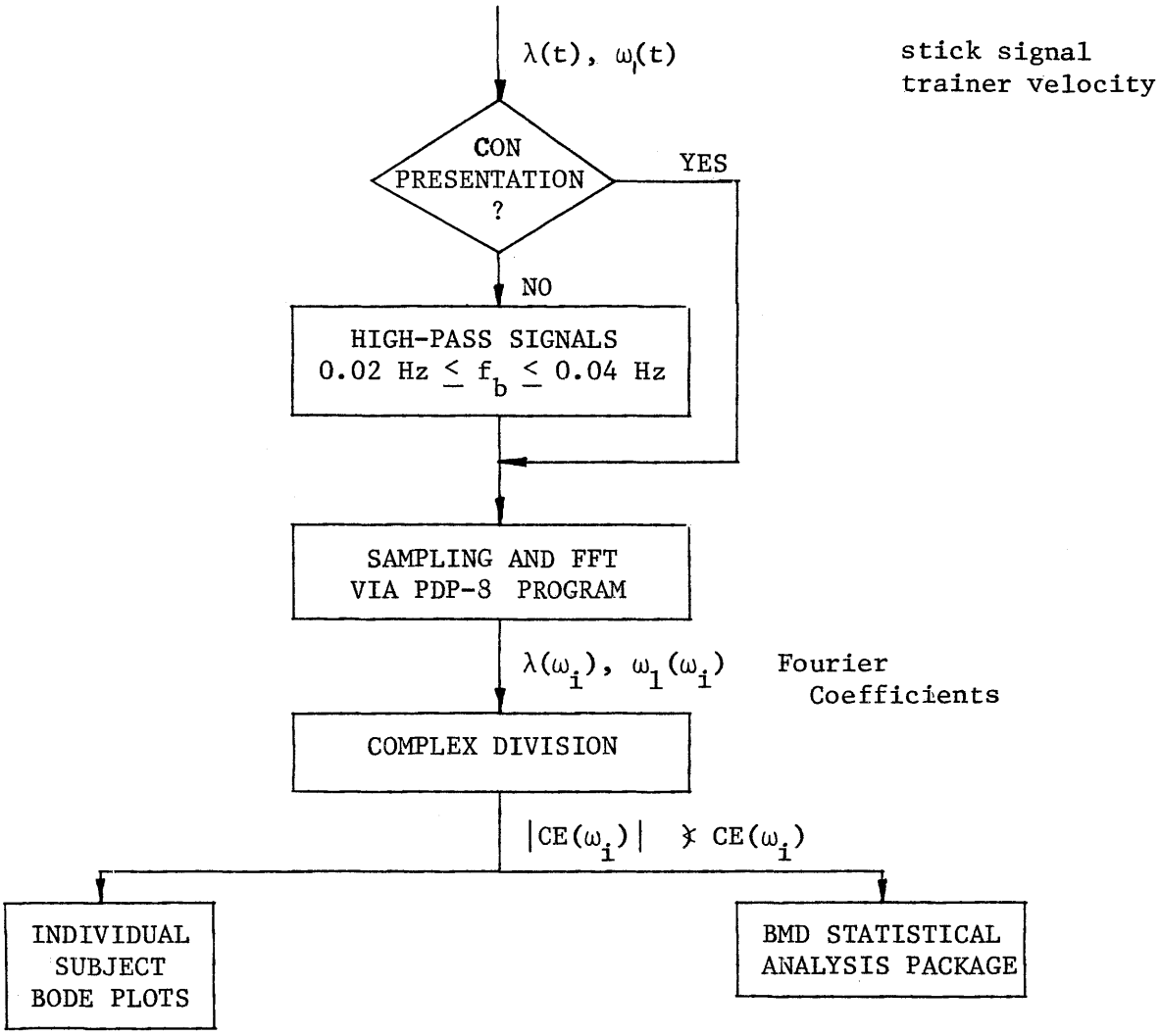

FIGURE 3.2: Data flow for describing function generation

3.2 Describing Function Results

This section presents the calculated operator describing function data in the conventional Bode plot format: amplitude ratio (AR) in decibels (dB) and phase in degrees, both plotted against frequency.

3.2.1 Describing Function Amplitude Ratios

Shown in Figure 3.3 is the amplitude ratio data associated with counterrotating visual field conditions (CON), obtained by pooling individual subject data across the six-subject test population. Data means are indicated by the solid dots, and one sigma deviations by the error bars. The simplest polynomial transfer function which fits the data reasonably well is a lag-lead, and is plotted as the solid curve in the figure. The particular parameter values displayed in the figure were obtained from a non-linear regression program which provides a least-squares fit to the data (BMD07R; Dixon, 1973). It should be recognized that the choice of a lag-lead function was motivated primarily by curve-fit considerations, and no attempt will be made at this point to justify this particular choice on the grounds of known semicircular canal transduction characteristics and/or human operator control strategy.

Shown in Figure 3.4 is the pooled AR data associated with the fixed visual field presentations (FIX), presentations which required the subjects to rely solely on vestibular (and proprioceptive) cues. Comparison with the previous figure shows a larger spread in the data at the lower

Figure 3.3: Amplitude Ratio Data for CON Presentation

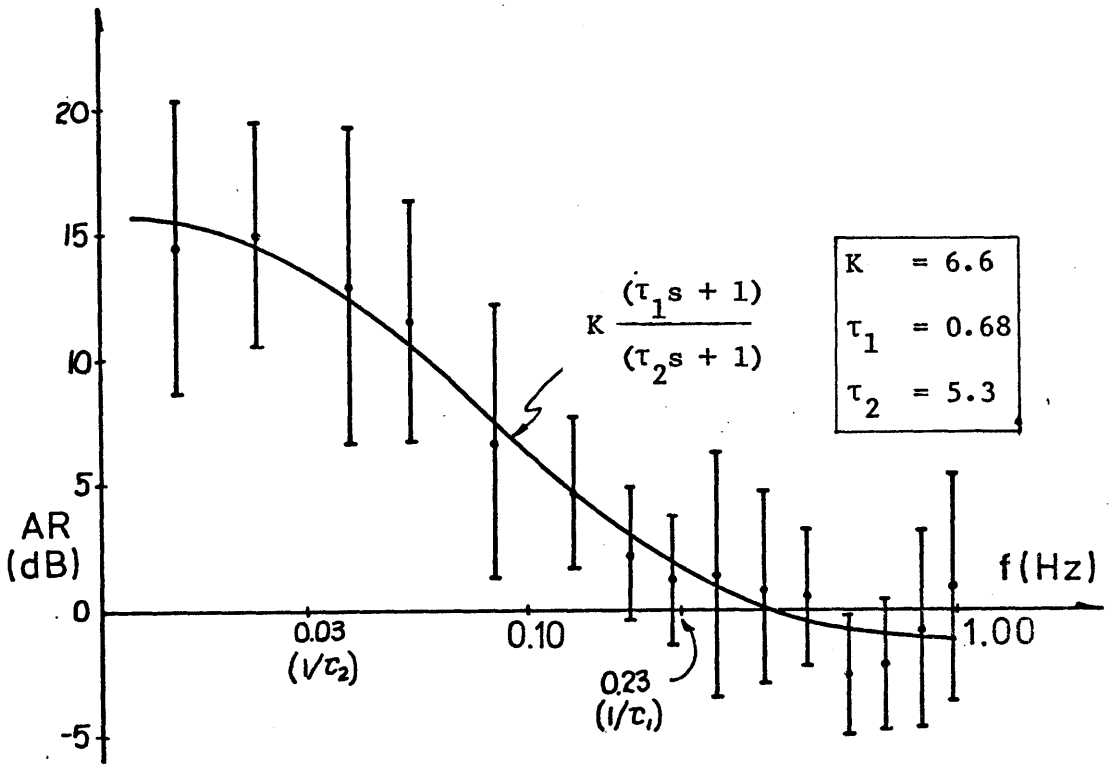

Figure 3.4 Amplitude Ratio Data for FIX Presentation

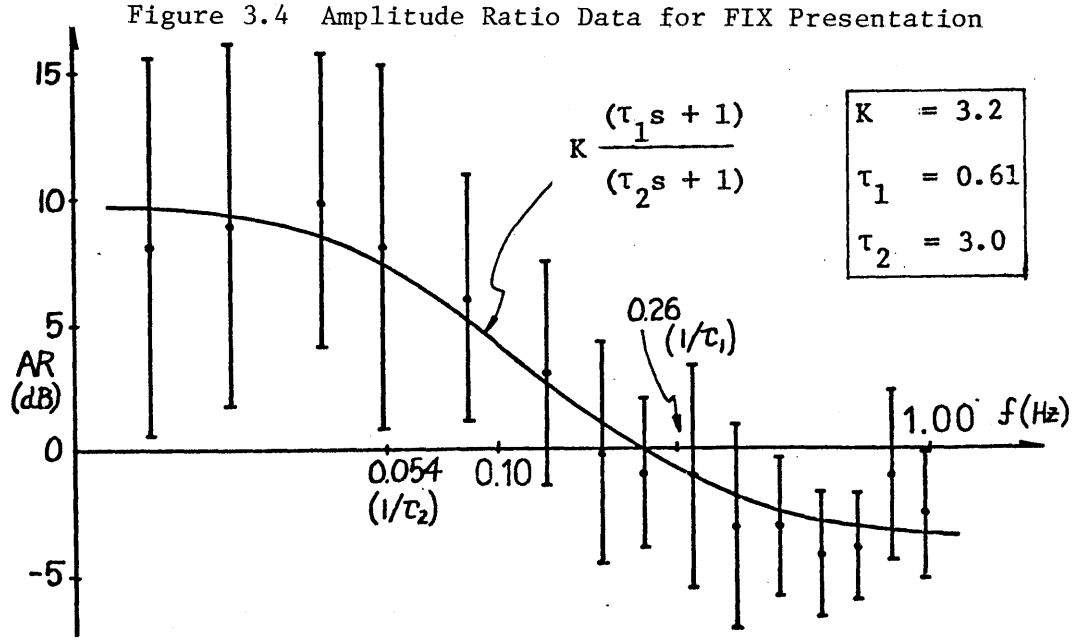

frequencies, reflecting perhaps the subject's greater uncertainty in the task when deprived of visual cues, especially at the low end of the spectrum.

Of greater significance, however, are the parameter value changes in the fitted lag-lead regression curve. Comparison with the values associated with a counterrotating field shows that the DC gain drops by a factor of two, the low frequency break ($1/\tau_2$) almost doubles, and the high frequency break ($1/\tau_1$) remains approximately unchanged. What this suggests is that the subjects, when deprived of valuable low frequency information provided by a counterrotating visual surround, are unwilling to use a high gain at low frequencies. This does not imply that gain is dropped throughout the frequency range, however, since the extension of the low frequency break ($1/\tau_2$) tends to compensate for any drop in DC gain, in the middle and high frequency ranges ($f \gtrsim 0.1$ Hz). The inference here, of course, is that the high frequency human operator dynamics are relatively unaffected by visual field motion, presumably because vestibular and proprioceptive cues are the primary sources of motion information in this frequency regime.

A test of this thesis is provided by the use of a constant velocity visual field (CV), which, as was seen in the previous chapter, induces a circularvection sensation and inappropriate low frequency stick compensation, resulting in a velocity drift of the trainer. Shown in Figure 3.5 is the pooled AR data associated with the CV field presentations, and it may be noted that the fitted curve is not markedly different from that associated with the FIX field case just described. The DC gains

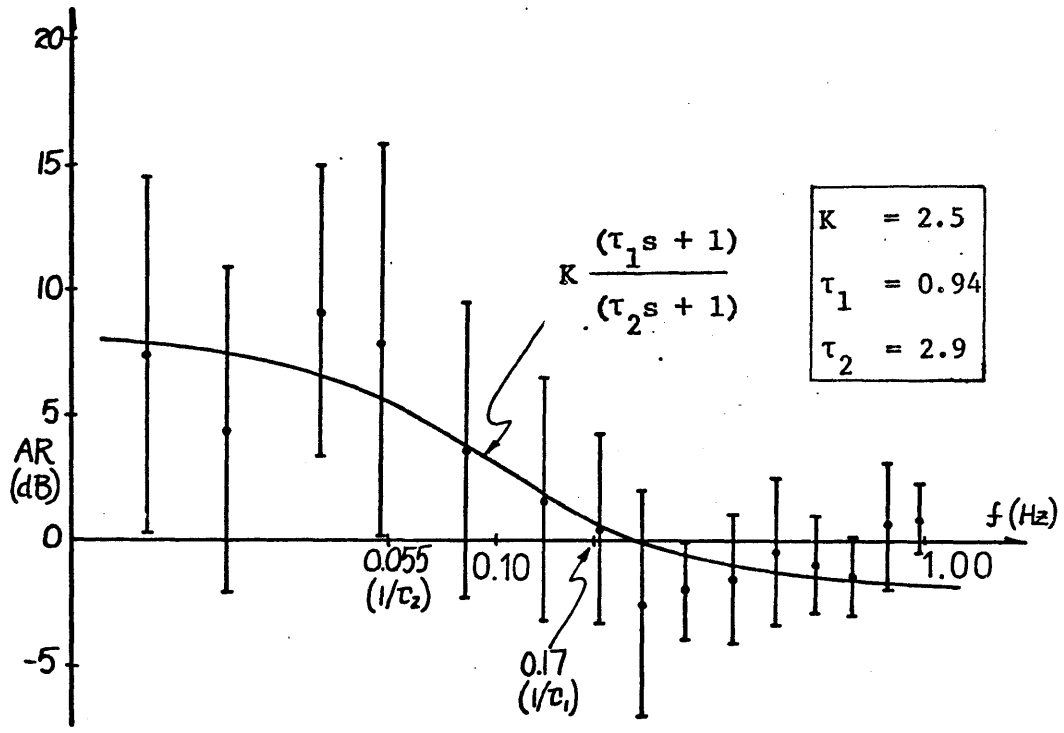

Figure 3.5: Amplitude Ratio Data for CV Presentation

are comparable, as are the low frequency breaks, and the data exhibits a similar increasing spread at the low frequencies, when compared with the counterrotating field data of Figure 3.3.

Additional characteristics of these three AR data sets will be discussed in section 3.3, with a closer look at the statistical significance of their differences, and their implications for functional modelling.

3.2.2 Describing Function Phases

Shown in Figure 3.6 is the phase data associated with counter-rotating visual field conditions (CON), again obtained by pooling across the six-subject test population. The dashed line represents the phase expected from the lag-lead function fit to the corresponding amplitude ratio data (recall Figure 3.3). It should be clear from the figure that the expected phase curve provides a poor fit to the data points. However, by assuming the presence of a transport lag or dead-time of τ_d seconds, the phase curve can be shifted down to the solid curve shown, and thus better approximate the observed lag. Such an addition to the lag-lead function does not, of course, affect the previously computed AR curve, and thus a lag-lead with dead-time provides a reasonable fit to both the gain and phase data, although it is clear that the latter is less well modelled than the former.

The particular choice of 0.40 seconds for τ_d was obtained from a linear regression on the residual phase angles, that is, the difference between the phase observed and the phase calculated from the lag-lead transfer function alone. Since this residual must be made up by the dead-time term, $e^{-\tau_d s}$, and since the dead-time's phase contribution is linear in frequency, i.e.:

$$\angle e^{-\tau_d s} = 2\pi f \tau_d = (2\pi\tau_d) f \qquad (3.8)$$

then it is a direct matter to linearly regress residual phase against frequency to obtain a value for τ_d. The statistical fit program used in this instance (BMD07R, Dixon, 1973) forced the regression through the origin, and furthermore provided an estimate of the dead-time variance.

It may be of interest to note that these calculations were performed with the three lag-lead parameters obtained from the fit to the pooled AR data. To check the effect of possible intersubject variation on the value of τ_d, a more lengthy approach was investigated, which consisted of calculating a lag-lead-gain parameter triplet fit to each subject's AR data, and using the resulting individual's transfer function as the basis for residual calculation, with subsequent regression to find τ_d. This approach was found not to yield significantly differ-

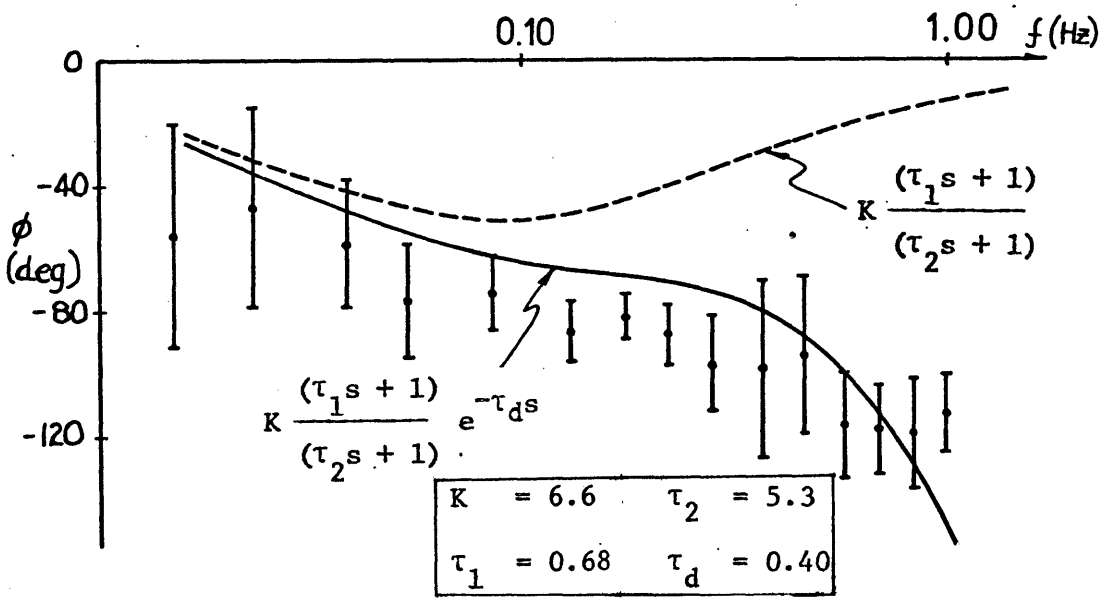

Figure 3.6: Phase Data for CON Presentation

ent values for τ_d, and thus was abandoned in favor of the simpler computational approach based on an overall population AR fit.

Shown in Figures 3.7 and 3.8 is the phase data associated with fixed and constant velocity visual field presentations (FIX and CV), along with the curve fits which minimize the residual error. Comparison with the phase data associated with the CON presentation (Figure 3.6) brings out two points which are immediately apparent. First, although all three presentations are characterized by comparable phase behavior

Figure 3.7: Phase Data for FIX Presentation

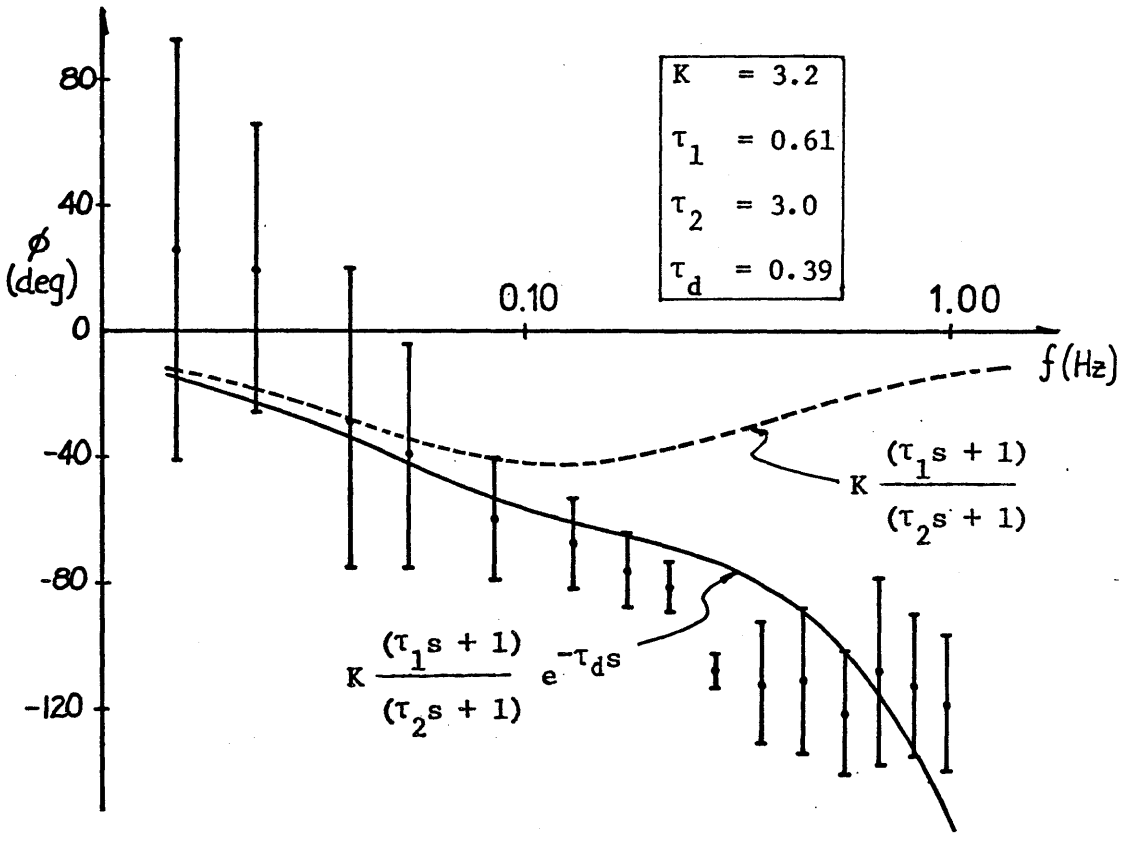

Figure 3.8: Phase Data for CV Presentation

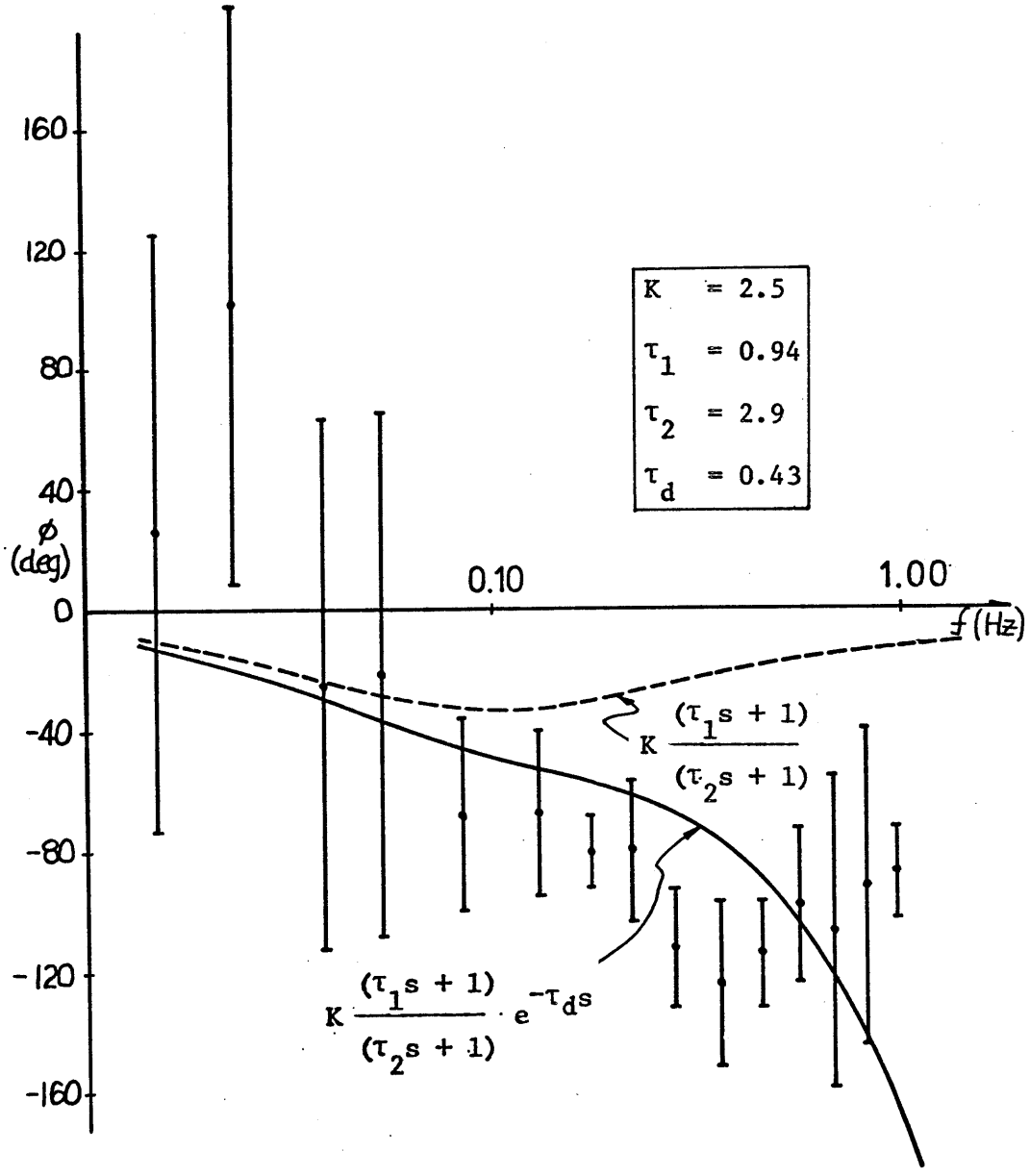

at mid- and high-frequencies, both the FIX and CV presentations result in considerably more phase lead at the low end of the spectrum. Recognizing that the vestibular channel provides more lead than is necessary for a low-frequency tracking task, the FIX and CV low-frequency leads may be indicative of a greater reliance on vestibular cues alone, behavior entirely consistent with operation in a visually-deprived environment. The second point to note is the greater variance at low frequencies, in the FIX and CV data, a characteristic paralleling that seen in the AR data, and supportive of the notion of subject uncertainty when deprived of important low-frequency visual cues.

3.3 Describing Function Model

The previous section has concentrated on some of the qualitative aspects of the frequency characteristics of the derived operator transfer function data. This section will look more closely at some of the characteristics of the fitted lag-lead model, and briefly discuss how the observed parameter changes with visual field presentation can be modelled.

3.3.1 Choice of Transfer Function Type

Before discussing the lag-lead model characteristics, it is appropriate to provide some justification for this particular choice of transfer function. Because the experimental approach does not allow us to separate control from estimation, justification of the model form cannot be made on the grounds of appealing to accepted dynamic models of rotatory vestibular sensation, since the operator control strategy C(s) is not known. It is possible, however, to motivate the use of a particular functional linear transfer function by considering how well it fits the data.

Several higher order transfer functions were fit to the amplitude ratio data in an effort to see if a signficant reduction in the fit error could be achieved. Reference to Figures 3.3, 3.4 and 3.5 shows both a gain attenuation at low frequencies and a gain increase at high frequencies for all three visual field conditions, suggesting that the basic lag-lead function fit could be improved by the addition of a low-frequency washout term and a high-frequency lead term. The resulting

model is:

$$CE(s) = K\underbrace{\left(\frac{\tau_1 s + 1}{\tau_2 s + 1}\right)}_{\text{lag-lead}}\underbrace{\left(\frac{\tau_3 s}{\tau_3 s + 1}\right)}_{\text{washout}}\underbrace{(\tau_4 s + 1)}_{\text{lead}} \tag{3.9}$$

where the dead-time term need not be considered for these AR fits.

As before, a non-linear regression program was used to generate least-squares parameter estimates. In this case, however, the presence of double poles and zeros resulted in numerical problems in the search algorithm, since the fitting function given above constrained the solution to real poles and zeros. To circumvent this problem, the transfer function was respecified in a more general format, allowing for complex pole allocation:

$$CE(s) = Ks\left(\frac{s^2 + 2\zeta_1\omega_1 s + \omega_1^2}{s^2 + 2\zeta_2\omega_2 s + \omega_2^2}\right)\left(\frac{\omega_2^2}{\omega_1^2}\right) \tag{3.10}$$

The results are shown in Figures 3.9, 3.10 and 3.11, each with its associated set of parameter values defining the transfer function. The most obvious point to be recognized is that the additional transfer function terms allow the curves to follow the mean data trends at both ends of the spectrum. In fact, if the only data to be fitted were the means at each frequency, we might expect a considerable reduction in the fit error for each visual field presentation, in comparison to the simple lag-lead curve fits.

However, the fit improvement is far from dramatic whan all the data point residuals are considered. Shown in Table 3.1 is the RMS residual associated with each field presentation, for the lag-lead AR fit. The

Figure 3.9: Extended Order Function Fit - (CON)

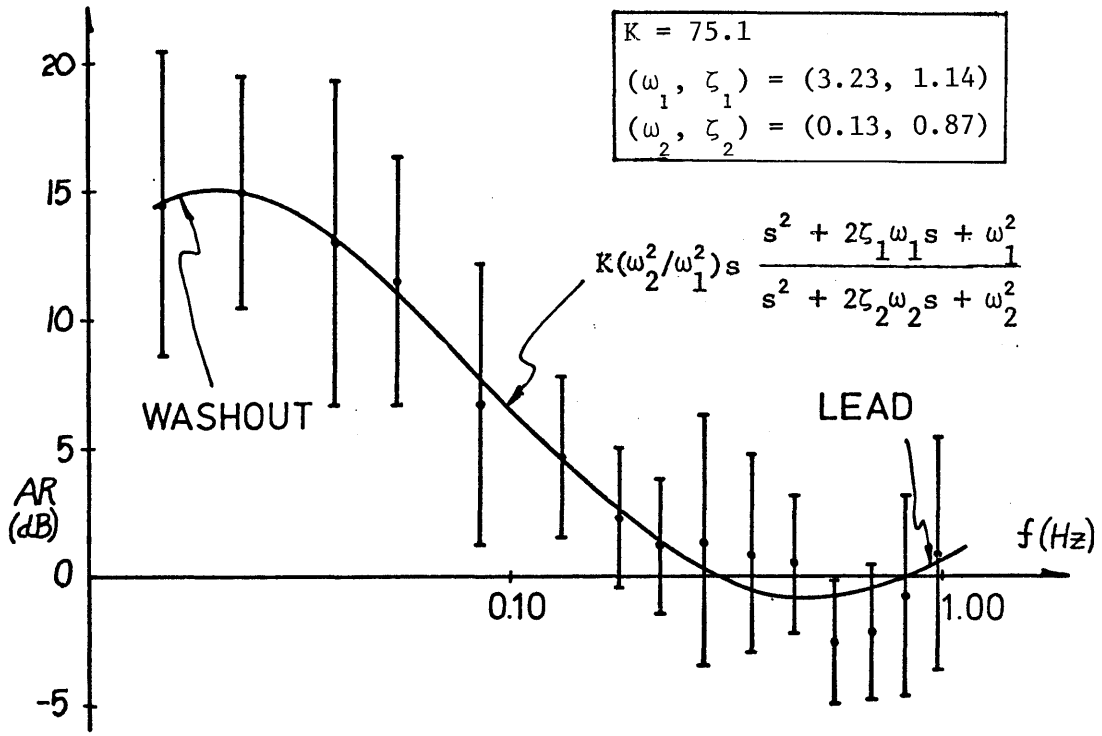

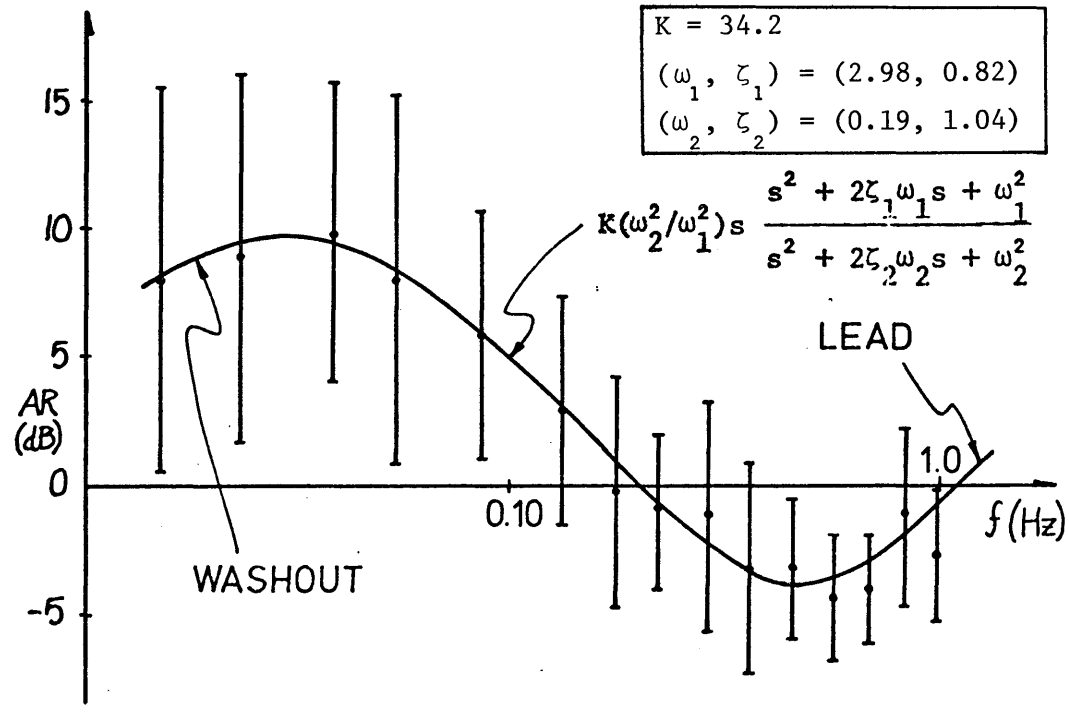

Figure 3.10: Extended Order Function Fit - (FIX)

Figure 3.11: Extended Order Function Fit - (CV)

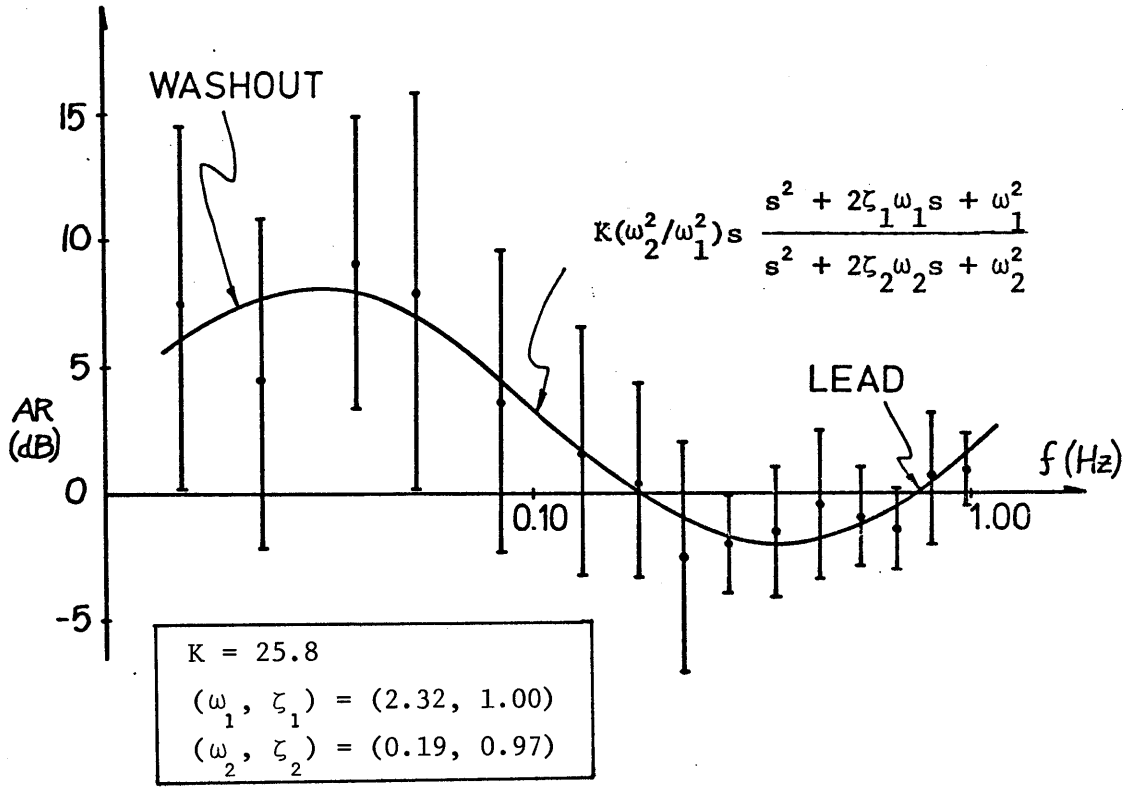

more than 20% increase seen in the progression from CON to FIX to CV presentations is consistent with our earlier observation regarding less data spread with a counterrotating confirming field. More to the point, however, is the small reduction in residual error associated with higher order transfer function curve fit. The maximum improvement of less than three percent is, of course, attributable to the spread in the overall population data, and thus, little in the way of predictive accuracy is to be gained by resorting to a model of higher order than a simple lag-lead, and the remainder of this section will be concerned with the characteristics of this simpler model.

VISUAL FIELD	RMS RESIDUAL (LAG-LEAD)	% REDUCTION IN RESIDUAL (LAG-LEAD + WASHOUT + LEAD)
CON	4.22	0.99
FIX	4.95	2.60
CV	5.09	1.74

Table 3.1 RMS Residual Fit Errors

3.3.2 Parameter Dependence on Visual Field Environment

Changes in parameter values as a function of visual field treatment have already been discussed to some extent in section 3.2. An overview of the fit results is provided by Figure 3.12, which illustrates parameter estimate values and their variances, for each field treatment.

3.3.2.1 DC Gain

From the figure, it is evident that the gains for the FIX and CV presentations are comparable. This is verified by an F-test on the variances which shows them to be not significantly different ($F_{5,5} = 1.34$, $P > 0.2$) and a t-test which shows the parameter estimates to be not significantly different ($t = 0.26$, $\nu = 10$, $P > 0.2$). The pooled statistics for the FIX and CV presentations are given by:

$$K = 2.85 \qquad \sigma_K = 0.34 \qquad N = 12 \tag{3.11}$$

Comparing these pooled statistics with the gain estimates from the CON presentations, an F-test shows the variances to be significantly different ($F_{5,11} = 7.84$, $P < 0.005$), and a Welch t-test (Afifi and Azen, 1972) leads to a similar conclusion regarding the parameter estimates ($t = 9.36$, $\nu = 5$, $P < 0.005$), confirming our original comments concerning the gain differences between CON and either FIX or CV presentations. That is, when subjects are deprived of valuable low frequency visual information, they are unwilling to use high gain at low frequencies.

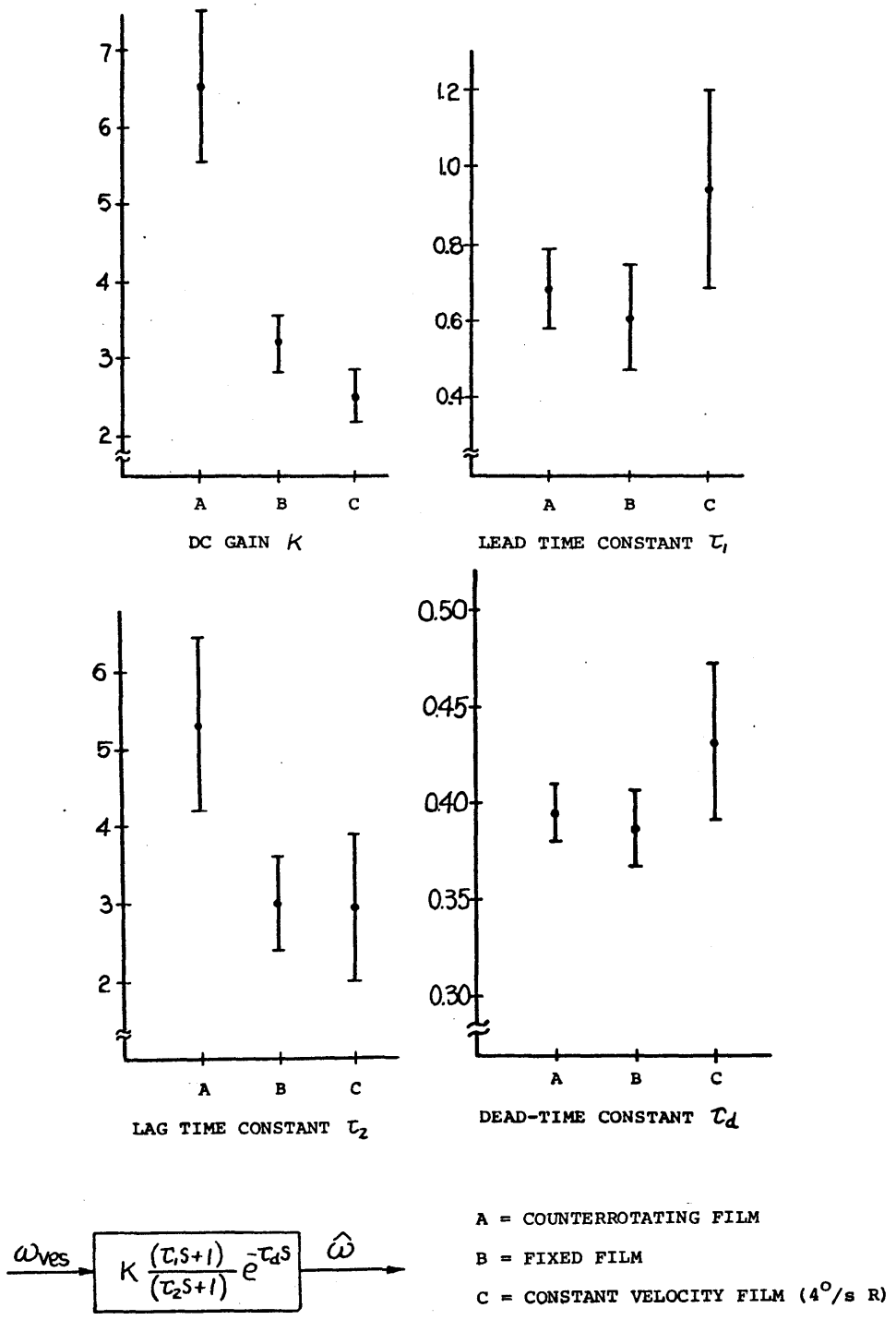

Figure 3.12: Parameter Dependence on Visual Field Type

3.3.2.2 Lead-time Constant τ_1

The situation is not as clear-cut with comparisons of the lead-time constant τ_1, as should be apparent from Figure 3.12. A comparison between the CON and FIX presentations shows their associated time constants to be comparable: an F-test on the variances shows no significant difference ($F_{5,5} = 1,50$, $P > 0.1$) as does a t-test on the parameter estimates ($t = 1.04$, $\nu = 10$, $P > 0.1$). The pooled statistics for the CON and FIX presentations are given by:

$$\tau_1 = 0.65\,s \qquad \sigma_{\tau_1} = 0.12\,s \qquad N = 12 \tag{3.12}$$

Comparing these pooled results with the results from the CV presentations, an F-test shows the variances to be significantly different ($F_{5,11} = 5.15$, $P < 0.01$) and a Welch t-test leads to a similar conclusion regarding the estimates themselves ($t = 2.59$, $\nu = 6$) although the confidence level is an order-of-magnitude lower than was seen in the previous gain comparison ($P < 0.05$). If we were to accept the null hypothesis at this confidence level (that is, fail to see a significant difference between the two parameter estimates), then the pooled statistics for all three visual field presentations would be given by:

$$\tau_1 = 0.74s \qquad \sigma_{\tau_1} = 0.18s \qquad N = 18 \tag{3.13}$$

Thus, we are suggesting that, for all three field presentations, the high frequency break is approximately constant, in spite of the marginally significant difference seen with the CV presentations.

3.3.2.3 Lag-time Constant τ_2

As is evident from Figure 3.12, the dependence of the lag-time constant τ_2 on field presentation completely parallels the previously-described gain behavior. Comparing the estimates associated with FIX and CV presentations shows no significant differences: an F-test on the variances ($F_{5,5} = 1.83$, $P > 0.1$) and a t-test on the parameter estimates ($t = 0.11$, $\nu = 10$, $P > 0.1$) suggest that the data be pooled, to result in the following statistics for the FIX and CV lag-times:

$$\tau_2 = 2.94s \qquad \sigma_{\tau_2} = 0.77s \qquad N = 12 \qquad (3.14)$$

Comparing these pooled results with the results from the CON presentations, an F-test shows the variances not to be significantly different ($F_{5,11} = 2.10$, $P > 0.1$); however, a t-test shows a highly significant difference between the parameter estimates ($t = 5.24$, $\nu = 16$, $P < 0.005$), confirming our original comments concerning the lag-time differences between CON and either FIX or CV presentations. Specifically, the large lag time associated with CON presentations drops significantly with either FIX or CV presentations, thus paralleling the DC gain drop seen earlier.

3.3.2.4 Dead time Constant τ_d

Reference to Figure 3.12 shows a parallel between the dead-time constant τ_d and the lead-time constant τ_1, in terms of visual field dependence. Comparing the CON and FIX dead-time constants shows them

to be statistically equivalent: an F-test on the variances shows no significant difference ($F_{5,5} = 2.04$, $P > 0.1$) and neither does a t-test on the parameter estimates ($t = 0.82$, $\nu = 10$, $P > 0.1$). The pooled statistics for the CON and FIX presentation are given by:

$$\tau_d = 0.39\,s \qquad \sigma_{\tau_d} = 0.017\,s \qquad N=12 \qquad (3.15)$$

Comparing these pooled statistics with the dead-time estimates from the CV presentations, an F-test shows a significant difference in the variances ($F_{5,11} = 5.82$, $P < 0.01$) and a Welch t-test leads to a similar conclusion regarding the estimates themselves ($t = 2.23$, $\nu = 6$), although again, as in the case of the lead-time comparison, the confidence level ($P < 0.05$) is considerably lower than seen in the previous gain and lag-time comparisons. If we were to ignore the difference and pool the dead-time values for the three cases, the following statistics would result:

$$\tau_d = 0.41\,s \qquad \sigma_{\tau_d} = 0.028\,s \qquad N = 18 \qquad (3.16)$$

Thus, we are suggesting that, for all three field presentations, the dead-time constant is approximately constant, in spite of the marginally significant difference seen with the CON presentations.

3.3.2.5 Simplified Parametric Model

The major findings of the previous section may be summarized in a schematic fashion as shown in Figure 3.13, which shows the three amplitude ratio asymptotes. The suggestion here is that the DC gain drops significantly when going from a CON presentation to either a FIX or CV presentation, and that the difference in gains associated with the latter two presentations is not statistically significant. The same can be said

regarding the decrease in lag-time τ_2, a change which provides compensation, at mid- and high-frequencies, for the DC gain drop. As was just noted, the observed difference in lead-time breaks may or may not be significant, but it would appear that the high-frequency gain $K\tau_1/\tau_2$ is comparable among the three conditions, again supporting the notion of estimator indifference to visual inputs when the vestibular signal consists of high-frequency components.

Thus, with a fixed or constant velocity visual field, the simplified parametric model predicts a vestibular DC gain drop, with a corresponding change in the lag-time, so as to maintain approximately the same mid- and high-frequency gain curve associated with a counterrotating visual field. The changes in lead-time and dead-time seen in the data may or may not be statistically significant, and a simplified model would incorporate them as constants independent of visual field presentation type.

Figure 3.13: Change in DF Gain due to Change in Visual Field Presentation

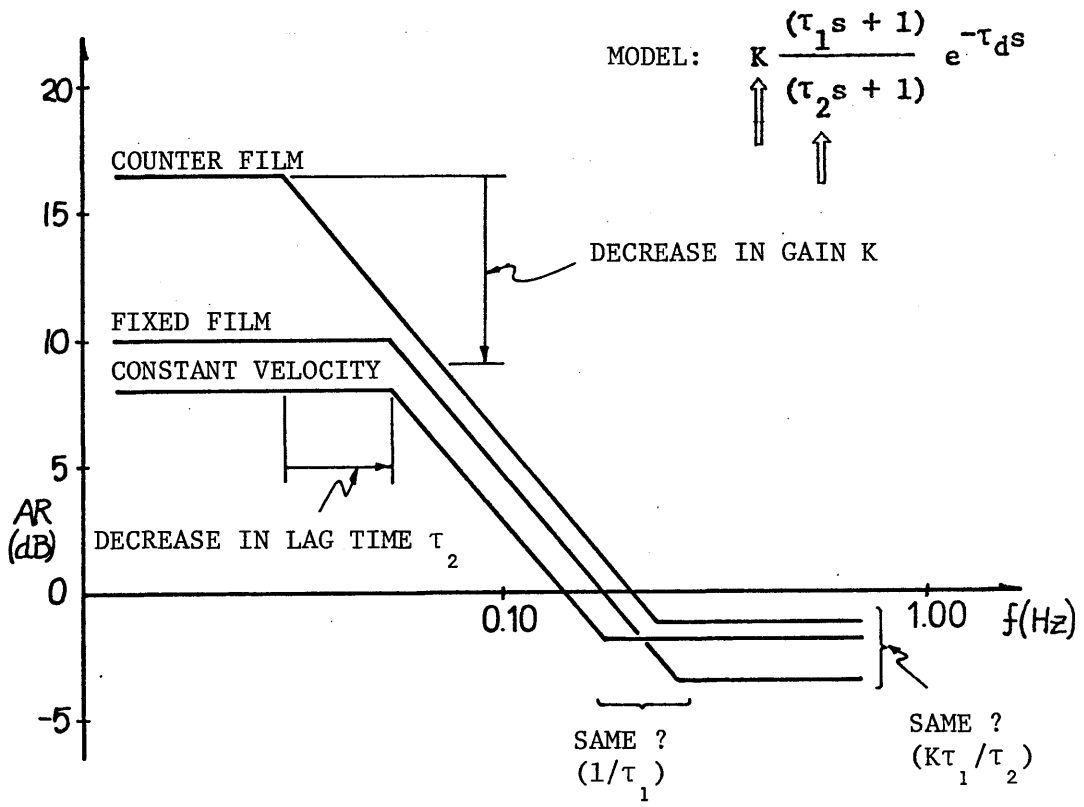

3.4 Summary

The single channel describing function model analyzed in this chapter was based on a simple lag-lead plus dead-time fit to the amplitude ratio and phase data obtained from the velocity-nulling experiments described in Chapter 2. The functional form was justified on the basis of little improvement seen in curve fitting error when going to a higher order function, and the particular parameter values chosen were seen to be dependent on the visual field environment in which the subject was operating. The parameters which changed most significantly were gain and lag-time, parameters associated with low-frequency response, confirming the results of the previous chapter regarding visual dominance of low-frequency sensation. Conversely, the high-frequency characteristics of the derived describing functions showed considerably less dependence on type of visual field presentation, suggesting that the subject relies almost completely on vestibular information at the high end of the test spectrum.

The model presented here is primarily a "vestibular" model, in that the describing function relates dynamic vestibular inputs to operator behavior and visual input is treated in a quasi-static manner. That is, the type of visual field is seen as determining the particular parameter vector associated with the lag-lead vestibular model, in accordance with the model of Figure 3.1, and is to be contrasted to the parallel channel model described in the previous chapter. This model approach of visual modulation of vestibular dynamics is consistent with some of the previously described results of analogous studies (Young, et al, 1973; Henn,

1974), but fails to provide any explanation for the dynamics of motion sensation elicited by purely visual means; any effort in this direction clearly requires a larger range of visual inputs to be provided to the subject. This problem of developing a dual-channel dynamic model will be considered at length in the next chapter.

It was noted at the beginning of this chapter that the experimental approach used provides no means by which separate control and estimation blocks can be derived from the overall operator describing function data. Thus, unless one can specify the control block as unity, there is no justification for assuming the lag-lead model to be an appropriate descriptor of the operator's sensory dynamics. In fact, a lag-lead perceptual model would, under fixed visual field conditions, predict sensations contrary to those expected from the high-pass dynamics of the canals, and more pertinently, contrary to observed sensation attenuation at low frequencies. Furthermore, it is unlikely that the control block is without dynamics; from our knowledge of human operator dynamics, it is much more likely to approximate an integrator, and thus the inferred estimator model must correspondingly differ from the lag-lead model discussed above.

This is not to suggest that the changes seen in describing fucntion behavior cannot be entirely ascribed to changes in the estimator dynamics, and, in fact, the changes seen are completely consistent with the notion of complementary cue dominance in the frequency domain. However, it should be clear that a closer look at control strategy dynamics is called for; this is the objective of the human operator analysis presented as part of the experimental approach of the next chapter.

CHAPTER IV

DUAL-CHANNEL DYNAMIC MODEL

The analysis and modelling efforts of the previous two chapters concentrated on the effect of low-frequency visual cues on motion perception. The object of the present chapter is to demonstrate how the modelling effort can be extended to an investigation of dynamic response to a wider spectrum of visual motion cues. Specifically, we wish to propose a human operator dual-input describing function (DIDF) which adequately models a subject's sensation in response to combined cue stimulation, in a situation in which both visual and vestibular cues contain wide bandwidth information.

As noted in the introduction, some work has already been done in specifying the dynamic characteristics of subjective response to a step change in visual field velocity; however, very little attention has been given to characterizing response to time-varying visual stimuli. It is felt that any dual-input modelling effort must consider other visual cues besides simple constant velocity field motion; the experimental design to be presented here will allow for this option. Furthermore, because of the anticipated interaction dynamics between visual and vestibular cues, it would seem appropriate to provide an experimental situation in which both cues are presented simultaneously, and in which both are time-varying. Essentially, we are suggesting a direct extension of the previous experimental results, by utilizing a wider range of visual motion cues.

The dual-input experiment described in this chapter, and the subsequent functional analysis, are based on the linear dual-channel model sketched in figure 4.1, repeated from the introduction (a negative sign preceeds E_2 in anticipation of visual cue sign reversal). The model presumes that each pathway provides a motion sensation estimate, to be combined additively for an overall subjective velocity estimate. This type of model has already been introduced to explain visual dominance of low-frequency sensation (recall figure 2.11), although it must be recalled that no statement was possible there regarding the specific dynamics of the visual pathway, because of the restricted class of visual cues used. The objective here will be to specify these dynamics and, furthermore, to verify the high-pass characteristics of the vestibular pathway. The outcome of such a modelling effort will then allow us to evaluate the applicability of a linear dual-channel functional model to describing subjective response to simultaneous cue presentation. In particular, it will provide a direct test of the complementary filtering hypothesis.

Figure 4.1: Linear Parallel Channel Model

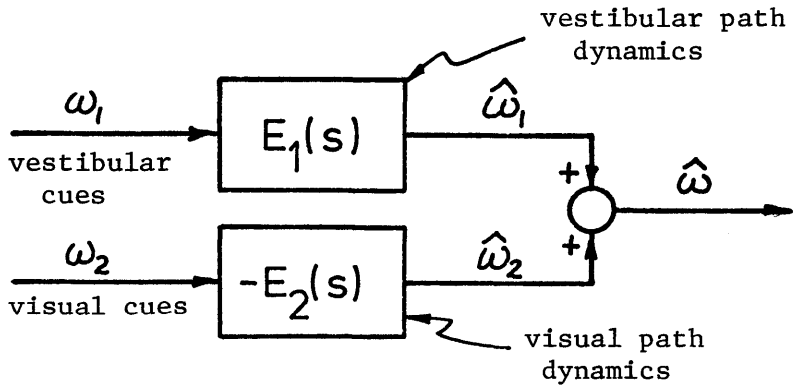

This chapter is organized into 6 sections. Section 4.1 describes the general experimental approach utilizing the time-varying inputs and based on the loop task of nulling perceived velocity, the measurement technique used in the previous experiment. Section 4.2 then presents a more detailed description of the actual experiment, while section 4.3 provides the analytic background showing how estimates of the model's two transfer functions can be extracted from the response data. The results, in both the the time and frequency domain, are presented in section 4.4; this section also demonstrates how the overall operator describing function can be corrected for by an independent measure of human operator dynamics. The resulting dual-channel estimator model is then discussed in section 4.5, with some attention given to its predictions in single cue presentation situations, and in situations in which visual and vestibular cues perfectly complement one another. Finally, section 4.6 summarizes the results and motivates the need for a closer look at non-linear interaction dynamics.

4.1 General Experimental Approach

The results presented in the last two chapters were based on measurements made on the velocity-nulling behavior of subjects presented with simultaneous visual and vestibular motion cues. The same approach will be used here, but less emphasis will be placed on the determination of vestibularly-induced sensation. In particular, the last experiment allowed the subject to control only his actual motion and restricted the visual motion cues to constant velocity or counterrotating visual fields. A more balanced experimental design is called for, however, to derive a dual-channel dynamic response model.

One fairly direct means of accomplishing this, within the framework of a perceived velocity-nulling task, is to provide the subject with control not only over his own motion, but also over peripheral visual field velocity. This allows him to null either visually-induced or vestibularly-induced sensations of motion, by providing the appropriate compensatory commands.

The same equipment used earlier is used in the current experimental effort: the trainer, which provides for actual motion of the subject, the projector system, which provides for peripheral visual field cues, and the control wheel, which gives the subject control over the two. In the first experiment, noise was injected into the trainer drive, requiring the subject to continuously provide compensatory wheel deflections for vestibularly induced sensations; in the present experiment, noise can also be injected into the projector drive, so that any visually

induced motion sensations must also be compensated for by the subject. By choosing the two disturbance signals to be uncorrelated, simultaneous nulling of both cues can be made to be an impossible task objective. Clearly, the subsequent analysis can then be based on whichever portion of either cue the subject chooses to null.

Figure 4.2 is a functional block diagram of the experiment, with the same type of schematic model of the human operator introduced earlier. Trainer velocity control is as in the previous experiment. Field velocity, however, is determined by both wheel deflection and the second disturbance input. It should be noted that the sign of the wheel signal is changed prior to being sent to the projector drive, to make the resulting visual field motion consistent with trainer motion (i.e. right wheel deflection results in right trainer motion and left field motion). To ensure that the visual field dynamics mimic trainer response, a prefilter F is added to the projector drive G (which has a relatively high bandwidth), so that, as shown on the figure, FG = P. Thus, without a visual field disturbance signal, the experiment is functionally equivalent to the counterrotating series conducted earlier.

It should be recognized that the same type of linear feedback model of the subject is presumed as in the previous chapters: a linear control strategy C(s) operating on perceived error, whose output is summed with a remnant component to yield total operator response. As before, we should expect the operator dynamics (C) to be imbedded in any input-output measurements we make, and this will be shown to be the case in the later analysis of section 4.3.1. Although it was not found necessary in

Figure 4.2: Closed-loop velocity-nulling task (dual disturbance input)

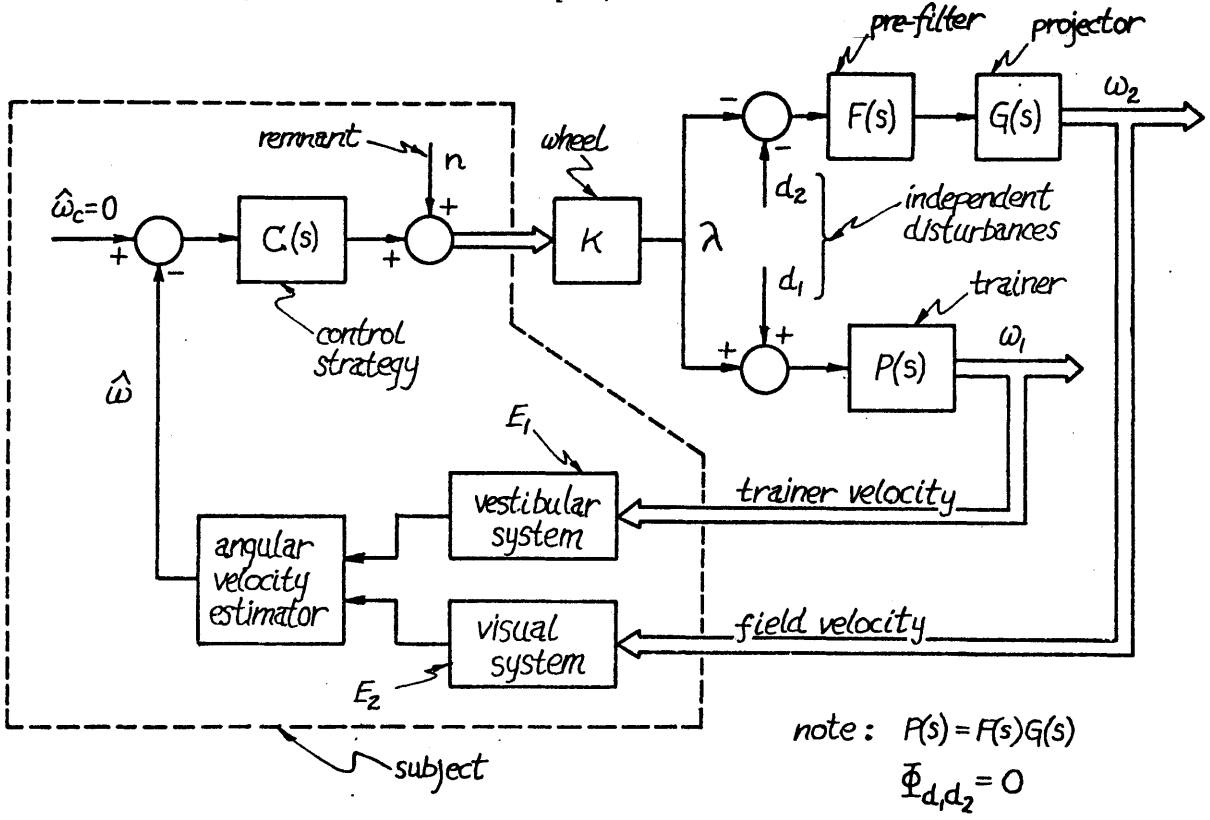

the analysis of the previous experimental data, it is clearly desirable here to provide some means of correcting the response for the operator dynamics, in order to arrive at a functional model of the subject's dual channel estimator dynamics. Section 4.4.3 briefly describes a subsidiary experiment directed at an independent measure of the operator dynamics, and subsequent analysis shows how this information can be used to infer the estimator dynamics. For the present, however, we need only be concerned with the functional modelling of overall input-output response.

4.2 Experimental Description

This section gives a brief description of the hardware implementing the loop of figure 4.2, the characteristics of the disturbance signals used, and the protocol used in the experimental runs.

4.2.1 Hardware Description

As noted above, the same basic equipment used earlier is used in the current experiment, the primary difference being in the loop network configuration which interconnects the trainer, projector, and control wheel. As before, the GPS 290T analog computer serves as the primary interconnection device, allowing for wheel command of both trainer and projector, and providing the interface for the digital computer generated disturbance signals (see below). Prefiltering of the projector drive signal is also accomplished on the analog computer, via a second-order filter which mimics the velocity servo characteristics of the trainer drive:

$$(\omega/\omega_c)_{proj} = \omega_n^2/(s^2 + 2\zeta_n\omega_n s + \omega_n^2) \qquad (4.1)$$

where, as in (2.1), the break frequency is 0.90 Hz and the damping ratio is 0.7. Details of the analog circuitry are given in Appendix A, as are the results of input-output testing of the prefiltered projector velocity servo loop. It suffices to note here that the dynamic response of the projected visual field is indistinguishable from that of the trainer.

The same peripheral field stripe pattern is used as before, with

the images projected on the trainer's side windows. The control wheel is used exclusively throughout this experiment, to avoid possible centering cues afforded by the spring-centered control stick. Finally, the same supplementary equipment is used (tape deck, etc), including headphones for communication and audio cue masking during a run.

4.2.2 Disturbance Signals

The disturbance signals injected into the trainer and projector drive loops are generated by the real-time operation of a PDP-8 digital computer, as before. Each signal is created by summing individual sinusoids, with subsequent timed digital-to-analog conversion and scaling provided by the analog computer. A listing of the digital program is given in Appendix A, which also details the analog circuitry.

Each disturbance signal is a pseudo-random zero mean signal with a period of 128 seconds, consisting of a sum of 12 sinusoids spanning the frequency range from 0.01 to 1.0 Hz. Each frequency component is an integral prime multiple of a base frequency of 1/128 Hz (0.00781 Hz), allowing the two signals to be formally defined as follows:

$$d_1(t) = \sum_{i=1}^{12} a_i \sin n_i \omega_0 t \qquad d_2(t) = \sum_{i=1}^{12} b_i \sin m_i \omega_0 t \qquad (4.2)$$

where $\omega_0 = 2\pi/T$ and $T = 128$ s, and where the n_i and m_i are alternating primes of an ascending series. This interleaving of the two line spectra assures a zero correlation between the two disturbances:

$$\Phi_{d_1 d_2}(\omega) = \Phi_{d_2 d_1}(\omega) = 0 \qquad (4.3)$$

and the choice of prime numbers also avoids the problem of possible harmonic ambiguities.

Each line spectrum follows that of a double lag-lead with a roll-off at 0.15 Hz, dropping 20 dB to level off at 0.48 Hz. This allows for a more gradual transition, from high power at low frequencies to low power at high frequencies, than the "shelf" disturbance spectrum chosen for the previous experiment. The overall power envelopes are roughly similar, however, since the lag-lead function midpoint approximates the shelf break. A more detailed look at the frequency characteristics of the disturbance signals used in this experiment is given in Appendix A.

4.2.3 Protocol and Experimental Design

The same six subjects who had taken part in the previous experimental series participated in the current dual-input nulling task. All were in normal health with normal peripheral vision, and having no known vestibular dysfunction. Each subject was instructed as to the nature of the velocity-nulling task and specifically told to keep the trainer as motionless as possible by concentrating on his own sense of motion and by providing the appropriate compensatory control wheel deflections. Each subject was also instructed that at times the task might become more difficult than in his previous experience, and if this happened, to simply concentrate more strongly on sense of self-motion, and compensate accordingly.

Prior to an actual run, each subject was given the opportunity to control trainer motion, with the door open, to observe how much control power was available to him, and to get an approximate idea of the trainer's response dyanmics. Then, with no wheel input, the disturbance signal was injected into the trainer drive so that the subject could obtain some estimate of the amplitude and frequency content of the signal he would be controlling against. Finally, with his head supported by a headrest and looking forward, he was given a practice session of two minutes with the door closed and with a counterrotating visual field motion providing confirming visual motion cues (CON mode of last experiment). During this time the subject wore the headphones, and background music volume was adjusted to ensure that any mechanical sounds form the trainer were inaudible, but remaining at a comfort level acceptable to the subject.

Each run lasted for approximately 8 minutes (4 periods of each disturbance signal), during which time the subject was required to provide continuous velocity-nulling compensation. Throughout the run, the vestibular disturbance (d_1) was continuously fed to the trainer drive. The visual environment, however, alternated between the previously discussed counterrotating field mode (CON) which provided accurate confirmation of vestibular cues, and the dual-input mode (DI) in which visual field velocity was determined by combining the subject's wheel signal with the visual disturbance signal (d_2), as illustrated in the loop diagram of figure 4.2. Two presentations of each field mode were given, the start of each synchronized with the start of a new period of the vestibular signal, and alternated with one another:

Series A: CON, DI, CON, DI

Series B: DI, CON, DI, CON

Three subjects received series A and three received series B, to provide balance for fatigue and learning.

At the end of a run, each subject was questioned as to whether he may have been consciously using other cues besides motion sensation to null trainer velocity. No one felt that any extraneous cues were available for inferring self-motion.

4.3 Analytic Approach

The approach to constructing a linear dual-channel model is fairly straightforward: simply derive two describing functions relating subject response to each of the two motion axes (visual and vestibular), and then use these describing functions to derive transfer function descriptions of each estimator channel. The derivation details are given in the next section, followed by a discussion to the implementation of the identification method.

4.3.1 Identification Method

The loop diagram of the velocity nulling task is repeated in figure 4.3, with the subject functionally represented by a linear dual-channel estimator, providing the velocity estimate for subsequent compensatory wheel deflections. The operator remnant, n, is presumed to be uncorrelated with both of the loop disturbances, d_1 and d_2.

Our objective is to show how the estimator transfer functions, E_1 and E_2, may be solved for in terms of the three loop inputs, d_1, d_2, and n, and the three measurable loop outputs, ω_1, ω_2, and λ. From block diagram algebra, the three outputs are related to the three inputs thusly:

$$\lambda(s) = \frac{1}{\Delta}\,[n(s) - PCE_1 d_1(s) - PCE_2 d_2(s)] \qquad (a)$$

$$\omega_1(s) = \frac{P}{\Delta}\,[n(s) + (1 + PCE_2)d_1(s) - PCE_2 d_2(s)] \qquad (b) \qquad (4.4)$$

$$\omega_2(s) = -\frac{P}{\Delta}\,[n(s) - PCE_1 d_1(s) + (1 + PCE_1)d_2(s)] \qquad (c)$$

where

$$\Delta \equiv 1 + PC(E_1 + E_2) \qquad (4.5)$$

and where, as before, we have tacitly assumed wheel gain to be unity, thus effectively measuring the operator output in terms of commanded velocity (deg/s) rather than wheel deflection (deg).

Figure 4.3: Linearized model of dual-input experiment

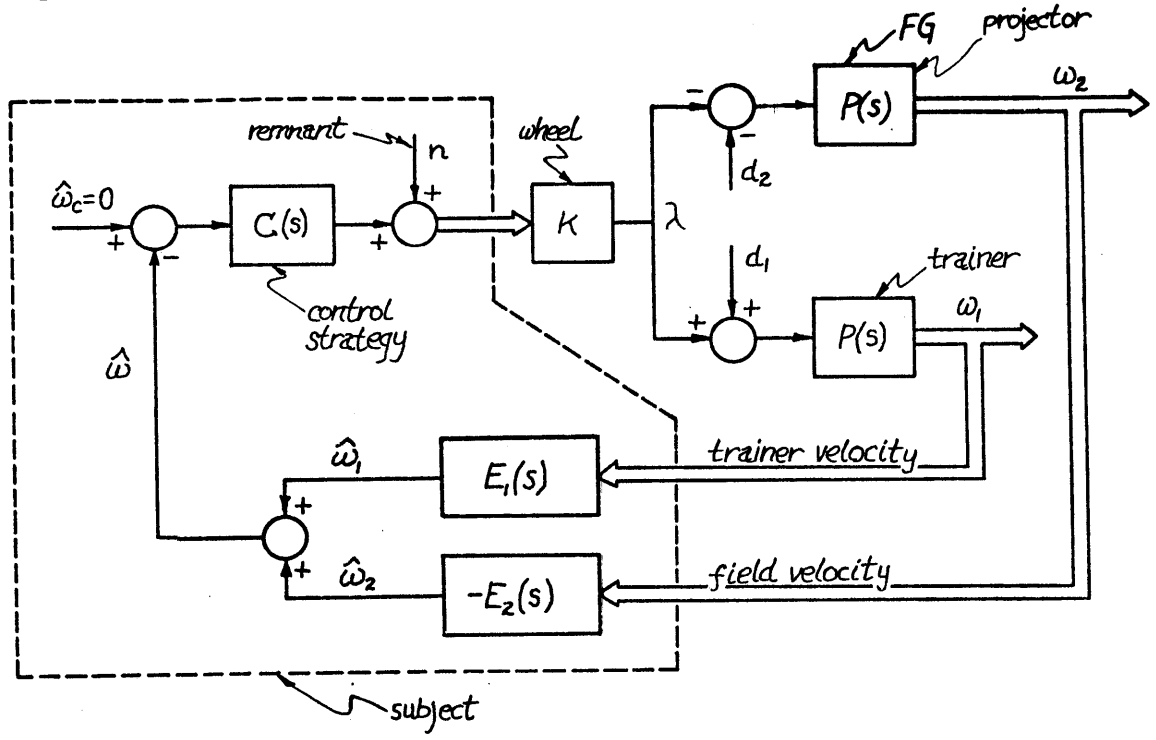

We can now make use of auto- and cross-power spectral density functions to solve for E_1 and E_2. Correlating d_1 with λ and ω_1, we have, from (4.4a) and (4.4b),

$$\Phi_{d_1\lambda} = \frac{1}{\Delta}[\Phi_{d_1 n} - PCE_1\Phi_{d_1 d_1} - PCE_2\Phi_{d_1 d_2}] \quad \text{(a)}$$

$$\Phi_{d_1\omega_1} = \frac{P}{\Delta}[\Phi_{d_1 n} + (1 + PCE_2)\Phi_{d_1 d_1} - PCE_2\Phi_{d_1 d_2}] \quad \text{(b)} \qquad (4.6)$$

Since the remnant is defined to be uncorrelated with the input disturbances, then

$$\Phi_{d_1 n} = \Phi_{d_2 n} = 0 \tag{4.7}$$

Further, we recall that the experimental design is such that d_1 and d_2 are uncorrelated, so that:

$$\Phi_{d_1 d_2} = \Phi_{d_2 d_1} = 0 \tag{4.3}$$

Thus, dividing (4.6a) by (4.6b) and using (4.7) and (4.3) to simplify the result, we find that

$$\Phi_{d_1 \lambda}/\Phi_{d_1 \omega_1} = -CE_1/(1 + PCE_2) \tag{4.8a}$$

In a similar fashion, it may be shown that

$$\Phi_{d_2 \lambda}/\Phi_{d_2 \omega_2} = CE_2/(1 + PCE_1) \tag{4.8b}$$

Since the left-hand-sides of (4.8) are computable from the measured outputs of the experiment, we define

$$\alpha_1 \equiv \Phi_{d_1 \lambda}/\Phi_{d_1 \omega_1} \qquad \alpha_2 \equiv \Phi_{d_2 \lambda}/\Phi_{d_2 \omega_2} \tag{4.9}$$

so that substituting into (4.8) allows for a solution for CE_1 and CE_2.

$$\begin{aligned} CE_1 &= \alpha_1(1 + P\alpha_2)/[1 + P^2\alpha_1\alpha_2] \qquad \text{(a)} \\ CE_2 &= \alpha_2(1 - P\alpha_1)/[1 + P^2\alpha_1\alpha_2] \qquad \text{(b)} \end{aligned} \tag{4.10}$$

As we expected, the control strategy C is imbedded with the estimators E_1 and E_2, and cannot be separated from them without additional input-output testing. What is obviously called for is an independent measure

of C, which can then be divided out from the expressions above. This is discussed in more detail in section 4.4.3; for now, however, we may continue to work with the control cascaded describing functions, CE_i.

As in the analysis of the single channel data of the previous chapter, it was found computationally more convenient to work directly with the Fourier transforms of the loop signals, rather than with their cross-power spectral densities. Appendix B presents a derivation showing that if the operator's remnant is small with respect to the loop disturbances, then the α_i of (4.9) can be computed according to the following method:

$$\alpha_i(f_{ij}) = \lambda(f_{ij})/\omega_i(f_{ij}) \qquad (i = 1,2) \qquad (4.11)$$

where f_{ij} represents the jth frequency contained in the disturbance d_i (recall (4.2)). In essence, we are computing two transfer functions, one relating stick deflection to trainer velocity, and the other to field velocity. The former is computed only at the trainer disturbance frequencies, while the latter only at the projector disturbance frequencies. Of course, this is made possible by the fact that the disturbances are composed of mutually exclusive frequency components.

It should be recognized that this implies that α_1 and α_2 will not be defined at the same frequencies, so that the computations for the CE_i indicated by (4.10) cannot be made. What is required is an assumption of continuity, in the frequency domain, of the transfer functions introduced by the linear model. This then allows for an interpolation across frequency to obtain the needed α_1 and α_2 values. That is, one can

interpolate between the α_1 values defined at the f_{1j} frequencies to obtain values for α_1 at the f_{2j} frequencies, and conversely for α_2. With α_1 and α_2 both defined in this manner at all the input frequencies introduced by both d_1 and d_2, (4.10) may then be used to define the describing functions CE_1 and CE_2, for all disturbance frequencies. This was the approach used in the data processing which followed the α_i calculations of (4.11).

To this point, the discussion has concentrated on dual-channel model calculations from dual-input (DI) experimental data. As noted in section 4.2.3, the DI presentations are alternated with counterrotating field presentations (CON). Clearly, the operator identification technique of the last chapter is applicable for these field presentations, so that (3.5) may be used to calculate the describing functions associated with CON presentations.

4.3.2 Implementation of the Identification Method

The operational details of implementing the describing function calculations are worth commenting on briefly. To obtain the Fourier transforms of the wheel, trainer, and projector signals, a digital program was written for a PDP-11 using standard routines supplied by Digital Equipment Corporation (1975). The program was used to sample the three signals at 8 Hz for 128 seconds, calculate the complex Fourier coefficients, convert to amplitude and phase format, and store the results on a diskpack for later use. As was the case for data sampling

in the previous experiment, the sample length was chosen to match the disturbance signals' periods, while the sample rate was chosen as a compromise between maximum sample buffer size and a desired high sample rate.

One of two FORTRAN programs was used to calculate the appropriate operator describing functions. For CON presentations, the signal amplitude and phase data was retrieved from the diskpack file, and used to calculate operator gain and phase at the disturbance frequencies, according to (3.5). For DI presentations, the calculation of the α_i was performed first, according to (4.11), and the two describing functions, CE_1 and CE_2 then calculated according to (4.10). Individual results were then stored on the diskpack for later use for obtaining average population trends, generating individual response plots, and/or for further processing via the UCLA BMD statistical software package (Dixon, 1973).

Figure 4.4 summarizes the data processing flow used in determining the operator describing functions. Program listings are given in Appendix C.

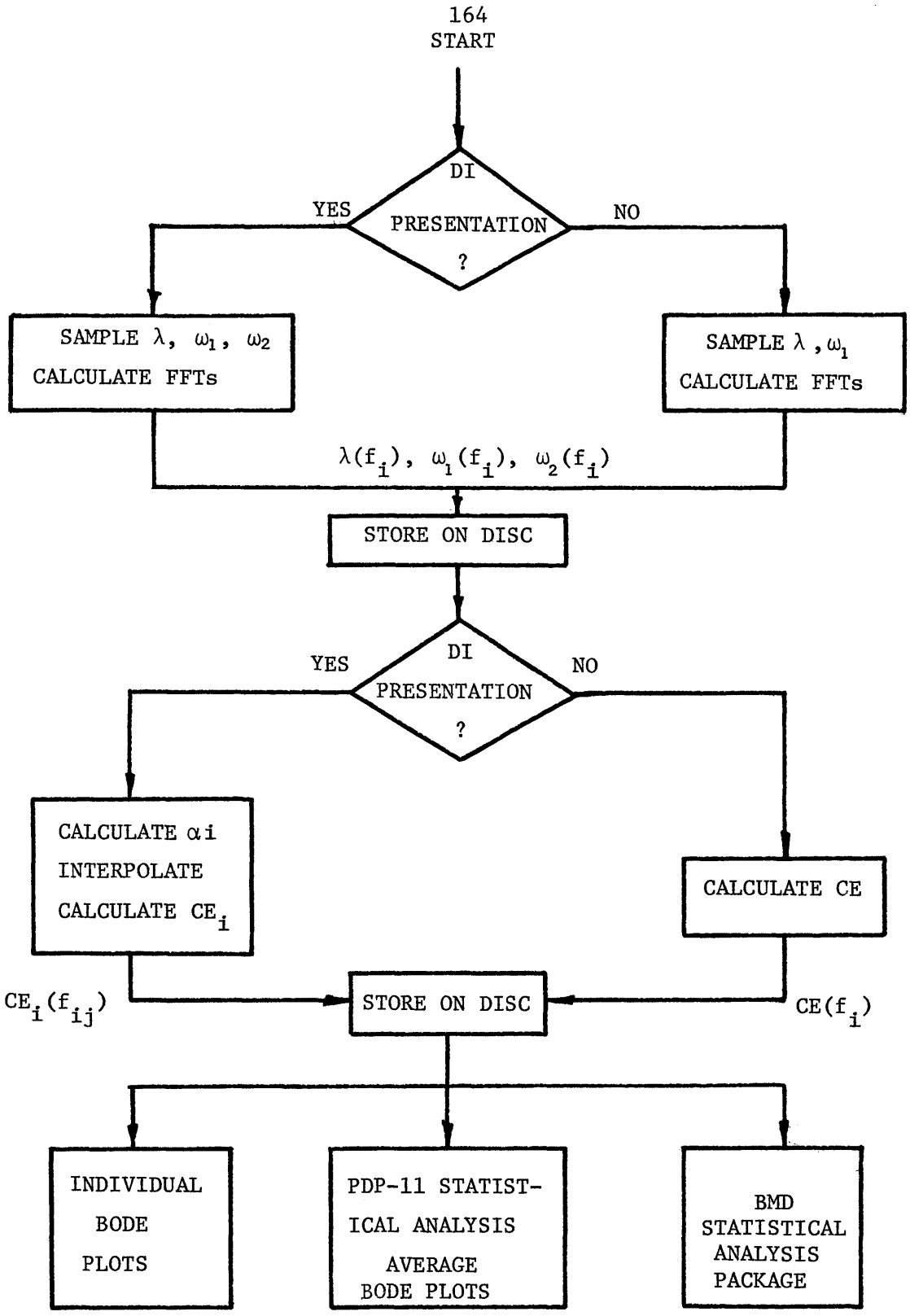

Figure 4.4: Data Flow for Describing Function Generation

4.4 Experimental Results

This section presents an illustrative time history response to a dual-input field presentation, and frequency domain results for both counterrotating and dual-input presentations. Also presented here are results from a subsidiary manual control experiment, and the inferred estimator transfer functions based on the measured manual control response dynamics.

4.4.1 Time Histories of Subject Response

Shown in figure 4.5 are time histories of a portion of one subject's run, showing the vestibular disturbance d_1, the visual disturbance d_2, the trainer and visual field velocities ω_1 and ω_2, and the subject's compensatory response λ. The first portion (CON mode) illustrates the good velocity-nulling performance we expect when the subject is presented with a counterrotating visual field, and specifically shows his ability to null out low frequency trainer motion, presumably because of the corroborating visual motion cue provided. The second portion (DI mode) illustrates poorer performance, especially with regard to nulling out low-frequency drift in the trainer velocity. Presumably, his low frequency stick response is primarily dedicated to nulling out the low frequency portion of the visual field velocity disturbance, as evidenced by the contrasting lack of drift seen in the field velocity history.

Figure 4.5: Dual-Input Disturbance Nulling

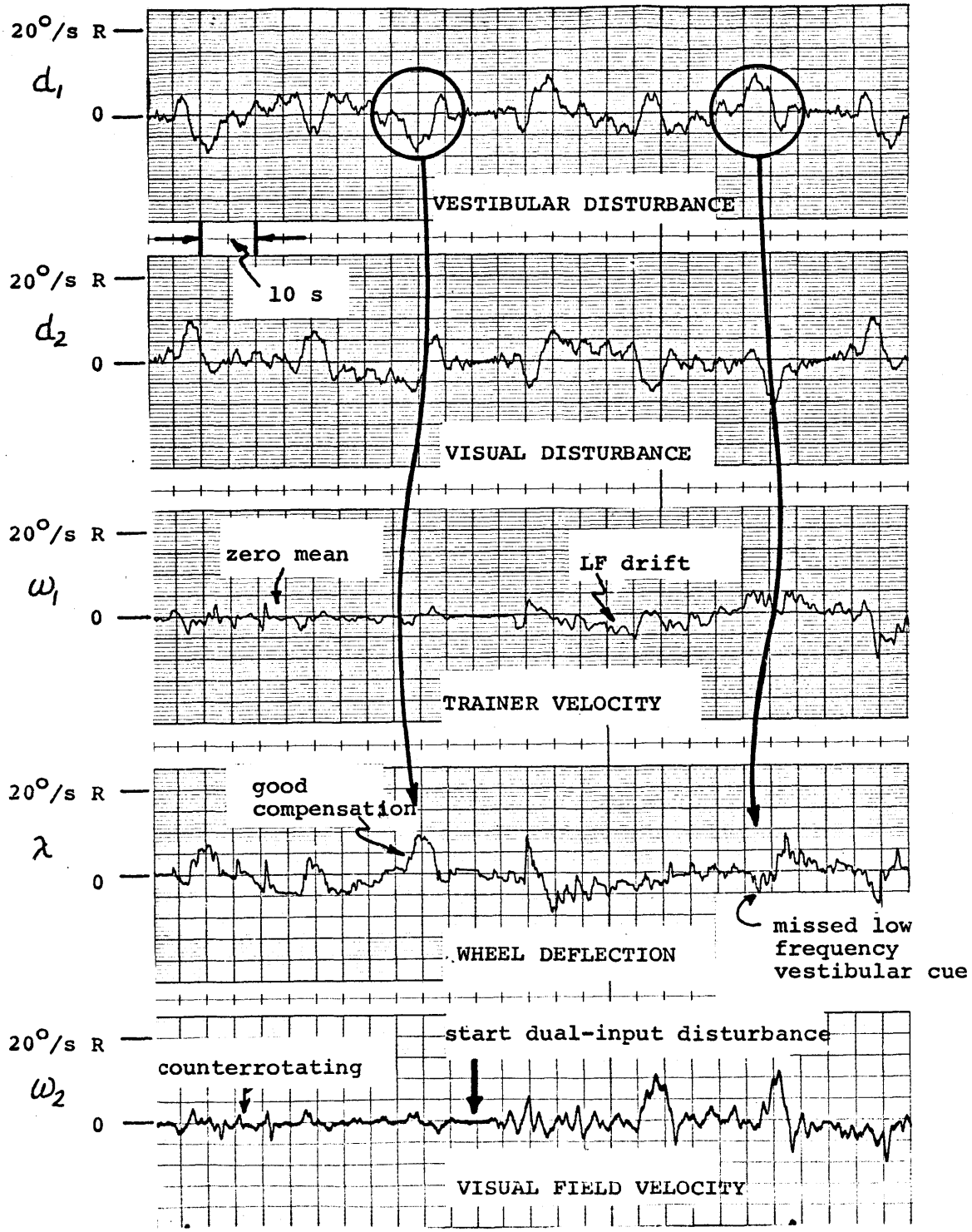

4.4.2 Describing Function Results

More definitive observations on subject response can be made in the frequency domain. The next two sections will present the describing functions associated with the two types of visual field presentations used.

4.4.2.1 Describing Functions for CON Presentations

Shown in figure 4.6 is the amplitude ratio data associated with counterrotating visual field conditions (CON), obtained by pooling individual subject data across the six-subject test population. Also shown are two transfer function fits: one a lag-lead and the other a simple integrator with lead. The particular parameter values displayed in the figure were obtained from a non-linear regression program which provides a least-squares fit to the data (BMD07R; Dixon, 1973).

The choice of a lag-lead function was motivated by its earlier successful application to similar data obtained under counterrotating field conditions, and reported on in the previous chapter in section 3.3. A brief comparison of the two data sets will be considered later in section 4.5.1. What is of interest to note here, however, is that the fit due to the integrator with lead follows the data almost as well as the lag-lead, and clearly provides for a simpler functional description.

Also shown in figure 4.6 is the phase data associated with the same CON presentation, again obtained by pooling across the six-subject test population. The dashed line represents the phase expected from the

Figure 4.6: Describing Functions for Counterrotating Visual Field

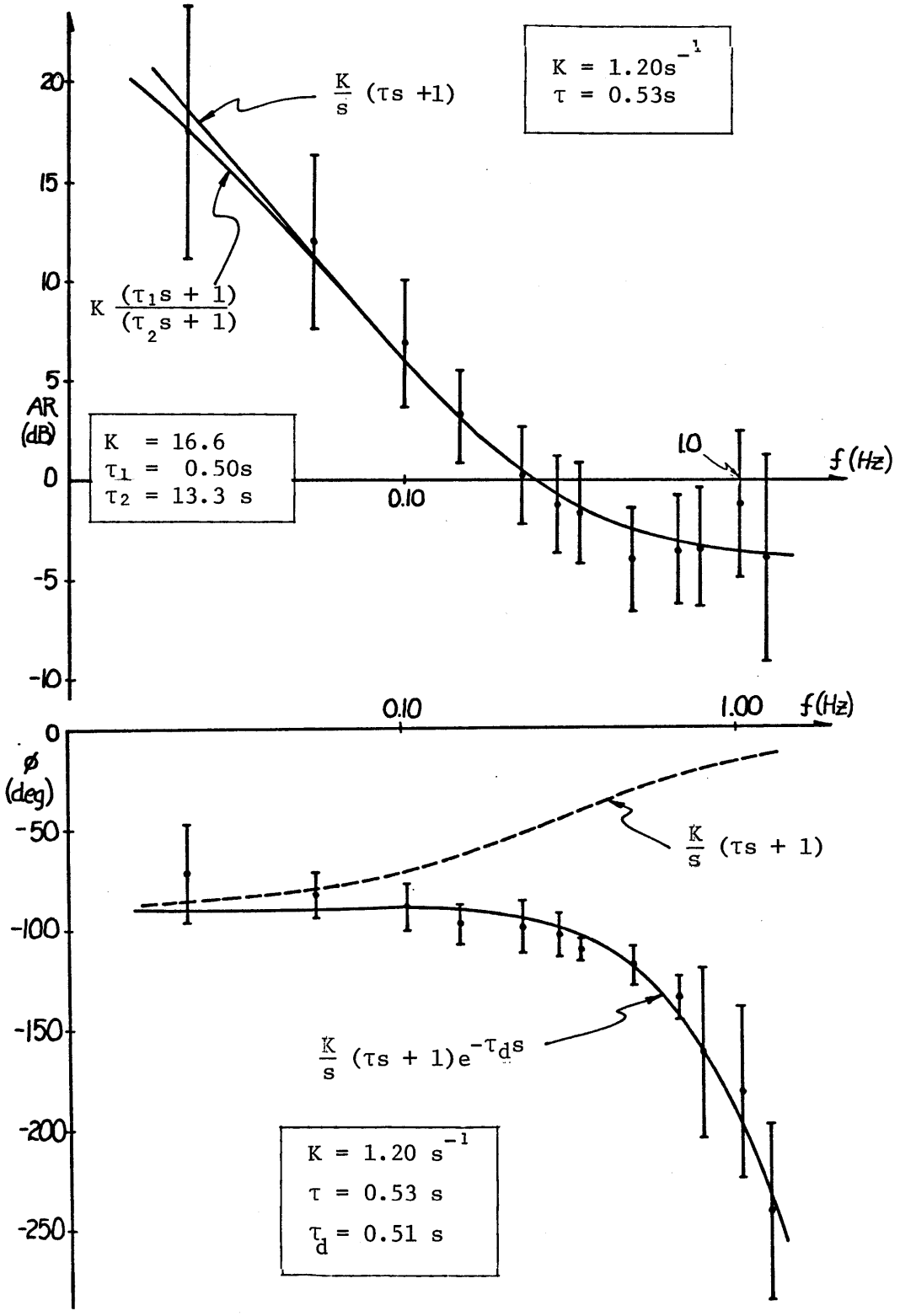

integrator-plus-lead function just illustrated, and the solid line the expected phase when an additional dead-time is incorporated into the transfer function. As in the previous chapter, the dead-time was calculated from a linear regression on the phase residuals, according to (3.7) and the accompanying computational description.

From the two figures, it would appear that the subject response data associated with counterrotating field conditions can be fit reasonably well with a fairly simple transfer function. The adequacy of fit will be discussed further in section 4.5.1, as well as its functional significance. It suffices here to note that the low-frequency qualities of the response data are reminiscent of a manual control cross-over model (McRuer and Krendel, 1959), in which the human operator is functionally modelled as an integrator when controlling a unity gain plant.

4.4.2.2 Describing Functions for DI Presentations

Shown in figure 4.7 are the describing functions calculated for the dual-channel model, obtained under dual-input visual field conditions (DI). The six-subject gain and phase averages are shown, along with smooth curves sketched in to indicate trends in frequency. Although various transfer functions were fit to the two data sets, they will not be discussed here; instead, the results of a more specific curve fitting exercise will be deferred to section 4.4.3. Some of the obvious features of the data trends are clearly worth commenting on here, however.

Figure 4.7: Dual-Input Describing Functions
(uncorrected for operator dynamics)

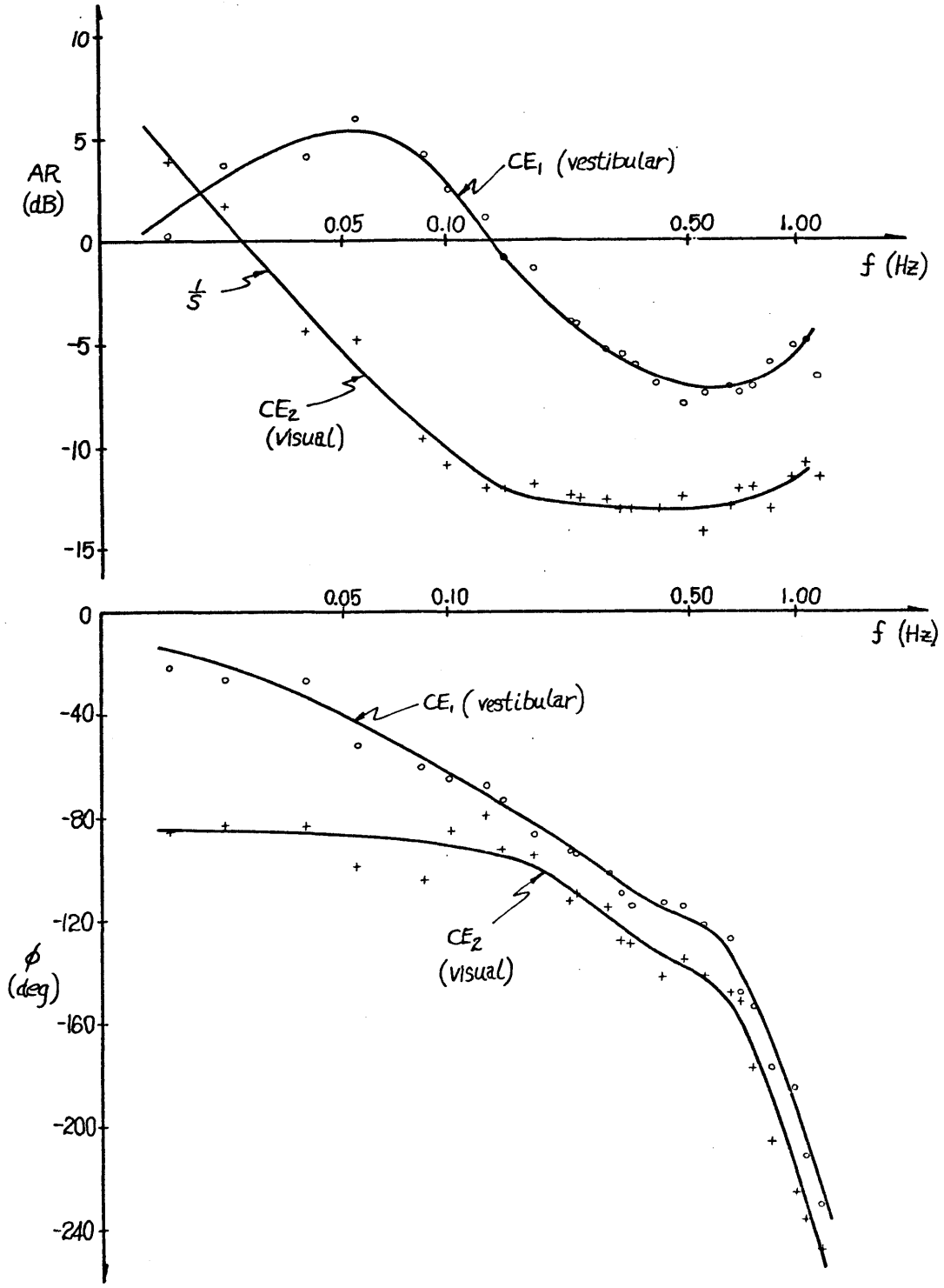

The "vestibular" gain, CE_1 follows what might be expected from a lag-lead, augmented by a lead at high frequencies and a washout at low frequencies. This washout characteristic is entirely consistent with our notion of negligible canal response at low frequencies, and, of course, is not inconsistent with the dual channel model proposed in section 2.4 (recall figure 2.11).

The Bode plots defining the "visual" transfer function, CE_2, show quite contrasting behavior. At low frequencies, the gain is higher than in the vestibular channel, supporting the earlier drift rate findings in which the dominance of a DC visual cue was demonstrated. Up to approximately 0.1 Hz, the visual channel behaves as a simple integrator (in gain and phase), which is again suggestive of the influence of manual control dynamics on our computed estimate of a cascaded estimator/controller describing function. Although the visual gain levels off at about 0.1 Hz, it remains considerably smaller ($\simeq$ 10 dB) than the vestibular gain, at frequencies above the gain crossover point ($f \simeq 0.02$ Hz). A linear complementary filter model of estimator dynamics thus does not appear to be an unreasonable functional model of combined cue processing.

4.4.3 Computed Estimator Describing Function Results

As noted in the introduction to this chapter, and demonstrated by the analysis of section 4.3, the subject's control strategy C is imbedded in the describing function results just presented. Thus, the objective of determining the linear estimator functions E_1 and E_2 has yet to be met. This motivated the design of another experimental series aimed at

determining the control strategy, so that its effect could be divided out of the results already obtained.

A brief description of the design of this experiment is given in the next section, which also presents the resulting measured human operator dynamics to be used shortly in deriving the estimator response functions.

4.4.3.1 Human Operator Dynamics

4.4.3.1.1 Experiment Description

Subjects, seated in the trainer, were given the task of nulling the velocity of the projected stripe pattern, by using the control wheel to compensate against a disturbance signal injected into the projector drive. The trainer remained stationary throughout the task, and the subject was informed of this prior to the experiment. In addition, to avoid any possibility of circularvection induced by visual field motion, the side windows were made opaque and the moving stripe pattern used earlier was projected on the trainer's front window. No sensations of self-motion were introduced by this arrangement, as indicated by post-test questioning of the subjects.

The task is thus a standard human operator pursuit tracking task, in which field velocity is the variable to be nulled. Figure 4.8 is a block diagram of the nulling task, with the subject drawn as a linear operator with remnant. It is presumed that the subject generates an internal estimate of visual field velocity, through an accurate estimator which is fast with respect to the motion sensation dynamics we are trying

to investigate; hence the unity gain. A negative feedback structure for the subject is also presumed, with the velocity estimate differenced with the task objective, to generate an error signal for control action. This is then acted upon by the subject's control dynamics, here presumed to approximate the corresponding control block used to model his behavior in the self-velocity nulling task.

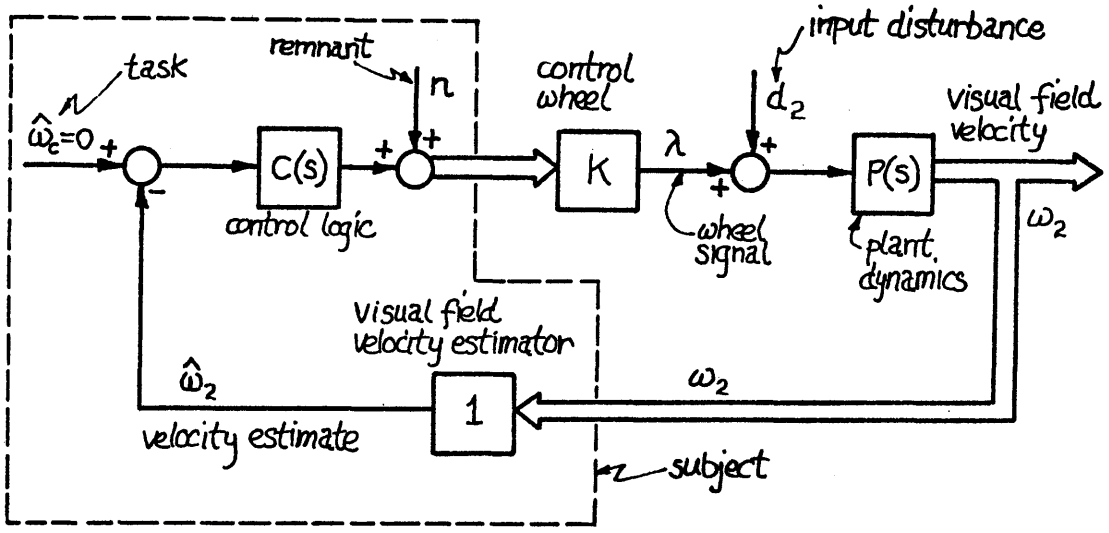

Figure 4.8: Visual field velocity-nulling task.

Note that the control wheel polarity is opposite that used in the self-velocity nulling task, to be consistent with the objective of field velocity nulling. Here, a right wheel deflection results in right field motion. The loop disturbance, d_2, is the same as used in the visual field loop of the previous task. Further, the projector drive signal is also filtered as before, so that the subject sees the same dynamic response, P, to his control actions.

Of course, it can be argued that the subject's control strategy in this experiment will differ from that used in the motion nulling experiments, simply on the basis that the tasks are different. However, this can be countered by noting that the same control wheel, plant dynamics, and visual loop input disturbance are used in both experimental series. In addition, the tasks are similar in that a nulling of perceived velocity is being asked of the subject, in one case self-velocity and the other, visual field velocity. Since there is obviously no conclusive way to disect the control strategy from the estimators proposed in the parallel channel model, it seems reasonable to assume an identity between the control logics of the two tasks, especially in view of task similarities.

4.4.3.1.2 Experiment Results

Six subjects attempted to maintain zero field velocity for two full presentations of the disturbance signal. For each presentation, FFT's were performed on the wheel deflection and field velocity histories, and gain and phase were computed at each frequency of the input disturbance, in a manner completely paralleling the input-output analysis of Chapter 3. Figure 4-9 shows the resulting six-subject average Bode plots, with one-sigma deviations indicated by the error bars. Also shown is a least squares fit, to the gain data, of a simple integrator with lead. The dead-time τ_d was calculated from a least squares fit to the phase residuals based on the fitted gain function. Although the fit could certainly be improved by the choice of a higher order transfer function, the simplified operator model of integrator-plus-lead will be seen to be adequate for the purpose of the analysis to follow.

From the figure, the gain trends are quite obvious: integration at low frequencies followed by a mid-frequency lead break, similar to what was seen in the amplitude ratio data defining the "visual" estimator function CE_2 (recall figure 4.7). The phase trends are also similar, although the current manual control describing function seems to exhibit more phase lag than computed for the function CE_2. The similarity overall, however, is quite striking, and suggests that a considerable portion of the frequency response associated with the cascaded control/estimator functions CE_i is, in fact, due to the operator response function C.

Figure 4.9: Operator Describing Function for Visual Field Velocity Nulling Task.

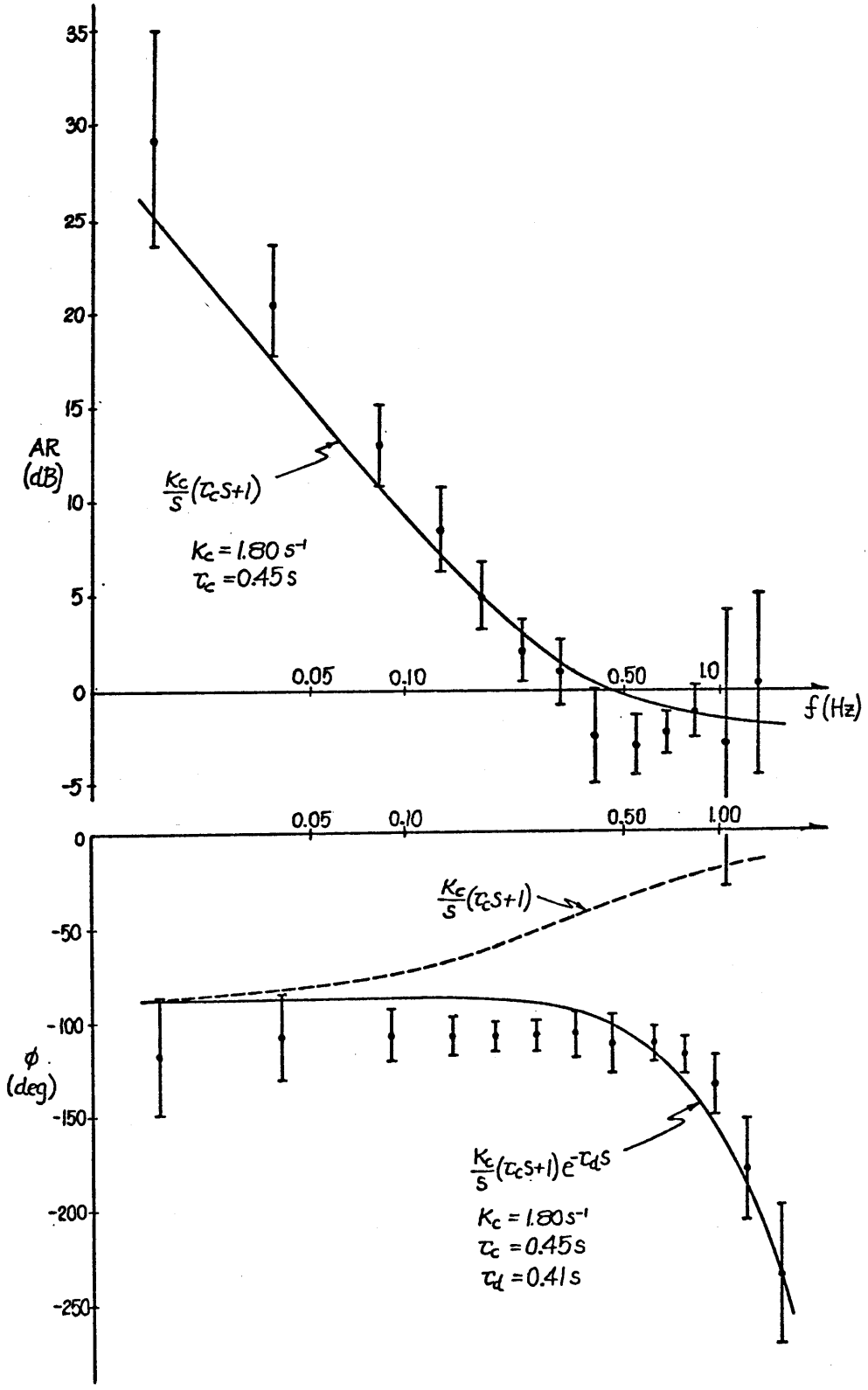

4.4.3.2 Estimator Function Calculation

Four of the subjects participated in both the self-velocity nulling experiment and the manual control task just described. Thus, for each individual, at each test frequency common to the two experiments, the gain and phase data of the overall describing function (CE, CE_1, or CE_2) can be adjusted by the gain and phase data defining the operator dynamics (C). Specifically, the overall describing function gains can be divided by the operator gains, and their phases subtracted, to infer the appropriate estimator function gain and phase.

It is appropriate to briefly describe how this calculation was implemented. The operator dynamics are only computed at the "visual" test frequencies contained in the second disturbance signal, d_2, because of the experiment's design. Thus, it is necessary to interpolate across frequencies to obtain estimates of operator gain and phase at the frequencies contained in the "vestibular" disturbance signal, d_1. This was done for each individual, for each set of response data associated with a full presentation of the disturbance signal. Since there are two periods of the disturbance signal sequentially presented to the subject during the manual control task, full-frequency operator response data was generated for the two presentations: "early" and "late" data sets.

It may be recalled from section 4.2.3 that the self-velocity nulling experiment consists of two presentations of each of the two visual field modes. Thus, there are "early" and "late" data sets associated with the two CON presentations and "early" and "late" data sets associated with the two DI presentations. Thus, for the CON presentations, the "early"

data set can be divided by the "early" operator dynamics data and similarly for the "late" data set. Naturally, the same approach can be taken with the response data during the DI presentations. This implementation thus not only corrects response data by an individual's own manual control characteristics, but also provides some compensation for possible fatigue and learning during the course of the task.

4.4.3.3 Estimator Function for Counterrotating Field Presentation

Shown in Figure 4.10 are the four-subject gain and phase averages obtained by dividing the counterrotating field nulling response data of figure 4.6 by the operator response data of figure 4.9, on an individual-by-individual basis. What should be evident from this division is that most of the describing function variation with frequency is due to human operator dynamics (C) and not to estimator dynamics (E). Also shown on the figure is a least-squares fit of a simple gain with dead-time, providing a rough approximation to both the gain and phase trends with frequency.

The data suggest that the estimator is fairly flat across the spectrum of interest, the implication being that sensed velocity is accurately estimated when vestibular information is exactly corroborated by visual motion cues, as it is under CON presentation conditions. The characterization of the estimator function as a simple DC gain could clearly be improved upon by the use of a higher order function, such as a lead-lag, but it is not felt that the overall spread warrants the use of such a fit. The simple fit shown is functionally more appealing when one

Figure 4.10: Velocity Estimator Describing Function: Counterrotating Visual Field

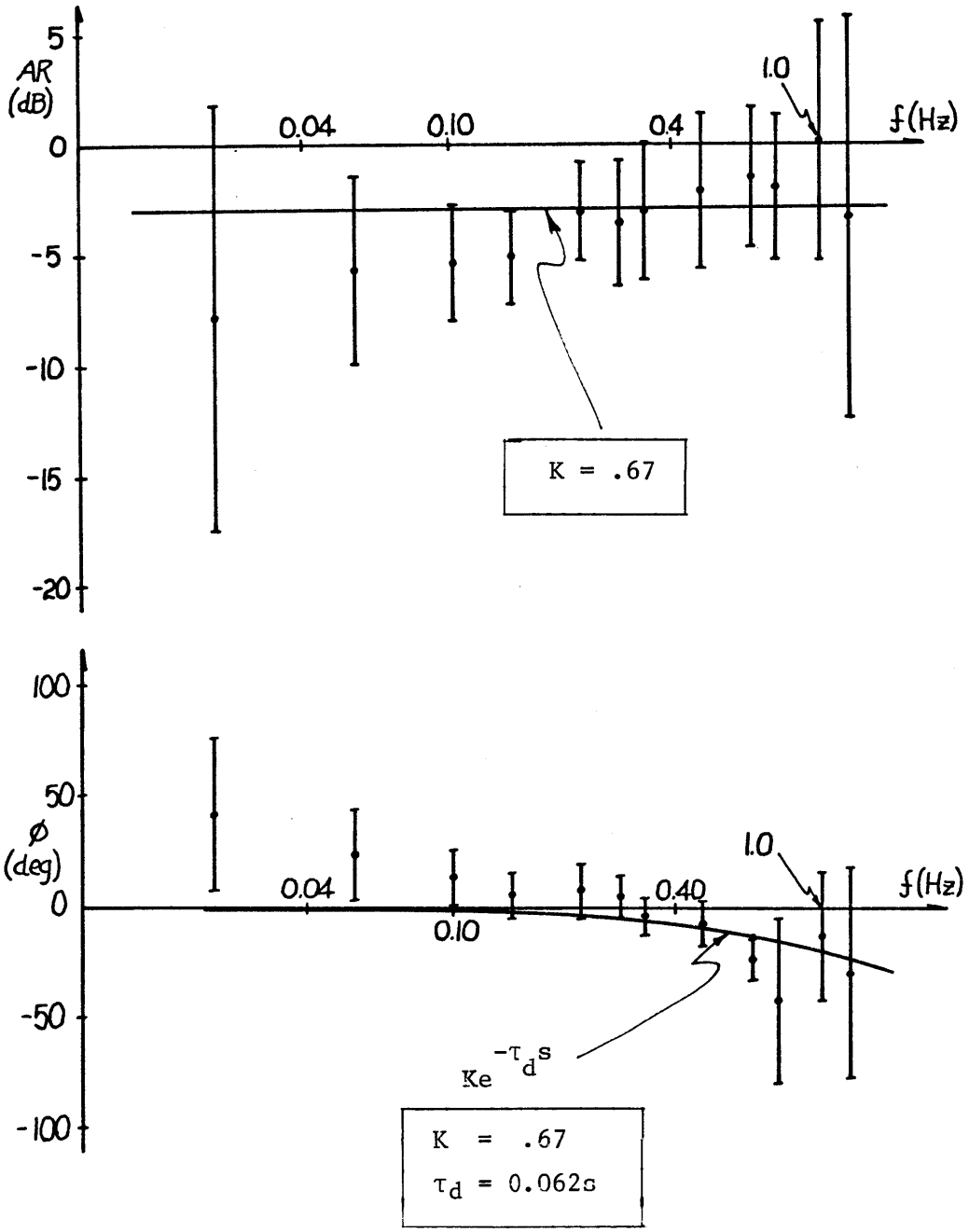

speculates on what would be considered desirable frequency response characteristics for an accurate estimator: flat gain and nearly zero phase across the input spectrum.

These data trends will be further discussed in section 4.5.1.

4.4.3.4 Estimator Functions for Dual-Input Field Presentation

Shown in figures 4.11 and 4.12 are the four subject gain and phase averages obtained by dividing the dual-input response data of figure 4.7 by the operator response data of figure 4.9, on an individual-by-individual basis. Also shown are smooth curves associated with two linear transfer functions providing a least-squares fit to the data.

The vestibular channel data (figure 4.11) exhibit, at first glance, the AC characteristic we would associate with the canals: both the rapid gain drop and phase lead with decreasing frequency are qualitatively well-modelled by a washout filter. However, the break frequency is quite high: the washout time constant is 0.94 s from the fit, which is an order of magnitude smaller than the 10 s time constant we would expect from the canals (Melvill Jones et al, 1964). The discrepancy is even larger when compared with the 13.8 s value calculated from the drift measurement in section 2.4.2. Finally, it is appropriate to note that we might expect unity gain at the high test frequencies; the data, in contrast, is better fit with half that gain.

The visual gain (figure 4.12) is a good deal lower than the vestibular gain, over much of the frequency range, with crossover occuring only at the very low end ($f \simeq 0.02$ Hz). In this region, the gain is

Figure 4.11: Vestibular Channel Velocity Estimator Describing Function: Dual-input Disturbances

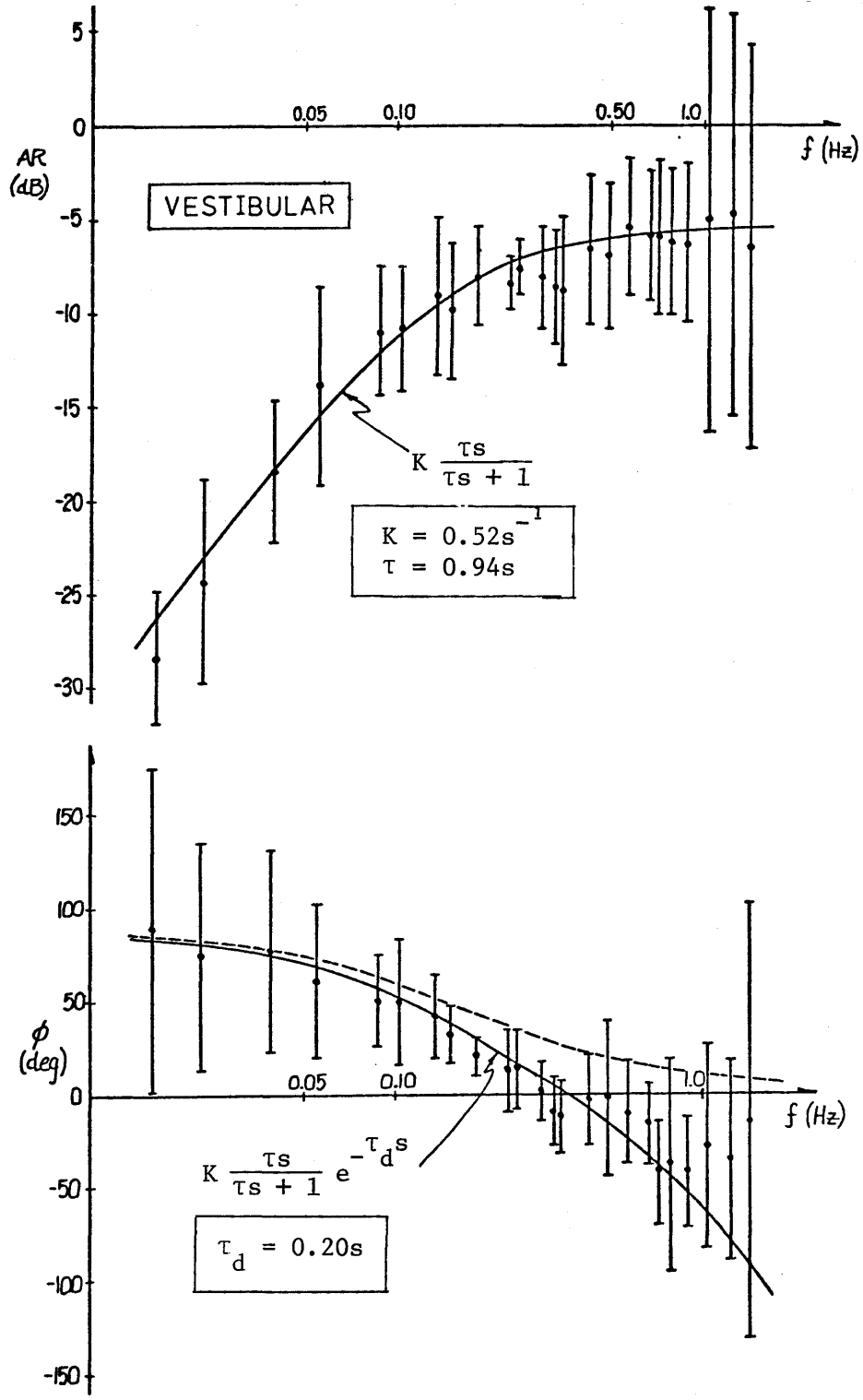

Figure 4.12: Visual Channel Velocity Estimator Describing Function: Dual-input Disturbances

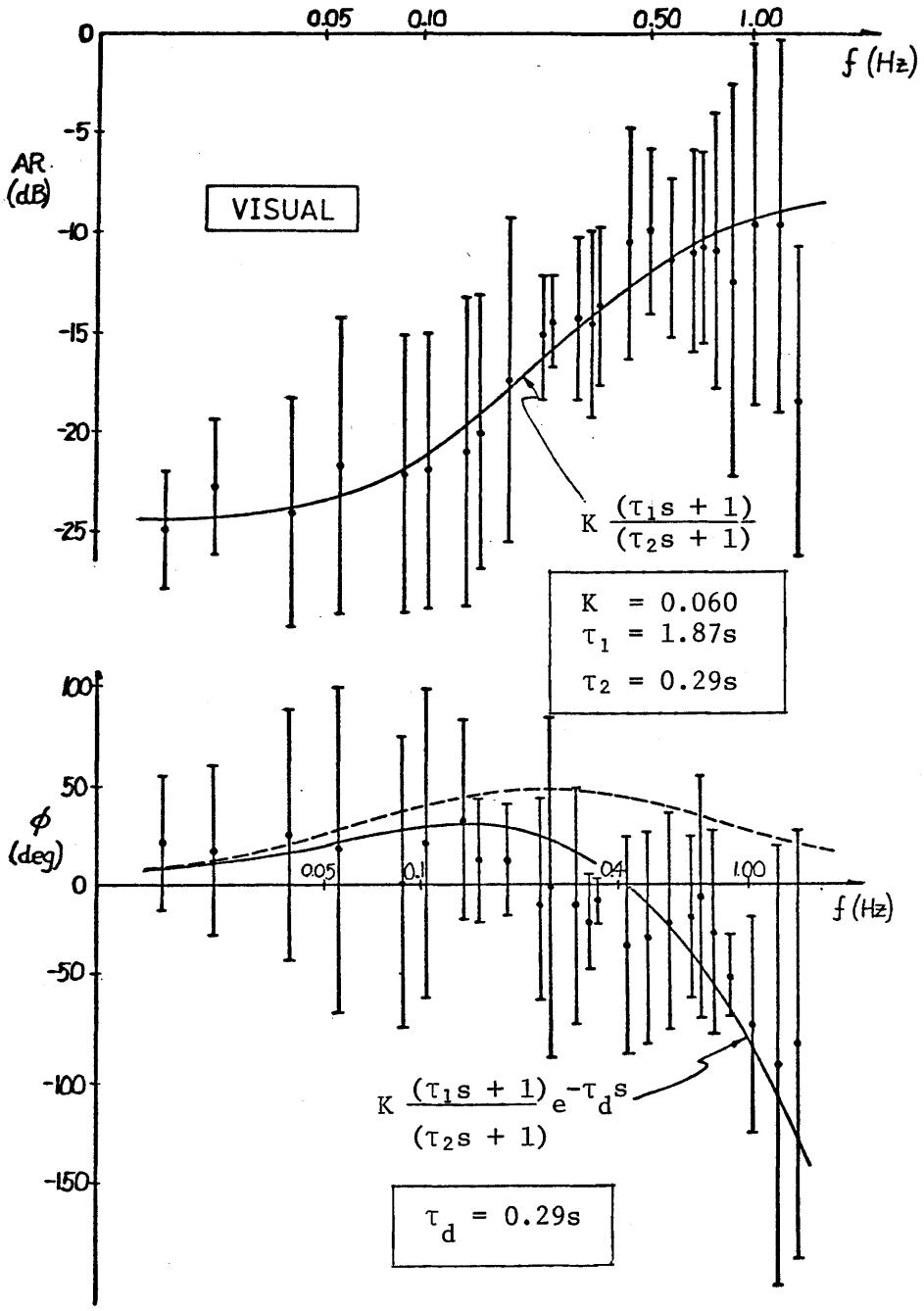

approximately constant with frequency, behavior which is qualitatively consistent with the idea of DC visual cue dominance. However, we might expect the DC gain to be approximately unity; certainly not the -25 dB seen in the data. Furthermore, if the visual channel were to be truly complementary to the vestibular channel, we would expect a roll-off near 0.1 Hz. Just the opposite occurs, however.

4.5 Dual-Input Describing Function Model

The previous section has concentrated on some of the qualitative aspects of the derived operator transfer function data associated with the two types of visual field presentations used in the nulling experiments (CON and DI). At this point, it is appropriate to consider how these results can be functionally described within the framework of the linear dual-channel estimator model of figure 4.1 proposed at the beginning of this chapter. Since two types of field presentations were utilized in the experiments, the results associated with each will be discussed separately in the next two subsections.

4.5.1 Model Implications from CON Presentation Data

4.5.1.1 Relation to Earlier CON Presentation Results

Before discussing how the counterrotating field data can be related to the dual channel model, it is appropriate to briefly discuss how these results relate to the counterrotating field data obtained from the experiment of the previous chapter. Shown in figure 4.13 are the amplitude ratio plots for both presentation sets, combining the data of figures 3.3 and 4.6 for convenient comparison. Although both exhibit the same trends with frequency, it is clear that higher low-frequency gains and lower high-frequency gains characterize the CON data associated with the current experiment. The result is a higher crossover frequency, and low-frequency behavior which closely follows what would be expected from a simple integrator. A statistical test on the parameters of the two fitted

Figure 4.13: Describing Functions for Counterrotating Visual Field-Gain Comparison

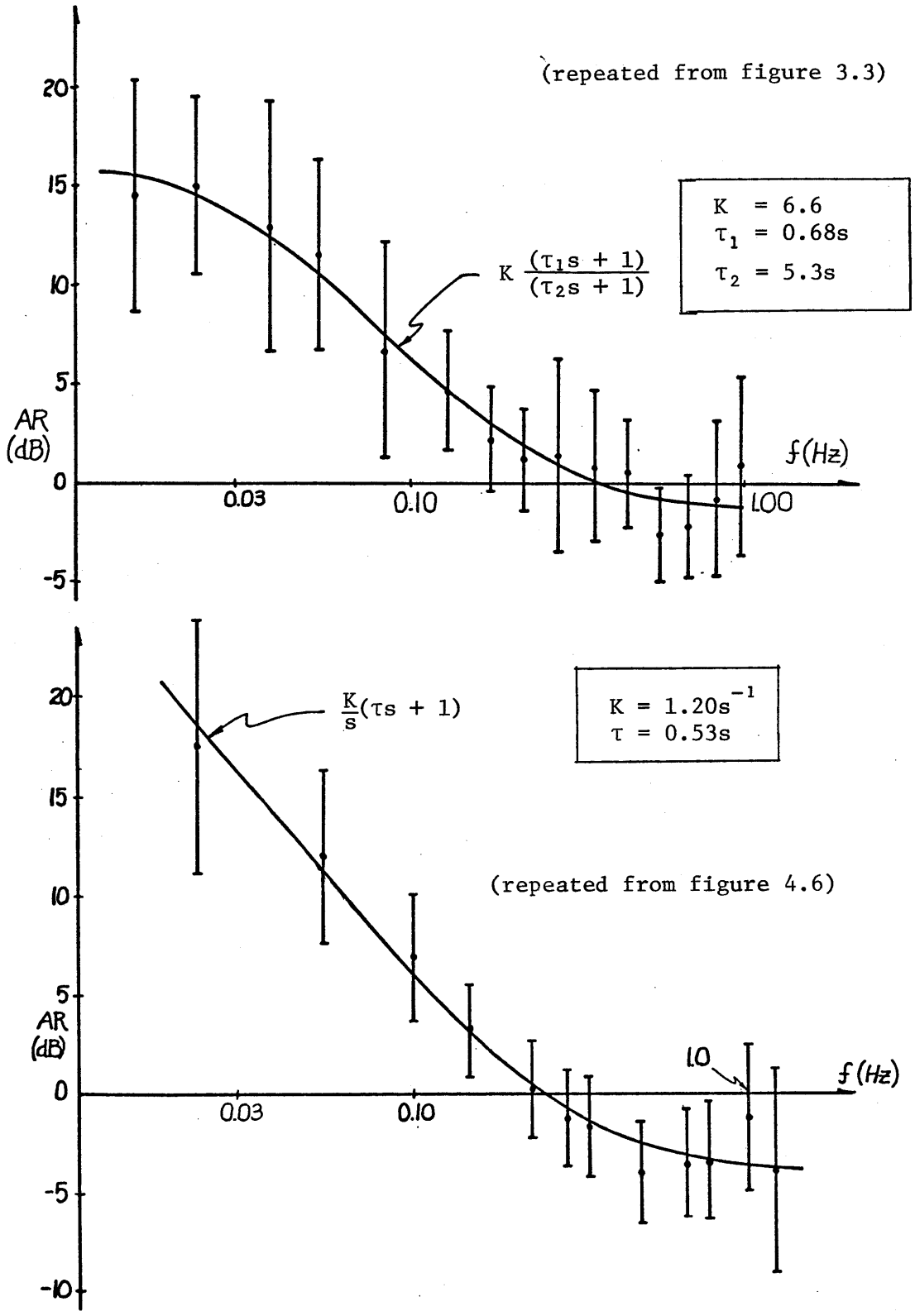

lag-lead functions could be conducted (paralleling the approach used in the previous chapter in which different field presentations were compared), but it should be clear, from the parameter values given, that the two transfer functions are not statistically equivalent.

Although the same subjects were given the same nulling task in the two experiments, it should be recalled that in the earlier experiment, the subjects used a spring loaded stick for disturbance compensation, whereas in the currrent experiments they used the control wheel. Furthermore, the trainer disturbance signals differ between the two experiments, the earlier consisting of 15 sinusoids following a shelf power spectrum, and the current one consisting of 12 sinusoids following a double lag-lead power spectrum. Thus, we might very well expect some differences in the derived transfer functions, even though both are associated with the same type of counterrotating visual field motion cue.

4.5.1.2 Integrator-Plus-Lead Model

More pertinent to the dual-channel modelling effort, however, is the fact that the amplitude ratio data from the current experiment appears to be as well-fit with a simple integrator-plus-lead as it does with a lag-lead. This may be seen directly by a visual comparison of the two fitted curves, by referring back to figure 4.6. The very low value of the lag break frequency ($1/\tau_2$) found by the regression program means that the two curves are almost indistinguishable over the frequency range we are considering. This is also seen by a direct comparison of the parameter values for the two fits. From Table 4.1, the lead time

constants are not significantly different ($p > 0.1$), as we might expect, and the ratio of lag-lead gain to lag time constant (K/τ_2) takes on a value of 1.25, a close approximation to the DC gain of the integrator-plus-lead. Thus, the two functions are effectively equivalent over the frequency range of interest.

In addition to its simplicity, the integrator-plus-lead function is a more attractive alternative because of the smaller variance in its fitted parameter values. From table 4.1, it is seen that the variance in the estimates of both gain and lag-time constant are relatively large for the lag-lead function, whereas the variance in the DC gain for the integrator-plus-lead is relatively small. For this reason, and in the interest of economy of description, the choice of integrator-plus-lead is more appropriate than the lag-lead, as a linear descriptor of subject response to this task.

Table 4.1: Curve Fit Parameters for CON Presentation

FUNCTION	PARAMETERS					
	K	σ_K	τ_1	σ_{τ_1}	τ_2	σ_{τ_2}
$\frac{K}{s}(\tau_1 s + 1)$	1.20	0.07	0.53	0.05	-	-
$K\frac{(\tau_1 s + 1)}{(\tau_2 s + 1)}$	16.57	10.96	0.50	0.06	13.28	9.40

Other functions were fit to the same data to investigate fit improvement with the use of higher-order functions. Although a better following of the mean data at the high end of the spectrum can be obtained by incorporating an additional lead term, it was found that the overall residual fit error is not significantly reduced, due to the data spread. This is the same result found in the previous chapter in which the effectiveness of higher order fits was considered (recall section 3.3.1), and thus might have been anticipated. What this suggests, then, is that the integrator-plus-lead function is not only a parsimonious descriptor of subject response, but that it is sufficiently accurate for the six subject population data being considered.

4.5.1.3 Relation to Human Operator Dynamics

With this choice of function to describe self-velocity nulling performance in a counterrotating field environment, it is a direct matter to compare fitted parameter values with those associated with the manual control task of visual field velocity-nulling. It may be recalled from figure 4.9 that an integrator-plus-lead function was fitted to the visual pursuit task data; thus, parameter values may be statistically compared. Shown in table 4.2 are the fit parameters associated with the two tasks, along with the standard deviations of their estimates.

In comparing the DC gains for these two tasks, an F-test shows the variances to be not significantly different ($F_{5,5} = 1.38$, $p > 0.2$), but a t-test on the parameter estimates themselves shows the gains to be

Table 4.2: Integrator-plus-lead Curve Fit Parameters

TASK	PARAMETERS			
	K	σ_K	τ_1	σ_{τ_1}
SELF VELOCITY NULLING (CE)	1.20	0.074	0.53	0.054
FIELD VELOCITY NULLING (C)	1.80	0.087	0.47	0.057

significantly different ($t = 12.8$, $\nu = 10$, $p < 0.001$). The higher gain in the manual control task is certainly not unreasonable, in view of the increased difficulty of the self-velocity nulling task; that is, we might expect lower loop gain if subjects take a more conservative approach in providing compensatory control. A similar comparison of the lead-times for the two fits shows them to be comparable. An F-test on the variances shows them to be not significantly different ($F_{5,5} = 1.06$, $p > 0.2$), and a t-test on the parameter estimates themselves shows them to be only marginally significantly different ($t = 1.86$, $\nu = 10$, $p < 0.05$).

In spite of the task differences, then, both sets of response data can be reasonably well fit with a simple integrator-plus-lead. The major difference between the two fits is in the DC gain level, with a significantly higher gain occurring in the manual control task, as might be expected. Thus, the suggestion is that most of the gain variation with frequency, seen in the self-velocity nulling task, is due to manual control dynamics, and not estimator dynamics. More succinctly, the CE dynamics are due to C and not E.

In fact, we might propose that the estimator can be modelled with a simple gain, for the task of nulling self-velocity in a counterrotating visual field environment. An estimate of the gain is obtained by simply dividing the DC gains of the two previous curve fits given in table 4.2:

$$|E| \simeq K_1/K_2 = 0.67 = -3.52 \text{ dB} \qquad (4.12)$$

A closer look at the validity of such an approximation is afforded by the corrected data of figure 4.10, in which manual control dynamics are divided out of self-velocity nullling response, on an individual-by-individual basis (for the four subjects participating in both experiments). As noted earlier, the fitted DC gain value was -3.50 dB. Although it should be recognized that the exceptionally close agreement between this value and the value given in (4.12) is unwarranted by the data spread, the fact they are not far apart suggests that a simple DC gain model for the estimator is not unreasonable.

This is also supported by the phase data of figure 4.10, in which the fitted dead-time constant is found to be 0.062 s. Since the standard deviation of this estimate is 0.079 s, a t-test shows the fitted dead-time to be not significantly different from zero ($t = 1.92$, $\nu = 5$, $p > 0.05$). Thus, a simple DC gain appears to be a reasonable model for estimator response in the given task.

4.5.1.4 Dual Channel Model Implications

To relate these observations to the dual-channel model proposed at the beginning of this chapter, and illustrated in figure 4.1, it is only

necessary to recognize that what is measured under counterrotating field conditions is the sum of the two estimator blocks. That is, with field velocity being the negative of trainer velocity ($\omega_2 = -\omega_1$) the dual-channel model predicts a velocity sensation given by

$$\hat{\omega} = E_1\omega_1 - E_2\omega_2 = (E_1 + E_2)\omega_1 \tag{4.13}$$

Since the estimator describing function of figure 4.10 relates trainer velocity ω_1 to perceived velocity $\hat{\omega}$, then it follows that

$$E = E_1 + E_2 \tag{4.14}$$

so that what is being measured is the sum of the two channels.

Any conclusions regarding E can thus be made for the two channel sum. In particular, we are suggesting that the two channels sum to provide a relatively flat frequency response across the test spectrum, with little phase lag. This is precisely the result we would expect from a complementary filter structure, in which each channel exactly compensates for the other channel's gain and phase variation with frequency. Thus, if the vestibular channel were to be modelled as a simple washout, i.e

$$E_1 = K_1 \frac{\tau s}{\tau s + 1} \tag{4.15a}$$

then, we would expect the visual channel to be its complement:

$$E_2 = K_2 - E_1 = \frac{\tau s(K_2 - K_1) + K_2}{\tau s + 1}$$

So that, with $K_2 = K_1$, the visual dynamics would be given by a simple lag function:

$$E_2 = \frac{K_1}{\tau s + 1} \tag{4.15b}$$

and the summed two channel gain would be the constant K_1 across all frequencies.

From the parameter fit made earlier, it might be argued that the gain constant K_1 is approximately -3.5 dB. However, this is inconsistent with the results of circularvection studies, since the model would predict, via (4.15b), that steady state self-velocity sensation would only be a fraction of the visual field speed, which we know not to be the case (Brandt et al, 1973).

Of course, this gain problem can be resolved by assigning the 3.5 dB attenuation to the operator dynamic block, C, for this particular nulling task. That is, by assuming that the subject drops his loop gain by 3.5 dB when going from the field velocity nulling task to the self-velocity nulling task, then the summed estimator dynamics ($E_1 + E_2$) can be assigned a unity gain. Not only is this consistent with our notion of accurate velocity estimation in a counterrotating visual field environment, but a unity gain allows for consistent single cue model predictions, via (4.15). Thus by assigning the gain drop to the operator dynamics, we can provide a reasonable functional description of subjective sensation by proposing a linear dual-channel complementary filter, with the vestibular path providing high-frequency information to complement low-frequency visual motion cues.

4.5.2 Model Implications from the DI Presentation Data

The computed estimator describing functions, obtained under DI field conditions and shown in figures 4.11 and 4.12, have already been discussed to some extent. Basically, it was noted that the vestibular break frequency is an order of magnitude higher than what we would expect from canal dynamics and what is actually observed under standard vestibular testing of subjective sensation. Further, the very low DC gain seen in the visual channel is entirely at odds with what is seen in circularvection responses, in which subjective sensation eventually grows to the full magnitude of visual field velocity. Finally, the gain increase with frequency seen in the visual channel is contrary to the observed latencies and slow rise times of circularvection, and, of course, is entirely different from what is predicted by the low-pass portion of the proposed complementary filter structure (recall (4.15b)).

Although some of these differences might be ascribed to possible variations in operator dynamics due to task differences, a direct comparison of subject response in the two types of visual field environments, CON and DI, suggests that the problems associated with the linear dual-channel model are fairly fundamental. Shown in figure 4.14 are the gain and phase data averages, repeated from figure 4.10, defining the estimator function E associated with velocity-nulling under counterrotating field conditions. Also shown are gain and phase averages

Figure 4.14: Estimator Function Comparison - CON vs. DI

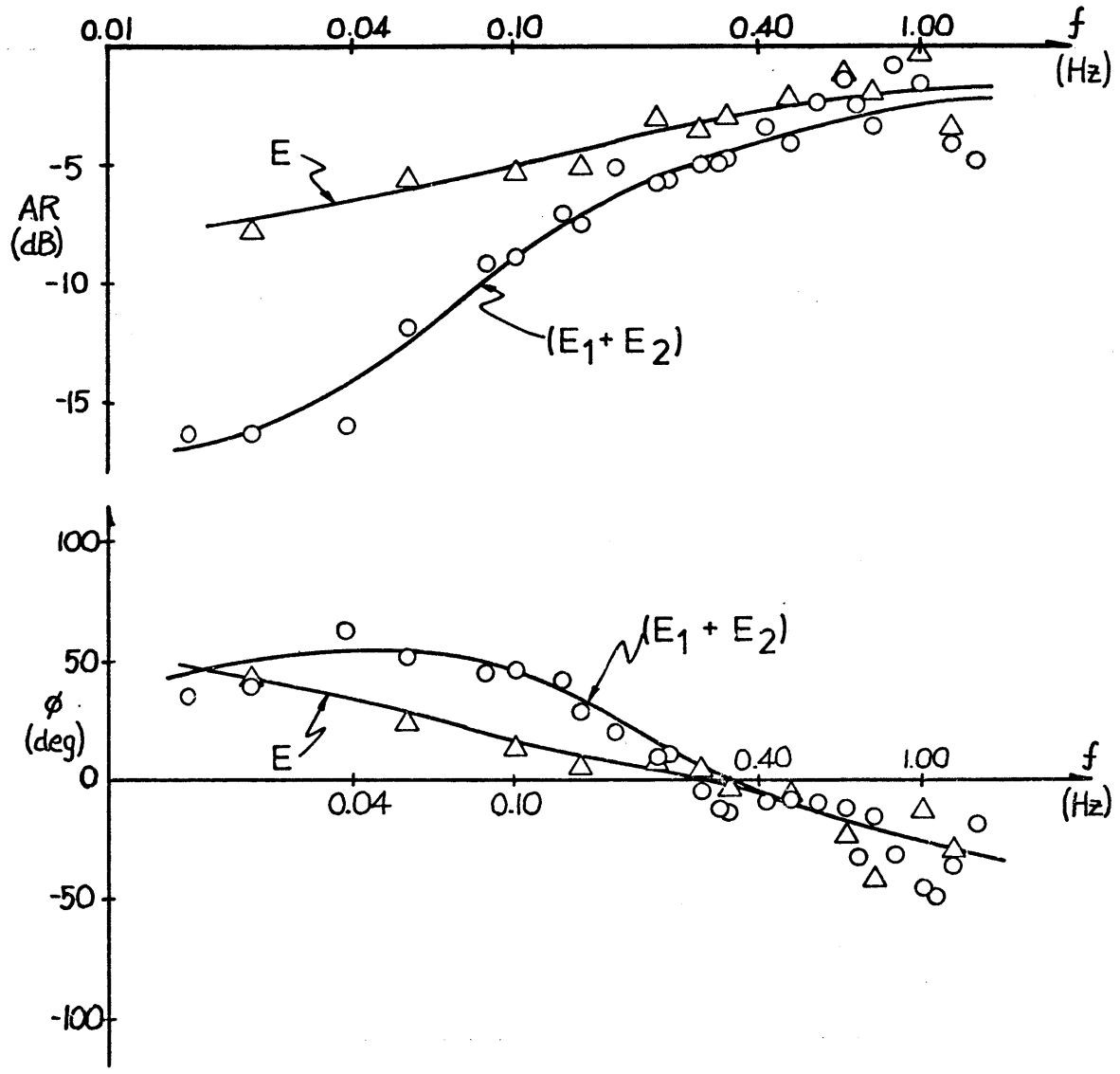

defining the summed response of the two channels of the dual-channel model ($E_1 + E_2$). These were obtained from the DI experimental data by summing E_1 with E_2 for each individual, and then averaging over the four-subject population. Smooth curves are drawn through both data sets to indicate trends.

If the linear dual-channel model is to be an accurate descriptor of combined cue processing, then, from (4.14), we would expect the two data sets of figure 4.14 to be indistinguishable; that is, we would expect the summed response ($E_1 + E_2$) to equal the counterrotating field response (E). Although the phases are relatively close, the fact that we see a 5 to 10 dB difference in low frequency amplitude ratios suggests that the linear model provides an inadequate description of subjective velocity estimation. It should be recognized that this inconsistency is based on data generated entirely within the framework of the experimental series discussed in this chapter. The additional inconsistencies with the results of past single-cue studies have already been noted.

Thus, although the inferred estimator describing function associated with CON presentations supports the complementary filter notion, the dual-channel model inferred from the DI presentations runs into serious difficulties when we atttempt to predict single or complementary cue response. Clearly, for the complementary filter model to be a valid descriptor of subjective sensation, it must be applicable to both types of cue presentation situations.

4.6 Summary

Subjects were given active control over their own rotational velocity while seated in a modified aircraft trainer, with a task objective of maintaining themselves fixed in space. A disturbance input to the trainer drive required each subject to continuously provide compensation via a control wheel. Visual motion cues presented in the subject's peripheral field were of two types: a) counterrotating with respect to actual subject velocity, providing an absolute measure of trainer velocity; and b) independent of actual subject velocity and under potential control of the subject. This second type of field motion was implemented by driving the projection system with a second independent disturbance, and allowing the subject's control wheel motions to directly influence field speed. Six subjects participated in the velocity-nulling task, each receiving two presentations of each field type.

By correlating subject response to each of the disturbance inputs, it is possible to see which portion of each cue the subject feels obliged to null, in order to maintain a sense of being motionless in space. This chapter has shown how this general response measure can be formulated analytically, by assuming a linear dual-channel model of motion perception cascaded with a linear human operator transfer function: the former is motivated by the earlier discussions concerning complementary filtering of combined cues, while the latter is motivated by the known non-unity gain characteristics evidenced in typical manual control tasks. In particular, it is shown here how the structure and specific parameters of such

a cascaded model can be inferred from the response data, and further, how the manual control dynamics may be eliminated from the response data, by separate testing in a related manual control task.

The corrected response data allows for the inference of a linear dual-channel estimator model, consisting of a washout operating on vestibular cues and a lead-lag operating on visual cues, the two filter outputs being summed for an overall estimate of self-motion. The washout function is consistent with known canal response, but the one second time constant is an order-of-magnitude lower than what has been measured in past vestibular testing. The visual path lead-lag is also inconsistent with single cue circularvection studies done in the past, since the DC gain is far too low to account for steady-state CV response, and the high frequency gain increase is counter to observed latencies and response times seen in CV testing.

An additional check on the linear model's validity is provided by the inferred estimator model associated with subject response under counterrotating visual field conditions. In this case, the complementary filter hypothesis is supported by the approximately flat response seen in the estimator describing function data. However, a comparison of this data with the response predicted from the dual-input data shows a large gain discrepancy below 0.10 Hz, implying that a linear summation of filtered cues is an inadequate model of subjective response to combined cue presentation. Thus, this model would appear to be only appropriate for fairly simple cue combinations, such as those described in

chapter 2 and successfully modelled there. The more general case investigated here, that of response to independent wide bandwidth motion cues, appears to be ill-described by a linear dual-channel model. What this suggests is that a closer look be given to the applicability of a non-linear dual-cue functional model which is the subject of the next chapter.

CHAPTER V

NON-LINEAR CONFLICT MODEL

The analysis and modelling efforts of the previous three chapters presumed a linear estimator structure for the functional modelling of visual and vestibular cue mixing. The object of the present chapter is to demonstrate how a non-linear cue conflict model can generalize on the results already obtained and simultaneously provide a means of resolving the apparent inconsistencies of the linear analysis presented in the last chapter. In particular, we wish to show that cue mixing need not be restricted to a simple linear addition of two independent sensory channels, and, in fact, that the postulation of an interaction between two channels leads to model predictions which are more consistent with observed single and dual-cue subjective response studies.

It was demonstrated in Chapter 2, that a linear complementary filter model of cue mixing provides predictions of subjective response which are not inconsistent with the low-frequency behavior observed in simple dual cue experiments. That is, when wide bandwidth vestibular cues are combined with constant velocity visual motion cues, a linear complementary filter adequately models inferred subjective sensation of self-motion. The high-frequency "vestibular" response characteristics discussed in Chapter 3 also support such a modelling approach. However, the linear modelling effort of Chapter 4, in which wide bandwidth stimuli were provided to both sensory channels, resulted in separate channel dynamics

which are apparently inconsistent with the results of single-cue studies. Of course, this can be resolved by proposing that simultaneous cue presentation involves a mixing of the two cues at different frequencies: that is, proposing that a vestibular cue at one frequency affects a visual cue at another, and vice versa. As suggested in the previous chapter, this points to the need for a reevaluation of our assumption of system linearity.

It was noted in the introductory chapter that the cue conflict hypothesis points to an alternative modelling approach which has the potential for providing at least a qualitative explanation for some of the results found in earlier combined cue experiments and visually-induced motion studies. The dual-input experiment of the last chapter places the subject in a high conflict situation, since he is presented with time-varying independent cues. Thus, a conflict model may prove to be an entirely appropriate structure within which to formulate an accurate descriptive functional model of combined cue sensation. This chapter will provide an evaluation of such a modelling approach.

The type of conflict model under consideration has already been described in general terms in the introduction; repeated in figure 5.1 is a block diagram of a dual channel model incorporating a cue conflict measurement and a selective weighting logic. As discussed previously, the motivation for this type of structure rests on the results of single cue experiments, in particular, subjective response to illusory visual motion cues. The premise, of course, is that cue weighting, and thus the resulting sensation, is determined by the amount of intercue conflict:

acceptance of either cue depends on the amount of corroboration provided by the complementary cue.

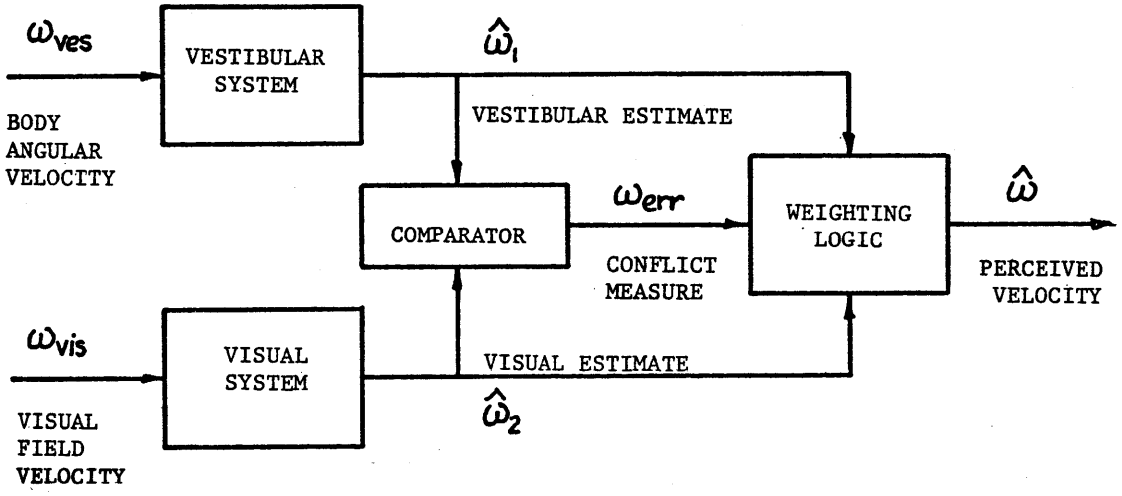

Figure 5.1 Dual input conflict model - Overview

Before describing this model in more detail, it is appropriate at this point to briefly note the general approach to be used in this chapter, for the development and evaluation of a cue conflict model. It should be clear that the analytic techniques of linear systems identification are of little help here: one must resort to a modelling effort based heavily on model simulation, in an attempt to match experimentally observed response characteristics. The approach, then, will be to propose a fairly simple functional model based on cue conflict, and motivated by the results of single cue studies. Model fidelity can then be evaluated

by simulating response to simple inputs, to provide some assurance that model response will be consistent with subjective data obtained from single cue studies. A further test is, of course, provided by simulating model response in the velocity-nulling task of the last chapter, and the model's frequency response can be compared with the corresponding subject describing function data. Naturally, this is an iterative exercise with no guarantee of optimality, nor, for that matter, convergence. It does, however, provide a means of developing a non-linear model with the capability of resolving the linear system inconsistencies of the last chapter.

This chapter is organized into four sections. Section 5.1 describes a simplified cue conflict model, and motivates its structure and parameter assignment by appealing to fairly basic considerations of visual-vestibular cue mixing. Section 5.2 then discusses simulated model response, in both open-loop and closed-loop test situations. In the former, simple step inputs are provided to the model, and the resulting time histories of the model response are described to provide some insight as to estimator operating characteristics. In the latter closed-loop simulations, the model is made part of a simulated velocity-nulling loop, in order to emulate the behavior recorded and described in the preceeding chapter. Also discussed here are model shortcomings which motivate the proposed modifications of section 5.3, followed by simulated model response to provide some measure of how effective these modifications are. Finally, section 5.4 summarizes the model development effort, and identifies the need for continued experimentation aimed at isolating functional non-linearities of cue mixing.

5.1 Cue Conflict Model

5.1.1 Model Structure

The basic structure of the cue conflict model has already been discussed in some detail. Shown in figure 5.2 is a functional diagram of the model, showing how the visual and vestibular cues are weighted in a complementary fashion according to the gain K. By restricting K to range between zero and one, a large K implies visual cue dominance and a gating out of vestibular sensation; with K small, the reverse occurs. The weighting gain is dependent on a measure of cue conflict, ω_{err}, which in turn, is derived directly from the two cues. The vestibular sensory dynamics are approximated by the low frequency portion of the torsion pendulum model (recall section 2.4). No visual sensory dynamics are modelled, for two reasons: the lack of experimental data for single channel visual cue response, and the relatively wide-band motion detection response of the visual system.

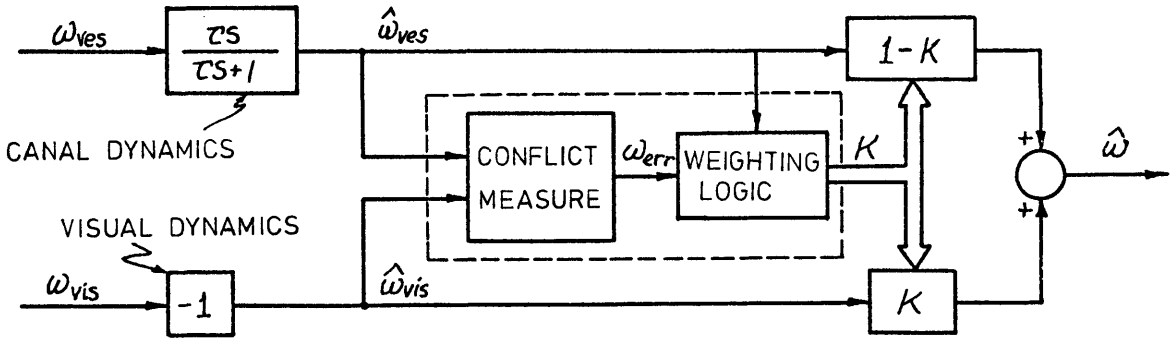

Figure 5.2 Dual-input conflict model - Functional diagram

A simple conflict measure can be motivated by considering, for example, self-motion in an inertially-fixed visual field environment (corresponding to the earlier CON field presentations). Although, this is clearly a zero conflict situation, a direct comparison of the two cues would lead to a discrepancy, because of the differences in the dynamic response of the two sensory channels. One is thus led to propose an internal model of canal dynamics, through which the visual information can then be compared with the actual vestibular signal. Effectively, then, conflict is based on high frequency cue content.

A weighting schema can then be proposed fairly directly. Since the conflict signal is a measure of high frequency agreement, and the vestibular system provides "reliable" information at high frequency, then it would seem reasonable to heavily weight this information whenever a high conflict situation is detected. The converse might be proposed with low conflict: heavily weight the visual cue. However, this approach is only reasonable at low frequencies, when we know the vestibular channel will be providing a null signal. At high frequencies, this weighting discards confirming vestibular information which clearly could be used to improve the velocity estimate. With no apriori knowledge of each channel's noise characteristics, an estimate can be obtained by simply averaging the cues. Thus, in a low conflict situation, we propose cue averaging, unless we have a small vestibular signal, in which case we heavily weight the visual cue.

An implementation of this type of conflict measure and weighting schema is shown in figure 5.3. The visual cue is high-passed through an

internal model of the vestibular dynamics to generate an expected vestibular signal, ω^{exp}, which is then differenced with the actual vestibular signal and passed through a rectifier. To allow for a long term resolution of steady state conflict, an adaptation operator acts on the rectified signal to generate the actual conflict signal, ω_{err}. The motivation for this adaptation operator will be discussed in the following section.

The symmetric weighting function is implemented with a cosine bell, for modelling simplicity. As illustrated, a large conflict signal (i.e. when $|\omega_{err}| > \varepsilon$) drives the visual path gain to zero, whereas a small one drives it to a peak weighting value which varies between 1/2 and 1, depending on the amplitude of the vestibular signal (and implemented via an additional bell function). Thus, in a low conflict situation, the cues can either be averaged or the visual cue passed straight through, depending on whether or not the vestibular signal is large or small, respectively.

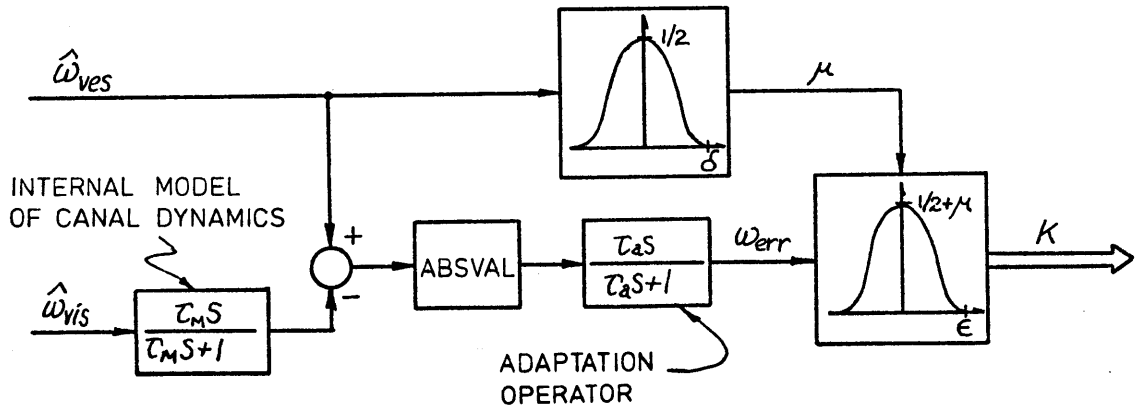

Figure 5.3 Conflict measure and weighting function

5.1.2 Model Parameters

Five parameters determine model behavior: the vestibular and vestibular model time constants, τ and τ_m, respectively; the two velocity magnitude measures, δ and ε; and the adaptation time constant, τ_a. This section provides a brief justification for setting these parameters appropriately.

As noted earlier, a reasonable value for the vestibular time constant τ is between 10 and 15 seconds (Melvill Jones et al, 1964). Although a choice of 13.8 s could be made on the basis of the CV drift rate averages discussed in section 2.4.2, a 10 s value provides us with an order-of-magnitude baseline with which to work. A similar argument holds for the model's time constant, τ_m, associated with the internal model of canal transduction. A 10 s value assigned to this time constant not only provides us with a rough order of magnitude, but avoids the problem of internal model mismatch, an area which is beyond the scope of the current model verification effort.

The velocity magnitude measures, δ and ε, can be assigned values by appealing to past work in defining vestibular threshold behavior. In particular, if we presume that cue conflict detection is characterized by the same type of behavior associated with vestibular pulse detection, then the conflict threshold ε may be chosen to equal the Meulder product of 2.5°/s (Oosterveld, 1970), the product which relates the magnitude of detected acceleration pulses to their duration. For model simplicity, we assume the measure of vestibular pulse size, δ, to be identical to ε.

The adaptation operator incorporated in the model provides for some flexibility in determining how long a steady-state intercue conflict should be allowed to continue. It may be recalled from section 2.3.1 that subjects place themselves in a potentially high-conflict situation by constantly accelerating the trainer to the right, in response to a right-moving constant velocity visual field. Since the subject's left CV illusion constantly opposes his rightward vestibular sensation, a model without an adaptation operator would predict constant conflict, and thus, a gating out of the visual motion information. If, instead, the conflict signal is washed out by an adaptation operator, a low conflict situation eventually results, allowing for an averaging of the two cues, behavior entirely consistent with the model analysis of section 2.4.2. A rough value for the adaptation time constant, τ_a, can thus be chosen on the basis of typical trainer acceleration latencies seen in the velocity nulling-task under CV conditions: a reasonable value would appear to be 10 s.

5.1.3 Cue Conflict Model

Shown in figure 5.4 is a block diagram of the proposed cue conflict model, based on the structure motivated earlier and on the parameter discussion given above.

Figure 5.4. Dual-Input Cue Conflict Model

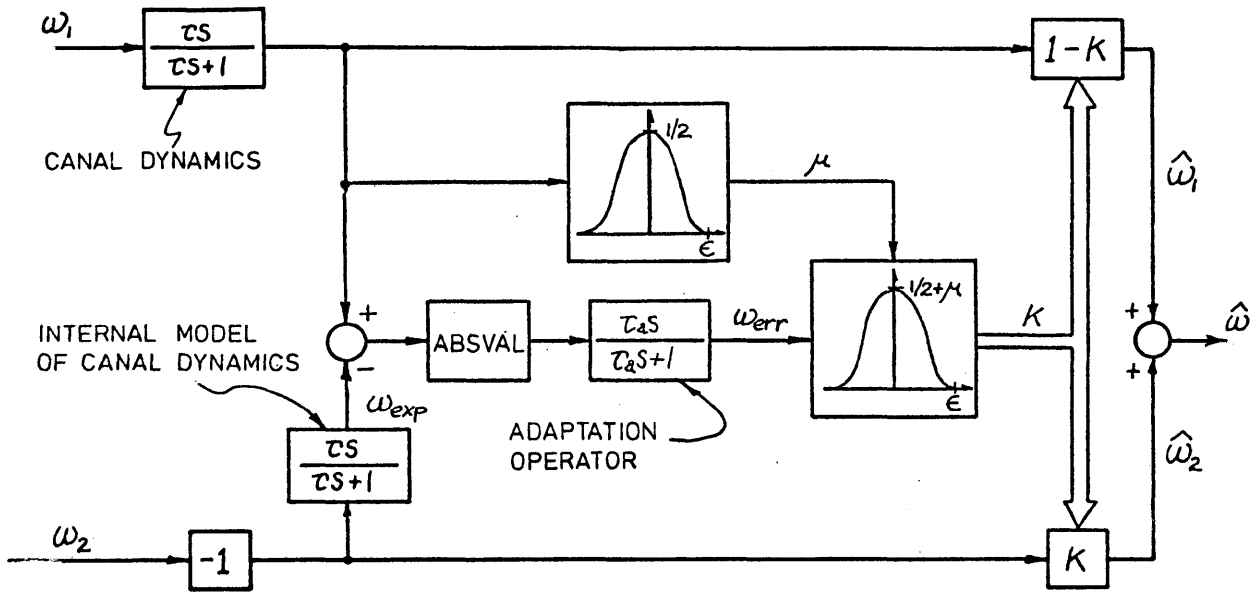

5.2 Simulated Model Response

Digital simulation of model behavior was conducted to evaluate model predictions in the face of simple cue inputs (such as velocity steps), and as part of two different closed-loop nulling tasks, simulating the experiments discussed in the previous chapters. A brief description of the simulation approach is given below, followed by time and frequency domain results characterizing model response.

5.2.1 Simulation Method

A general purpose digital simulation package was written in FORTRAN for use on a PDP-11/34, consisting of an executive program responsible

for simulation timing and data file maintenance, and a library of subroutines which provided a general purpose capability of functional simulation (Zacharias, 1977). It suffices to note here that the library routines implemented various linear and non-linear input-output functions (e.g., adder, integrator, multiplier, lead-lag, etc.) and the executive structure allowed for modular testing and verification of program subunits prior to large scale simulation. Trapezoidal integration was used for programming simplicity, and a relatively small integration step size (T = 1/128 s) was used to insure integration accuracy, at the expense of simulation run-time.

Two basic types of simulations were conducted. The first consisted of simple input-output testing of the non-linear estimator of figure 5.4, in which perceived velocity $\hat{\omega}$ was computed as a function of visual and vestibular motion cues. The second consisted of a loop simulation in which the estimator was placed in the simulated loop structure of figure 5.5, thus providing a test of model response in a closed-loop velocity-nulling environment. As earlier, the subject is modelled as a controller cascaded with an estimator. For the simulations, the control block C is modelled as an integrator-plus-lead, motivated by the discussion of section 4.4.3, and defined by figure 4.9:

$$C(s) = (K_c/s)(\tau_c s+1)e^{-\tau_d s} \tag{5.1}$$

where the parameters are given by

$$K_c = 1.80\ s^{-1} \qquad \tau_c = 0.45\ s \qquad \tau_d = 0.41\ s \tag{5.2}$$

Note that no control remnant is simulated.

External to the subject are shown the two visual and vestibular paths, each with identical dynamics (P) as used in the dual-input (DI) experiment of the previous chapter:

$$P(s) = \omega_n^2/(s^2 + 2\zeta_n\omega_n s + \omega_n^2) \tag{5.3}$$

where

$$(\omega_n, \zeta_n) = (5.65, 0.70) \tag{5.4}$$

The loop disturbances d_1 and d_2 are calculated for the simulation to be exactly the same as those used in the actual experiments, and thus, with the diagram's switch in the DI position, allows for two possible conflicting cue inputs to be presented to the estimator model. With the switch in the CON position, model response in a confirming situation can be investigated.

Figure 5.5 Conflict Model in Simulated Nulling Task

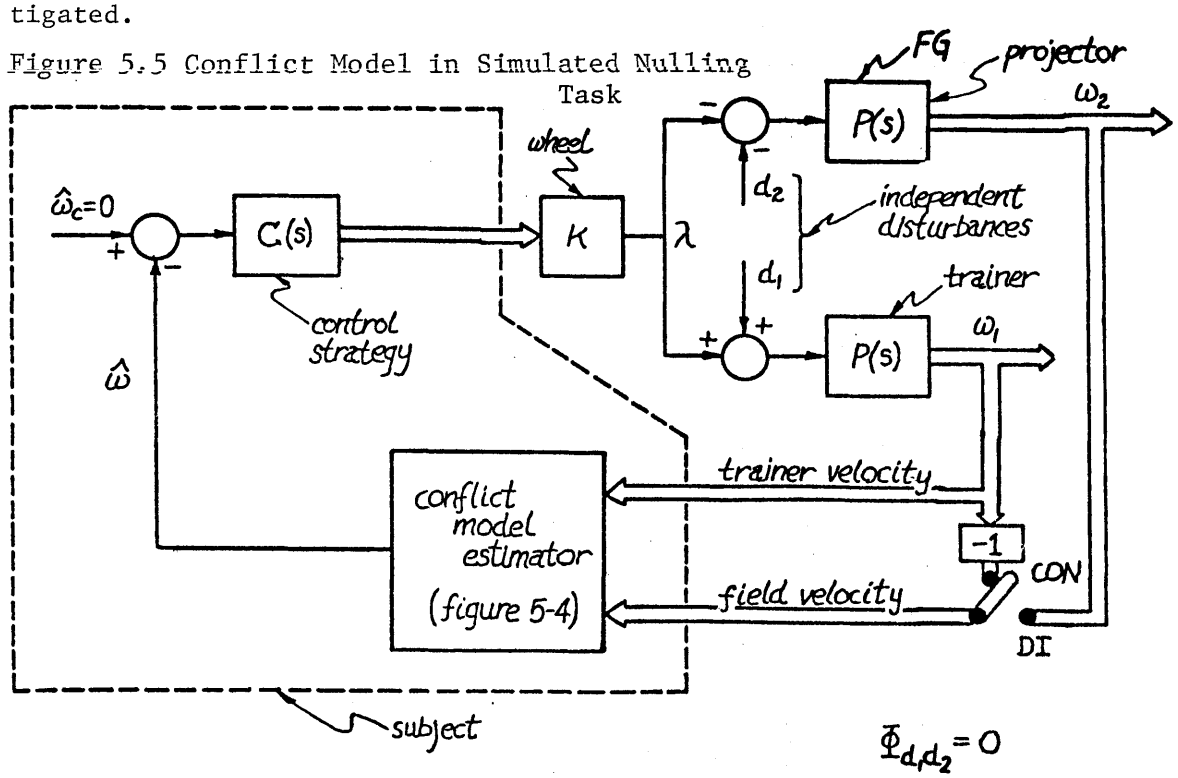

One final note regarding the simulation studies should be made. As is clear from the model diagram of figure 5.4, no provision is made for an estimator time delay operating on the velocity estimate output, although one could certainly argue for the presence of a delay by recalling the phase data discussion of the previous chapter (recall section 4.4.3). However, for simulation purposes, it is more convenient to assign the entire operator delay to the manual control block, C, and simply assume that velocity estimates are processed with a minimum computational delay. Thus, the open-loop responses to be discussed in the next section will not exhibit a delay term contribution, whereas the closed-loop responses will. Naturally, the net effect in the simulated closed-loop responses will be unaffected as to the controller/estimator allocation of dead-time, so that a complete allocation to the control block C will suffice for the model simulation studies. The particular delay time value appropriate to the experimental situation will be discussed further in section 5.2.3.

5.2.2 Open-Loop Step Response

Figures 5.6a through d show time histories of the model's response to simple open-loop visual and vestibular cues.

Figure 5.6a is the model's prediction of subjective response to a 5°/s step in angular velocity, with a subject-fixed visual field (FIX presentation). Although the response appears to be characterized by two exponentials, only the first portion is truly exponential, and is due to

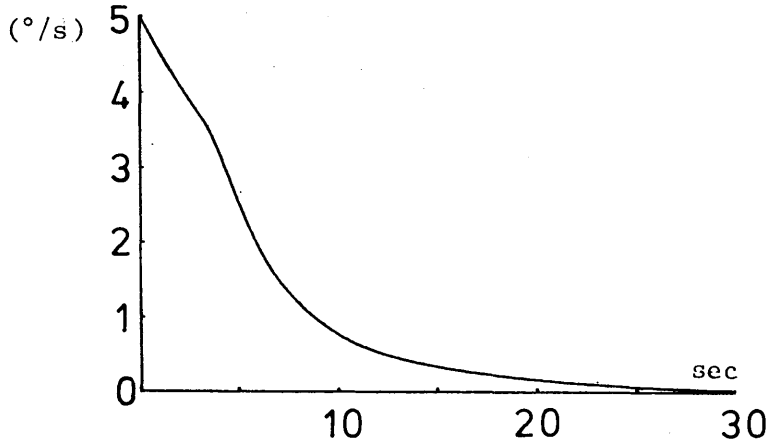

Figure 5.6a: Vestibular Step Response (FIX)

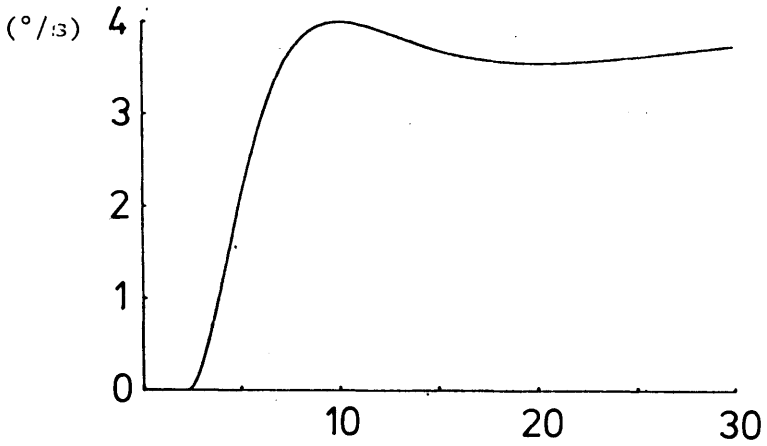

Figure 5.6b: Visual Step Response (CV)

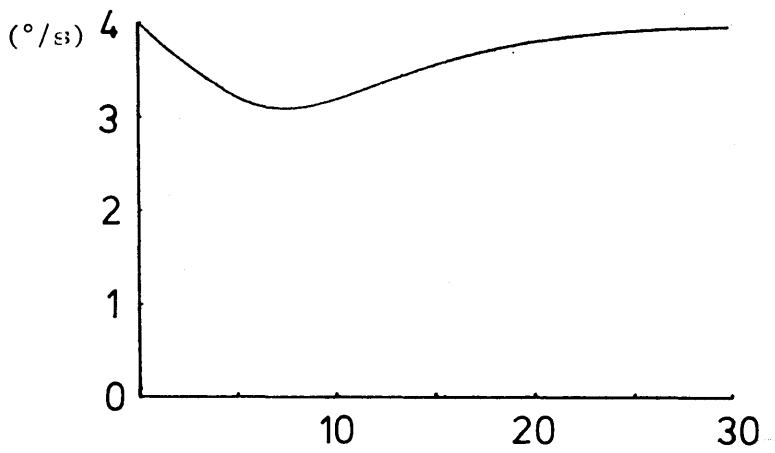

Figure 5.6c: Response to Visual and Vestibular Step (CON)

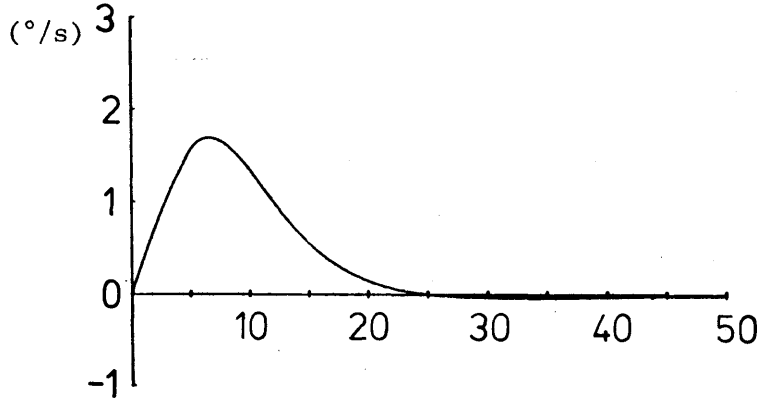

Figure 5.6d: Response to Visual Step and Vestibular Ramp

the fact that the canals provide the only information during the initial high conflict phase. As the conflict decreases with time, the null visual signal is weighted more heavily, and the response thus decays more rapidly.

Figure 5.6b shows model response to a left 4°/s step in visual field velocity, in the absence of confirming vestibular cues (CV presentation). Again, because of the initially high conflict level, the null vestibular cue is the basis for sensation resulting in the response latency seen. As the expected vestibular signal (ω^{exp} of figure 5.4) drops to zero and matches the actual null signal from the canals, the conflict lessens and the weighting on the visual cue increases to unity. The undershoot is caused by the adaptation operator acting on the conflict signal, temporarily increasing the conflict level.

Figure 5.6c shows the model response to confirming visual and vestibular velocity steps (CON presentation). Since this is a zero conflict situation, the initially large vestibular signal dictates that both cues be averaged, which results in a sensation drop-off due to the decaying canal response. As the vestibular signal grows smaller, however, the weighting emphasizes the DC visual cue, bringing the subjective response back to the true velocity level.

Figure 5.6d shows model response to a constant field velocity of 4°/s combined with a constant body acceleration of $0.4°/s^2$, both to the right. The initial response is due to the vestibular path, but is turned around as the oppositely-directed circularvection illusion takes hold. The conflict gradually decreases, because of the adaptation operator, but the vestibular signal remains at a constant level ($\tau\alpha \simeq 4°/s$), so that

in the steady state, both cues are averaged. Since they are of opposite sign, the net result is approximately zero sensation, and agrees with what is observed experimentally, under CV visual field conditions (recall section 2.4.2).

Figures 5.7a through c show similar response histories to input step magnitudes ranging between 1°/s and 5°/s.

Figure 5.7a illustrates vestibular step response, and shows how the apparent double exponential decay pattern disappears as the step magnitude drops below 2.5°/s. This is due to the fact that with smaller step inputs, cue conflict is smaller, which results in an earlier weighting of the null visual signal. Thus, the apparent simple exponential decay is, in actuality, a result of the weighting function shift to emphasize the visual channel information.

Figure 5.7b illustrates visual step response, parameterized against visual field velocity magnitude, and demonstrates how both response latency and rise time decrease with this magnitude. Again, as in the previous case, this is due to an earlier weighting of the constant velocity visual field information, as apparent cue conflict decreases with smaller step inputs. It is also appropriate to note the model's increasing undershoot with step magnitude, followed by eventual recovery. This is due to a temporary increase in the conflict signal magnitude, due to the action of the adaptation operator in processing the decaying exponential which characterizes the expected vestibular signal.

Figure 5.7c shows model response to confirming visual and vestibular

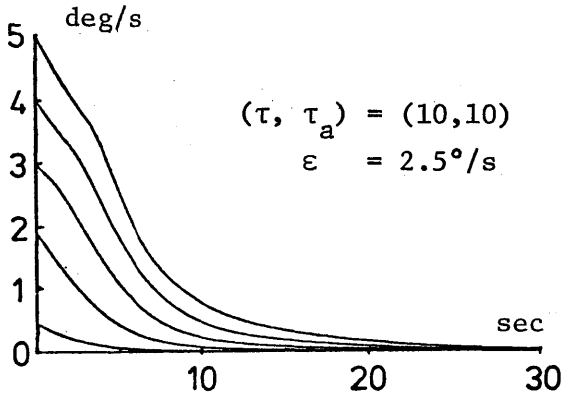

Figure 5.7a: Vestibular Step Response

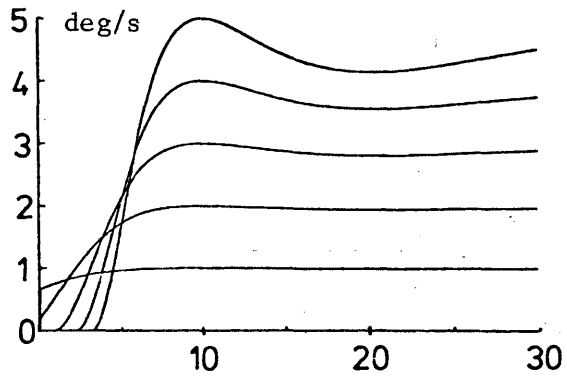

Figure 5.7b: Visual Step Response

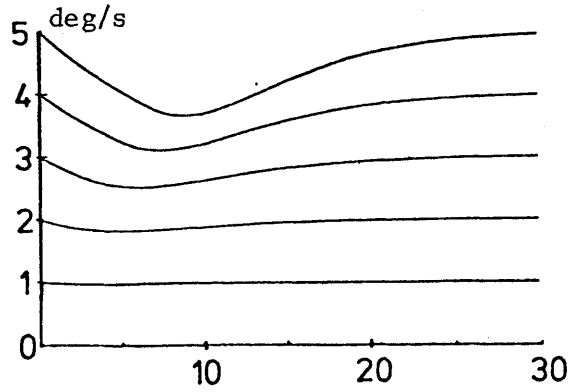

Figure 5.7c: Response to Visual and Vestibular Steps

velocity steps of varying magnitudes. As shown earlier, the rapid rise is due to the initial acceptance of the vestibular cue, and the steady maintenance of that sensation is due to the total gradual acceptance of the visual cue. The transition from one to the other, however, shows a more pronounced drop off as step magnitude increases. This is due to the visual path gain failing to rise sufficiently rapidly to offset the exponential decay of the vestibular signal. To see this, it is necessary to refer to the estimator diagram of figure 5.4 and recognize that the conflict signal, ω_{err}, remains zero throughout the confirming dual-cue presentation. Thus, the weighting gain is given by

$$K = \lambda + 1/2$$

However, λ ranges between zero and 1/2:

$$\lambda: 0 \rightarrow 1/2$$

so that the two path gains range in a complementary fashion:

$$K_{vis}: \quad 1/2 \rightarrow 1$$

$$K_{ves}: \quad 1/2 \rightarrow 0$$

over the course of the dual-cue presentation. Since the vestibular gain drops to zero, the decaying vestibular signal provides a rapidly diminishing contribution to overall estimator output, a contribution which is not adequately offset by increasing step magnitudes, since this transition period is proportional to the time it takes for the vestibular signal to decay to zero.

With the above reservations in mind, it would appear that the conflict model provides reasonable matches to subjective response dynamics, in simple open-loop cue presentation situations. Additional transient

response characteristics will be addressed later; for now, however, it is of interest to examine the model's ability to fit the cue mixing data obtained from the closed-loop nulling experiments of the last chapter.

5.2.3 Closed-Loop Response

Digital simulation of model response was conducted to evaluate model predictions when placed in a simulated closed-loop velocity-nulling task, as illustrated in Figure 5.5. Simulations were conducted for one period of the disturbance input (T = 128 s), and the simulated trainer velocity, visual field velocity, and control wheel deflections were stored throughout the run for later processing. This allowed for plotting of the response histories, and for additional frequency response measures.

Frequency analysis of the simulated response histories was conducted in exactly the same manner as was used in the processing of the experimental data. That is, the three stored response histories (λ, ω_1 and ω_2) were processed by the same digital programs, which calculated the overall operator describing function relating control output to velocity cue inputs, and which were described earlier in Section 4.3.2. Thus, for simulated CON presentations, the describing function CE was calculated from model response, whereas for the DI presentations, CE_1 and CE_2 were calculated. To eliminate the human operator transfer function, C, from the response data, gain and phase were calculated from (5.1) and subtracted from the overall input-output data inferred from the model, to arrive at estimates of E, for the CON presentations, and of E_1 and E_2 for the DI presentations. This computational approach thus allows for a direct

comparison of the estimator functions calculated from the experimental data with those associated with the simulated closed-loop model response.

This section will discuss the results of the simulation runs conducted, in an effort to provide some motivation for model parameter choice, and response senstivity to parameter variations. The following sections will interleave time histories with frequency domain results, to provide insight as to the non-linear model's response characteristics.

5.2.3.1 Choice of Model Delay Time

The issue of delay time assignment was addressed earlier, and it was noted that in the closed-loop simulation studies, it is computationally more convenient to allocate all of the delay time to the control block, C. Of interest now is the particular value assigned to the delay time parameter, τ_d. From the human operator experimental results described in section 4.4.3, it was shown that a value of 0.41 s provided a reasonable fit to the phase data, and thus might be considered a manual control delay typifying the visual field velocity-nulling task. From the inferred estimator describing function data obtained under counterrotating field conditions, it was noted in the previous chapter that the estimator delay time is effectively zero (recall figure 4.10); thus, an appropriate value for τ_d under CON presentation conditions would appear to be approximately 0.4 s.

Under the dual-input (DI) presentation conditions, the additional lag in estimating self-velocity, and acting on it, is evident from the estimator phase plots for E_1 and E_2 given in figures 4.11 and 4.12. For the

vestibular channel (E_1), a delay time of 0.20 s is indicated, whereas for the visual channel (E_2), a longer delay of 0.29 s is indicated. Since we have decided to consolidate these delays as part of the control function, an appropriate value for τ_d under DI presentation conditions would appear to be 0.65 s, a value approximately equalling the average of the estimator delays summed with the manual control delay of 0.4 s. Clearly, this is an approximation which ignores interchannel differences, but would appear to be not unreasonable, in light of the phase data spread of figures 4.11 and 4.12.

Thus, for the simulations presented below, a delay time of 0.4 s is used for the CON presentations, and a delay of 0.65 s is used for DI presentations.

5.2.3.2 Response with Nominal Loop Gain

Shown in figure 5.8 are model response histories obtained under counterrotating field conditions (CON), in which field velocity is the negative of trainer velocity, so that the estimator is provided with non-conflicting motion cues. The nominal manual control gain is used ($K_C = 1.8\ s^{-1}$), and it is evident that this relatively high value results in a tendency for some oscillatory behavior in the trainer velocity, ω_1, although peak values remain below approximately 2°/s. A comparison with the experimentally obtained history of figure 2.3a shows larger peak excursions, although both the model and the actual data show that a zero mean trainer velocity is maintained throughout the presentation, an expected result in the absence of any internally modelled vestibular bias

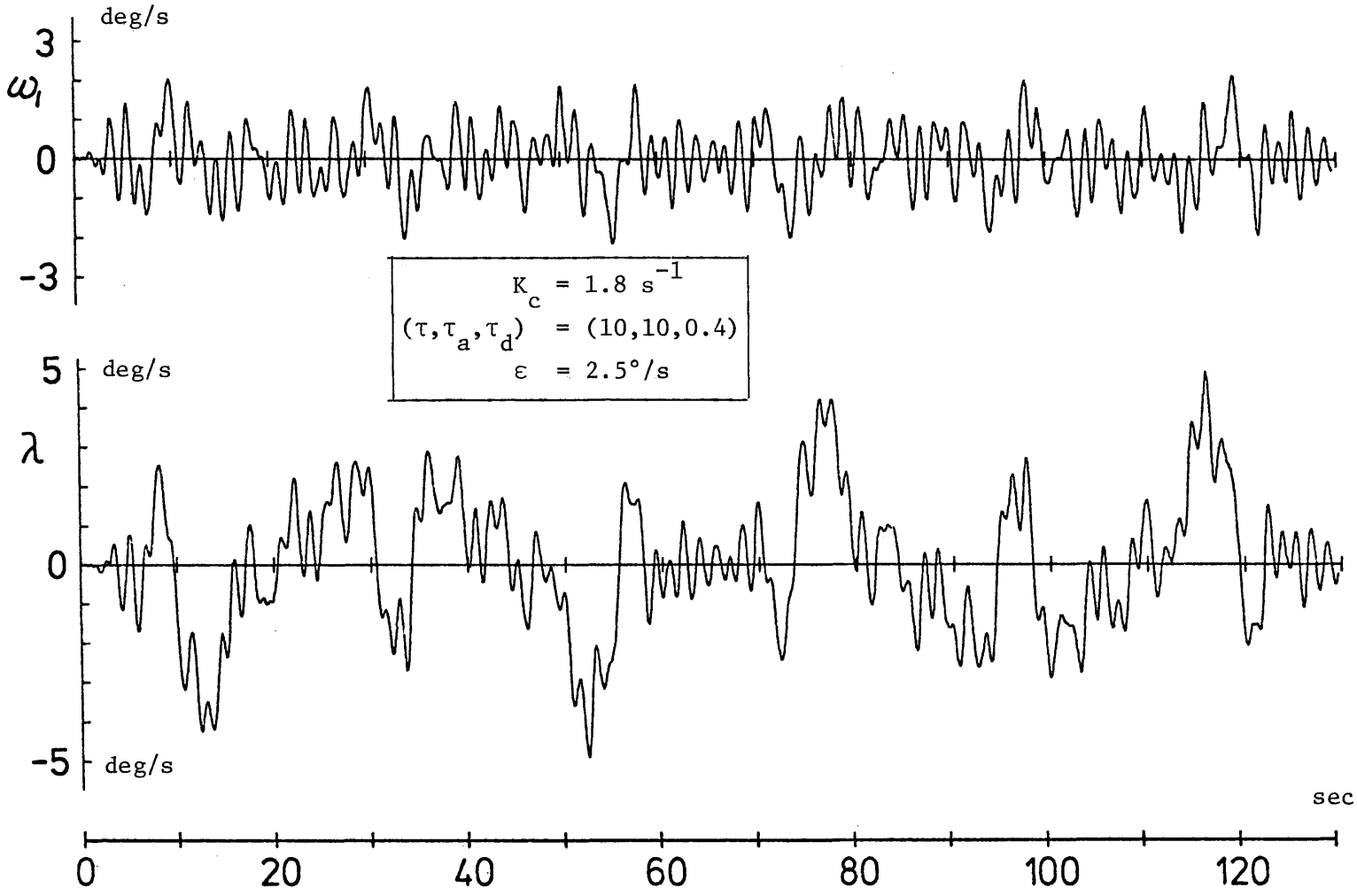

Figure 5.8: Model Response with Counterrotating Field (CON; nominal parameter values).

(recall the discussion of section 2.4).

Figure 5.9 provides for a direct comparison of the model's frequency response inferred from the simulation, with the experimentally derived estimator data discussed earlier in Chapter 4 and repeated here from figure 4.10. The open circles indicate model response, while the bars indicated measured data. From the amplitude ratio data, it should be clear that the model's gain is too high. It may be recalled that a curve fit of a simple gain to the experimental data resulted in a DC gain value of -3.5 dB (see figure 4.10), and this would appear to be approximately the amount by which model gain exceeds the experimental gain.

A more dramatic indication of an inappropriately high gain is provided by a simulation of model behavior under DI conditions, using the longer delay time of 0.65 s and a control gain of 1.8 s^{-1}. Shown in figure 5.10 are the time histories from such a run; the divergent amplitude coupled with the approximately constant limit cycle frequency suggests that the high gain and long dead time is an inappropriate combination if we are to ensure loop stability.

A prediction of the divergent oscillation frequency can be made from a fairly simple, though approximate, linear analysis of the loop dynamics. If we assume a divergent response, then the control response λ will be large with respect to either of the disturbances, d_1 and d_2. From the loop diagram of figure 5.5, this implies that field velocity will be approximately the negative of trainer velocity ($\omega_2 \simeq -\omega_1$), so that the conflict estimator model will be presented with corroborating motion cues. From the model diagram of figure 5.4, this implies that the weighting gain

Figure 5.9: Model Frequency Response with Counterrotating Field (CON; nominal parameter values)

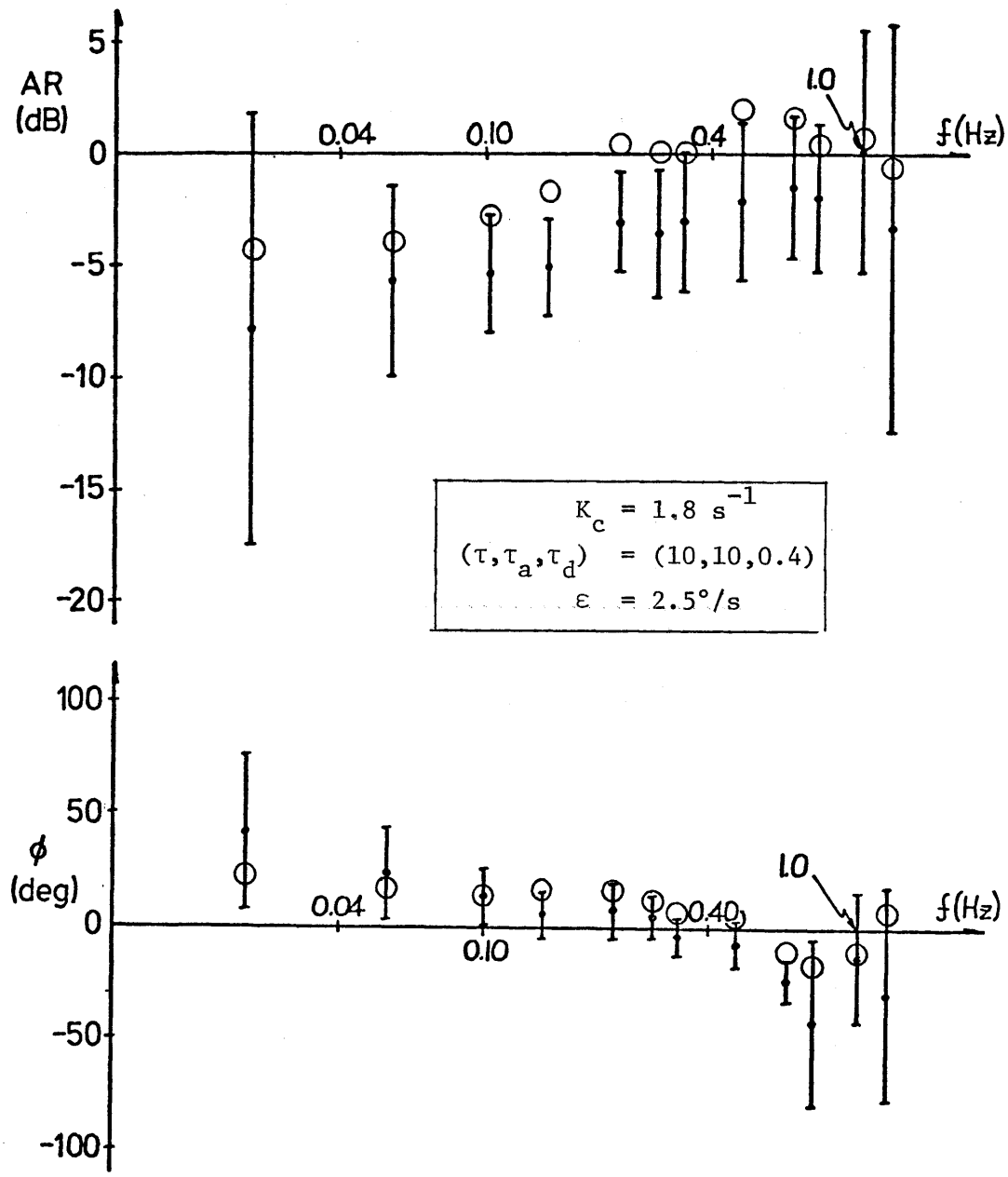

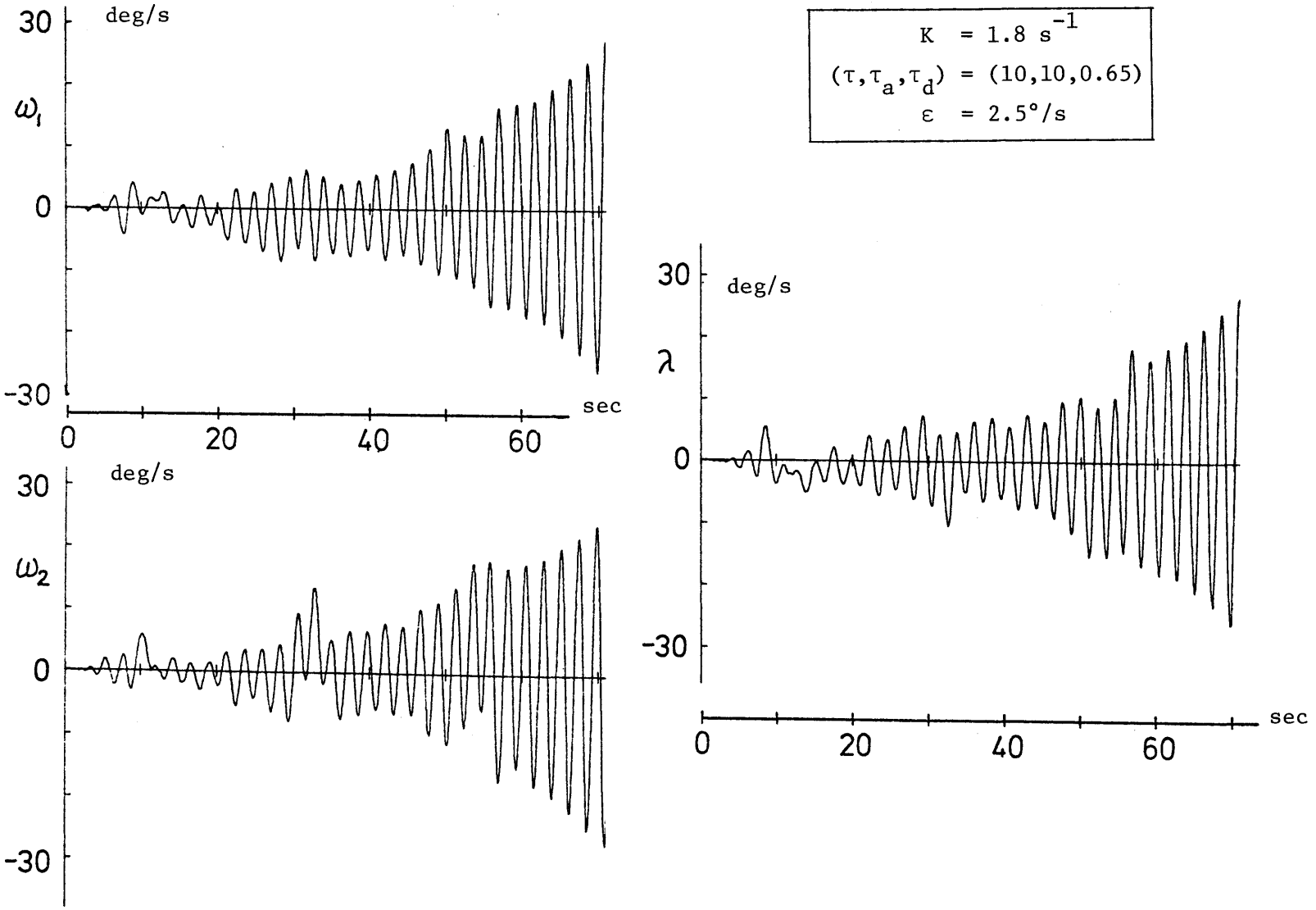

Figure 5.10: Model Response in Dual-Input Nulling Task (DI; nominal parameter values).

K will equal 1/2, since the vestibular signal ω_1 is presumed large. Thus, estimator output can be approximated as a linear function of trainer velocity:

$$\hat{\omega} = \frac{1}{2}((2\tau s+1)/(\tau s+1))\omega_1 \tag{5.5}$$

so that, from the loop diagram of figure 5.5, the control law definition of (5.1) and the plant dynamics of (5.3), the following closed-loop transfer function results, relating actual trainer velocity ω_1 to the commanded velocity, ω_c:

$$\omega_1/\omega_c = PC/(1 + PCE) \tag{5.6}$$

where the open-loop transfer function is given by:

$$PCE = \left(\frac{K_c\omega_n^2}{2}\right)\left(\frac{1}{s}\right)\frac{(\tau_c s+1)(2\tau s+1)}{(\tau s+1)(s^2+2\zeta_n\omega_n s+\omega_n^2)}e^{-\tau_d s} \tag{5.7}$$

Bode plots defining the open-loop transfer function PCE are given in figure 5.11, obtained by using the relation just derived, in conjunction with the parameter values used in the divergent simulation of DI response. What should be clear from the figure is the greater than unity gain at the phase crossover frequency of 0.43 Hz. Thus, an assumption of divergence and an approximate linear analysis leads to a prediction of a model limit cycle frequency of 0.43 Hz. A spectral analysis of the divergent response histories of figure 5.10 shows the fundamental frequency component to be 0.43 Hz, within the frequency resolution (Δf = 0.008 Hz) imposed by the sample duration (T = 128 s).

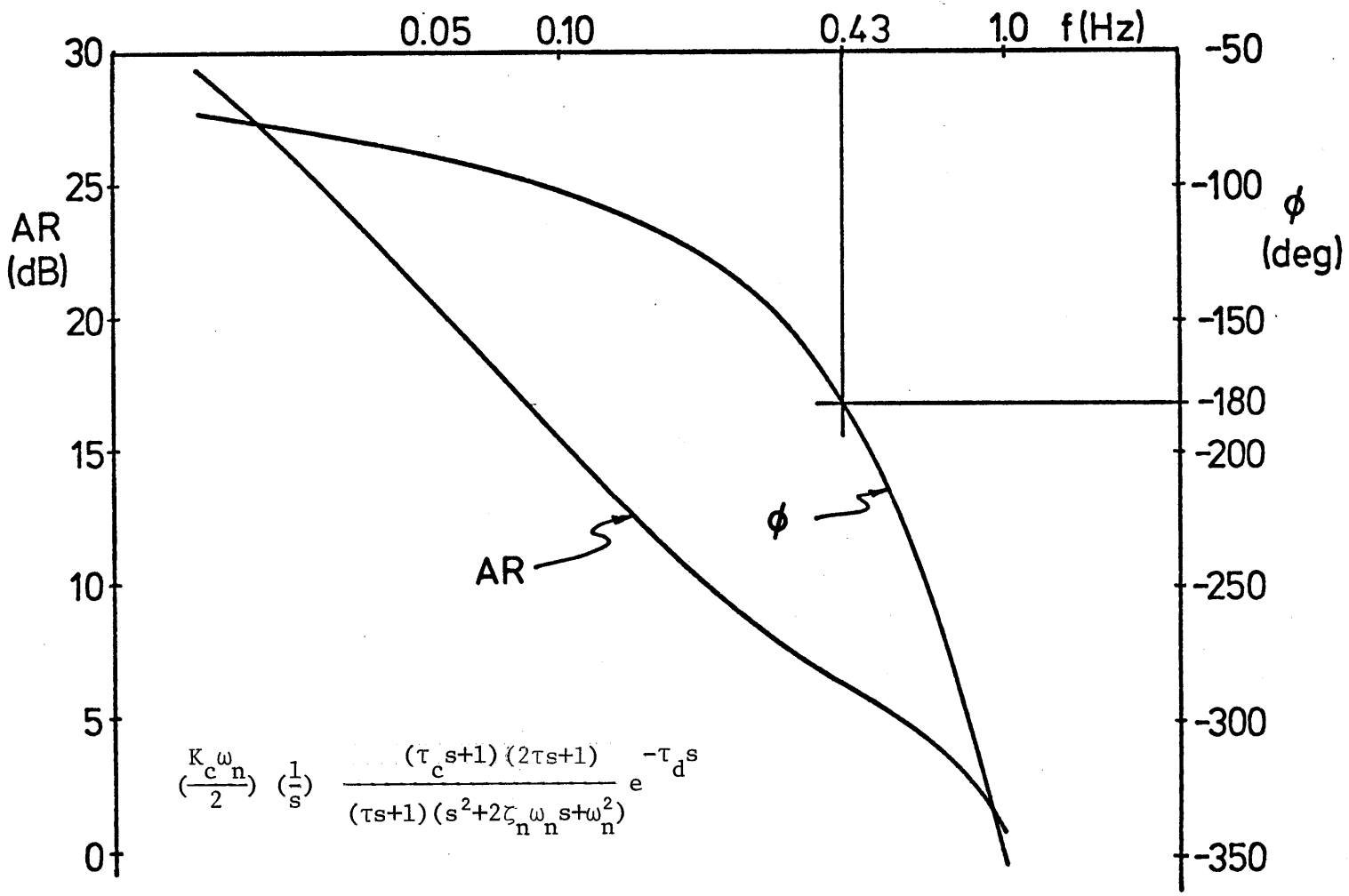

Figure 5.11: Bode Plots for Open-Loop Transfer Function PCE.

5.2.3.3 Response with Lowered Loop Gain

With the simulated response under CON field conditions suggesting a gain which is 3.5 dB too high, and with the divergent response obtained under DI field conditions, it is appropriate to investigate model behavior with a lowered loop gain. Earlier, in section 4.5.1, it was argued that it is not unreasonable to assign a lower gain to the human operator block, because of the difference in task difficulty between nulling visual field velocity and nulling self-velocity. This section will thus describe simulated model response while part of a lower gain loop, effected by a drop in the manual control gain K_c.

Shown in figure 5.12 are model response histories obtained under counterrotating field conditions (CON), from a simulation in which the control gain was dropped by 3.5 dB, from 1.8 s^{-1} to 1.2 s^{-1}. Again, the estimator is presented with non-conflicting motion cues, but since the control is not as tight, the trainer velocity exhibits larger peak excursions in this lowered gain case, when compared with the response histories of figure 5.8. What should also be clear is that the lowered gain results in considerably less oscillatory behavior, suggesting a greater phase margin in the equivalent linear system.

Figure 5.13 illustrates the inferred frequency response of the estimator operating in this lower gain environment. Again, the experimentally derived data is also presented, for direct comparison. What should be clear is that the model provides a considerably better fit to the gain data, in terms of fitting both the low frequency gain, and the gain variation with increasing frequency. The fit might be improved

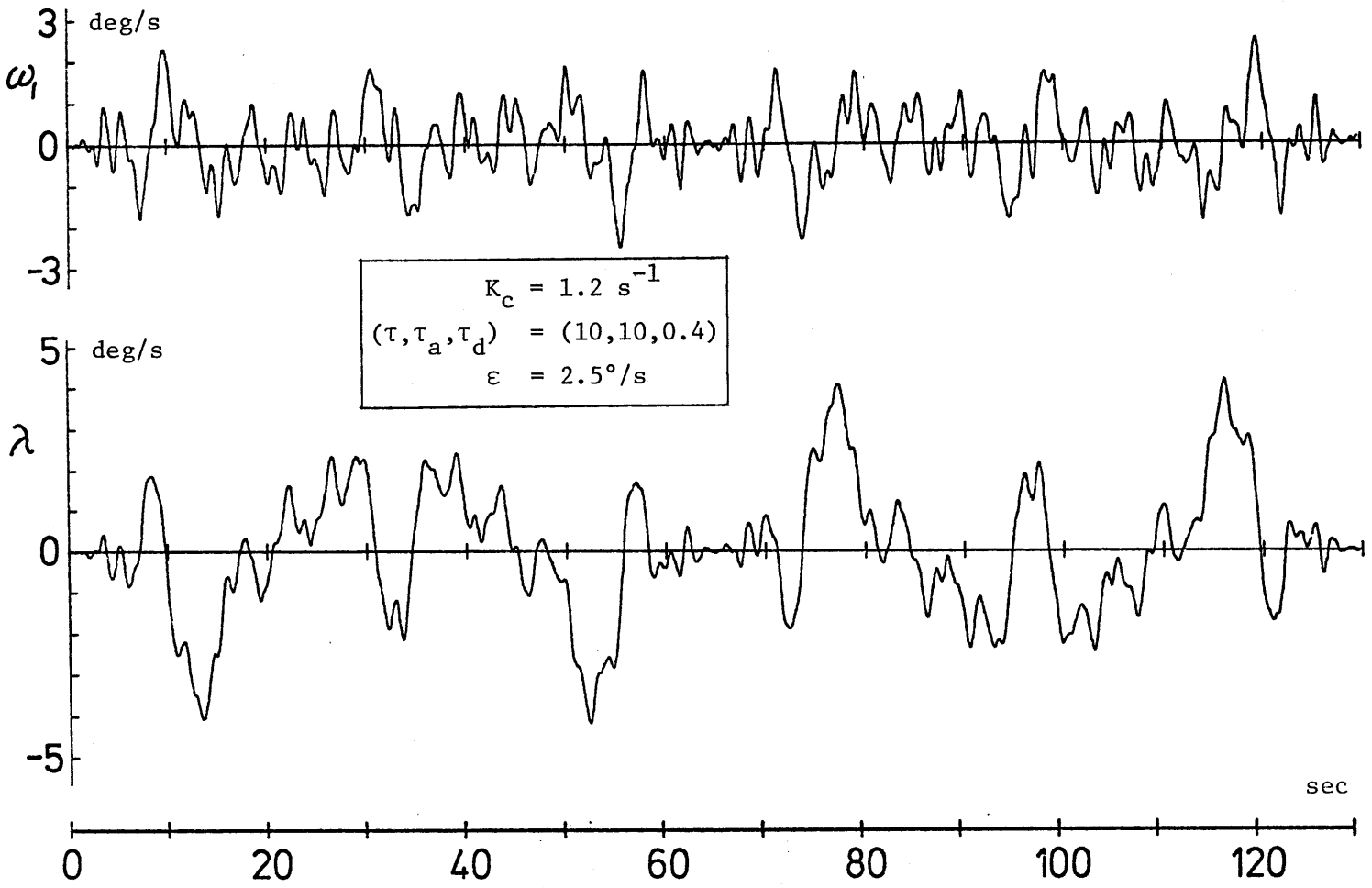

Figure 5.12: Model Response with Counterrotating Visual Field (CON; lowered gain).

Figure 5.13: Model Frequency Response with Counterrotating Field (CON; lowered gain)

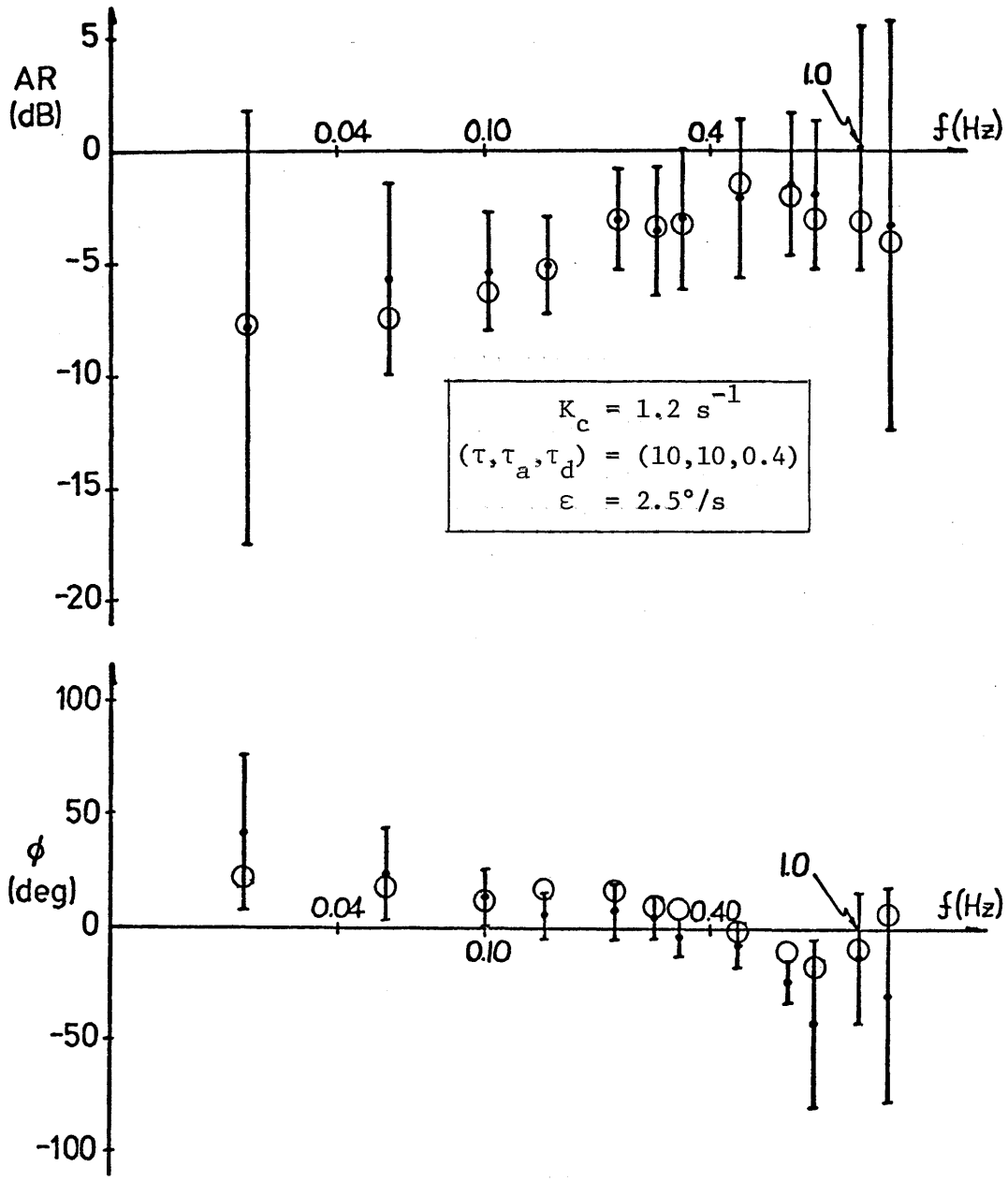

upon by varying the control gain slightly, but this has not been done, since the primary objective here is to illustrate how model response in a simulated closed-loop environment can mimic the experimentally derived velocity-nulling data trends. It is also worth noting the phase fit of figure 5.13, in which the model mimics both the observed low frequency lead and the relatively small increase in phase lag with increasing frequency. This correspondence between model and observed response, under counterrotating field conditions, suggests that the lowered control gain is an appropriate modification to the model parameter choice made earlier in this chapter. It is now of interest to consider how this gain change affects model response under dual-input conditions.

Model response,under DI conditions and with a lowered control gain, is shown in figure 5.14. In contrast to the divergence seen earlier, the loop is now quite stable, although the peak trainer velocity excursions are larger than those seen under CON conditions (compare with figure 5.12). This, of course, might well be expected, since the two motion cues are non-corroborating. Of more interest, however, is the frequency response data to be inferred from these simulated histories.

Shown in figure 5.15 are the amplitude ratios for both the vestibular and visual estimator functions (E_1 and E_2 respectively), with the model response data superimposed upon the dual-input data derived from the experiment of the previous chapter, and repeated from figures 4.11 and 4.12. As may be seen, the major data trends are reasonably well-followed by the simulated model response. In particular, the 10 s vestibular time constant used in the model is transformed to an effective one-second time

Figure 5.14: Model Response in Dual-Input Nulling Task
(DI; lowered gain)

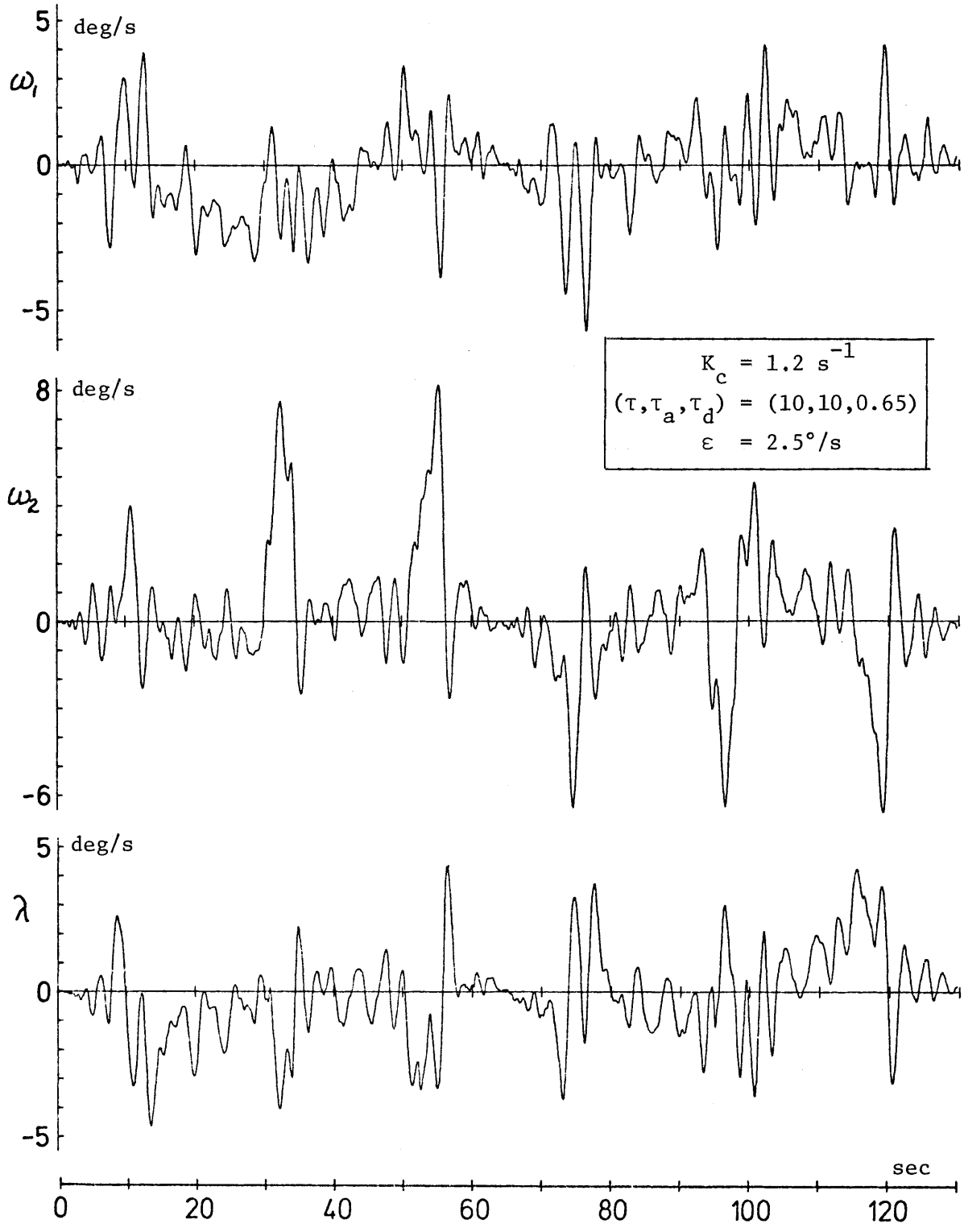

Figure 5.15: Model Frequency Response in Dual-Input Nulling Task (DI; lowered gain)

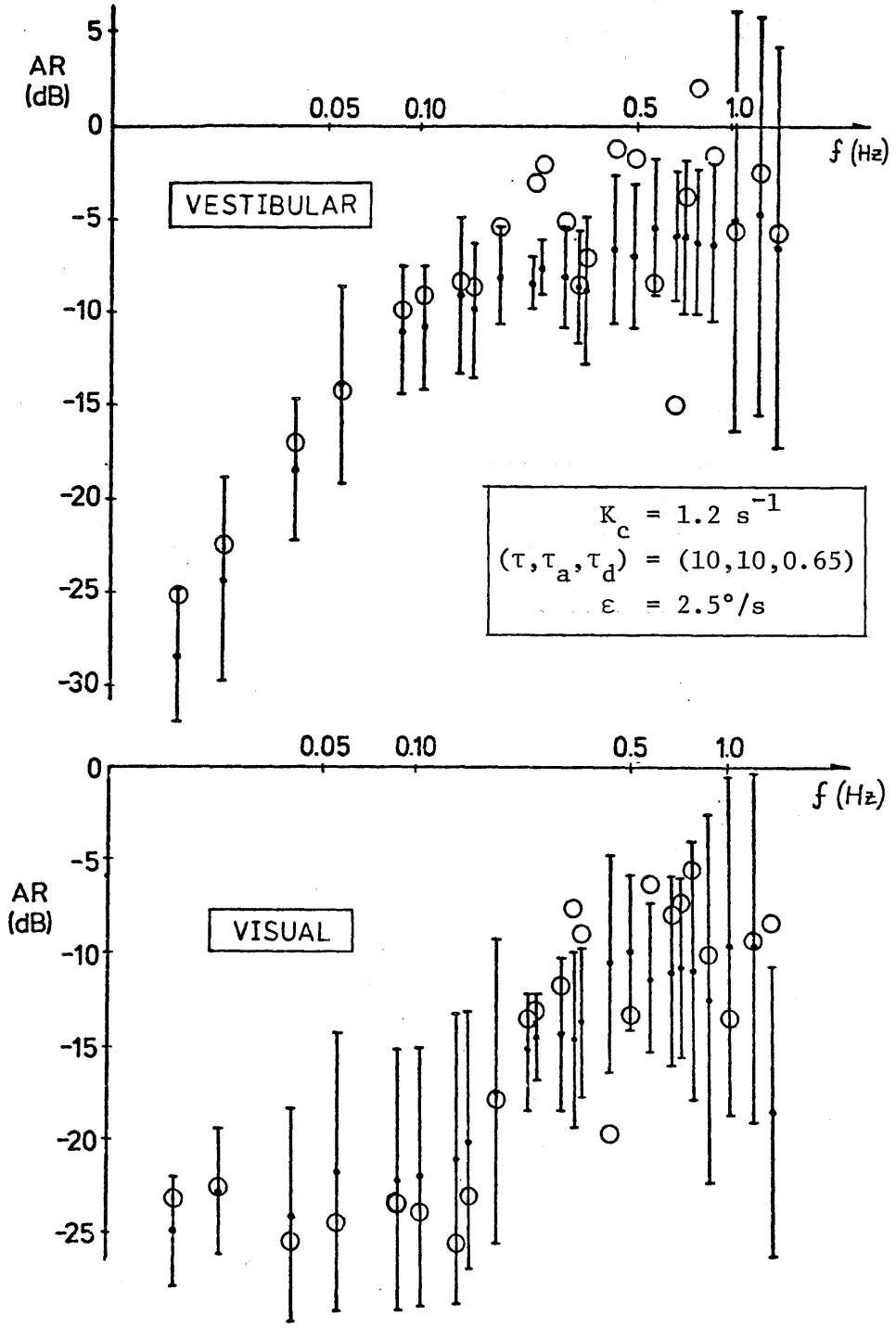

constant by the conflicting visual cues. Similarly, conflicting vestibular cues effectively drop the unity gain used in the model's visual channel, by 25 dB at low frequencies; at higher frequencies, the conflict lessens because of the decreased magnitudes of the loop disturbance (recall the amplitude spectra defined in Appendix A), and the visual gain rises correspondingly. This gain rise thus need not be attributed to a high frequency visual lead term, a term which would be required by a linear model and one which is inconsistent with our knowledge of circularvection response.

The conflict model thus provides a means of fitting the experimentally derived results obtained from the dual-input nulling task, while maintaining consistency with the results of single cue experiments. A comparison with the earlier linear system fit illustrated in figures 4.11 and 4.12, in which a high break frequency washout was used for the vestibular channel and a low gain lead-lag was used for the visual channel, makes it clear that the conflict model does a poorer job of fitting the experimental data, in terms of minimizing residual fit error. However, since the linear model is fundamentally untenable from the discussion concluding the previous chapter, this only suggests that there is room for improvement in the choice of parameter values to be used with the non-linear conflict model estimator.

An improvement in the vestibular channel fit may be made by dropping the control gain K_c by an additional 2.5 dB, so that it is reduced by 6 dB from its originally proposed value of 1.8 s^{-1}. The resulting amplitude ratios for both channels are shown in figure 5.16,

Figure 5.16: Model Frequency Response in Dual-Input Velocity Nulling Task (DI; gain halved)

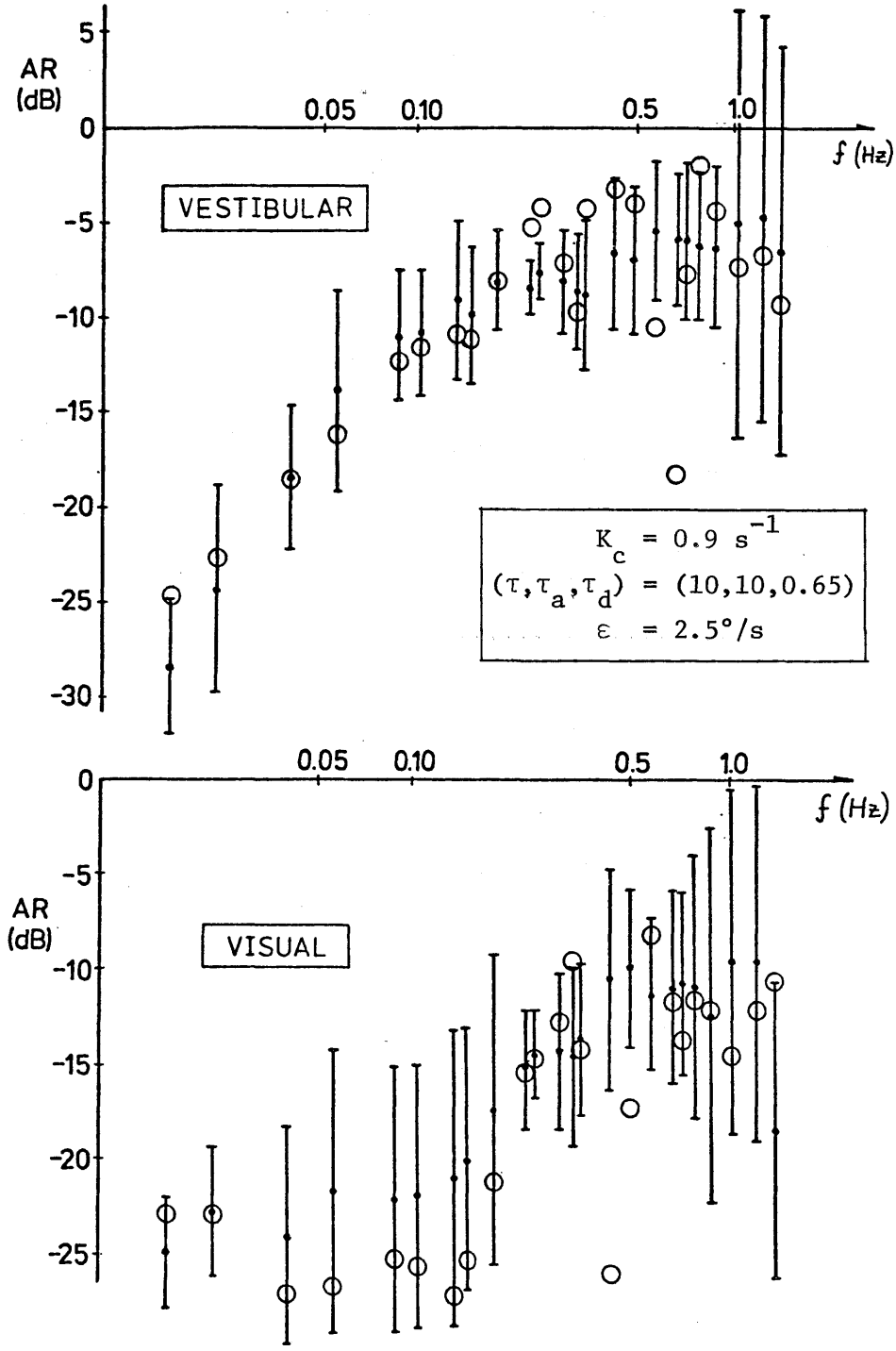

where, as in the case just discussed, the gain trends are still matched by the model response. Here, however, the measured vestibular gain of approximately -6 dB at the high frequency end is better matched by the simulated model response. This is, however, at the expense of a poorer match of the visual channel data, as may be seen by comparing the model response from both figures 5.15 and 5.16.

5.2.3.4 Response with Shorter Adaptation Time

From the model description given earlier, it should be apparent that a large amplitude conflict signal (recall ω_{err} of figure 5.4) will result in a heavy weighting of vestibular cues by the model, in preference to any visual motion cues which may be available. The results of the previous simulation suggests that this balance point be shifted slightly, in favor of visual channel information, and there are two ways of accomplishing this: expansion of the conflict threshold ε, or diminution of the adaptation time τ_a. The former makes the conflict signal smaller relative to the model's conflict standard, while the latter results in a more rapid attenuation of any steady-state or low frequency conflict between channels. Since the major discrepancy between model response and the experimental data occurs in the low frequency visual channel gain (figure 5.16), then it is appropriate to consider the effect of lowering the adaptation time constant, τ_a, on model response.

Figure 5.17 shows the calculated dual-channel gains associated with the closed loop behavior of the model simulated in the dual-input nulling

Figure 5.17: Model Frequency Response in Dual-Input Nulling Task
(DI; adaptation time constant halved)

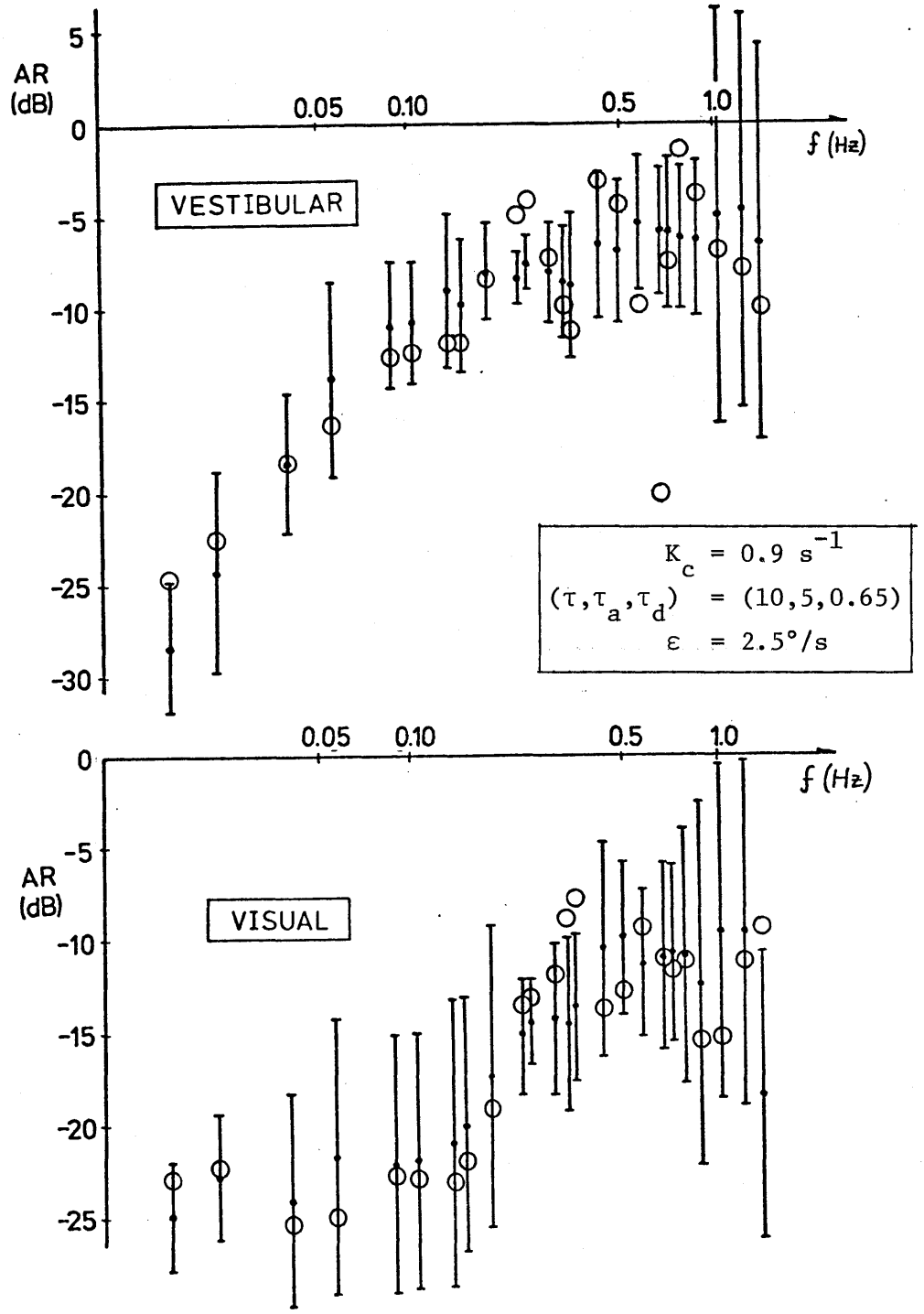

task, with the adaptation time constant halved, from 10 s to 5 s. A comparison with the model response shown in figure 5.16, in which the adaptation time is 10 s, reveals little change in the vestibular channel gain $|E_1|$; however, the visual channel gain fit is improved at low and mid-frequencies by a general gain increase due to the incorporation of a reduced adaptation time. Further reduction in the value assigned to τ_a results in additional visual channel gain increases, to the detriment of the model fit illustrated in figure 5.17. As in the case of the loop gain variations described in the previous section, a more finely-grained parameter search could be instituted to optimize the choice of τ_a, but this has not been done, as the main objective here is to demonstrate how the conflict model can fit the dual-input data with parameter choices based on fairly simple arguments, augmented with parameter value changes motivated by data fitting accuracy.

Since the model's adaptation operator acts only on the internal conflict signal ω_{err}, and since counterrotating visual field conditions give rise to zero conflict at all times, the proposed change in the adaptation time constant has no effect on model predictions for subject velocity-nulling under CON presentation conditions. Thus, the model predictions presented previously in figure 5.13 remain unchanged for the current choice of τ_a.

5.2.3.5 Response with Variations in Threshold Magnitude

It was noted above that the relative emphasis between visual and vestibular cues could also be directly affected by the magnitude of the

conflict threshold parameter, ε. By doubling its originally proposed 2.5^{o}/s value, a given cue conflict magnitude becomes less inhibitory of visual channel information, and one would expect an overall increase in visual channel gain, when measured in a simulated dual-input nulling task. Shown in figure 5.18 are the computed channel gains for just this case. A comparison with the corresponding predictions of figure 5.17, in which the conflict threshold is half as large, shows that the most significant changes occur in the visual channel. A general gain rise across frequency is evident, with the largest increase at low frequency, where the disturbances are larger and where one would expect the most conflict to exist. Needless to say, the model fit is significantly poorer because of this visual cue amplification by the choice of a large threshold value.

The converse effect also holds true: assigning a small value to the conflict threshold parameter results in visual channel attenuation. This is shown in figure 5.19, in which ε takes on the value of 1^{o}/s. Again, most of the effect is seen in the visual channel, the exceptionally low gains being due to the small conflict threshold effectively gating out most of the visual channel information.

As in the case of the parameters discussed earlier, no attempt has been made to minimize the model fit error by careful selection of the threshold size. It should be evident from the discussion just given that the 2.5^{o}/s value appears to be a reasonable value in terms of fit accuracy, since bracketing values of 1°/s and 5°/s result in significantly poorer model fits. Thus there would appear to be no strong justification for

Figure 5.18: Model Frequency Response in Dual-Input Nulling Task (DI; conflict threshold doubled)

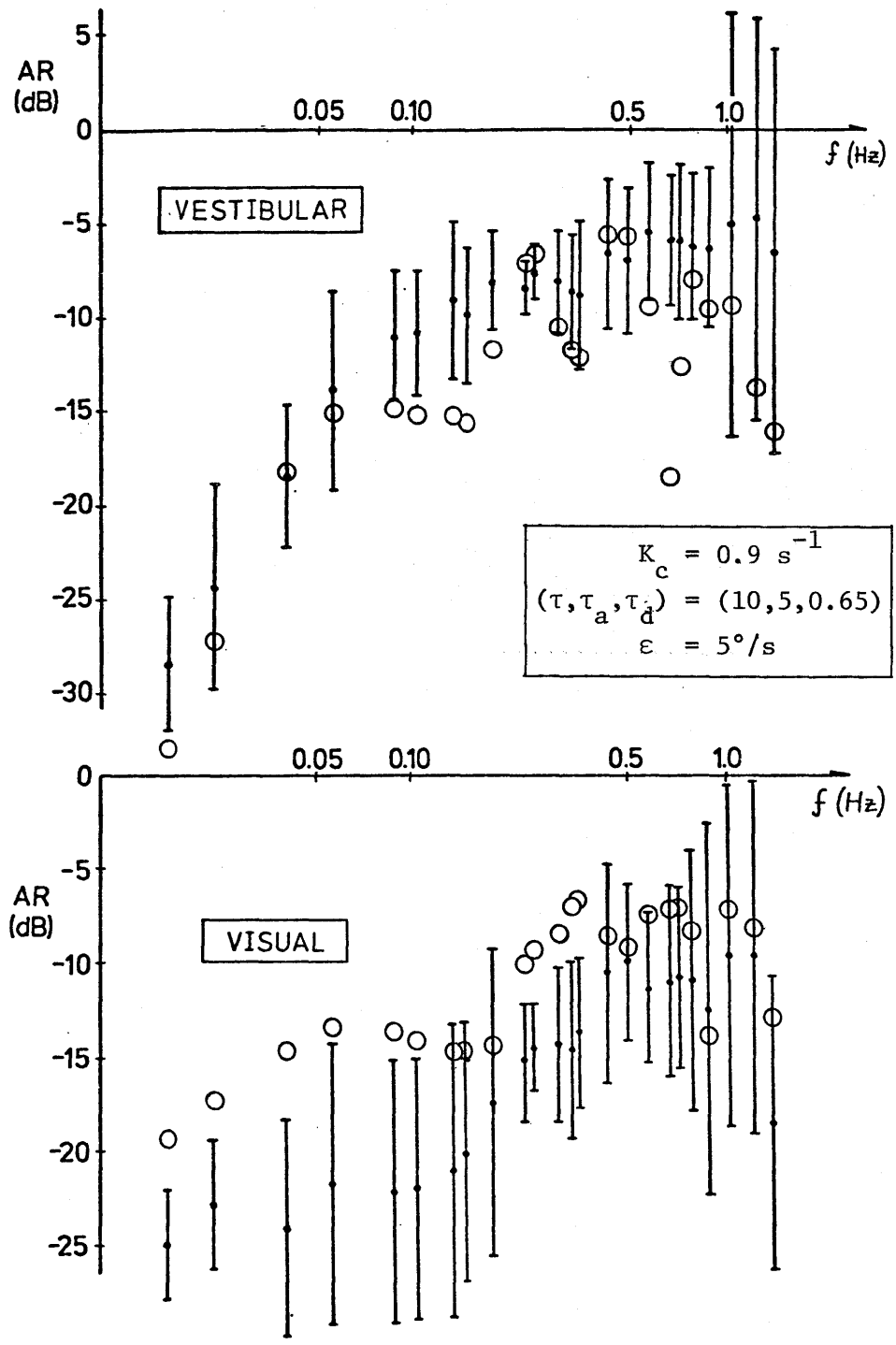

Figure 5.19: Model Frequency Response in Dual Input Nulling Task (DI; conflict threshold halved)

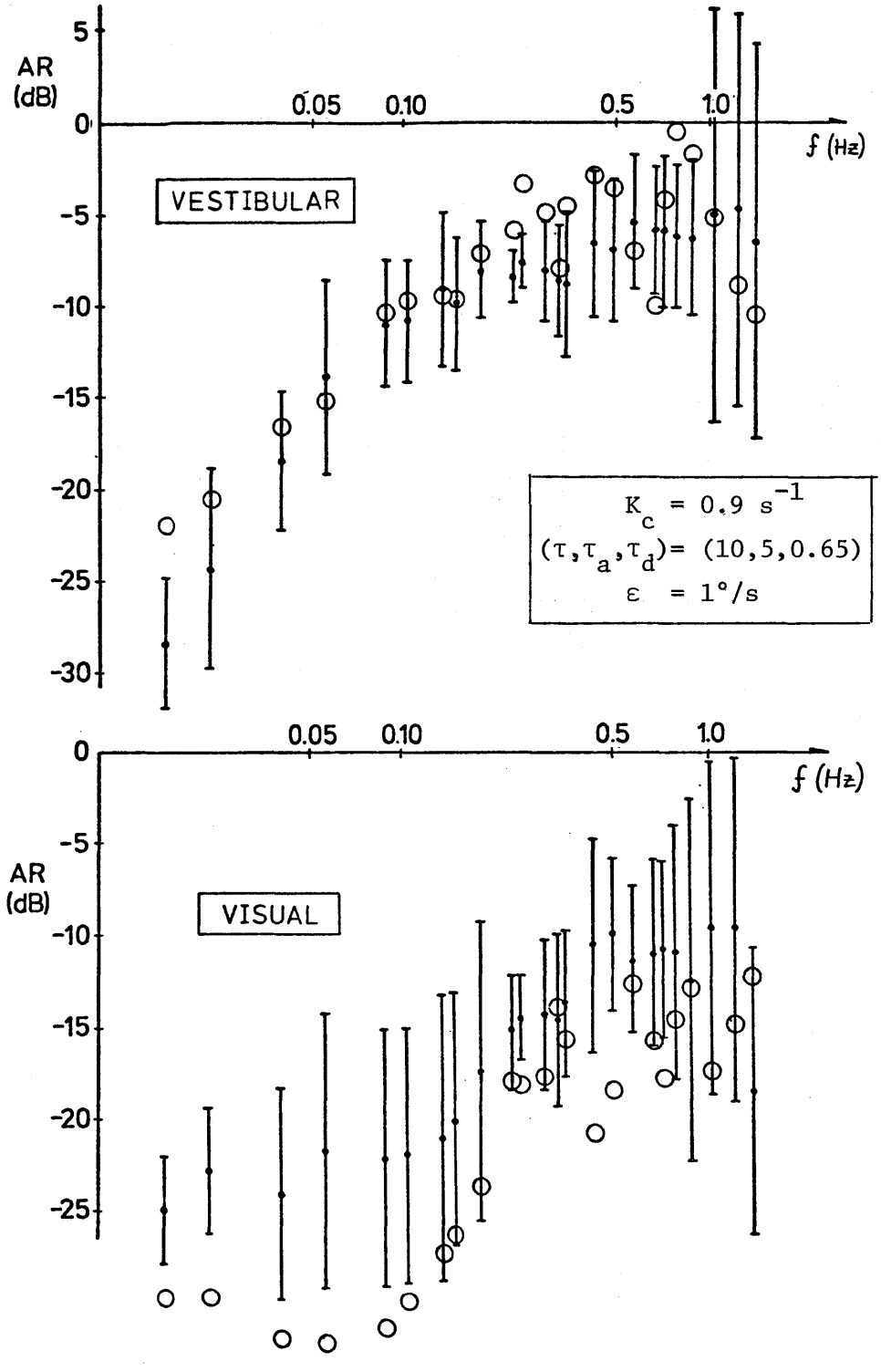

suggesting that the originally proposed 2.5°/s value for ε be changed.

5.2.3.6 Phase Dependence on Delay Time

To this point, the model's ability to match the dual-input velocity-nulling data has been based on fitting gain trends, and the question of phase data fitting has not been addressed. Shown in figure 5.20 is the experimental phase data for both visual and vestibular channels, repeated from figures 4.11 and 4.12, and the superimposed model response, using the same simulation parameters used to generate the gain results of figure 5.17. In general, it might be noted that the phase match between the model and data is not as close as the gain match. In the vestibular channel, the model fails to predict the low-frequency lead evident in the experimental results and compounds the fit discrepancy by predicting an excessive lag at the high-frequency end. In the visual channel, the model agrees with the approximately zero lead at low frequency, but again predicts excessive lag at the upper frequencies.

The high frequency phase mismatch in both channels can be readily alleviated by reducing the delay time constant τ_d. For the results shown in figure 5.20, a value of 0.65 was used, based on the parameter selection arguments presented at the beginning of this section. No constraints are violated, however, by reducing this value, and shown in figures 5.21a and 5.21b are the model predictions with a reduced delay time of 0.50 s. As might be expected, this change has little effect on the predicted gain behavior with frequency, as a comparison with the corresponding results of figure 5.17 will show. The major effect is in the model's improved

Figure 5.20: Model Phase Response in Dual-Input Nulling Task

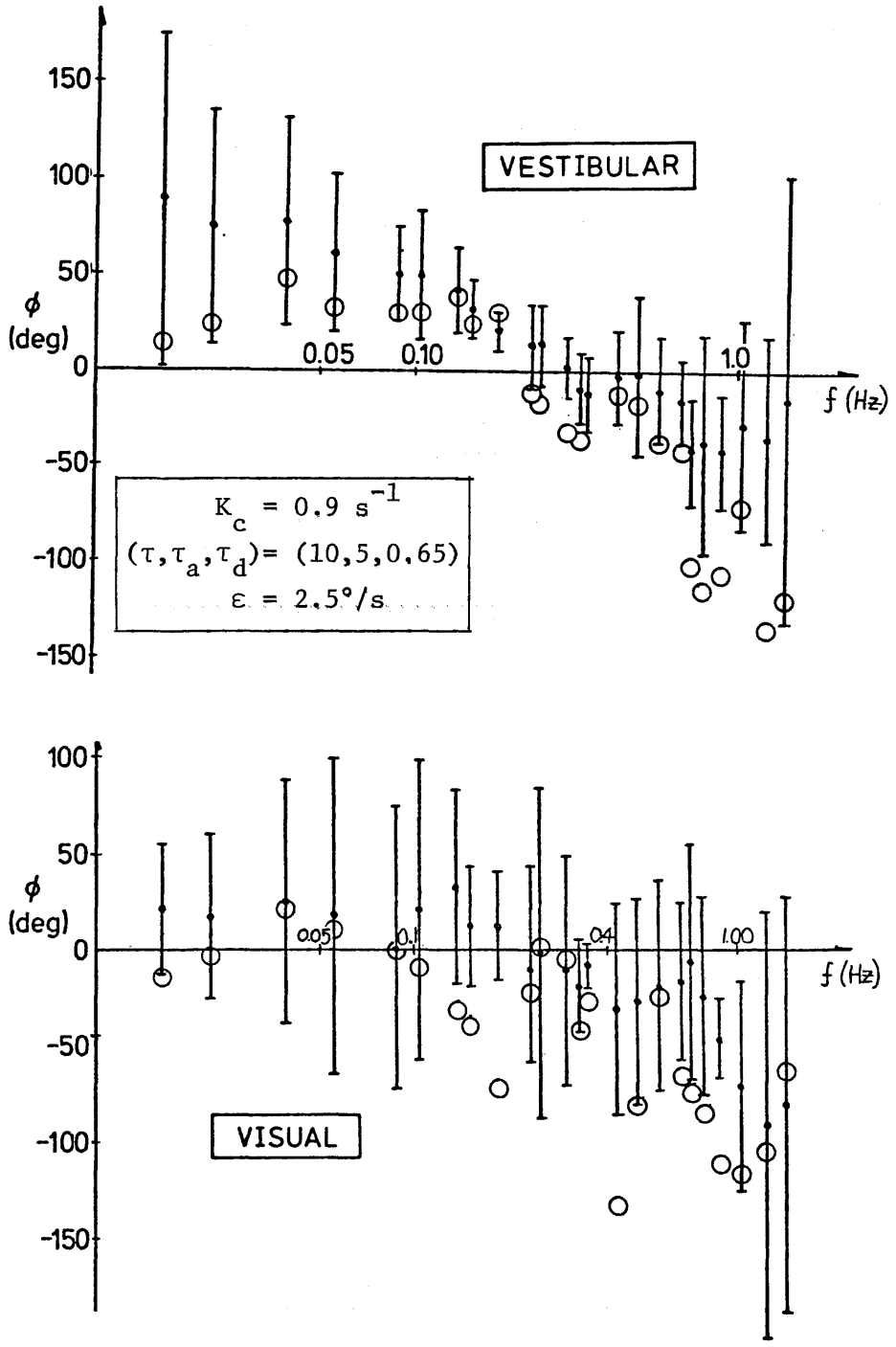

Figure 5.21a: Model Frequency Response in Dual-Input Nulling Task (vestibular channel, nominal gain)

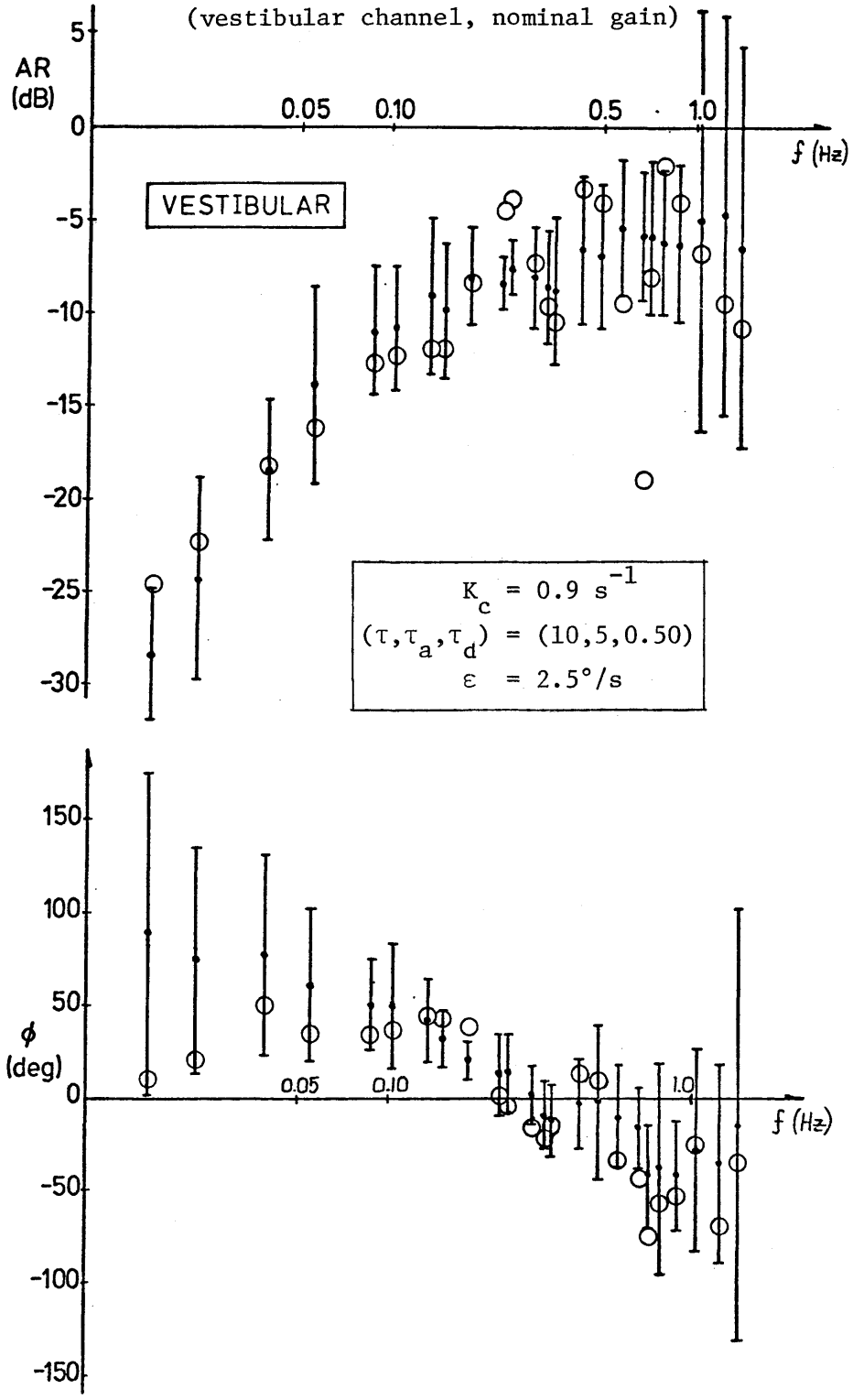

Figure 5.21b: Model Frequency Response in Dual-Input Nulling Task

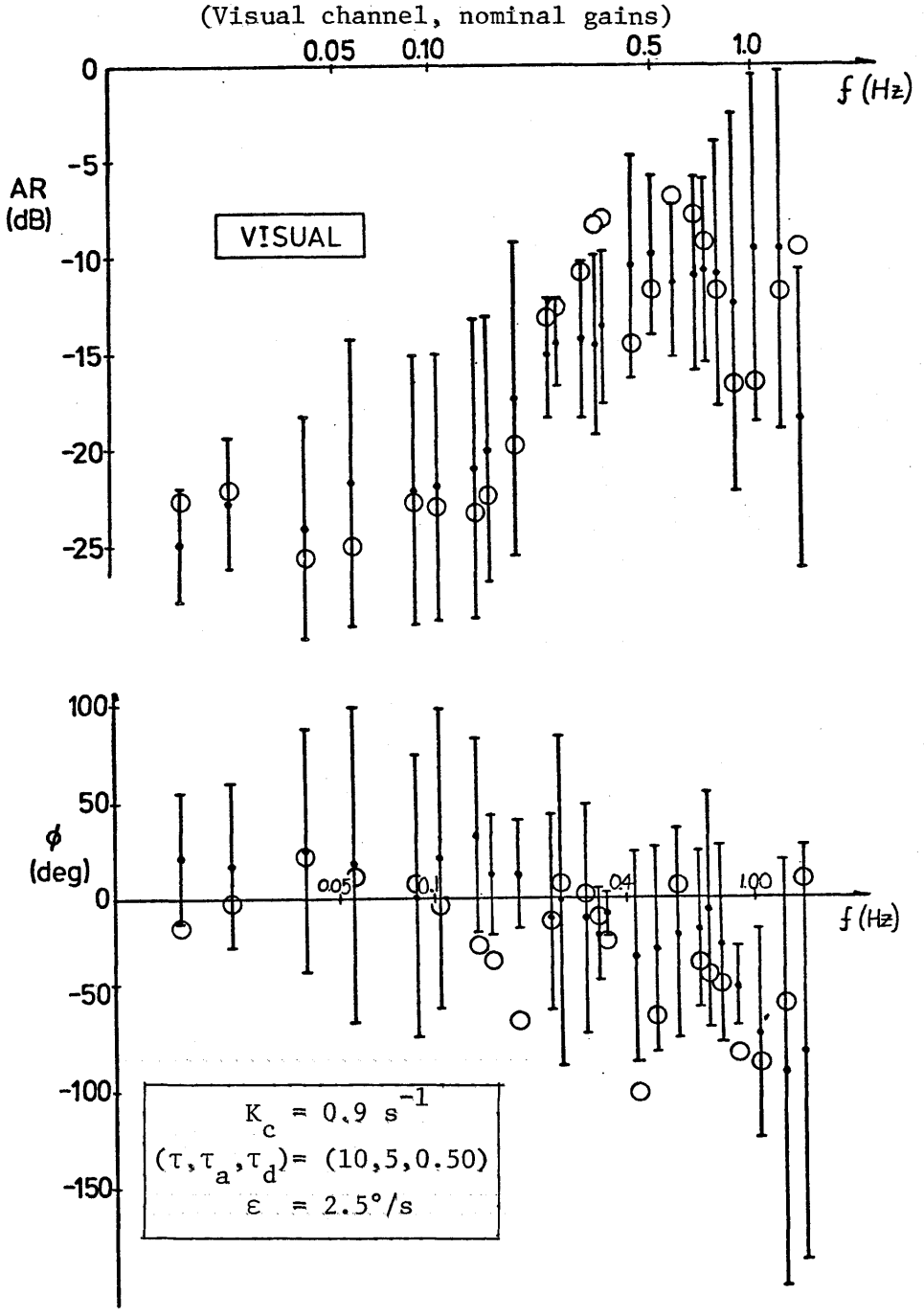

fit of the phase data, when compared with the predicted phase response of figure 5.20, associated with the longer delay time.

Again, it is worth noting that no effort has been made to optimize this choice in terms of minimizing the phase residuals. Naturally, smaller delay time values result in a reduction of high-frequency lag, and values smaller than 0.50 s begin to result in a poorer phase fit due to excessive high-frequency lead relative to the experimentally derived response. This behavior, coupled with the notion that the delay time might be expected to be greater than that associated with velocity-nulling under counterrotating field conditions (τ_d = 0.40 s), suggests that a delay of 0.50 s is a more appropriate choice than the originally proposed 0.65 s value. It should be recognized, however, that neither choice corrects the model's failure to match the low-frequency vestibular lead characterizing the experimentally derived response data.

5.2.3.7 Summary of Closed-Loop Response Behavior

This section has shown how the conflict model of figure 5.4, in conjunction with the linear human operator dynamics of (5.1), can mimic the frequency characteristics of the estimator functions derived from the velocity-nulling experiments of the last chapter, under both counterrotating and dual-input visual field conditions. Approximately flat frequency response from the model is obtained with CON presentations (figure 5.13), while the DI presentations result in a model matching of

both the relatively high break frequency vestibular washout and the low gain visual lead-lag (figure 5.17).

Four parameters dictate model behavior. The delay time constant τ_d was initially chosen on the basis of the phase data of the previous chapter: a value of 0.40 s was assigned to the model for CON nulling runs, and 0.65 s chosen for DI runs, both representing the lumped time delay due to both estimator and controller. The requirement of better matching the DI phase data called for a reduction of the delay time in the latter case, from 0.65 s to 0.50 s. In a similar fashion, two values were assigned to the control gain K_c, depending on field presentation type: 1.2 s^{-1} during CON runs, and 0.9 s^{-1} during DI runs, both lowered from the original value of 1.8 s^{-1} which was based on manual control performance in the visual field velocity nulling-task. This gain reduction necessitated a reduction in the adaptation time constant τ_a, from its original 10 s value to 5 s, to maintain a reasonable model fit with the visual channel DI experimental data. Finally, it was shown that the threshold magnitude parameter was adequately approximated by a value of $2.5^{o}/s$, higher and lower values leading to considerable visual channel gain mismatch between model predictions and derived experimental results.

The model's frequency response with this choice of parameters has already been illustrated. Figure 5.13 shows gain and phase under CON field conditions, while figure 5.21 shows the corresponding dual-channel response, when operating under DI cue presentation conditions. As was noted earlier, the conflict model fails to fit the data as well as the fitted linear functions introduced in the previous chapter (and

illustrated in figures 4.11 and 4.12). It does, however, match the trends reasonably well, without being inconsistent with single cue response expectations, a capability which is not matched by a linear model based on the functional fits of the previous chapter.

5.2.4 Open-Loop Step Response: Magnitude Dependence

At this point, it is appropriate to reconsider the model's open-loop transient response, to simulated velocity step inputs. It may be recalled that three model parameters dictate response in the open-loop situation (τ, τ_a, and ε), and one of them, the adaptation time constant τ_a, was reassigned a new value based on the frequency response analysis just conducted. Thus, a reexamination of step response behavior is called for to ensure that this parameter value change has not significantly changed the model response from that discussed earlier.

Shown in Figure 5.22 are step response histories for simple vestibular steps, simple visual steps, and combined corroborating steps, all parameterized against input step size, which ranges from 1°/s to 5°/s. In the figure, the left column of responses results from the 5 s value assigned to τ_a, while the right column is repeated from figure 5.7, in which τ_a was assigned a value of 10 s. A direct comparison of the two responses to confirming cue presentation (figures 5.22c and 5.22f) shows them to be identical, which is to be expected, since the conflict signal is zero in both cases, and a change in adaptation time has no effect on a null signal. Differences are evident in the single cue responses, however. Comparing figures 5.22a and 5.22d shows that the shorter adaptation time leads to a more rapid vestibular decay, which is due to the fact that the cue conflict signal (ω_{err} of figure 5.4) is washed out more rapidly, leading to an earlier weighting of the null visual information. Similarly, a comparison of figures 5.22b and 5.22e shows an earlier acceptance of the visual motion cue step, again due to the faster conflict signal decay, and

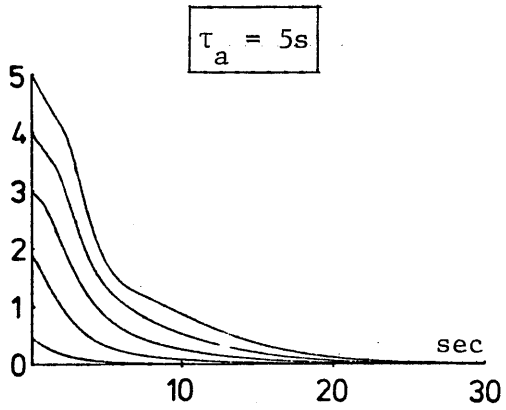

Figure 5.22a: Vestibular Step Response

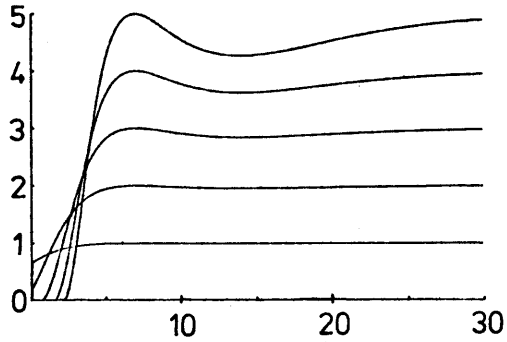

Figure 5.22b: Visual Step Response

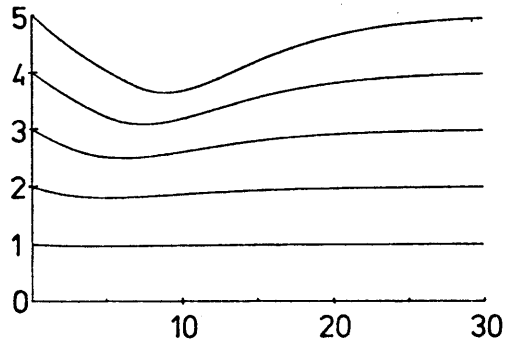

Figure 5.22c: Response to Visual and Vestibular Steps

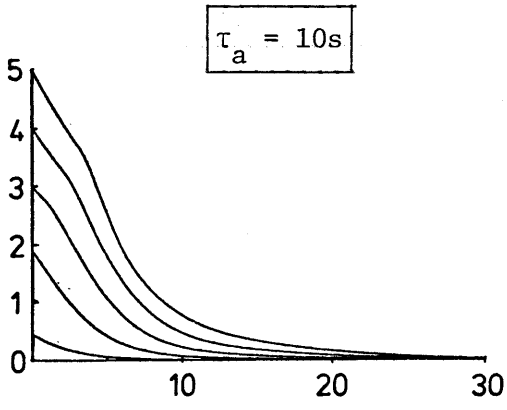

Figure 5.22d: Vestibular Step Response

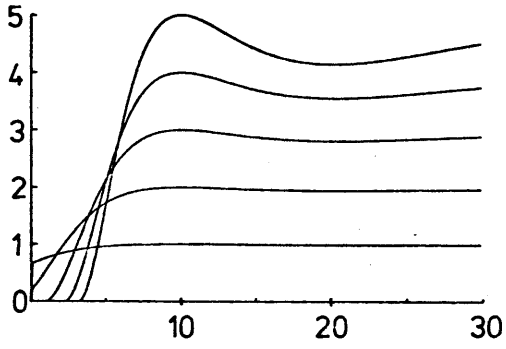

Figure 5.22e: Visual Step Response

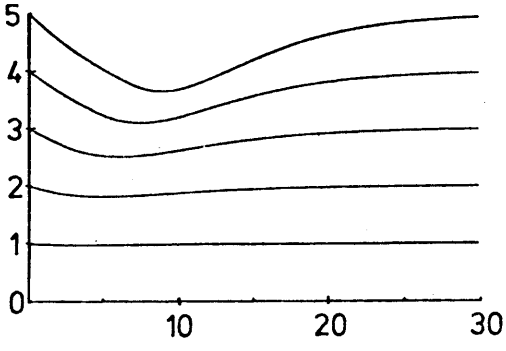

Figure 5.22f: Response to Visual and Vestibular Steps

is manifested by shorter response latencies and rise times. On the whole, however, the responses in the two cases are similar, and the choice of the shorter adaptation time does not significantly change the conflict model's step response behavior, which has already been discussed in detail in section 5.2.2.

Of more interest, perhaps, is model response in the face of large magnitude step inputs. It should be recognized that the modelling effort, to this point, has been concerned with matching responses to fairly small inputs (in both the step response and loop nulling simulations), and an examination of large amplitude behavior can provide a check on the descriptive accuracy of the conflict model, as proposed. Shown in figure 5.23 are histories of open-loop simulated step responses, similar in format to those just presented, but with input step magnitudes ranging from 5°/s to 60°/s. A comparison with the smaller magnitude step responses of figure 5.22 shows a considerably different response pattern to large amplitude inputs, and, in particular, shows that the model fails to adequately match known subjective responses to large velocity step inputs, especially in the single vestibular and single visual cue input cases (figures 5.23a and b).

The vestibular response of figure 5.23 exhibits the 10 s time constant decaying exponential associated with the washout model of the canal dynamics (recall the model of figure 5.4), but also is characterized by a disquieting 'notch' in the response history, approximately 7 s after stimulus presentation. This is caused by the internal conflict signal ω_{err} passing through zero at this time, which results in a weighting of the null visual

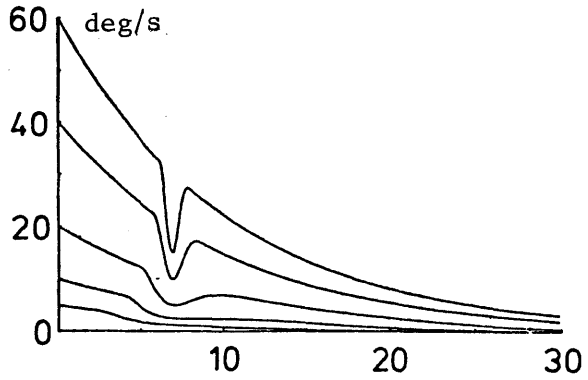

Figure 5.23a: Vestibular Step Response

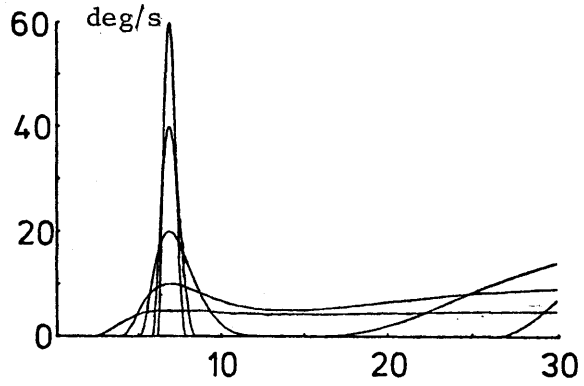

Figure 5.23b: Visual Step Response

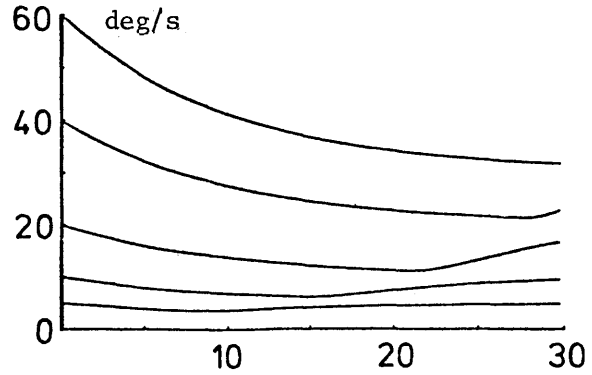

Figure 5.23c: Response to Visual and Vestibular Steps

cue, in turn causing the response to drop towards zero momentarily. This is seen fairly directly by recognizing that, with a vestibular step input ω_0, the conflict model of figure 5.4 predicts a conflict signal given by

$$\omega_{err}(s) = \omega_0 s/\left[(s + 1/\tau_a)(s + 1/\tau)\right] \tag{5.8}$$

so that the conflict signal will pass through zero at time T, where T is defined by

$$\omega_{err}(T) = (\omega_0/(\tau_a-\tau))[\tau_a e^{-T/\tau} - \tau e^{-T/\tau_a}] = 0 \tag{5.9}$$

so that

$$T = (1/\tau_a - 1/\tau)^{-1} \ln(\tau/\tau_a) \tag{5.10}$$

which yields a value of 6.93s with τ and τ_a assigned values of 10 s and 5 s, respectively. Since ω_{err} only passes through zero momentarily, the notch effect in the vestibular response is only transitory: as the conflict signal grows more negative, and larger in absolute value, the null visual signal becomes unweighted, and the response resumes its normal vestibular decay pattern, as seen in figure 5.23a.

A similar argument holds true for the visual step response of figure 5.23b, since the error signal is identical. The consequences are more severe, however, since the visual channel information is only momentarily weighted, and a spike type response results, followed by an eventual very slow acceptance of the visual cue. Such behavior is entirely contrary to known circularvection response (Brandt et al, 1973), in which self-velocity sensation grows monotonically following a few seconds latency, to reach saturation within 10 or 20 s, a value which appears to be independent of

velocity step magnitude (over the range of 10°/s to 90°/s). This response disparity clearly needs to be corrected for in the model, and the discussion to follow shortly will address this problem.

The final response shown in figure 5.23, that due to the presentation of confirming visual and vestibular cues, also shows the effect of large conflict signal propagation, although not to the extent that the single cue responses do. The initial rapid rise due to the vestibular domination gradually falls off, but at a rate slower than in the single vestibular cue case, because of the complementary visual cue contribution. However, since the vestibular cue remains relatively large throughout the time period shown, the model tends to average the cues, resulting in a depressed response considerably lower than the step input to the model. Only for the smaller input steps, in which the conflict signal has dropped to near zero in the 30 s shown, does the response show a recovery tendency to the appropriate steady-state value dictated by the input step magnitude.

5.3 Conflict Model with Conflict Signal Limiting

The previous section has shown that the conflict model proposed at the beginning of this chapter does a reasonable job of fitting the frequency response data associated with the two nulling tasks described in the last chapter, with small magnitude step response characteristics which appear to mimic single cue subjective response studies. However, the model's response to large magnitude steps contrasts sharply with measured subjective sensation, and the discussion of the previous section has pointed to the source of the problem: the generation and propagation of a large conflict signal, with an undesireable zero-crossing characteristic attributable to the adaptation operator responding to a decaying exponential input. The objective of this section is to discuss this aspect of the modelling problem in greater detail, and suggest a means of resolving the disparity between model predictions and the measured subjective response.

5.3.1 Conflict Signal Limiting

The model's undesirable response to large step inputs can be traced to two factors: the generation of a large conflict signal which effectively inhibits the incorporation of visual cue information for long periods of time, and the action of the adaptation operator on this signal which changes a simple decaying exponential into a biphasic waveform, to result in the vestibular notch and visual pulse seen in the histories of figure 5.23. The former problem suggests that some sort of error limiting be incorporated

into the model, while the latter suggests that a modified washout filter be utilized, one which provides a monotonic output for a similar input.

Several limiting schemes might be suggested for the model of figure 5.4. Limiting the visual signal input to the conflict logic would improve the circularvection response, but latencies proportional to step magnitude would result, in contrast with observed behavior. Further, large magnitude confirming cues would no longer result in a zero conflict signal, model behavior which is counterintuitive to the notion of a zero conflict measure when confirming cues are present. Limiting the conflict signal itself is more appealing, but still would result in an increased time to acceptance of visual channel information, with increasing conflict levels. Again, this would not agree with the observed latency and rise time insensitivity to large amplitude visual steps. Clearly, other approaches are possible, but most seem to suffer from the same shortcomings.

Of course, any limiting scheme would still be subject to the problem introduced by the adaptation operator acting on the limited signal. Shown in Figure 5.24 is a response schematic in which it is presumed that the conflict model of figure 5.4 incorporates a limiter between the cue summer and the adaptation operator. With a single step input in either channel, the cue summer output is a decaying exponential. The limiter clips this signal, and the adaptation washout, seeing a constant input, generates a decaying output for the initial period of the response. As the input exponential drops below the limit, the washout begins generating the biphasic response shown. Clearly, with large amplitude inputs, the output of the adaptation operator will reach a large negative value, following

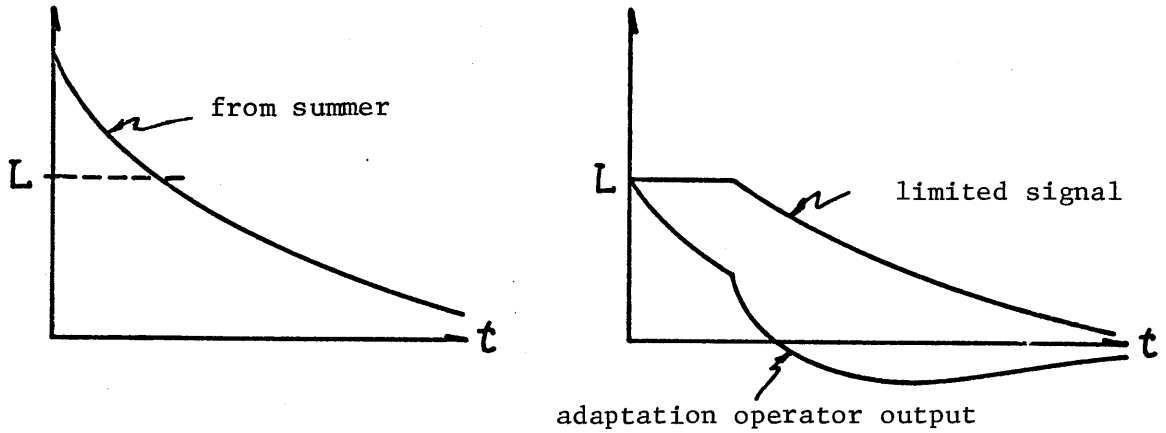

Figure 5.24 Adaptation Operator Zero Crossing Behavior

a zero crossing, and the same type of response behavior will be seen as in figure 5.23. What this calls for is a modification to the washout characteristics of the adaptation operator.

5.3.2 Modified Conflict Model

One means of avoiding the undershoot of figure 5.24 is to modify the washout filter to account for the difference between input and output, and selectively ignore input changes which would lead to zero crossover behavior. Figure 5.25 schematizes the response of such a modified washout filter, to a step change in the input level. In all three cases, the filter output decays exponentially from the initial constant portion of the input ($t < T$), mimicking normal washout behavior. In the first case, the input makes a step increase, the filter output jumps by the same amount, and then exponentially decays from that point. In the second case, the input makes a step decrease, but not to the current low level of the output; no change is seen in the filter output. In the last case, the input drops to below the current level of the output, the filter output jumps to this new level, and then continues its exponential decay from that point.

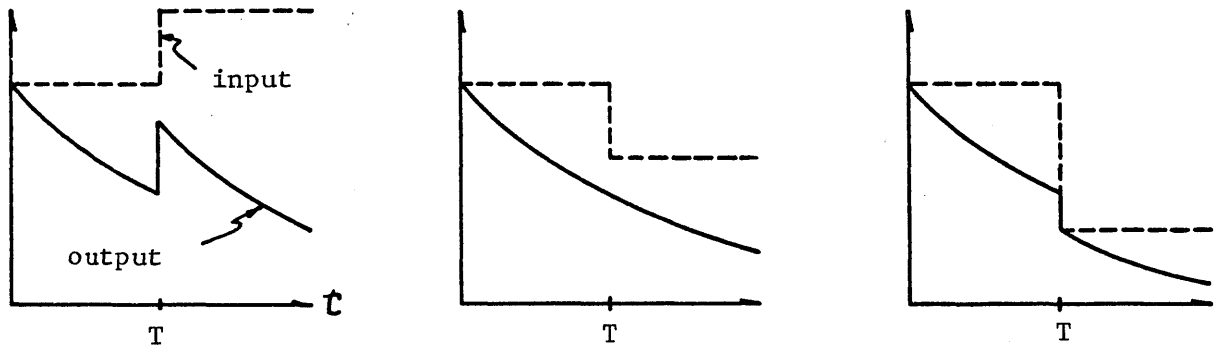

Figure 5.25 Modified washout behavior

With this specification of step response, the modified filter mimics washout response by the incorporation of an exponential decay characteristic, yet avoids the zero crossover problem incurred by the washout when provided with a monotonically decreasing input (as seen in figure 5.24). Such a modified washout filter was programmed as part of the digital simulation library package.

With this functional block available, the originally proposed conflict model may be modified to incorporate both a limiter and the modified washout function. Shown in figure 5.26 is the same model block diagram which was presented earlier in figure 5.4, with the modified

Figure 5.26: Modified Dual-input Cue Conflict Model

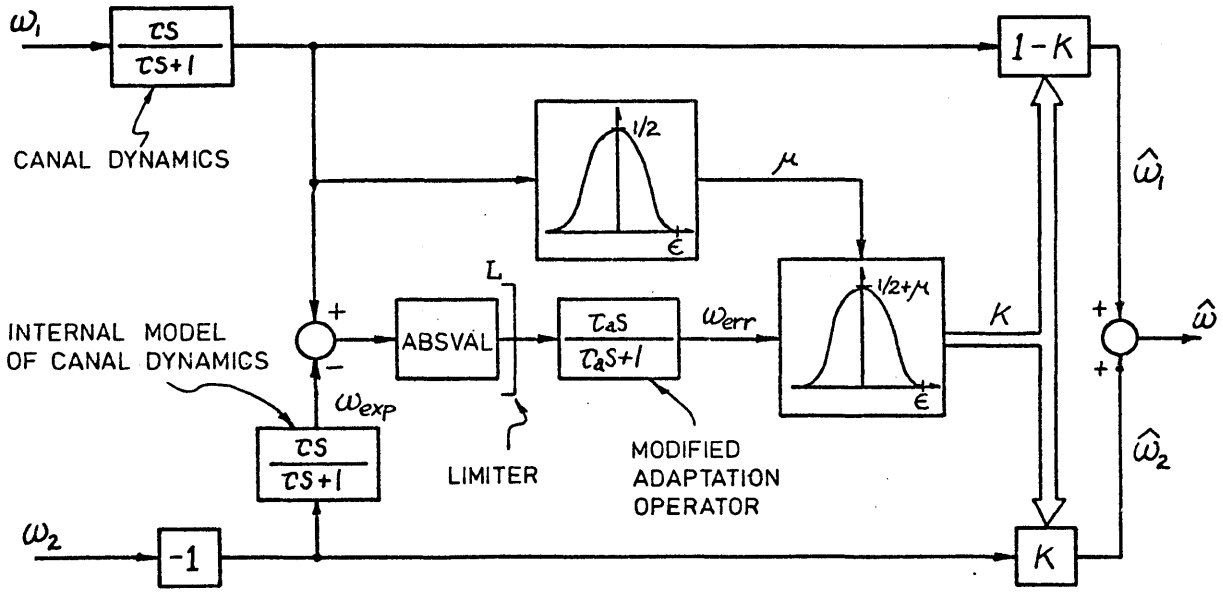

portion outlined in the center path. The original adaptation operator is replaced by a limiter and the modified washout function. For purposes of comparison, the same 5 s adaptation time constant is used in the simulation results to follow. The limiter is assigned a value of 7.5°/s, to provide for reasonable circularvection latency times when operating the model with the previously assigned conflict threshold value of 2.5°/s.

5.3.3 Modified Conflict Model Simulation Results

Shown in figure 5.27 are large amplitude open-loop step responses obtained with the modified conflict model. A direct comparison with the analogous results of figure 5.23 makes it clear that the limiter and modified washout function result in model response which is decidedly improved. The vestibular response of figure 5.27a exhibits the apparent dual time constant decay seen earlier in the small amplitude step simulations, without the notch artifact midway through the response. The transition from one decay rate to another occurs at the same point in time, for all steps larger than the limit value of 7.5°/s, since this is the point at which the conflict signal becomes (and remains) smaller than the conflict threshold value of 2.5°/s.

Similar behavior is seen in the model's response to visual motion steps in figure 5.27b. Since the conflict signal drops to the 2.5°/s threshold value at the same point in time, for all step inputs greater than the 7.5°/s limit, visual channel information begins to be accepted at the same point in time, for the four large inputs shown in the figure. Thus, the response latency of approximately six seconds is independent of step input,

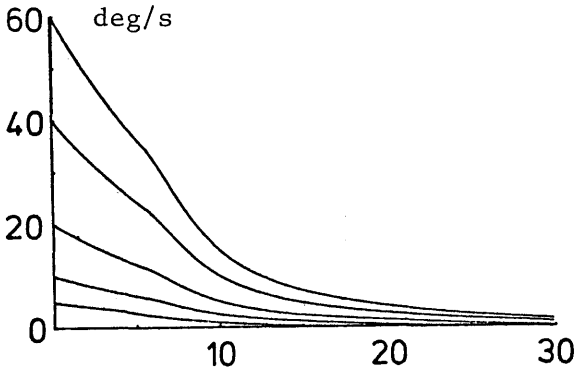

Figure 5.27a: Vestibular Step Response

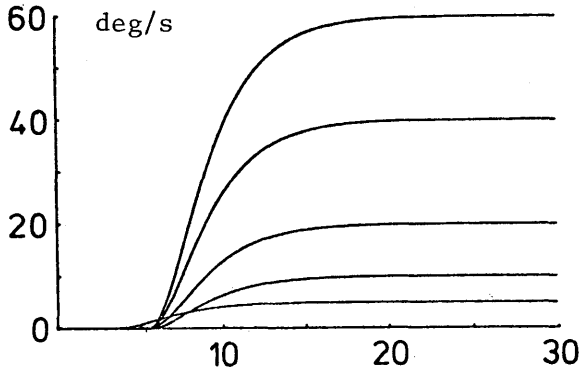

Figure 5.27b: Visual Step Response

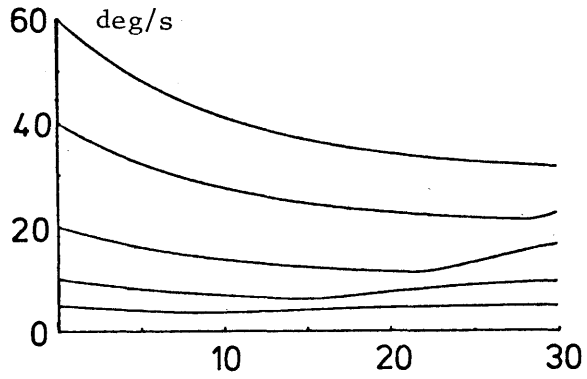

Figure 5.27c: Response to Visual and Vestibular Steps

for large steps. The same argument holds, of course, for rise time insensitivity to step input size. The smallest step response shown, that of 5°/s (below the limit value) results in a reduced latency, as in the earlier simulation studies, and yet smaller inputs will show proportionately smaller latencies and rise times.

The model's response in the face of confirming motion cues, shown in figure 5.27c, is identical to the earlier results obtained without the limiter and illustrated in figure 5.23. This, of course, is due to the fact that the model modification has been restricted to the computation of the cue conflict signal, and since that signal is zero under this cue presentation condition, the modification is effectively non-functional.

This large amplitude step response of the modified model is encouraging; however, an examination of the model's predicted frequency response in the simulated dual-input nulling task shows an exceptionally poor fit to experimentally based data. Shown in figures 5.28a and b are the predictions generated from the simulation of the modified model, superimposed on the experimental results. The vestibular channel fit at low frequencies is poor, with too much gain and insufficient phase lead. A comparison with the unmodified model response of figure 5.21a shows perhaps a slight improvement in the high frequency gain fit, although a quantitative measure of the residuals would be necessary to make a definitive statement on the degree of improvement.

The greatest effect the modification has on model behavior is on the visual channel data fit, as may be seen from figure 5.28b. Except for very low frequencies and a small mid-frequency band, the predicted visual gain

Figure 5.28a: Modified Model Response in Dual-Input Nulling Task (vestibular channel)

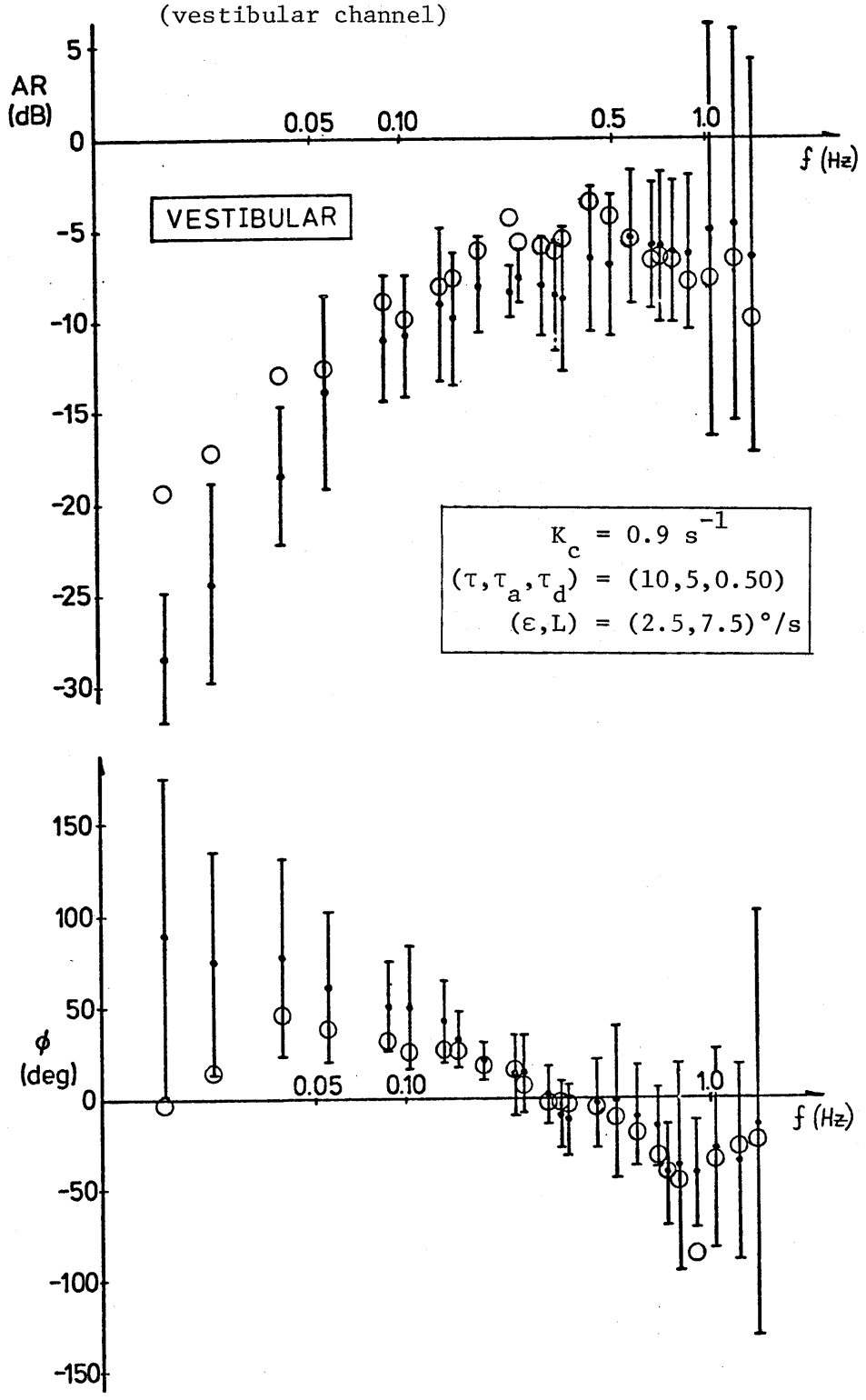

Figure 5.28b: Modified Model Frequency Response in Dual-Input Nulling Task (visual channel)

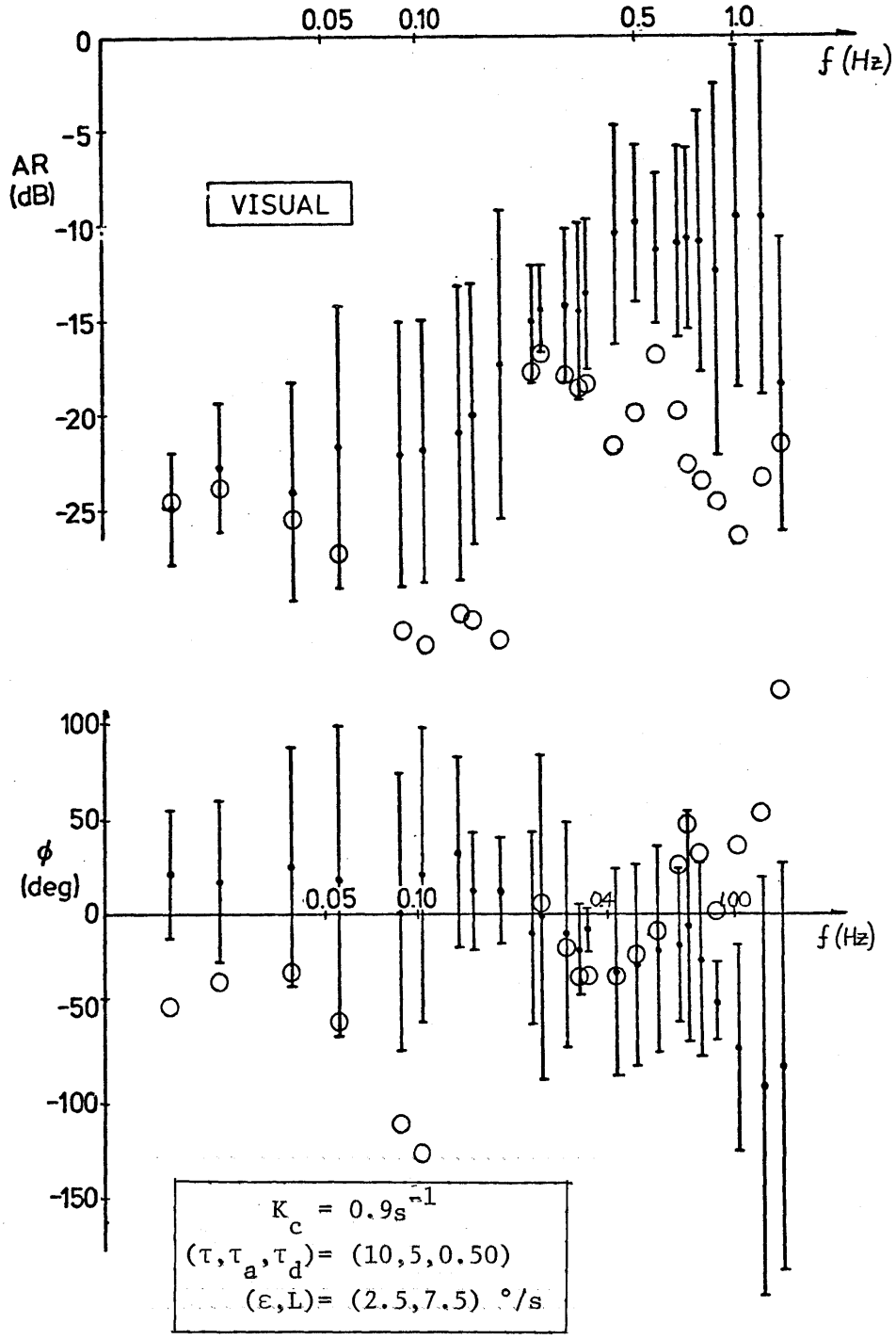

is considerably smaller than the actual gain, resulting in an even poorer fit than in the vestibular channel. The phase fit is worse yet, with some model points not shown because of their failure to remain within the axis limits drawn. A comparison with the unmodified model's predictions for the visual channel, shown in figure 5.21b, allows for a relative judgment as to the goodness of fit attainable without the proposed modifications.

It should be clear that some adjustment in model frequency response can be made by suitable parameter value selection, conducted in a manner similar to that used for model development in section 5.2. In fact, some effort was devoted to improving the modified model's frequency response, but met with little success in terms of matching the fit accuracy obtained with the unmodified model. This is not to suggest that a more exhaustive search of the parameter space would not lead to a fit improvement; however, it is not deemed worth the effort for two reasons. First, it may prove more fruitful to examine the applicability of alternative means of conflict signal limiting and subsequent high-pass filtering, modifications which are needed in the originally proposed cue conflict model, and which may be better implemented in ways other than those proposed earlier in this section. Second, the main objective of the modified model was to demonstrate its capability in mimicking subjective response to large single and combined cue step inputs. It was successful in this task, and although failing to adequately fit the frequency response data, points out the feasibility of such an approach, and suggests that a single model, based on the central conflict measure, can be developed which adequately fits both time and frequency domain experimental data.

5.4 Summary

A dual-input model, based on the cue conflict hypothesis described in the introductory chapter, has been proposed in an attempt to explain the trends in the estimator describing function data presented in the last chapter. Since these trends imply that a simple linear filtering of simultaneous cues results in predictions of single cue response which are inconsistent with measured subjective response, a non-linear filtering scheme is proposed, with cue weighting dependent on the amount of cue conflict present. An internal model of canal dynamics is used to provide a self-consistent measure of interchannel conflict, which, when large, results in a heavy weighting of vestibular information. When small, the visual information is either averaged in, or accepted completely to the exclusion of the vestibular information, depending on whether the vestibular signal is large or small, respectively.

The proposed model of figure 5.4 is fairly simple in structure, and requires the specification of three parameter values to determine its response characteristics: a vestibular time constant, an adaptation time constant, and an error threshold. The initial parameter value assignment was based on observed single cue response behavior, and verified in the case of small amplitude step inputs, by the use of a digital computer simulation of the model's dynamic response. The responses show an apparent two time constant exponential decay to vestibular steps, and qualitatively follow subjective response under circularvection conditions. When the model is presented with confirming visual and vestibular step inputs, response accurately follows true velocity, except for a transient dip due

to the cue averaging property of the model.

Examination of model behavior in a simulation of the closed-loop velocity-nulling task of the previous chapter shows the model to be quite capable of fitting the data, after suitable adjustment of the two parameters used to specify the human operator dynamics. The adjustments suggest that operator dynamics change between operating in a counter-rotating visual field environment (CON) and operating under independent dual-input conditions (DI). Specifically, operator gain is higher and latency (delay time) is lower under CON conditions, possibly because of the operator's greater confidence in the appropriateness of his compensatory actions, and thus willingness to use a higher gain with less indecision.

The gain and latency adjustments made to the human operator dynamics prompted a subsequent change in the originally proposed adaptation time constant value from 10 s to 5 s, to improve the model's fit to the DI estimator describing function data. Further adjustments of model parameters were not made, since substantial changes in the conflict threshold of 2.5°/s degraded the model's fit accuracy, and the vestibular time constant was originally chosen to agree with the fairly well-established value of 10 s.

Additional simulations of model behavior were conducted, to investigate open-loop response to large amplitude steps. Because of large signal propagation through the model's conflict measurement logic, coupled with the adaptation operator's tendency to generate biphasic outputs, vestibular step response fails to show the earlier apparent two time constant decay;

instead, a momentary drop-out of the signal occurs, because of an inappropriate transient acceptance of null visual information as the conflict signal is momentarily driven to zero. This type of conflict signal behavior is also manifested under circularvection conditions, resulting in a prediction of a pulsatile subjective response.

To remedy this behavior, conflict signal limiting is proposed, in combination with a modified adaptation operator, which ensures an avoidance of the earlier biphasic conflict signal waveform. Simulation of a modified conflict model incorporating these changes shows large amplitude step response to be considerably improved, with both visual and vestibular responses qualitatively mimicking observed subjective response. However, a simulation of the model in the closed-loop dual-input nulling task shows a considerable discrepancy between model predictions and measured responses. The suggestion is that although conflict signal limiting demonstrates the feasibility of matching large amplitude step responses behavior with the conflict model, the particular implementation of the modified adaptation operator merits further study. This problem is not pursued here, as the main objective was to demonstrate how conflict signal limiting could improve on the large amplitude step response predicted by the model, especially in circularvection presentations.

It should be clear that model modification, and subsequent analysis and simulation, could be continued in an effort to better fit both the frequency response data of the last chapter and the transient response reported on in the literature (Peters, 1969; Brandt et al, 1973). However

it is felt that effort would be better directed toward further combined cue experimentation aimed directly at exercising conflict model predictions when non-conflicting cues presentations are made. The objective, of course, would be to isolate and verify smaller portions of the model, to allow for an eventual modular development in contrast to the model matching exercise presented here, an approach which was necessitated by the apparently contradictory results of the previous chapter.

CHAPTER VI

SUMMARY, CONCLUSIONS AND RECOMMENDATIONS FOR FUTURE WORK

6.1 Summary and Conclusions

Several experiments were conducted, and models proposed, to provide a functional explanation of how vestibular rotatory motion cues are integrated with peripheral visual field motion cues to result in a subjective sensation of self-motion. The type of motion investigated was rotation about earth-vertical, and the behavioral measure used was a subject's compensatory control response in attempting to null his own sensation of self-velocity. The closed-loop velocity-nulling task was configured so as to allow the experimenter control over both vestibular and visual inputs to the subject, and implemented via the use of a modified aircraft trainer and a peripheral visual field projection system, both capable of being independently driven as velocity servos to provide the desired motion cues to the subject.

Initial experiments investigated velocity-nulling behavior in the face of a pseudo-random vestibular disturbance applied to the trainer drive, combined with a peripheral visual field cue which was either: (a) stationary with respect to the subject, depriving him of important visual motion cue information; (b) counterrotating with respect to the subject so as to appear inertially fixed, thus providing the subject with visual motion cues which corroborated his vestibular sensations; or (c) moving at constant velocity with respect to the subject, providing him with an illusory sensation of self-motion counter to field motion.

The experimental results confirmed the importance of visual cues in determining the low frequency components of perceived velocity, and a simple model based on the complementary filter hypothesis was shown to be consistent with the low-frequency trends observed in subject acceleration histories. The model processes both cues linearly and in parallel, summing the filtered cues to provide an internal estimate of self-motion. By the presumption of an output bias on the vestibular channel, constant acceleration during visual cue deprivation is predicted by the model, in accordance with the experimental results. By further assuming the visual channel to be a low-pass unity-gain filter (an assumption consistent with single cue studies), it is shown how the model fits the measured response under both counterrotating and constant velocity visual field conditions, and, further, how the long vestibular time constant can be extracted from the measured data, within the context of the proposed model.

The experimental results also confirmed the importance of vestibular cues in determining the high frequency components of perceived velocity. Describing function data, relating subject compensatory response to actual self-motion, is shown to be adequately fit with a simple lag-lead transfer function (with cascaded dead-time), whose parameters depend on the type of visual field cue presented to the subject during the nulling task. With confirming visual cues, the subject exhibits a high gain at low frequency, which drops signficantly when the visual field is either held stationary or moving at constant velocity. However, since the transfer function's lag time constant exhibits a corresponding drop with visual field type, the mid- and high-frequency describing function gain remains

relatively insensitive to visual field treatment. This suggests that subject response at these frequencies is unaffected by visual cues, and supports the notion of vestibular dominance of high-frequency motion sensation.

This demonstrated frequency complementarity of visual and vestibular cue integration confirms the earlier assertions of other researchers, assertions based primarily on the results of single cue psychophysical studies and dual cue neurophysiological studies. The research presented here extends the scope of this earlier work by providing quantitative measures of response to simultaneous cue presentation, which are then used as a basis for proposing the functional model of a linear complementary cue filter. Because the proposed model is more than a qualitative descriptor of cue processing, it is amenable to direct experimental verification. This prompted the design of a second experimental series aimed at validating the linear functional model.

Again velocity-nulling behavior was used as the behavioral measure of subjective sensation, but the experimental protocol provided for simultaneous presentation of conflicting visual and vestibular motion cues. This approach allows for the determination of two human operator describing functions, one relating subject compensatory response to actual self-motion, and the other to motion of the visual field. By the use of a second experimental series measuring manual control dynamics, these describing functions were then corrected for the dynamics of operator nulling behavior, and the resulting dual channel estimator was

linearly modelled in the frequency domain.

By patterning the estimator structure after the complementary filter model proposed earlier, it is shown that the linearity assumptions of cue processing are inappropriate, in the more general experimental environment of independent cue presentation. Specifically, it is shown how the inferred vestibular channel dynamics are best modelled with a washout filter having a time constant which is an order of magnitude smaller than that associated with the response properties of the semicircular canals. Further, the inferred visual channel dynamics are best modelled with a low gain lead-lag, having a gain which is too low to account for subjective response during the visual illusion of circularvection, and a lead which is inconsistent with the low frequency response characteristics associated with visually-induced motion illusions.

This motivated the development of a non-linear functional model for cue mixing, based on the conflict hypothesis which suggests that selective cue weighting is based on an internally-generated measure of intercue conflict. Simulation of the model, in both open- and closed-loop cue presentation conditions, demonstrated its ability to fit the experimentally derived estimator describing functions, while retaining the capability of following the response trends observed in single cue studies, and reported in the literature. Although response to large amplitude inputs is shown to result in poorer response matches, it is demonstrated how simple modifications to the model might be used to extend its applicability to a larger range of simultaneous cue presentation conditions.

6.2 Recommendations for Future Work

Validating the conflict model of combined cue processing should continue, since it is, at present, the only proposed functional description of subjective sensation dependence on vestibular and peripheral visual field motion cues. The effort should be based both on current neurophysiological data, describing unit response to combined cue presentation, and on extended behavioral testing which allows for a measurement of subjective sensation under similar cue presentation conditions. With the neurophysiological data, it is felt that a model matching effort is most appropriate, with reliance on extensive model simulation to develop a good fit to the data. The extended subjective testing should concentrate on isolating independent functional characteristics of the model, such as channel weighting behavior as a function of cue conflict amplitude, and cue conflict signal dependence on cue disparity. By attempting to isolate model features in this manner, a more modular approach to model verification can take place, and thus support an independent validation of specific model features.

It should be clear that the experimental and analytic approach presented here can be extended to other types of motion, with the most promising carryover appearing to be linear motion in the horizontal plane. Here, presumably, the otoliths would be the vestibular acceleration sensors, and peripheral visual field motion would provide low frequency information driving subjective sensation of translational velocity. Studies in other axes are, of course, compounded by otolith-canal interactions, which are still in the

process of being modelled; however, the cue conflict model may provide a means of functionally describing these interactions, and allow for an eventual integration with visual motion cues.

Finally, it is appropriate to point out that intercue conflict plays an important role in the evaluation of ground-based aircraft simulators and further may also be implicated as a possible cause of motion sickness. Clearly, these are two areas which may benefit from a closer look at cue conflict, and, in particular, may benefit from an application of the conflict model, in predicting intercue disparity thresholds for simulator fidelity, and in correlating motion sickness incidence with cue disparity magnitude.

APPENDIX A

EQUIPMENT DESCRIPTION

This appendix describes the hardware, software and performance capabilities of the equipment used in both velocity-nulling tasks and in the visual field velocity-nulling task.

A.1 Hardware

The enclosed platform used for subject rotation is a modified small aircraft trainer, the Link GAT-1 trainer (General Precision Systems, 1968), driven in yaw rotation only, as a velocity servo as illustrated in Figure A.1.

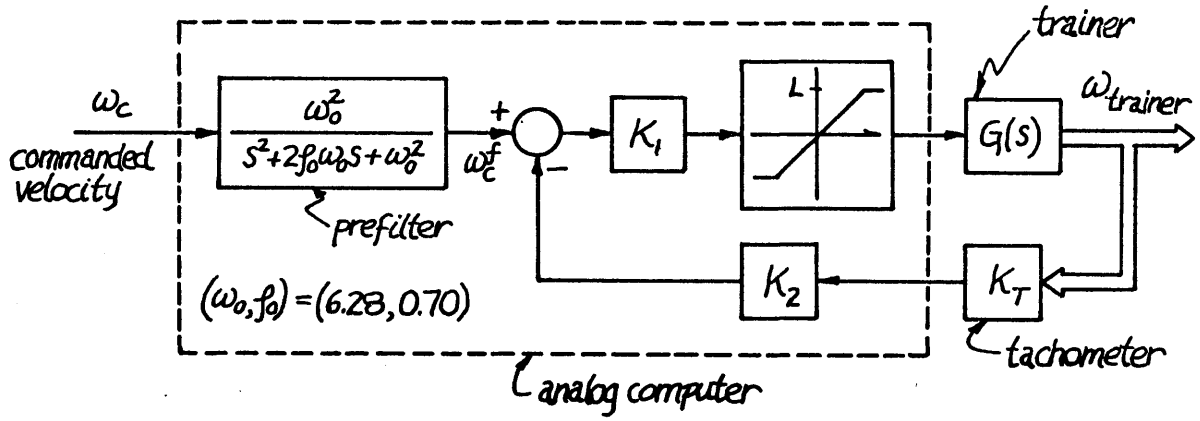

Figure A.1 Trainer drive loop

Loop closure via tachometer feedback is provided by the GPS290T analog computer, as is command signal pre-filtering and error signal limiting to

avoid trainer drive resonance at high frequencies and to avoid overdriving the trainer power amplifiers, respectively. Individual gains are given in the analog block diagram of Section A.2, and the closed-loop frequency response of the trainer is given in Section A.3.

Visual motion cues are presented to the subject via the translucent windows of the trainer, upon each of which is projected appropriate visual cues by a trainer-mounted slide projector, lens, mirror, and servo-drive system (Murphy, 1972). The drive allows velocity control of a film loop passing through the projector and containing the stripe pattern, and, thus, velocity control of the projected images. For the self velocity-nulling experiments, the trainer's two side windows are used and the optics arranged so that when the image on one window moves forward, the other window's image moves aft. The front window is made opaque. For the visual field velocity-nulling experiments, the side windows are made opaque, and the front window only is used.

When the subject is seated in the trainer looking forward, with his head supported by the headrest, the side windows subtend approximately 64° in the vertical direction, measured from subject eye position. They subtend approximately 52° in the forward direction and 12° aft, resulting in a projected image exceeding normal peripheral visual field limits. The front window subtends approximately 45° in the vertical direction, and 60° horizontally. The alternating black and white stripes projected to all windows subtend angles of approximately 12°.

Analog circuitry is used to scale the projector drive input appropriately, so that commands can be given in equivalent angular velocity units

(see analog block diagram of Section A.2). This allows for scaled tachometer crossfeed during counterrotating field operation, constant voltage input for constant velocity operation, or filtered analog signal input during dual-input operation. In the last case, prefiltering is used to simulate the closed-loop trainer dynamics, since the projector drive has a wider bandwidth than the trainer. This is illustrated in Figure A.2.

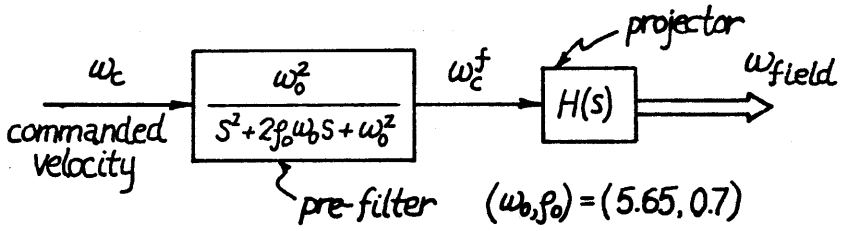

Figure A.2 Film drive

Individual gains are given in the analog block diagram of the next section, and the frequency response of the prefiltered projector system is given in Section A.3.

Two manual controls are used in the experiment: a spring center-loaded stick, and a horizontally mounted wheel. Spring stiffness for the stick is quite low, and full deflection is limited to ± 30°, which through analog circuit scaling results in a velocity command of 20°/s. No centering cue is provided by the wheel, and full defection is limited to a half turn in either direction; with analog scaling, this also corresponds to a velocity command of 20°/s. With both stick and wheel, the direction of trainer motion corresponds with deflection direction, while visual field motion is oppositely signed. Analog circuitry is shown in the next section.

A.2 Software

A.2.1 Analog Computer Program

The analog computer program, for processing of trainer, projector, and control wheel/stick signals is shown in Figure A.3. On the left-hand side are shown the analog trunk lines which send signals to the strip chart recorder (SC) and the tape deck (TD), for monitoring and recording the experimental data. Trainer velocity, visual field velocity, and loop disturbances are all scaled at (5°/s)/volt. Control stick/wheel deflection is scaled at (full deflection)/(4 volts), which is equivalent to (5°/s)/volt in terms of commanded velocity. Also shown on the left-hand side are the two loop disturbances (d_1 and d_2), generated by the digital program, and interfaced via the two D/A channels shown. Disturbance signal scaling is (5°/s)/volt. On the right hand side are shown the analog and link trunk lines which connect the analog computer with the trainer, projector and control stick/wheel.

Indicated on the diagram are the two second-order prefilters, one for the trainer loop to avoid drive resonance, and one for the projector loop to allow for a mimicking of trainer drive dynamics by the projector loop. Switch A provides for different scale factors for the manual controller, because of the difference in voltage/deflection gain between stick and wheel. Switch B determines whether or not the visual field is to counterrotate with respect to the trainer (CON mode); if not, switch C determines the alternate mode (CV, FIX, or DI). Finally, switch D decides

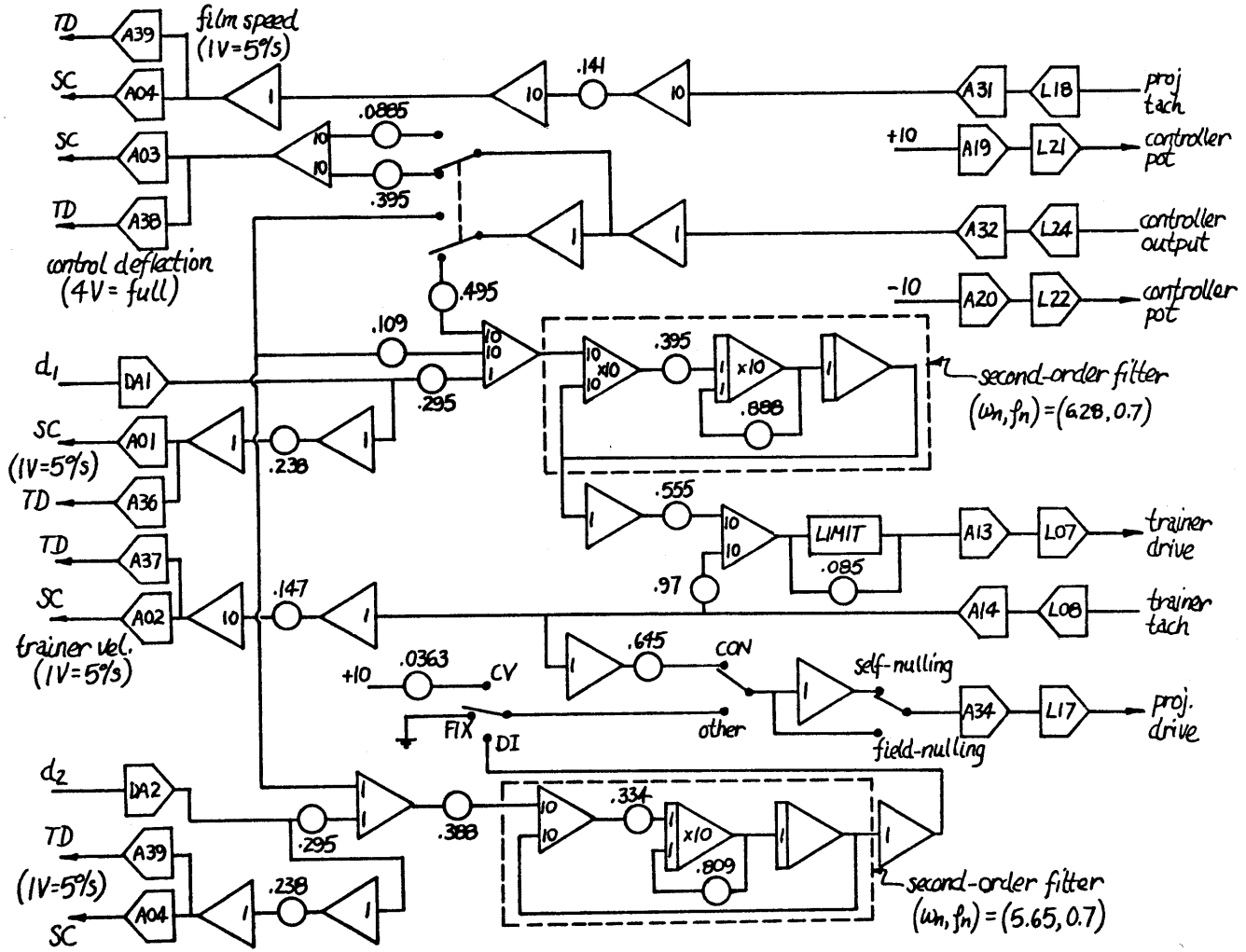

Figure A.3 Analog Computer Block Diagram

between a self-velocity nulling experiment (SN) or a field velocity nulling experiment (FN); for the latter, switch B is set to "OTHER" and Switch C is set to "DI".

The analog computer is also used to provide a means of initiating and interrupting digital program execution. Shown in Figure A.4 is the interrupt logic, in which a comparator is used to sense momentary microswitch closure, and subsequently change the first bit of the PDP-8 digital input word (SL1). This circuit allowed interrupt capability from the computer room, the trainer room, or via slip rings, from within the trainer.

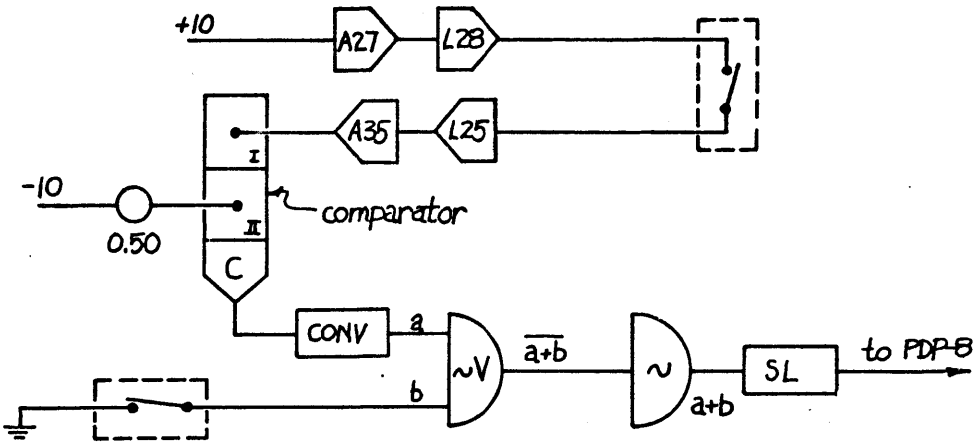

Figure A.4: Interrupt Logic

A.2.2 Digital Computer Program

A listing of the digital program used for disturbance signal generation is given at the end of this section, and is a modified version of an earlier single channel program written at the MVL (Van Houtte, 1970). With an

interrupt signal for starting, the program generates two pseudo-random signals, each composed of a sum of sinusoids and generated by timed D-to-A conversion. The trainer loop disturbance d_1 is output at DA1 and the projector loop disturbance d_2 is output at DA2 (see Figure A.3). In general, the signals are given by:

$$d_1(t) = \sum_{i=1}^{N_1} a_i \sin n_i \omega_0 t \qquad \text{(a)}$$

$$d_2(t) = \sum_{i=1}^{N_2} b_i \sin m_i \omega_0 t \qquad \text{(b)} \qquad \text{(A.1)}$$

where $\omega_0 = 2\pi/T$ and the period T is 128 s. The component amplitudes (a_i, b_i), frequency multiples (n_i, m_i) and the number of terms are program specified parameters. The amplitudes chosen depend on the particular experiment in which the program is used, but for all experiments, rapid start-up transient in the two disturbances are avoided by alternating the signs of the amplitudes, according to:

$$\text{sign}(a_{i+1}) = -\text{sign}\ (a_i) \qquad \text{sign}(b_{i+1}) = -\ \text{sign}\ (b_i) \qquad \text{(A.2a)}$$

where

$$\text{sign}(a_1) = 1 \qquad \text{sign}(b_1) = 1 \qquad \text{(A.2b)}$$

For the single disturbance loop experiments described in Chapters 2 and 3, the second channel output of the program is not used. For the first channel (d_1 of (A.1)), the number of terms N_1 is set to 15, and the frequency multiples (n_i) are defined by Table A.1. The amplitudes are defined by the shelf spectrum in Figure A-5a, with the 20 dB shelf break at 0.25 Hz. The zero dB reference level amplitude is 2°/s.

Table A.1 Frequency multiples for disturbance signals

SINGLE INPUT EXPERIMENT	DUAL INPUT EXPERIMENT	
d_1	d_1	d_2
2	3	2
3	7	5
5	13	11
7	19	17
11	29	23
17	37	31
23	43	41
29	61	53
37	83	71
47	97	89
59	127	109
73	151	137
89		
107		
127		

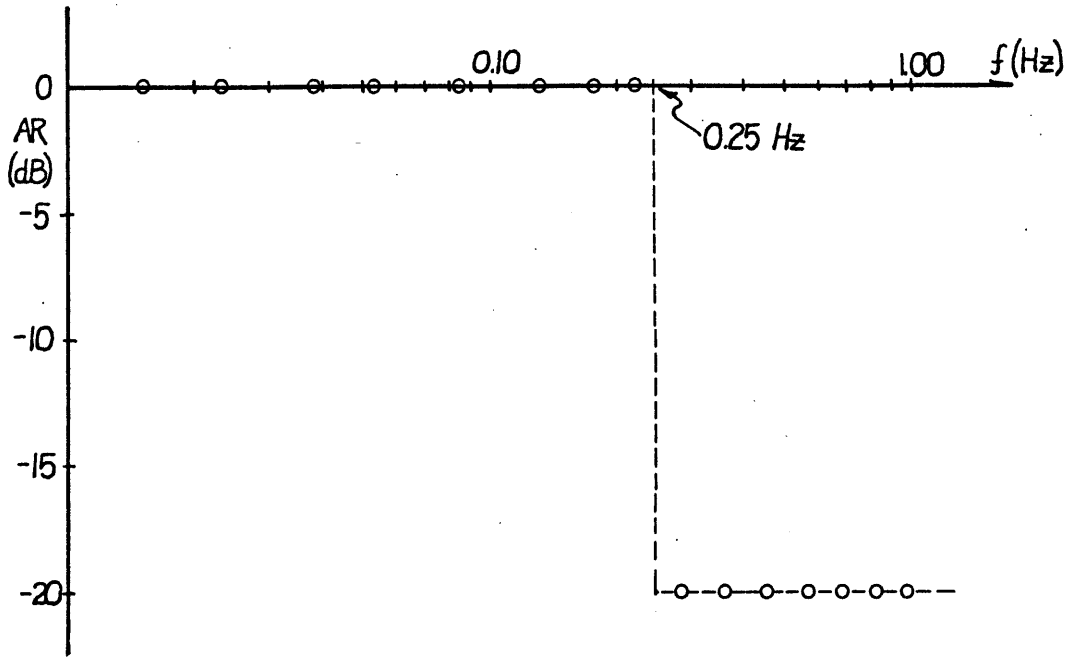

Figure A.5a: Disturbance Spectrum for Single Input Tasks

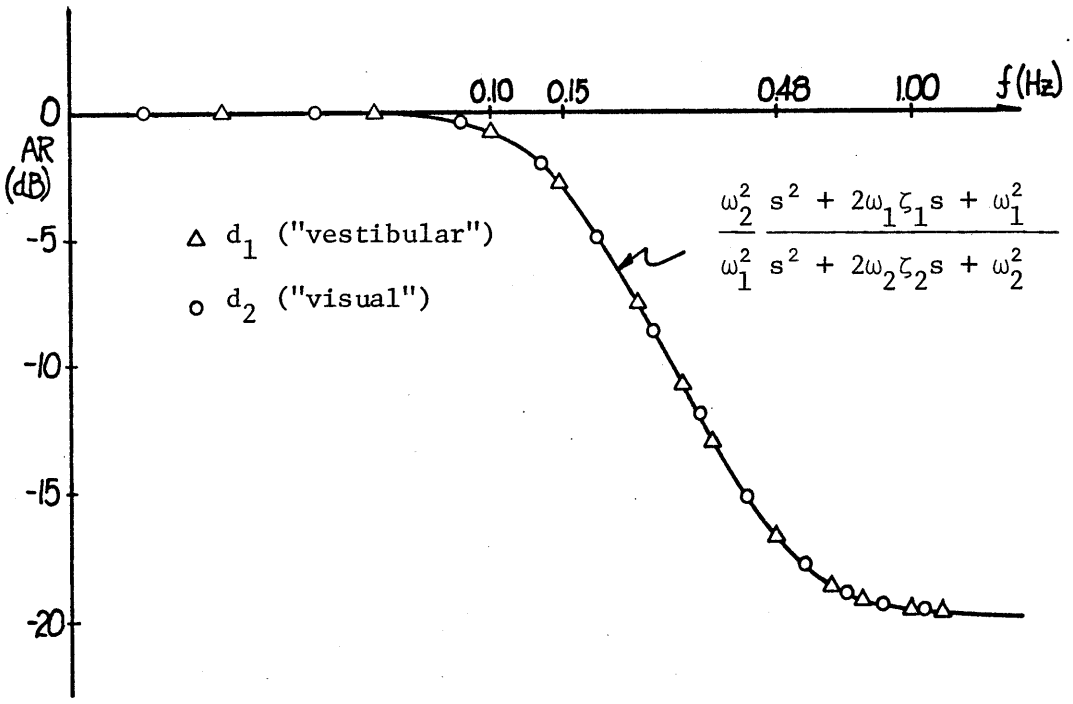

Figure A.5b: Disturbance Spectrum for Dual Input Task

For the dual disturbance loop experiments described in Chapter 4, both channels are used, and each signal consists of 12 terms (N_1 and N_2). The frequency multiples n_i and m_i are chosen as alternating primes of an ascending series to assure zero correlation between the signals, and are defined by Table A.1. The signal amplitudes are defined by the spectrum of figure A-5b, which shows how the components are interleaved, and how both spectra follow the AR curve associated with a double lag-lead transfer function, given by:

$$\frac{\omega_2^2}{\omega_1^2}\,\frac{s^2+2\zeta_1\omega_1 s+\omega_1^2}{s^2+2\zeta_2\omega_2 s+\omega_2^2} \qquad \text{(A-3a)}$$

where

$$(\omega_1,\omega_2) = (0.475,\ 0.150)\ \text{Hz}$$
$$(\zeta_1,\zeta_2) = (0.707,\ 0.707) \qquad \text{(A.3b)}$$

The lag and lead break frequencies are chosen to give a more gradual transition between the large low frequency amplitudes and the small high frequency amplitudes, with the transition point chosen to approximate the 0.25 Hz break frequency used in the single input experiment disturbance spectrum of Figure A.5a. The zero dB reference level amplitude is 2°/s.

For the visual field velocity-nulling experiments described in Chapter 4, only the second channel is used, and is generated with the same stored parameters as used in the dual disturbance experiments just noted.

Operation of the program requires that the hybrid clock be set for a 31.25 msec interval (T = 32 s). Program start is at location 200, the beginning of a wait loop which can be interrupted via microswitch closure to start disturbance generation. Subsequent switch closure will interrupt signal generation and reset the program to the wait loop.

Listing for Disturbance Signal Generation Program

```
                *100
0100  0600  PRAND,RAND
0101  1050  PMUL,SMUL
0102  7401  PSINE,SINE
0103  0000  TEMPH1,0
0104  0000  TEMPH2,0

                *200
0200  7300  WAIT,  CLA CLL
0201  6552        DAL1
0202  6554        DAL2
0203  6551        DACX
0204  6301        CL01
0205  6304        CL02
0206  7300        CLA CLL
0207  7604        LAS
0210  7010        RAR
0211  7430        SZL
0212  5216        JMP START
0213  4245        JMS INTRPT
0214  7420        SNL
0215  5206        JMP .-7

0216  7300  START, CLA CLL
0217  7120        STL
0220  4500        JMS I PRAND

0221  7100  CALC,  CLL
0222  4500        JMS I PRAND
0223  4225        JMS OUTPUT
0224  5221        JMP CALC

0225  0000  OUTPUT,0
0226  7300        CLA CLL
0227  6461        SNAF
0230  7410        SKP
0231  5227        JMP .-2
0232  6454        CLAF
0233  1103        TAD TEMPH1
0234  6552        DAL1
0235  7200        CLA
0236  1104        TAD TEMPH2
0237  6554        DAL2
0240  6551        DACX
0241  4245        JMS INTRPT
0242  7430        SZL
0243  5200        JMP WAIT
0244  5625        JMP I OUTPUT

0245  0000  INTRPT,0
0246  7300        CLA CLL
0247  6435        LASI
0250  7004        RAL
0251  7420        SNL
0252  5645        JMP I INTRPT
0253  7300        CLA CLL
0254  1265        TAD MIN6
0255  6461        SNAF
0256  5260        JMP .+2
0257  5255        JMP .-2
0260  6454        CLAF
0261  7001        IAC
0262  7510        SPA
0263  5255        JMP .-6
0264  5645        JMP I INTRPT
0265  7771  MIN6,  7771

                *400

                    DECIMAL

0400  0003  DELT00,3
0401  0007  DELT01,7
0402  0015  DELT02,13
0403  0023  DELT03,19
0404  0035  DELT04,29
0405  0045  DELT05,37
0406  0053  DELT06,43
0407  0075  DELT07,61
0410  0123  DELT08,83
0411  0141  DELT09,97
0412  0177  DELT10,127
0413  0227  DELT11,151
0414  0345  DELT12,229
0415  0000  DELT13,0
0416  0000  DELT14,0
0417  0000  DELT15,0
0420  0000  DELT16,0
0421  0000  DELT17,0
0422  0000  DELT18,0
0423  0000  DELT19,0

0424  0002  DELT20,2
0425  0005  DELT21,5
0426  0013  DELT22,11
0427  0021  DELT23,17
0430  0027  DELT24,23
0431  0037  DELT25,31
0432  0051  DELT26,41
0433  0065  DELT27,53
0434  0107  DELT28,71
0435  0131  DELT29,89
0436  0155  DELT30,109
0437  0211  DELT31,137
0440  0255  DELT32,173
0441  0407  DELT33,263
0442  0000  DELT34,0
0443  0000  DELT35,0
```

```
0444  0000  DELT36,0
0445  0000  DELT37,0
0446  0000  DELT38,0
0447  0000  DELT39,0

0450  0632  COEF00,410
0451  7157  COEF01,-401
0452  0570  COEF02,376
0453  7325  COEF03,-299
0454  0250  COEF04,168
0455  7612  COEF05,-118
0456  0132  COEF06,90
0457  7704  COEF07,-60
0460  0060  COEF08,48
0461  7723  COEF09,-45
0462  0052  COEF10,42
0463  7726  COEF11,-42
0464  0051  COEF12,41
0465  0000  COEF13,0
0466  0000  COEF14,0
0467  0000  COEF15,0
0470  0000  COEF16,0
0471  0000  COEF17,0
0472  0000  COEF18,0
0473  0000  COEF19,0

0474  0632  COEF20,410
0475  7153  COEF21,-405
0476  0614  COEF22,396
0477  7276  COEF23,-322
0500  0347  COEF24,231
0501  7552  COEF25,-150
0502  0147  COEF26,103
0503  7672  COEF27,-70
0504  0064  COEF28,52
0505  7723  COEF29,-45
0506  0053  COEF30,43
0507  7726  COEF31,-42
0510  0051  COEF32,41
0511  7727  COEF33,-41
0512  0000  COEF34,0
0513  0000  COEF35,0
0514  0000  COEF36,0
0515  0000  COEF37,0
0516  0000  COEF38,0
0517  0000  COEF39,0

0520  0000  ANGL00,0
```

OCTAL

```
                *600
0600  0000  RAND,0
0601  7420        SNL
0602  5215        JMP REPEAT
0603  7240        SMA
0604  1277        TAD LANGL
0605  3010        DCA 10
0606  1310        TAD NUMB
0607  3305        DCA CNTR
0610  3410        DCA I 10
0611  2305        ISZ CNTR
0612  5210        JMP .-2
0613  3303        DCA TEMPH
0614  5600        JMP I RAND

0615  7200  REPEAT,CLA
0616  1277        TAD LANGL
0617  3302        DCA PANGL
0620  1275        TAD LDELT
0621  3300        DCA PDELT
0622  1276        TAD LCOEF
0623  3301        DCA PCOEF
0624  1310        TAD NUMB
0625  3305        DCA CNTR
0626  1311        TAD NUMB1
0627  3306        DCA CNTR1
0630  3303        DCA TEMPH
0631  3304        DCA TEMPL

0632  1702  LOOP,  TAD I PANGL
0633  1700        TAD I PDELT
0634  3702        DCA I PANGL
0635  1702        TAD I PANGL
0636  7000        NOP
0637  4502        JMS I PSINE
0640  7421        MQL
0641  1701        TAD I PCOEF
0642  4501        JMS I PMUL
0643  1303        TAD TEMPH
0644  3303        DCA TEMPH
0645  7100        CLL
0646  7501        MQA
0647  1304        TAD TEMPL
0650  3304        DCA TEMPL
0651  7430        SZL
0652  2303        ISZ TEMPH
0653  7000        NOP
0654  2302        ISZ PANGL
0655  2300        ISZ PDELT
0656  2301        ISZ PCOEF
0657  2305        ISZ CNTR
0660  5265        JMP .+5
0661  7200        CLA
0662  1303        TAD TEMPH
```

```
0663  3104          DCA TEMPH2
0664  5600          JMP I RAND
0665  2306          ISZ CNTR1
0666  5232          JMP LOOP
0667  7200          CLA
0670  1303          TAD TEMPH
0671  3103          DCA TEMPH1
0672  3303          DCA TEMPH
0673  3304          DCA TEMPL
0674  5232          JMP LOOP

0675  0400    LDELT,DELT00
0676  0450    LCOEF,COEF00
0677  0520    LANGL,ANGL00
0700  0000    PDELT,0
0701  0000    PCOEF,0
0702  0000    PANGL,0
0703  0000    TEMPH,0
0704  0000    TEMPL,0
0705  0000    CNTR,0
0706  0000    CNTR1,0
0707  2000    C2000,2000
0710  7730    NUMB,-50
0711  7754    NUMB1,-24

              *7401

7401  0000    SINE,0
7402  3301    DCA ANGLE
7403  1301    TAD ANGLE
7404  7104    CLL RAL
7405  7430    SZL
7406  5216    JMP OP2
7407  7500    OP1,SMA
7410  5231    JMP CASE1
7411  0276    AND C3777
7412  7640    SZA CLA
7413  5226    JMP CASE2
7414  7050    CMA RAR
7415  5601    JMP I SINE
7416  7500    OP2,SMA
7417  5236    JMP CASE3
7420  0276    AND C3777
7421  7640    SZA CLA
7422  5233    JMP CASE4
7423  7326    SP2
7424  1276    TAD C3777
7425  5601    JMP I  SINE

7426  1301    CASE2,TAD ANGLE
7427  7041    CIA
7430  3301    DCA ANGLE

7431  4241    CASE1,JMS GET
7432  5601    JMP I SINE

7433  1301    CASE4,TAD ANGLE
7434  7041    CIA
7435  3301    DCA ANGLE

7436  4241    CASE3,JMS GET
7437  7041    CIA
7440  5601    JMP I SINE

7441  0000    GET,0
7442  7300    CLL CLA
7443  1301    TAD ANGLE
7444  7012    RTR
7445  7012    RTR
7446  0277    AND C0077
7447  1242    TAD SINTAB
7450  3265    DCA SINLOC
7451  1665    TAD I SINLOC
7452  3302    DCA A
7453  2265    ISZ SINLOC
7454  1665    TAD I SINLOC
7455  3303    DCA B
7456  1301    TAD ANGLE
7457  0300    AND C0017
7460  3265    DCA MLTPR
7461  1302    TAD A
7462  7041    CIA
7463  1303    TAD B
7464  7425    MUL MUY
7465  0000    MLTPR,0
7466  7501    MQA
7467  1300    TAD C0017
7470  7417    LSR
7471  0003    0003
7472  1302    TAD A
7473  7010    RAR
7474  4304    JMS PLUS
7475  5641    JMP I GET

7476  3777    C3777,3777
7477  0077    C0077,0077
7500  0017    C0017,0017
7501  0000    ANGLE,0
7502  0000    A,0
7503  0000    B,0

              SINLOC=MLTPR
```

```
                SINTAB=GET+1

7504  0000  PLUS,0
7505  7500  SMA
7506  5704  JMP I PLUS
7507  3302  DCA A
7510  7240  SM1
7511  1302  TAD A
7512  2301  ISZ ANGLE
7513  5305  JMP PLUS+1
7514  7402  HLT


                *7300

7300  0000  0000
7301  0144  0144
7302  0311  0311
7303  0455  0455
7304  0621  0621
7305  0765  0765
7306  1131  1131
7307  1274  1274

7310  1437  1437
7311  1601  1601
7312  1743  1743
7313  2104  2104
7314  2244  2244
7315  2404  2404
7316  2543  2543
7317  2701  2701

7320  3037  3037
7321  3173  3173
7322  3326  3326
7323  3461  3461
7324  3612  3612
7325  3742  3742
7326  4071  4071
7327  4216  4216

7330  4343  4343
7331  4465  4465
7332  4607  4607
7333  4727  4727
7334  5045  5045
7335  5162  5162
7336  5275  5275
7337  5407  5407

7340  5517  5517
7341  5625  5625
7342  5731  5731
7343  6034  6034
7344  6135  6135
7345  6233  6233
7346  6330  6330
7347  6423  6423

7350  6514  6514
7351  6603  6603
7352  6670  6670
7353  6752  6752
7354  7033  7033
7355  7111  7111
7356  7165  7165
7357  7237  7237

7360  7306  7306
7361  7354  7354
7362  7417  7417
7363  7457  7457
7364  7516  7516
7365  7552  7552
7366  7603  7603
7367  7633  7633

7370  7657  7657
7371  7702  7702
7372  7722  7722
7373  7737  7737
7374  7752  7752
7375  7763  7763
7376  7771  7771
7377  7775  7775

                *7400
7400  7776  7776

                *1000
1000  0000  SDVI,0
1001  7100  CLL
1002  7500  SMA
1003  5215  JMP POS
1004  7060  CMA CML
1005  3306  DCA HIGH
1006  7501  MQA
1007  7041  CIA
1010  7420  SNL
1011  2306  ISZ HIGH
1012  7421  MQL
1013  7120  CLL CML
1014  7410  SKP
1015  3306  POS,DCA HIGH
1016  1303  TAD DIVSOR
```

```
1017  7510  SPA
1020  7061  CIA CML
1021  3227  DCA DVSOR
1022  7420  SNL
1023  7040  CMA
1024  3302  DCA SIGN
1025  1306  TAD HIGH
1026  7407  DVI
1027  0000  DVSOR,0
1030  7430  SZL
1031  7402  HLT
1032  3304  DCA REMAIN
1033  7501  MQA
1034  3305  DCA QUOT
1035  1304  TAD REMAIN
1036  7141  CIA CLL
1037  7004  RAL
1040  1227  TAD DVSOR
1041  7710  SPA CLA
1042  7101  IAC CLL
1043  1305  TAD QUOT
1044  2302  ISZ SIGN
1045  7041  CIA
1046  7100  CLL
1047  5600  JMP I SDVI

1050  0000  SMUL,0
1051  7100  CLL
1052  7510  SPA
1053  7061  CIA CML
1054  3265  DCA MLTPLR
1055  7501  MQA
1056  7510  SPA
1057  7061  CIA CML
1060  7421  MQL
1061  7430  SZL
1062  7040  CMA
1063  3302  DCA SIGN
1064  7405  MUY
1065  0000  MLTPLR,0
1066  2302  ISZ SIGN
1067  5650  JMP I SMUL
1070  3265  DCA HIGHER
1071  7501  MQA
1072  7141  CLL CIA
1073  7421  MQL
1074  1265  TAD HIGHER
1075  7040  CMA
1076  7430  SZL
1077  7001  IAC
1100  7100  CLL
1101  5650  JMP I SMUL
1102  0000  SIGN,0
1103  0000  DIVSOR,0

1104  0000  REMAIN,0
1105  0000  QUOT,  0
1106  0000  HIGH,  0
            HIGHER=MLTPLR
```

A.3 Plant Dynamics

As noted in the text, the trainer was found to exhibit a resonance at about 1.5 Hz, due to the mechanical properties of the load and drive system. To avoid this, an analog pre-filter (see figure A.3) was added, to ensure linear operation and reliable velocity feedback information over a lower frequency range. The resulting pre-filtered trainer response gain can be approximated with a unity gain second-order filter, P(s).

This low-pass characteristic of the pre-filtered trainer necessitates the use of a pre-filter in the projector drive circuit, to ensure that the projector dynamics mimic those of the trainer, when the projector is driven independenly during DI experiments. The pre-filter is implemented on the analog computer (see figure A-3) and is second-order, with a break frequency of 0.92 Hz and a damping ratio of 0.70.

To ensure that the trainer and projector transfer functions, with their associated pre-filters, were close approximations of one another, input-output testing was performed on each. Shown in Figure A.6 are the computed gain and phase for both trainer and projector at the test frequencies used in the experiments. Superimposed on the data are the gain and phase curves associated with a second-order unity gain filter:

$$P(s) = \omega_n^2/(s^2 + 2\zeta_n\omega_n s + \omega_n^2) \qquad (A.4a)$$

where the parameters were chosen to fit the measured response and are given by:

$$(\omega_n,\zeta_n) = (5.65,\ 0.70) \qquad (A.4b)$$

It should be clear from the figure that the frequency responses of the trainer and projector are practically indistinguishable, and that both can be adequately modelled by the linear transfer function given above.

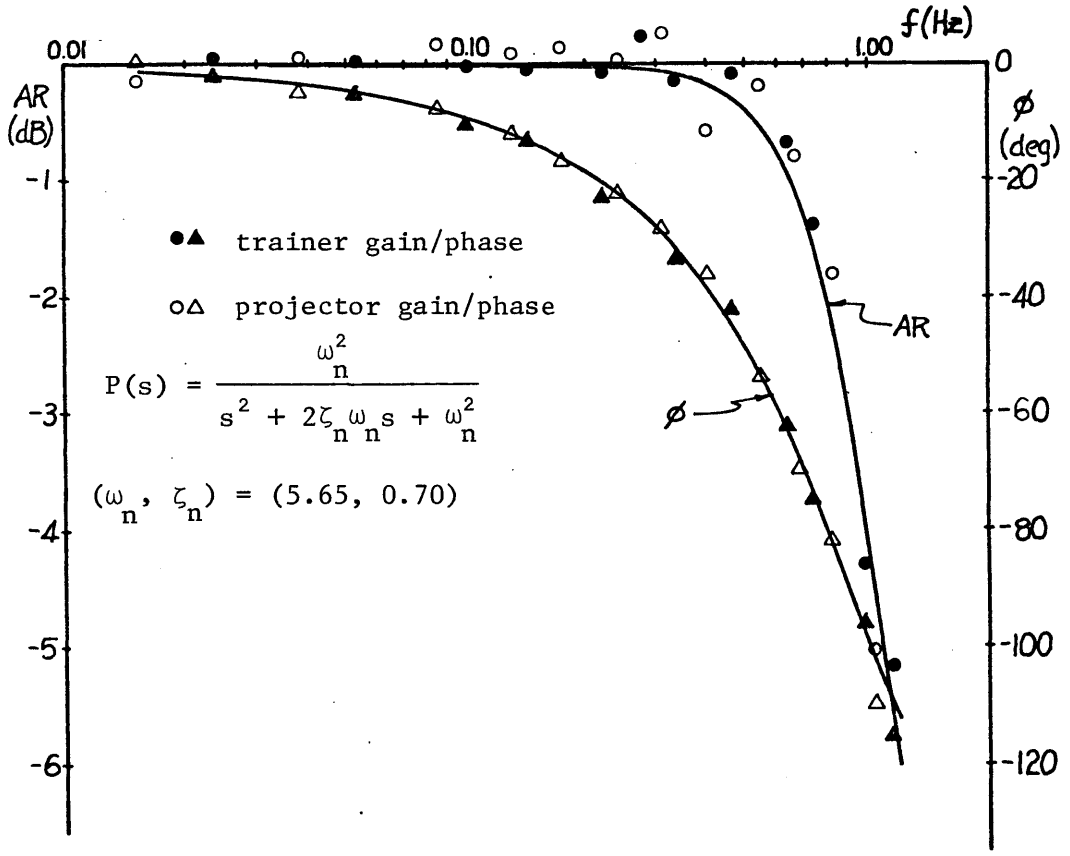

Figure A.6: Dynamics of Trainer and Projector

APPENDIX B

DESCRIBING FUNCTION CALCULATIONS

This appendix demonstrates how the various describing functions presented in the text can be calculated in an approximate fashion directly from the Fourier transforms of the human operator's inputs and outputs. Section B.1 presents the general method of correcting power spectrum measurements for the presence of operator remnant, while section B.2 describes how this correction is implemented. Section B.3 then presents remnant corrected describing function data and compares it directly to the uncorrected data, showing that the difference is insignificant, when viewed in light of the spread characterizing the averaged population responses.

B.1 Remnant Correction Method

The method of correcting operator response for the presence of remnant power is patterned after the approach described by Shirley (1968), with a modification for dual-channel operator input.

B.1.1 Dual-Input Calculations

For the dual-input experiment of Chapter 4, the three measured loop variables, λ, ω_1, and ω_2, are given by (4.4):

$$\lambda(s) = (1/\Delta)[n(s) - PH_1 d_1(s) - PH_2 d_2(s)] \qquad (a)$$

$$\omega_1(s) = (P/\Delta)[n(s) + (1 + PH_2)d_1(s) - PH_2 d_2(s)] \qquad (b) \qquad (B.1)$$

$$\omega_2(s) = -(P/\Delta)[n(s) - PH_1 d_1(s) + (1 + PH_1)d_2(s) \qquad (c)$$

where

$$\Delta \equiv 1 + P(H_1 + H_2) \qquad (B.2a)$$

and where, for convenience, we have combined the estimator and control functions:

$$H \equiv CE_i \qquad (i = 1, 2) \qquad (B.2b)$$

Recognizing that the cross-power spectra of remnant n and disturbance d_i are zero (recall (4-3) and (4-7)), then, from (B-1), we have the following power spectral density expressions:

$$\Phi_{\lambda\lambda} = (1/|\Delta|^2)[\Phi_{nn} + |PH_1|^2\Phi_{d_1d_1} + |PH_2|^2\Phi_{d_2d_2}] \qquad (a)$$

$$\Phi_{\omega_1\omega_1} = (|P/\Delta|)^2[\Phi_{nn} + |1 + PH_2|^2\Phi_{d_1d_1} + |PH_2|^2\Phi_{d_2d_2}] \qquad (b) \qquad (B.3)$$

$$\Phi_{\omega_2\omega_2} = (|P/\Delta|)^2[\Phi_{nn} + |PH_1|^2\Phi_{d_1d_1} + |1 + KPH_1|^2\Phi_{d_2d_2}] \qquad (c)$$

Now, from (4.2), it may be recalled that the disturbance signals d_i are composed of orthogonal sinusoids:

$$d_1(t) = \Sigma\, a_i \sin n_i\omega_0 t \qquad d_2(t) = \Sigma\, b_i \sin m_i\omega_0 t \qquad (B.4)$$

where the n_i and m_i are alternating primes. Thus, if we define the two sets of disturbance frequencies as follows,

$$\Omega_1 \equiv \{n_1\omega_0,\ n_2\omega_0,\ \ldots.\} \qquad \Omega_2 \equiv \{m_1\omega_0,\ m_2\omega_0,\ \ldots\} \tag{B.5}$$

then, from (B.4)

$$\begin{aligned} \Phi_{d_1d_1} &= 0 \qquad \forall\ \omega \notin \Omega_1 \\ \Phi_{d_2d_2} &= 0 \qquad \forall\ \omega \notin \Omega_2 \end{aligned} \tag{B.6}$$

Further, if we define the set Ω of all disturbance frequencies

$$\Omega \equiv \{\Omega_1,\ \Omega_2\} \tag{B.7}$$

then

$$\Phi_{d_1d_1} = \Phi_{d_2d_2} = 0 \qquad \forall\ \omega \notin \Omega \tag{B.8}$$

If we now look at the control power at the frequencies not included in the disturbance signals, then from (B.3a), it follows that

$$\Phi_{\lambda\lambda} = \Phi_{nn}/|\Delta|^2 \qquad \forall\ \omega \notin \Omega \tag{B.9}$$

This is the control power injected by the operator between the spikes defined by the input disturbance frequencies, and is a relatively smooth looking function across frequency (McRuer and Krendel, 1959). Thus, we are motivated to define a control remnant power density which is smooth across frequency and which satisfies (B.9) above:

$$\hat{\Phi}_{\lambda\lambda} \equiv \Phi_{nn}/|\Delta|^2 \qquad \forall\ \omega \tag{B.10}$$

Note that

$$\begin{aligned} \Phi_{\lambda\lambda} &= \hat{\Phi}_{\lambda\lambda} \qquad \forall\ \omega \notin \Omega \\ &\neq \hat{\Phi}_{\lambda\lambda} \qquad \forall\ \omega \in \Omega \end{aligned} \tag{B.11}$$

We can now look at the ratio of control power to trainer velocity power, and specifically at the "vestibular" disturbance frequencies of d_1. From (B.3) and (B.6),

$$\Phi_{\lambda\lambda}/\Phi_{\omega_1\omega_1} = (1/|\Delta|^2)[\Phi_{nn} + |PH_1|^2\Phi_{d_1d_1}]/\Phi_{\omega_1\omega_1} \qquad \forall\ \omega\ \in \Omega_1 \qquad \text{(B.12)}$$

Use of (B.10) in the above expression results in

$$\Phi_{\lambda\lambda}/\Phi_{\omega_1\omega_1} = \hat{\Phi}_{\lambda\lambda}/\Phi_{\omega_1\omega_1} + |PH_1/\Delta|^2(\Phi_{d_1d_1}/\Phi_{\omega_1\omega_1}) \qquad \forall\ \omega\ \in \Omega_1 \qquad \text{(B.13)}$$

To eliminate the disturbance power from the expression above, we note, from (B.3a) and (B.8), that

$$\Phi_{\omega_1\omega_1} = |P/\Delta|^2[\Phi_{nn} + |1 + PH_2|^2\Phi_{d_1d_1}] \qquad \forall\ \omega\ \in \Omega_1 \qquad \text{(B.14)}$$

Solving this for $\Phi_{d_1d_1}$ and using (B.10) to eliminate Φ_{nn} results in

$$\Phi_{d_1d_1} = |(\Delta/P)/(1 + PH_2)|^2[\Phi_{\omega_1\omega_1} - |P|^2\hat{\Phi}_{\lambda\lambda}] \qquad \forall\ \omega\ \in \Omega_1 \qquad \text{(B.15)}$$

Substituting this into (B.13) then allows us to relate the remnant power to the total control power, as follows:

$$\Phi_{\lambda\lambda}/\Phi_{\omega_1\omega_1} = \hat{\Phi}_{\lambda\lambda}/\Phi_{\omega_1\omega_1} + |H_1/(1 + PH_2)|^2[1 - |P|^2(\hat{\Phi}_{\lambda\lambda}/\Phi_{\omega_1\omega_1})] \qquad \forall\ \omega\ \in \Omega_1 \qquad \text{(B.16)}$$

Thus, motivated by (4.8) and (4.9), we may define the following transfer function:

$$\alpha_1 \equiv -H_1/(1 + PH_2) \tag{B.17}$$

so that, from (B.16), we have

$$|\alpha_1| = \left\{ \left[\Phi_{\lambda\lambda}/\Phi_{\omega_1\omega_1} - \hat{\Phi}_{\lambda\lambda}/\Phi_{\omega_1\omega_1} \right] \Big/ \left[1 - |P|^2 (\Phi_{\lambda\lambda}/\Phi_{\omega_1\omega_1}) \right] \right\}^{1/2} \quad \forall\ \omega \in \Omega_1 \tag{B.18}$$

Note that the numerator tells us to subtract the remnant power appearing at the operator's output, and the denominator tells us to scale up the result according to the remnant power fed back to the operator via the plant P. Limiting behavior is as might be expected:

$$\begin{aligned} |\alpha_1| &\to (\Phi_{\lambda\lambda}/\Phi_{\omega_1\omega_1})^{1/2} \qquad \text{as} \qquad \hat{\Phi}_{\lambda\lambda} \to 0 \\ |\alpha_1| &\to 1/|P| \qquad\qquad\ \text{as} \qquad \hat{\Phi}_{\lambda\lambda} \to \infty \end{aligned} \tag{B.19}$$

That is, a small remnant implies that an input over output measure gives us a good approximation to α_1, whereas a large remnant results in the measurement simply reflecting the inverse of the plant dynamics.

The above development was concerned with the ratio of control power to trainer velocity power, evaluated at the "vestibular" disturbance frequencies (Ω_1). Clearly the same approach can be used with the ratio of control power to field velocity power, evaluated at the "visual" disturbance frequencies (Ω_2). The corresponding result is:

$$|\alpha_2| = \left\{ \left[\Phi_{\lambda\lambda}/\Phi_{\omega_2\omega_2} - \hat{\Phi}_{\lambda\lambda}/\Phi_{\omega_2\omega_2} \right] \Big/ \left[1 - |P|^2 (\hat{\Phi}_{\lambda\lambda}/\Phi_{\omega_2\omega_2}) \right] \right\}^{1/2} \quad \forall\ \omega \in \Omega_2 \tag{B.20}$$

where, motivated as before by (4.8) and (4.9), we have defined α_2 as follows:

$$|\alpha_2| \equiv H_2/(1 + PH_1) \tag{B.21}$$

From (B.20), the limiting behavior of α_2 is similar to that of α_1:

$$\begin{aligned} |\alpha_2| &\rightarrow (\Phi_{\lambda\lambda}/\Phi_{\omega_2\omega_2})^{1/2} \quad \text{as} \quad \hat{\Phi}_{\lambda\lambda} \rightarrow 0 \\ |\alpha_2| &\rightarrow 1/|P| \quad \text{as} \quad \hat{\Phi}_{\lambda\lambda} \rightarrow \infty \end{aligned} \tag{B.22}$$

Thus, (B.18) and (B.20) allow for the calculation of the α_i magnitudes, given the power spectra of the operator output, estimated remnant, trainer velocity, and field velocity. Section B.2 will discuss in more detail how this may be implemented using Fourier transforms of the signals.

B.1.2 Single-Input Calculations

The transform calculations appropriate to the two single input experments described in Chapters 2 and 4 can be considered special cases of the dual-input calculations just described.

For the self velocity-nulling experiments, only a "vestibular" transfer function is considered, and no visual loop disturbance is used. Thus, if we let

$$H_2 = d_2 = 0 \tag{B.23a}$$

and associate the combined estimator/control transfer function CE with H_1 in the previous section,

$$CE \equiv H_1 \tag{B.23b}$$

then, if we combine (B.17) with (B.18) and use (B.23) above, we find that

$$CE = \left\{\left[\Phi_{\lambda\lambda}/\Phi_{\omega_1\omega_1} - \hat{\Phi}_{\lambda\lambda}/\Phi_{\omega_1\omega_1}\right]\Big/\left[1 - |P|^2(\hat{\Phi}_{\lambda\lambda}/\Phi_{\omega_1\omega_1})\right]\right\}^{1/2}$$

$$\forall \ \omega \in \Omega_1 \tag{B.24}$$

which provides for a remnant corrected magnitude estimate of the operator's transfer function in the single-input self velocity-nulling task of Chapter 2.

A similar result can be derived for the field velocity-nulling experiment. Here the vestibular path is not part of the loop, and only a visual loop disturbance is used. Thus, if we let

$$H_1 = d_1 = 0 \tag{B.25a}$$

and associate the human operator transfer function C with H_2 of the previous section,

$$C \equiv H_2 \tag{B.25b}$$

Then, if we combine (B.20) with (B.21) and use (B.25) above, we find that

$$|C| = \left\{\left[\Phi_{\lambda\lambda}/\Phi_{\omega_2\omega_2} - \hat{\Phi}_{\lambda\lambda}/\Phi_{\omega_2\omega_2}\right]\Big/\left[1 - |P|^2(\hat{\Phi}_{\lambda\lambda}/\Phi_{\omega_2\omega_2})\right]\right\} \qquad \forall\ \omega \in \Omega_2 \tag{B.26}$$

which provides for a remnant corrected magnitude estimate of the operator's transfer function in the single-input field velocity nulling experiment of Chapter 4.

B.2 Implementation of Correction Method

The remnant correction method detailed in the previous section may be summarized by combining (B.18) and (B.20), to show how the magnitudes of the α_i transfer functions depend on the spectral densities of the measured variables:

$$|\alpha_i| = \left\{ \left[\Phi_{\lambda\lambda}/\Phi_{\omega_i\omega_i} - \hat{\Phi}_{\lambda\lambda}/\Phi_{\omega_i\omega_i} \right] \Big/ \left[1 - |P|^2 (\hat{\Phi}_{\lambda\lambda}/\Phi_{\omega_i\omega_i}) \right] \right\}^{1/2} \tag{B.27}$$

$$\forall \quad \omega \in \Omega_i \qquad (i = 1,2)$$

Implementation of this calculation is fairly straightforward. At each measurement frequency, a signal's power spectral density may be approximated by its measured power at that frequency divided by the frequency window of the measurement (Shirley, 1968; Magdaleno, 1972):

$$\Phi_{xx}(\omega) \simeq (A_x^2/2)/\Delta\omega \tag{B.28}$$

where A_x is the signal's amplitude at frequency ω, obtained from a Fourier transform of the signal, and where $\Delta\omega$ is determined by the signal sample length T, and given by $2\pi/T$. Thus, the signal's Fourier components may be used directly in the above calculations. The problem, of course, is in separating the remnant component of the control signal, $\hat{\Phi}_{\lambda\lambda}$, from the total control signal power, $\Phi_{\lambda\lambda}$, at the input disturbance frequencies.

Recognizing that the remnant spectral density is a continuous function of frequency (McRuer and Krendel, 1959; Levison et al, 1969), an estimate of the remnant at the loop disturbance frequencies ($\omega \in \Omega$) may be obtained

from the remnant observed at all frequencies in between ($\omega \notin \Omega$). One particular estimation approach is described by Magdelano (1972), in which averaging of neighboring components is used to infer the remnant power at the disturbance frequencies. A similar approach is used here.

Figure B.1 shows two control wheel amplitude spectra superimposed on one another, obtained from FFT processing of one subject's response during two dual-input presentations of the self velocity-nulling experiment described in Chapter 4. Circles show operator response at the "vestibular" disturbance frequencies contained in d_1 (Ω_1) and squares show response at the "visual" disturbance frequencies contained in d_2 (Ω_2). The dots indicate response power at all other frequencies which are multiples of the frequency window of 1/128 Hz. The smooth curve drawn is an approximating fit to this remnant power, and is defined as a constant below the break frequency shown and as a Gaussian function above the break frequency. This continuous function thus affords an estimate of the remnant power at the "visual" and "vestibular" disturbance frequencies.

For each individual, remnant curves may be fit in this manner to the subject's uncorrelated response, and then used to infer his remnant contribution at the measurement frequencies. Specifically, remnant amplitude may be estimated from the curve fit and then used to calculate remnant power spectral density according to (B.28). This yields $\hat{\Phi}_{\lambda\lambda}$ at each disturbance frequency. Total response power spectral density, $\Phi_{\lambda\lambda}$, may also be estimated from (B.28); in this case the amplitude is

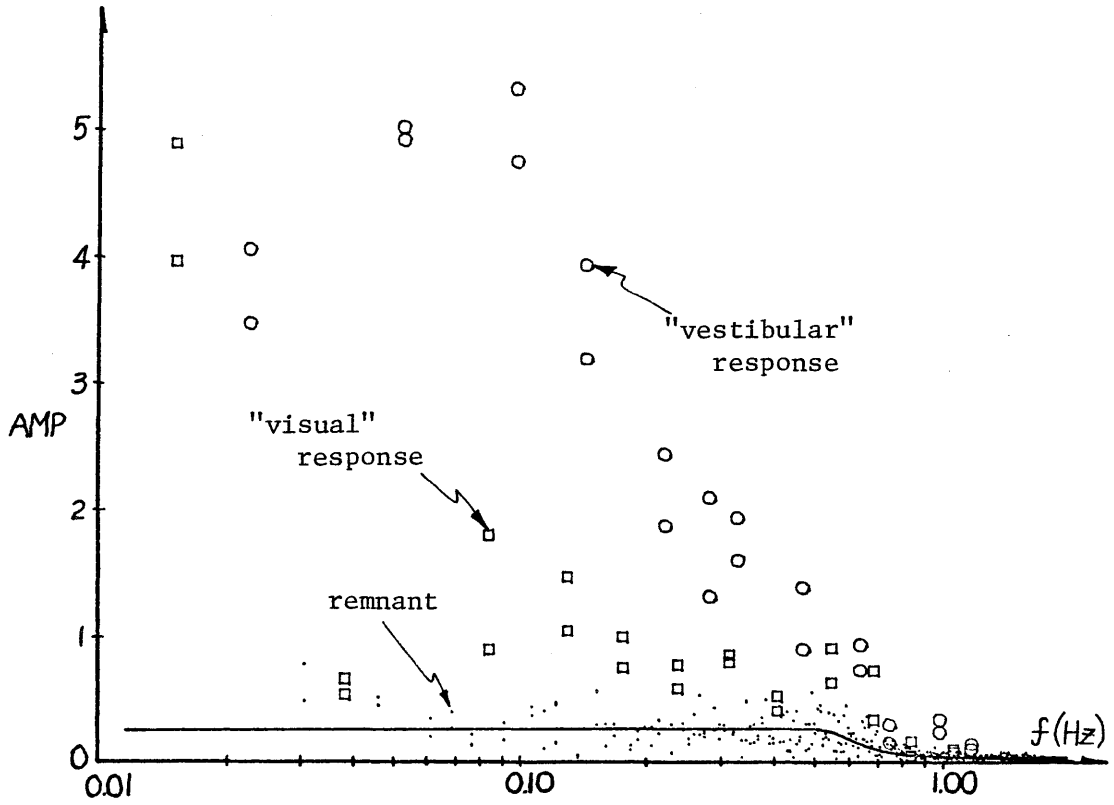

Figure B.1 Control wheel amplitude spectra

simply the measured amplitude obtained directly from the FFT (i.e., the amplitude indicated by the circles or squares of figure B.1). Since a ratio of power spectral densities eliminates the frequency window factor in (B.28), the α_i magnitudes can be calculated directly from (B.27) in the following manner:

$$|\alpha_i| = \left\{ \left[A^2_{\lambda}/A^2_{\omega_i} - A^2_r/A^2_{\omega_i} \right] \Big/ \left[1 - |P|^2 (A^2_r/A^2_{\omega_i}) \right] \right\}^{1/2} \qquad \forall\ \omega \in \Omega_i \tag{B.29}$$

where A_λ is control wheel response amplitude, A_{ω_i} is velocity amplitude (trainer or field), and A_r is control wheel remnant amplitude; the first two are measured at each disturbance frequency, while the last is inferred from the remnant curve. Knowledge of the plant amplitude ratio $|P|$, obtained from the response curves of appendix A, then allows for the calculation of $|\alpha_i|$. The same approach, of course, can be used to implement the single-input transfer function calculations specified by (B.24) and (B.26).

B.3 Response Data Corrected for Remnant Power

It should be clear from the preceeding discussion that the α_i transfer functions can be calculated directly from the Fourier components of the human operator's input and output signals, if remnant contributions are small. That is, from (B.19) and (B.22),

$$|\alpha_i| \simeq (\Phi_{\lambda\lambda}/\Phi_{\omega_i\omega_i})^{1/2} \qquad \text{if} \qquad \hat{\Phi}_{\lambda\lambda} \simeq 0 \tag{B.30}$$

when calculated at the appropriate disturbance frequencies. From (B.29), the equivalent expression, using Fourier transforms of the signals, is

$$|\alpha_i(f_{ij})| \simeq |\lambda(f_{ij})|/|\omega_i(f_{ij})| \qquad \text{if} \qquad \hat{\Phi}_{\lambda\lambda} \simeq 0 \tag{B.31a}$$

where f_{ij} represents the jth frequency contained in the loop disturbance signal d_i.

Since the remnant is considered to have a uniformly distributed phase angle at any given frequency, the calculated phase of α_i is not affected by the presence of remnant power. That is, independent of remnant magnitude, we have

$$\angle\, \alpha_i(f_{ij}) = \angle\, \lambda(f_{ij}) - \angle\, \omega_i(f_{ij}) \tag{B.31b}$$

Combining the last two relations results in a method of calculating the α_i directly from the signal transforms, valid for small remnant power:

$$\alpha_i(f_{ij}) \simeq \lambda(f_{ij})/\omega_i(f_{ij}) \qquad (\hat{\Phi}_{\lambda\lambda} \simeq 0) \tag{B.32}$$

The most direct method of validating the appropriateness of this approximation is to compare the calculated describing functions obtained with this method with those obtained by using the remnant correction method described in the previous section. Figure B.2 and B.3 present the calculated estimator describing function data obtained by using (B.32) and using the computational procedure detailed in Chapter 4; the figures are repeated from figures 4.11 and 4.12 in the text. It should be pointed out that neither the self velocity-nulling data nor the field velocity-nulling data (used for correcting the data for the presence of operator dynamics) was corrected for the presence of remnant power.

Also shown on the figure are circles indicating population means obtained by using the remnant correction method of the preceeding section, for both the self velocity-nulling data and the field velocity-nulling data. What should be clear is that the corrected data is not significantly different from the uncorrected data obtained by using (B.32) and assuming small remnant contributions at the disturbance frequencies. This suggests that the simpler method of direct calculation from the signal transforms is sufficiently adequate considering the spread of the experimental data.

Although this discussion has been primarily concerned with the dual-input experimental data of Chapter 4, the same argument holds for the single-input self velocity-nulling experiments of Chapters 2 and 3, and the subsidiary field-nulling experiment of Chapter 4. That is, from (B.24) and (B.26),

Figure B.2: Vestibular channel estimator: Remnant Corrections

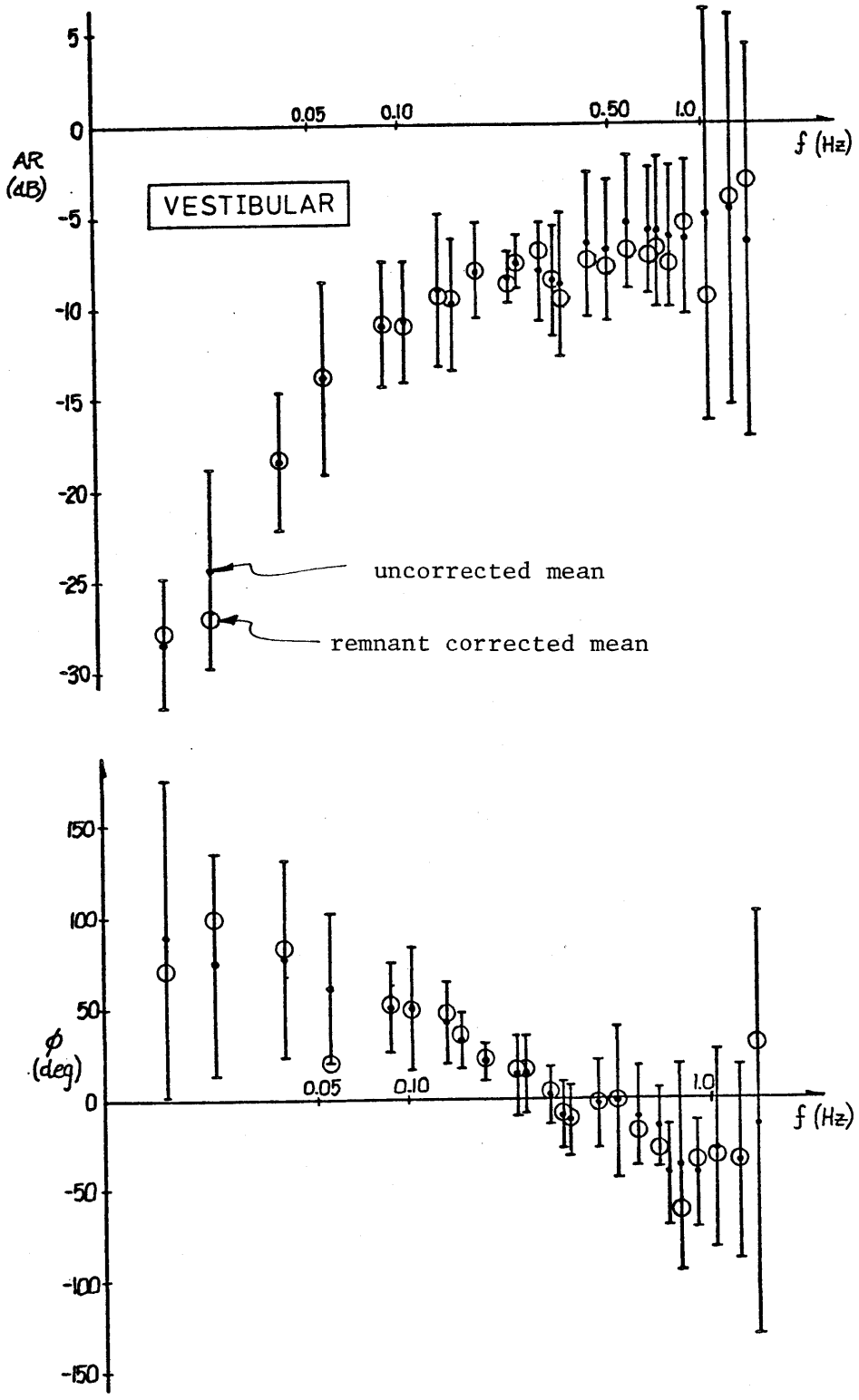

Figure B.3: Visual channel estimator: Remnant corrections

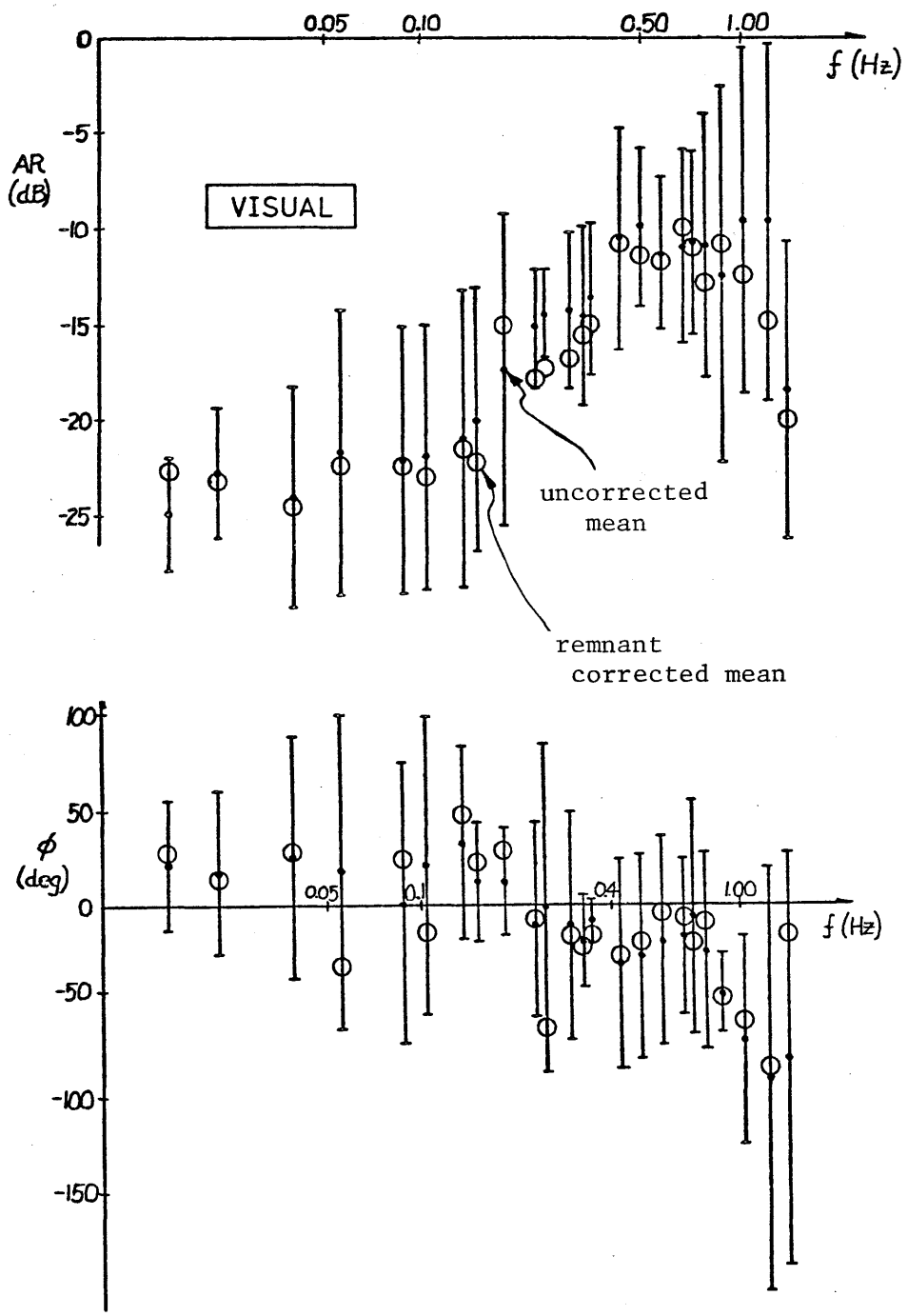

$$CE(f_{1j}) \simeq -\lambda(f_{1j})/\omega_1(f_{1j}) \quad \text{(a)}$$
$$C(f_{2j}) \simeq -\lambda(f_{2j})/\omega_2(f_{2j}) \quad \text{(b)} \qquad \text{(B.33)}$$

where, as before, f_{ij} is the jth frequency in disturbance d_i.

APPENDIX C

PROGRAM LISTING FOR PDP-11/34 PROCESSING

This appendix presents program listings used in PDP-11 processing of the recorded experimental data generated from the experiments described in chapter 4. For notational convenience below, the letters SI refer to single input loops, which correspond to either the CON presentation configuration of the velocity-nulling experiment, or to the field velocity-nulling experiment used to determine human operator response characteristics. The letters DI refer to dual-input loop, which corresponds to the DI presentation configuration of the velocity-nulling experiment.

Programs SISAM and DISAM are written in a hybrid of RT11 BATCH and SPARTA, and are used to sample and digitize the recorded experimental variables. For SISAM, it is assumed that trainer velocity is on analog-to digital channel AD8, and wheel deflection on AD9; for DISAM, the channel allocation is: trainer velocity AD8, projector velocity on AD9, and wheel deflection on AD10. Both programs sample for 128 s at 8 Hz, Fourier transform the input signals to obtain gain and phase, and then write this data onto a prespecified data file, assigned to a particular experiment type and subject.

Programs REMSI and REMDI are used to read these data files and generate amplitude spectra plots of trainer velocity, wheel deflection and, for the DI experimental series, projector velocity. No new files are generated by these programs.

Programs SIEXP and DIEXP are used to read the transformed data files also, and calculate the appropriate operator transfer functions. SIEXP can be used to calculate CE according to (3.6), which relates wheel deflection to trainer velocity; or, can be used similarly to calculate C alone, which relates wheel deflection to field velocity, in the manual control task. DIEXP is used to calculate CE_1 and CE_2 according to (4.10) and the algorithm description given in section 4.3. Both programs interpolate between test frequencies where necessary , and provide describing function output (gain and phase) at the TTY console. This data is also written onto a prespecified data file, assigned to the particular experiment type and subject.

Programs SIDIV and DIDIV operate on this data file to generate velocity estimator transfer functions which have been corrected for the effects of manual control dynamics. For each individual, SIDIV divides the describing function data defining CE by that defining C, to arrive at an estimator function E; DIDIV operation is similar, except that both CE_1 and CE_2 are corrected to yield two estimator transfer functions, E_1 and E_2. Both programs use complex arithmetic to effect the division and frequency interpolation when necessary. Describing function output (gain and phase) is provided at the TTY console, and also written onto a prespecified data file, assigned to the particular experiment type and subject.

Programs FILER1 AND FILER2 are used to generate condensed summary files of gain and phase information, associated with one test condition

experiment type. The format is chosen to be compatible with the input format of the BMD07R program (Dixon, 1973) used for later off-line processing and curve fitting.

Programs SIEXPC and DIEXPC are similar to SIEXP and DIEXP, respectively, but also provide for remnant corrected describing function outputs. The algorithms used are described in Appendix B.

```
\C
$JOB/LIST

$RT11
\LLOOP  \CLOOP:
\ER SPARTA
\DBBU S4 F2 1024
MOF
\@ENTER FILE NAME (WITH <, IF NEW)
\G
BSU S1
BSU S2
BSU S3
BSU S4
AAD S1 8 P C
C8 2 1 0 I
\@SAMPLE NOW
\G
\G
SAD S1 -2048
DDI S1
DID
DLO
DLO
DLO
SAD S2 -2048
DDI S2 0
FFT S1 S3
FFT S2 S4
FMP S3 S1 F1 F2
DDI F1
MOU F1 256 01
MOU F2 256 01
FMP S4 S2 F1 F2
MOU F1 256 01
MOU F2 256 01
MCL
EXT
\F
\C      GOTO -LOOP
\JLOOP  0\C
$EOJ
\L$$$$$$\F\ER BATCH
\D/R
\E\F
*
```

PROGRAM SISAM

```
\C
$JOB/LIST

$RT11
\LLOOP  \CLOOP:
\ER SPARTA
\DBBU S6 F2 1024
MOF
\@ENTER FILE NAME (WITH <, IF NEW)
\G
BSU S1
BSU S2
BSU S3
BSU S4
BSU S5
BSU S6
AAD S1 8 P C
C8 3 1 0 I
\@SAMPLE NOW
\G
\G
SAD S1 -2048
DDI S1
DID
DLO
DLO
DLO
SAD S2 -2048
DDI S2 0
SAD S3 -2048
DDI S3 0
FFT S1 S4
FFT S2 S5
FFT S3 S6
FMP S4 S1 F1 F2
DDI F1
MOU F1 256 01
MOU F2 256 01
FMP S5 S2 F1 F2
MOU F1 256 01
MOU F2 256 01
FMP S6 S3 F1 F2
MOU F1 256 01
MOU F2 256 01
MCL
EXT
\F
\C      GOTO -LOOP
\JLOOP  0\C
$EOJ
\L$$$$$$\F\ER BATCH
\D/R
\E\F
*
```

PROGRAM DISAM

```
FORTRAN IV      V01C-03A

      C
      C     PROGRAM REMSI.GLZ  2 DEC 76
      C
0001        DIMENSION XIN(1024),WEELG(256),WEELP(256),NF(19),
           1             FREQ(256),XMAX(2),XMIN(2),V(2,256),
           1          XOUT(2,256),XZ(2),VZ(2),YOUT(2,13)
0002        REAL LINKG(256),LINKP(256)
0003        INTEGER SF
      C
0004        EQUIVALENCE (XIN(  1),LINKG(1)),
           1                (XIN(257),LINKP(1)),
           1                (XIN(513),WEELG(1)),
           1                (XIN(769),WEELP(1))
      C
      C
0005        DEFINE FILE 1 (1,2048,U,NREC)
0006        WRITE(7,200)
0007      200 FORMAT(/////,5X,'ENTER INPUT FILENAME: '$)
0008        CALL ASSIGN(1,,-1)
0009        READ (1'1) XIN
0010        CALL CLOSE(1)
      C
0011        WRITE(7,211)
0012      211 FORMAT(5X,'ENTER 1 FOR LINK/STRIPE OR 2 FOR WHEEL: '$)
0013        READ(5,100) L
      C
0014        WRITE(7,210)
0015      210 FORMAT(5X,'ENTER SCALE FACTOR: '$)
0016        READ(5,100) SF
0017      100 FORMAT(I1)
      C
0018        SFGAIN=2**SF
      C
0019        XOUT(1,1)=0.
0020        XOUT(2,1)=0.
0021        XOUT(1,2)=0.
0022        XOUT(2,2)=0.
      C
0023        DO 5 I=3,256
0024        FREQ(I)=(I-1)/128.
0025        XOUT(1,I)=ALOG10(FREQ(I)) + 2.
0026        IF(L .EQ. 1) TEMP=LINKG(I)
0028        IF(L .EQ. 2) TEMP=WEELG(I)
0030        XOUT(2,I)=TEMP*SFGAIN
      C
0031        DO 10 J=1,13
0032        IF(I .NE. (NF(J)+1)) GO TO 10
0034        DO 15 K=1,2
0035        YOUT(K,J)=XOUT(K,I)
0036        XOUT(K,I)=XOUT(K,I-1)
0037       15 CONTINUE
0038       10 CONTINUE
0039        5 CONTINUE
      C
```

```
FORTRAN IV      V01C-03A

0040        WRITE(7,205)(FREQ(NF(I)+1),YOUT(2,I),I=1,13)
0041      205 FORMAT(2X,F6.3,5X,F10.2)
      C
0042        WRITE(7,201)
0043      201 FORMAT(//,5X,'ENTER YMIN,YMAX (2F7.2): '$)
0044        READ(5,202) XMIN(2),XMAX(2)
0045      202 FORMAT(2F7.2)
0046        XMAX(2)=(XMAX(2)-XMIN(2))*(301./300.)+XMIN(2)
      C
0047        CALL SCALER(1,XZ,XMAX,XMIN,VZ)
0048        CALL ZERO(VZ)
      C
0049        CALL SCALER(256,XOUT,XMAX,XMIN,V)
0050        CALL POINT(256,V)
      C
0051        CALL SCALER(13,YOUT,XMAX,XMIN,V)
0052        CALL CIRCLE(13,V)
0053        STOP
      C
0054        DATA XMIN/0.,0./
0055        DATA XMAX/2.86,300000./
0056        DATA XZ/0.,0./
      C
0057        DATA PI,RTD/3.14159,57.296/
      C     DATA NF/2,3,5,7,11,17,23,29,37,47,59,73,89,107,127,
      C     1           149,173,199,229/
      C     FREQS FOR D1 (VESTIBULAR)
      C     DATA NF/3,7,13,19,29,37,43,61,83,97,127,151,229,6*0/
      C     FREQS FOR D2 (VISUAL)
0058        DATA NF/2,5,11,17,23,31,41,53,71,89,109,137,173,6*0/
0059        END
*
```

```
      C
      C     PROGRAM REMDI.GLZ 27 DEC 76
      C
0001        DIMENSION XIN(1536),FILMG(256),FILMP(256),WEELG(256),
           1       WEELP(256),NF(26),FREQ(256),XMAX(2),XMIN(2),V(2,256),
           1     XOUT(2,256),XZ(2),VZ(2),YOUT(2,13),ZOUT(2,13)
      C
0002        REAL LINKG(256),LINKP(256)
0003        INTEGER SF
      C
0004        EQUIVALENCE     (XIN(   1),LINKG(1)),
           1                (XIN( 257),LINKP(1)),
           1                (XIN( 513),FILMG(1)),
           1                (XIN( 769),FILMP(1)),
           1                (XIN(1025),WEELG(1)),
           1                (XIN(1281),WEELP(1))
      C
0005      1 CONTINUE
0006        DEFINE FILE 1 (1,3072,U,NREC)
0007        WRITE(7,200)
0008      200 FORMAT(/////,5X,'ENTER INPUT FILENAME: '$)
      C
0009        CALL ASSIGN(1,,-1)
0010        READ (1'1) XIN
0011        CALL CLOSE(1)
      C
0012        WRITE(7,211)
0013      211 FORMAT(5X,'ENTER 1 FOR LINK, 2 FOR WHEEL, 3 FOR FILM: '$)
0014        READ(5,100) L
      C
0015        WRITE(7,210)
0016      210 FORMAT(5X,'ENTER SCALE FACTOR: '$)
0017        READ(5,100) SF
0018      100 FORMAT(I1)
      C
0019        SFGAIN=2**SF
      C
0020        XOUT(1,1)=0.
0021        XOUT(2,1)=0.
0022        XOUT(1,2)=0.
0023        XOUT(2,2)=0.
      C
0024        DO 5 I=3,256
0025        FREQ(I)=(I-1)/128.
0026        XOUT(1,I)=ALOG10(FREQ(I)) + 2.
0027        IF(L .EQ. 1) TEMP=LINKG(I)
0029        IF(L .EQ. 2) TEMP=WEELG(I)
0031        IF(L .EQ. 3) TEMP=FILMG(I)
0033        XOUT(2,I)=TEMP*SFGAIN
      C
0034        DO 10 J=1,13
0035        I1=2*J
0036        I2=I1-1
0037        IF(I .EQ. (NF(I1)+1)) GO TO 11  !CHECK FOR VES FREQS
```



```
0039        IF(I .EQ. (NF(I2)+1)) GO TO 12  !CHECK FOR VIS FREQS
0041        GO TO 10
0042     11 CONTINUE     !SET YOUT (CIRCLES) TO VES FREQ INPUTS
0043        DO 15 K=1,2
0044        YOUT(K,J)=XOUT(K,I)
0045     15 XOUT(K,I)=XOUT(K,I-1)
0046        GO TO 10
0047     12 CONTINUE     !SET ZOUT (SQUARES) TO VIS FREQ INPUTS
0048        DO 14 K=1,2
0049        ZOUT(K,J)=XOUT(K,I)
0050     14 XOUT(K,I)=XOUT(K,I-1)
0051     10 CONTINUE
0052      5 CONTINUE
      C
0053        WRITE(7,205)(FREQ(NF(I)+1),YOUT(2,I/2),I=2,26,2)
0054    205 FORMAT(2X,F6.3,5X,F10.2)
0055        WRITE(7,206)
0056    206 FORMAT(//)
0057        WRITE(7,205)(FREQ(NF(I)+1),ZOUT(2,(I+1)/2),I=1,25,2)
      C
0058        WRITE(7,201)
0059    201 FORMAT(//,5X,'ENTER YMIN,YMAX (2F7.2): '$)
0060        READ(5,202) XMIN(2),XMAX(2)
0061    202 FORMAT(2F7.2)
0062        XMAX(2)=(XMAX(2)-XMIN(2))*(301./300.)+XMIN(2)
      C
0063        CALL SCALER(1,XZ,XMAX,XMIN,VZ)
0064        CALL ZERO(VZ)
      C
0065        CALL SCALER(256,XOUT,XMAX,XMIN,V)
0066        CALL POINT(256,V)
      C
0067        CALL SCALER(13,YOUT,XMAX,XMIN,V)
0068        CALL CIRCLE(13,V)
      C
0069        CALL SCALER(13,ZOUT,XMAX,XMIN,V)
0070        CALL SQUARE(13,V)
      C
0071        STOP
      C
0072        DATA XMIN/0.,0./
0073        DATA XMAX/2.86,300000./
0074        DATA XZ/0.,0./
      C
0075        DATA PI,RTD/3.14159,57.296/
0076        DATA NF/2,3,5,7,11,13,17,19,23,29,31,37,41,43,53,61,71,
           1              83,89,97,109,127,137,151,173,229/
      C     FREQS FOR D1 (VESTIBULAR)
      C     DATA NF/3,7,13,19,29,37,43,61,83,97,127,151,229,6*0/
      C     FREQS FOR D2 (VISUAL)
      C     DATA NF/2,5,11,17,23,31,41,53,71,89,109,137,173,6*0/
0077        END
      *
```

```
      C
      C     PROGRAM SIEXP.GLZ 4 OCT 76
      C
0001        DIMENSION XIN(1024),WEELG(256),WEELP(256),NF(19),
           1          GAIN(19),PHASE(19),FREQ(19)
0002        REAL LINKG(256),LINKP(256)
0003        INTEGER SF(2)
      C
0004        EQUIVALENCE (XIN(  1),LINKG(1)),
           1            (XIN(257),LINKP(1)),
           1            (XIN(513),WEELG(1)),
           1            (XIN(769),WEELP(1))
      C
0005      1 CONTINUE
      C
0006        DEFINE FILE 1 (1,2048,U,NREC)
0007        WRITE(7,200)
0008    200 FORMAT(/////,5X,'ENTER INPUT FILENAME: '$)
0009        CALL ASSIGN(1,,-1)
0010        READ (1'1) XIN
0011        CALL CLOSE(1)
      C
0012        WRITE(7,210)
0013    210 FORMAT(5X,'ENTER SCALE FACTORS: '$)
0014        READ(5,100)(SF(I),I=1,2)
0015    100 FORMAT(2I1)
      C
0016        T1=2.**(SF(2)-SF(1))
0017        TEMP=2.*PI
0018        DO 5 I=1,13
0019        J=NF(I)+1
0020        GAIN(I)=20.*ALOG10(T1*WEELG(J)/LINKG(J))
0021        PHASE(I)=WEELP(J)-LINKP(J) + PI
0022        IF(PHASE(I) .GE. TEMP) PHASE(I)=PHASE(I)-TEMP
0024        IF(PHASE(I) .LT.   0.) PHASE(I)=PHASE(I)+TEMP
0026        PHASE(I)=RTD*(PHASE(I)-TEMP)
0027        FREQ(I)=NF(I)/128.
0028      5 CONTINUE
      C
0029        WRITE(7,220)
0030    220 FORMAT(5X,'N',2X,'NF',3X,'FREQ',8X,'GAIN',7X,'PHASE',
           1          //)
0031        WRITE(7,230)(I,NF(I),FREQ(I),GAIN(I),PHASE(I),I=1,13)
0032    230 FORMAT(2X,2I4,F7.3,2F12.2)
      C
0033        WRITE(7,240)
0034    240 FORMAT(//,5X,'ENTER OUTPUT FILENAME: '$)
0035        CALL ASSIGN(2,,-1)
0036        WRITE(2,250)(NF(I),FREQ(I),GAIN(I),PHASE(I),I=1,13)
0037    250 FORMAT(1X,I3,F5.3,2F8.3)
0038        CALL CLOSE(2)
      C
0039        GO TO 1
      C
```



```
0040        STOP
0041        DATA PI,RTD/3.14159,57.296/
      C     DATA NF/2,3,5,7,11,17,23,29,37,47,59,73,89,107,127,
      C     1           149,173,199,229/
      C     FREQS FOR D1 (VESTIBULAR)
0042        DATA NF/3,7,13,19,29,37,43,61,83,97,127,151,229,6*0/
      C     FREQS FOR D2 (VISUAL)
      C     DATA NF/2,5,11,17,23,31,41,53,71,89,109,137,173,6*0/
0043        END
*
```

```
FORTRAN IV      V01C-03A

      C
      C     PROGRAM DIEXP.GLZ 1 OCT 76
      C
0001        DIMENSION XIN(1536),FILMG(256),FILMP(256),WEELG(256),
           1       WEELP(256),NF(26),X1G(26),X2G(26),X1P(26),X2P(26),
           1       FREQ(26),PHASE(52),GAIN(52),PG(26),PP(26),
           1       Y1G(26),Y1P(26),Y2G(26),Y2P(26)
0002        REAL LINKG(256),LINKP(256)
0003        INTEGER SF(3)
0004        COMPLEX X1(26),X2(26),P(26),Y1(26),Y2(26),TEMPC
      C
0005        EQUIVALENCE     (XIN(   1),LINKG(1)),
           1                (XIN( 257),LINKP(1)),
           1                (XIN( 513),FILMG(1)),
           1                (XIN( 769),FILMP(1)),
           1                (XIN(1025),WEELG(1)),
           1                (XIN(1281),WEELP(1))
      C
0006        EQUIVALENCE     (PHASE( 1),X1P(1)),
           1                    (PHASE(27),X2P(1)),
           1                    (PHASE( 1),Y1P(1)),
           1                    (PHASE(27),Y2P(1)),
           1                    (GAIN( 1),Y1G(1)),
           1                    (GAIN(27),Y2G(1))
      C
0007      1 CONTINUE
0008        DEFINE FILE 1 (1,3072,U,NREC)
0009        WRITE(7,200)
0010      200 FORMAT(/////,5X,'ENTER INPUT FILENAME: '$)
      C
0011        CALL ASSIGN(1,,-1)
0012        READ (1'1) XIN
0013        CALL CLOSE(1)
      C
0014        WRITE(7,210)
0015      210 FORMAT(5X,'ENTER SCALE FACTORS: '$)
0016        READ(5,100) (SF(I),I=1,3)
0017      100 FORMAT(3I1)
      C
      C     CALC GAIN AND PHASE FOR X1 AND X2, FROM INPUTS
      C
0018        T1=2.**(SF(3)-SF(1))
0019        T2=2.**(SF(3)-SF(2))
0020        DO 5 I=1,13
0021        I1=2*I
0022        I2=I1-1
0023        J1=NF(I1)+1
0024        J2=NF(I2)+1
0025        X1G(I1)=T1*WEELG(J1)/LINKG(J1)
0026        X1P(I1)=WEELP(J1)-LINKP(J1)
0027        X2G(I2)=T2*WEELG(J2)/FILMG(J2)
0028        X2P(I2)=WEELP(J2)-FILMP(J2)
0029      5 CONTINUE
      C
```

```
FORTRAN IV      V01C-03A

0030        DO 10 I=1,26
0031      10 FREQ(I)=NF(I)/128.
      C
      C     LIMIT PHASE TO BETWEEN ZERO AND 2*PI
      C
0032        CALL AMOD(PHASE)
      C
      D     WRITE(7,220)(I,NF(I),FREQ(I),X1G(I),X1P(I)*RTD,X2G(I),
      D    1            X2P(I)*RTD, I=1,26)
      C
      C     USE ALIN TO INTERPOLATE POINTS NOT ORIGINALLY IN DATA
      C
0033        CALL ALIN(NF,X1G,2,24,0)
0034        CALL ALIN(NF,X1P,2,24,1)
0035        CALL ALIN(NF,X2G,1,23,0)
0036        CALL ALIN(NF,X2P,1,23,1)
      C
      C     ADDITIONAL CALC FOR END POINTS OF X1 AND X2
      C
0037        TEMP=1.*(NF(1)-NF(2))/(NF(4)-NF(2))
0038        X1G(1)=X1G(2)+TEMP*(X1G(4)-X1G(2))
0039        DELP=X1P(4)-X1P(2)
0040        X1P(1)=X1P(2)+TEMP*DELP
0041        IF(ABS(DELP) .GT. PI) X1P(I)=X1P(I)+PI
0043        TEMP=1.*(NF(26)-NF(23))/(NF(25)-NF(23))
0044        X2G(26)=X2G(23)+TEMP*(X2G(25)-X2G(23))
0045        DELP=X2P(25)-X2P(23)
0046        X2P(26)=X2P(23)+TEMP*DELP
0047        IF(ABS(DELP) .GT. PI) X2P(26)=X2P(26)+PI
      C
0049        CALL AMOD(PHASE)
      C
      C     DUMP OUT GAIN AND PHASE FOR X1 AND X2
      C
      D     WRITE(7,220)(I,NF(I),FREQ(I),X1G(I),X1P(I)*RTD,X2G(I),
      D    1                X2P(I)*RTD,I=1,26)
      C
      C
      C     CONVERT TO COMPLEX VECTORS FOR X1 AND X2 AND P
      C
0050        DO 20 I=1,26
0051        T1=X1G(I)*COS(X1P(I))
0052        T2=X1G(I)*SIN(X1P(I))
0053        X1(I)=CMPLX(T1,T2)
0054        T1=X2G(I)*COS(X2P(I))
0055        T2=X2G(I)*SIN(X2P(I))
0056        X2(I)=CMPLX(T1,T2)
0057        TEMP=10.**(PG(I)/20.)
0058        T1=TEMP*COS(PP(I)/RTD)
0059        T2=TEMP*SIN(PP(I)/RTD)
0060        P(I)=CMPLX(T1,T2)
      C
      C     CALC Y1 AND Y2 (COMPLEX)
      C
```

```
FORTRAN IV      V01C-03A

0061          TEMPC=P(I)*P(I)*X1(I)*X2(I)+1.
0062          Y1(I)=-X1(I)*(1.+P(I)*X2(I))/TEMPC
0063          Y2(I)=+X2(I)*(1.-P(I)*X1(I))/TEMPC
      C
      C       CONVERT TO GAIN AND PHASE NOTATION
      C
0064          Y1G(I)=CABS(Y1(I))
0065          Y1P(I)=ATAN2(AIMAG(Y1(I)),REAL(Y1(I)))
0066          Y2G(I)=CABS(Y2(I))
0067          Y2P(I)=ATAN2(AIMAG(Y2(I)),REAL(Y2(I)))
0068       20 CONTINUE
      C
      C       NOTE THAT WEVE DESTROYED X1P AND X2P
      C       ALSO, CHANGE OUTPUT GAIN TO DB
      C
0069          CALL AMOD(PHASE)
0070          DO 25 I=1,52
0071          GAIN(I)=20.*ALOG10(GAIN(I))
0072       25 CONTINUE
      C
0073          WRITE(7,230)
0074      230 FORMAT(//)
0075          WRITE(7,240)
0076      240 FORMAT(5X,'N',2X,'NF',3X,'FREQ',6X,'Y1GAIN',5X,'Y1PHASE',
             1            6X,'Y2GAIN',5X,'Y2PHASE',//)
      C
0077          TEMP=2.*PI
0078          DO 26 I=1,52
0079       26 PHASE(I)=RTD*(PHASE(I)-TEMP)
0080          WRITE(7,220)(I,NF(I),FREQ(I),Y1G(I),Y1P(I),Y2G(I),Y2P(I),
             1                    I=1,26)
0081      220 FORMAT(2X,2I4,F7.3,F12.4,F12.1,F12.4,F12.1)
      C
0082          WRITE(7,250)
0083      250 FORMAT(//,5X,'ENTER OUTPUT FILENAME: '$)
0084          CALL ASSIGN(2,,-1)
0085          WRITE(2,260)(NF(I),FREQ(I),Y1G(I),Y1P(I),Y2G(I),Y2P(I),
             1                  I=1,26)
0086      260 FORMAT(1X,I3,F5.3,4F8.3)
0087          CALL CLOSE(2)
      C
0088          GO TO 1
      C
0089          STOP
      C
0090          DATA RTD,PI/57.294,3.14159/
0091          DATA X1G,X1P,X2G,X2P/104*0./
0092          DATA XIN/1536*0./
0093          DATA NF/2,3,5,7,11,13,17,19,23,29,31,37,41,43,53,61,71,
             1            83,89,97,109,127,137,151,173,229/
      C
      C       PLANT GAIN AND PHASE GIVEN IN DB AND DEG,RESPECTIVELY
      C
0094          DATA PG/8*0.,-.01,-.02,-.02,-.05,-.07,-.08,-.19,-.33,-.58,
```

```
FORTRAN IV      V01C-03A

             1            -1.04,-1.32,-1.77,-2.56,-3.94,-4.77,-5.97,-7.84,
             1            -12.20/
0095          DATA PP/-1.4,-2.1,-3.5,-4.9,-7.7,-9.2,-12.0,-13.5,-16.4,
             1            -20.8,-22.3,-26.8,-29.9,-31.5,-39.5,-46.1,-54.6,
             1            -64.7,-69.7,-76.2,-85.5,-97.9,-103.8,-111.2,
             1            -120.6,-136.4/
0096          END
```

```
FORTRAN IV      V01C-03A

0001          SUBROUTINE ALIN(N,X,IS,IF,IFLAG)
0002          DIMENSION N(26),X(26)
0003          DO 5 I=IS,IF,2
0004          TEMP=X(I+2)-X(I)
0005          X(I+1)=X(I)+TEMP*(N(I+1)-N(I))/(N(I+2)-N(I))
0006          IF (IFLAG .EQ. 0) GO TO 5
0008          IF (ABS(TEMP) .GT. PI) X(I+1)=X(I+1)+PI
0010        5 CONTINUE
0011          RETURN
0012          DATA PI/3.14159/
0013          END
```

```
FORTRAN IV      V01C-03A

0001          SUBROUTINE AMOD(P)
0002          DIMENSION P(52)
0003          TEMP=2.*PI
0004          DO 1 I=1,52
0005          IF(P(I) .GE. TEMP) P(I)=P(I)-TEMP
0007          IF(P(1) .LT. 0.  ) P(I)=P(I)+TEMP
0009        1 CONTINUE
0010          RETURN
0011          DATA PI/3.14159/
0012          END
*
```

```
FORTRAN IV      V01C-03A

      C     PROGRAM SIDIV.GLZ 23 DEC 76
      C
0001        DIMENSION XL(26,2),XS(26,2),X(26,2),FREQ(26),NF(26)
      C
0002      1 CONTINUE
      C
0003        WRITE(7,210)
0004      210 FORMAT(5X,'ENTER NUMERATOR FILE:',//)
0005        CALL ASSIGN(1,,-1)
0006        WRITE(7,220)
0007      220 FORMAT(5X,'ENTER DENOM FILE:',//)
0008        CALL ASSIGN(2,,-1)
0009        READ(1,100)(XL(I,1),XL(I,2),I=2,26,2)
0010        READ(2,100)(XS(I,1),XS(I,2),I=1,25,2)
      C
      C     (9X,F8.3,8X,F8.3) FOR UNCORRECTED GAIN
      C     (17X,2F8.3)       FOR CORRECTED   GAIN
0011      100 FORMAT(9X,F8.3,8X,F8.3)
      C   100    FORMAT(17X,2F8.3)
0012        CALL CLOSE(1)
0013        CALL CLOSE(2)
      C
0014        DO 5 I=1,26
0015       5 FREQ(I)=NF(I)/128.
      C
0016        DO 10 J=1,2    !INTERPOLATE FOR MISSING XS POINTS
0017        XS(26,J)=(XS(25,J)-XS(23,J))*(FREQ(26)-FREQ(23))/
           1              (FREQ(25)-FREQ(23))+XS(23,J)
0018        DO 15 I=1,23,2
0019      15 XS(I+1,J)=(XS(I+2,J)-XS(I,J))*(FREQ(I+1)-FREQ(I))/
             1              (FREQ(I+2)-FREQ(I))+XS(I,J)
      C
0020        DO 20 I=2,26,2
0021        X(I,J)=XL(I,J)-XS(I,J)
0022      20 CONTINUE
0023        CONTINUE
0024      10 CONTINUE
      C
0025        WRITE(7,230)
0026      230 FORMAT(//,2X,'FREQ',6X,'GAIN',3X,'PHASE',//)
      C
0027        WRITE(7,200)(FREQ(I),X(I,1),X(I,2),I=2,26,2)
0028      200 FORMAT(1X,F6.3,2X,2F8.2)
      C
0029        WRITE(7,240)
0030      240 FORMAT(//,2X,'ENTER OUTPUT FILENAME:',//)
0031        CALL ASSIGN(3,,-1)
0032        WRITE(3,200)(FREQ(I),X(I,1),X(I,2),I=2,26,2)
0033        CALL CLOSE(3)
      C
0034        GO TO 1
      C
0035        DATA NF/2,3,5,7,11,13,17,19,23,29,31,37,41,43,53,61,71,
           1         83,89,97,109,127,137,151,173,229/
0036        DATA XL,XS/528999.,528999./
0037        STOP.
0038        END
$
```

```
FORTRAN IV      V01C-03A

      C     PROGRAM DIDIV.GLZ 30 DEC 76
      C
0001        DIMENSION Y(25,2,2),XS(25,2),X(25,2,2),FREQ(25),NF(25)
      C
0002      1 CONTINUE
      C
      C     CODE FOR INDIVIDUAL FILE DIVIDES
      C
0003        WRITE(7,210)
0004    210 FORMAT(5X,'ENTER NUMERATOR FILE:',//)
0005        CALL ASSIGN(1,,-1)
0006        WRITE(7,220)
0007    220 FORMAT(5X,'ENTER DENOM FILE:',//)
0008        CALL ASSIGN(2,,-1)
0009        READ(1,100)(Y(I,1,1),Y(I,2,1),Y(I,1,2),Y(I,2,2),I=1,25)
0010    100 FORMAT(9X,16X,2F8.3,16X,2F8.3)
      C  100    FORMAT(9X,4F8.3)      !UNCORRECTED FILES
0011        READ(2,110)(XS(I,1),XS(I,2),I=1,25,2)
      C    (9X,F8.3,8X,F8.3) FOR UNCORRECTED WHEEL AMP
      C    (17X,2F8.3)       FOR   CORRECTED WHEEL AMP
0012    110 FORMAT(9X,F8.3,8X,F8.3)
0013        CALL CLOSE(1)
0014        CALL CLOSE(2)
      C
      C     CODE FOR AVERAGE POPULATION DIVIDES
      C
      C     DO 2 I=1,4
      C     CALL ASSIGN(I,,-1)
      C   2   CONTINUE
      C     READ(1,100)(Y(I,1,1),I=1,25)
      C     READ(2,100)(Y(I,2,1),I=1,25)
      C     READ(3,100)(Y(I,1,2),I=1,25)
      C     READ(4,100)(Y(I,2,2),I=1,25)
      C     DO 3 I=1,4
      C   3   CALL CLOSE(I)
      C     CALL ASSIGN(1,,-1)
      C     CALL ASSIGN(2,,-1)
      C     READ(1,100)(XS(I,1),I=1,25,2)
      C     READ(2,100)(XS(I,2),I=1,25,2)
      C     CALL CLOSE(1)
      C     CALL CLOSE(2)
      C 100   FORMAT(8X,F8.2,14X)
      C
0015        DO 5 I=1,25
0016      5 FREQ(I)=NF(I)/128.
      C
0017        DO 10 K=1,2
0018        DO 11 J=1,2
      C     INTERPOLATE FOR MISSING XS POINTS
0019        DO 15 I=1,23,2
0020     15 XS(I+1,J)=(XS(I+2,J)-XS(I,J))*(FREQ(I+1)-FREQ(I))/
          1              (FREQ(I+2)-FREQ(I))+XS(I,J)
      C
0021        DO 20 I=1,25

FORTRAN IV      V01C-03A

0022        X(I,J,K)=Y(I,J,K)-XS(I,J)
0023     20 CONTINUE
0024     11 CONTINUE
0025     10 CONTINUE
      C
0026        WRITE(7,230)
0027    230 FORMAT(//,2X,'FREQ',9X,'X1GAIN',5X,'X1PHASE',
          1       6X,'X2GAIN',5X,'X2PHASE',//)
      C
0028        WRITE(7,235)(FREQ(I),X(I,1,1),X(I,2,1),X(I,1,2),X(I,2,2),
          1            I=1,25)
0029    235 FORMAT(1X,F6.3,2X,4F12.2)
      C
0030        WRITE(7,240)
0031    240 FORMAT(//,2X,'ENTER OUTPUT FILENAME:',//)
0032        CALL ASSIGN(3,,-1)
0033        WRITE(3,245)(FREQ(I),X(I,1,1),X(I,2,1),X(I,1,2),X(I,2,2),
          1            I=1,25)
0034    245 FORMAT(1X,F6.3,2X,4F8.3)
0035        CALL CLOSE(3)
      C
0036        GO TO 1
      C
0037        DATA NF/2,3,5,7,11,13,17,19,23,29,31,37,41,43,53,61,71,
          1       83,89,97,109,127,137,151,173/
0038        STOP
0039        END
*
```

```
FORTRAN IV      V01C-03A

      C
      C     PROGRAM FILER1.GLZ
      C
0001        DIMENSION GAIN(13),PHASE(13)
0002        INTEGER*4 NAME(4)
0003        CALL ASSIGN(1,,-1)
0004        CALL ASSIGN(2,,-1)
0005        L=2
0006        DO 5 J=1,8
0007        L=(L+1)/L
0008        CALL ASSIGN(3,,-1)
0009        READ(3,100)(GAIN(I),PHASE(I),I=1,13)
0010    100 FORMAT(9X,F8.3,8X,F8.3)
0011        CALL CLOSE(3)
0012        K=(J+1)/2
0013        WRITE(1,200) NAME(K),L,(GAIN(I),I=1,10)
0014    200 FORMAT(A4,I1,' ',10F6.2)
0015        WRITE(1,210) NAME(K),L,(GAIN(I),I=11,13)
0016    210 FORMAT(A4,I1,'C',3F6.2)
0017        WRITE(2,220) NAME(K),L,(PHASE(I),I=1,10)
0018    220 FORMAT(A4,I1,' ',10F6.1)
0019        WRITE(2,230) NAME(K),L,(PHASE(I),I=11,13)
0020    230 FORMAT(A4,I1,'C',3F6.1)
0021      5 CONTINUE
0022        CALL CLOSE(1)
0023        CALL CLOSE(2)
0024        STOP
0025        DATA NAME/'LH61','GZ61','BL61','JT61'/
0026        END
*
```

```
FORTRAN IV      V01C-03A

      C
      C     PROGRAM FILER2.GLZ
      C
0001        DIMENSION G1(25),G2(25),P1(25),P2(25)
0002        INTEGER*4 NAME(4)
0003        CALL ASSIGN(1,,-1)      !GAIN1 FILE
0004        CALL ASSIGN(2,,-1)      !GAIN2 FILE
0005        CALL ASSIGN(3,,-1)      !PHASE1 FILE
0006        CALL ASSIGN(4,,-1)      !PHASE2 FILE
0007        L=2
0008        DO 5 J=1,NCASE
0009        L=(L+1)/L
0010        CALL ASSIGN(5,,-1)
0011        READ(5,100)(G1(I),P1(I),G2(I),P2(I),I=1,25)
      C
      C     FOLLOWING 2 FORMATS FOR DIEXPC GENERATED FILES
      C 100     FORMAT(25X,2F8.3,16X,2F8.3)      !FOR CORRECTED DATA
      C 100 .   FORMAT(9X,2F8.3,16X,2F8.3,16X)   !FOR UNCORRECTED DATA
      C
      C     FOLLOWING FORMAT FOR DIEXP GENERATED FILES
0012    100 FORMAT(9X,4F8.3)
      C
0013        CALL CLOSE(5)
      C
0014        K=(J+1)/2
0015        WRITE(1,200) NAME(K),L,(G1(I),I=1,10)
0016    200 FORMAT(A4,I1,' ',10F6.2)
0017        WRITE(1,210) NAME(K),L,(G1(I),I=11,20)
0018    210 FORMAT(A4,I1,'C',10F6.2)
0019        WRITE(1,220) NAME(K),L,(G1(I),I=21,25)
0020    220 FORMAT(A4,I1,'C',5F6.2)
0021        WRITE(2,200) NAME(K),L,(G2(I),I=1,10)
0022        WRITE(2,210) NAME(K),L,(G2(I),I=11,20)
0023        WRITE(2,220) NAME(K),L,(G2(I),I=21,25)
0024        WRITE(3,230) NAME(K),L,(P1(I),I=1,10)
0025    230 FORMAT(A4,I1,' ',10F6.1)
0026        WRITE(3,240) NAME(K),L,(P1(I),I=11,20)
0027    240 FORMAT(A4,I1,'C',10F6.1)
0028        WRITE(3,250) NAME(K),L,(P1(I),I=21,25)
0029    250 FORMAT(A4,I1,'C',5F6.1)
0030        WRITE(4,230) NAME(K),L,(P2(I),I=1,10)
0031        WRITE(4,240) NAME(K),L,(P2(I),I=11,20)
0032        WRITE(4,250) NAME(K),L,(P2(I),I=21,25)
0033      5 CONTINUE
0034        CALL CLOSE(1)
0035        CALL CLOSE(2)
0036        CALL CLOSE(3)
0037        CALL CLOSE(4)
0038        STOP
0039        DATA NCASE/8/
0040        DATA NAME/'JT82','GZ82','BL82','LH82'/
0041        END
*
```

```
FORTRAN IV      V01C-03A

      C
      C     PROGRAM SIEXPC.GLZ 16 DEC 76
      C
0001        DIMENSION XIN(1024),WEELG(256),WEELP(256),NF(13),
           1            GAIN(13),PHASE(13),FREQ(13),
           1          ARU(13),ARC(13),PG(26),REM(13)
0002        REAL LINKG(256),LINKP(256),KGAIN,MU,NUM
0003        INTEGER SF(2)
      C
0004        EQUIVALENCE (XIN(  1),LINKG(1)),
           1                (XIN(257),LINKP(1)),
           1                (XIN(513),WEELG(1)),
           1                (XIN(769),WEELP(1))
      C
0005      1 CONTINUE
      C
0006        DEFINE FILE 1 (1,2048,U,NREC)
0007        WRITE(7,200)
0008      200 FORMAT(//////,5X,'ENTER INPUT FILENAME: '$)
0009        CALL ASSIGN(1,,-1)
0010        READ (1'1) XIN
0011        CALL CLOSE(1)
      C
0012        WRITE(7,210)
0013      210 FORMAT(5X,'ENTER SCALE FACTORS: '$)
0014        READ(5,100)(SF(I),I=1,2)
0015      100 FORMAT(2I1)
      C
0016        WRITE(7,220)
0017      220 FORMAT(5X,'ENTER K,MU,SIGL,SIGR,ALPH')
0018        READ(5,110) KGAIN,MU,SIGL,SIGR,ALPH
0019      110 FORMAT(5(F10.5,/))
      C
0020        T1=2.**SF(1)
0021        T2=2.**SF(2)
      C
      C     OUTER FREQUENCY LOOP
0022        DO 5 I=1,13
0023        IFLAG=0
0024        J=NF(I)+1
      C     L=2*I         !FOR VESTIBULAR FREQS
0025        L=2*I-1       !FOR VISUAL     FREQS
      C
0026        FREQ(I)=NF(I)/128.      !CALCULATE REMNANT
      C
0027        T3=(FREQ(I)-MU)/SIGL
0028        IF(T3 .LT. 0.) GO TO 10
0030        T3=T3*SIGL/SIGR
0031       10 CONTINUE
0032        REM(I)=KGAIN*EXP(-T3*T3/2.)
0033        IF(T3 .GT. 0.) REM(I)=REM(I)+ALPH*(1.-EXP(-T3))
      C
0035        GAINU=(T2/T1)*WEELG(J)/LINKG(J) !CALC UNCORRECTED STICK
0036        POWRU=GAINU*GAINU
```

```
FORTRAN IV      V01C-03A

0037        ARU(I)=20.*ALOG10(GAINU)
      C
0038        GAINR=REM(I)/(LINKG(J)*T1)    !CALC STICK REMNANT/LINK
0039        POWRR=GAINR*GAINR
      C
0040        NUM=POWRU-POWRR       !CALC NUMERATOR
      C
0041        IF(NUM .LT. EPS) IFLAG=1
      C
0043        PGAIN=10.**(PG(L)/20.)      !CALC DENOMINATOR
0044        DENOM=1.-PGAIN*PGAIN*POWRR
      C
0045      240 FORMAT(//)
0046        IF(DENOM .LT. EPS) IFLAG=1
      C
0048        IF(IFLAG .EQ. 0) GO TO 25  !CALC CORRECTED GAIN
0050        GAINC=GAINU
0051        GO TO 26
0052       25 GAINC=SQRT(NUM/DENOM)
0053       26 ARC(I)=20.*ALOG10(GAINC)
      C
0054        TEMP=2.*PI      !CALC PHASE
0055        PHASE(I)=WEELP(J)-LINKP(J) + PI
0056        IF(PHASE(I) .GE. TEMP) PHASE(I)=PHASE(I)-TEMP
0058        IF(PHASE(I) .LT.   0.) PHASE(I)=PHASE(I)+TEMP
0060        PHASE(I)=RTD*(PHASE(I)-TEMP)
      C
0061        5 CONTINUE
      C
0062        WRITE(7,250)
0063      250 FORMAT(5X,'N',2X,'NF',3X,'FREQ',8X,'GAIN',7X,'GAINC',
           1          7X,'PHASE', //)
0064        WRITE(7,255)(I,NF(I),FREQ(I),ARU(I),ARC(I),PHASE(I),I=1,13)
0065      255 FORMAT(2X,2I4,F7.3,3F12.2)
      C
0066        WRITE(7,260)
0067      260 FORMAT(//,5X,'ENTER OUTPUT FILENAME: '$)
0068        CALL ASSIGN(2,,-1)
0069        WRITE(2,270)(NF(I),FREQ(I),ARU(I),ARC(I),PHASE(I),I=1,13)
0070      270 FORMAT(1X,I3,F5.3,3F8.3)
0071        CALL CLOSE(2)
      C
0072        GO TO 1
      C
0073        STOP
0074        DATA EPS/.001/
0075        DATA PI,RTD/3.14159,57.296/
      C
      C     PLANT GAIN GIVEN IN DB
      C
0076        DATA PG/8*0.,-.01,-.02,-.02,-.05,-.07,-.08,-.19,-.33,-.58,
           1         -1.04,-1.32,-1.77,-2.56,-3.94,-4.77,-5.97,-7.84,
           1          -12.20/
      C
```

```
FORTRAN IV      V01C-03A

      C     DATA NF/2,3,5,7,11,13,17,19,23,29,31,37,41,43,53,61,71,
      C    1           83,89,97,109,127,137,151,173,229/
      C     FREQS FOR D1 (VESTIBULAR)
      C     DATA NF/3,7,13,19,29,37,43,61,83,97,127,151,229/
      C     FREQS FOR D2 (VISUAL)
0077        DATA NF/2,5,11,17,23,31,41,53,71,89,109,137,173/
0078        END
*
```

```
FORTRAN IV      V01C-03A

      C
      C     PROGRAM DIEXPC.GLZ 22 JAN 77
      C
0001        DIMENSION XIN(1536),FILMG(256),FILMP(256),WEELG(256),
           1       WEELP(256),NF(26),X1G(26),X2G(26),X1P(26),X2P(26),
           1       FREQ(26),PHASEX(52),PHASEY(104),GAIN(104),PG(26),
           1       PP(26),Y1G(26),Y1P(26),Y2G(26),Y2P(26),
           1     X1GC(26),X2GC(26),Y1GC(26),Y2GC(26),Y1PC(26),
           1     Y2PC(26),REM(26),TG(3)
      C
0002        REAL LINKG(256),LINKP(256),NUM,KGAIN,MU
0003        INTEGER SF(3)
0004        COMPLEX X1(26),X2(26),P(26),Y1(26),Y2(26),TEMPC,
           1          X1C(26),X2C(26),Y1C(26),Y2C(26)
      C
0005        EQUIVALENCE      (XIN(   1),LINKG(1)),
           1                 (XIN( 257),LINKP(1)),
           1                 (XIN( 513),FILMG(1)),
           1                 (XIN( 769),FILMP(1)),
           1                 (XIN(1025),WEELG(1)),
           1                 (XIN(1281),WEELP(1))
      C
0006        EQUIVALENCE      (PHASEX( 1),X1P(1)),
           1                     (PHASEX(27),X2P(1)),
           1                     (PHASEY( 1),Y1P(1)),
           1                     (PHASEY(27),Y2P(1)),
           1                   (PHASEY(53),Y1PC(1)),
           1                   (PHASEY(79),Y2PC(1)),
           1                     (GAIN( 1),Y1G(1)),
           1                     (GAIN(27),Y2G(1)),
           1                   (GAIN(53),Y1GC(1)),
           1                   (GAIN(79),Y2GC(1))
      C
0007      1 CONTINUE
0008        DEFINE FILE 1 (1,3072,U,NREC)
0009        WRITE(7,200)
0010      200 FORMAT(/////,5X,'ENTER INPUT FILENAME: '$)
      C
0011        CALL ASSIGN(1,,-1)
0012        READ (1'1) XIN
0013        CALL CLOSE(1)
      C
0014        WRITE(7,210)
0015      210 FORMAT(5X,'ENTER SCALE FACTORS: '$)
0016        READ(5,100) (SF(I),I=1,3)
0017      100 FORMAT(3I1)
      C
0018        WRITE(7,215)
0019      215 FORMAT(5X,'ENTER K,MU,SIGL,SIGR,ALPH')
0020        READ(5,110) KGAIN,MU,SIGL,SIGR,ALPH
0021      110 FORMAT($(F10.5,/))
      C
0022        DO 2 I=1,3
0023        TG(I)=2.**SF(I)
```

```
FORTRAN IV      V01C-03A

0024      2 CONTINUE
      C
0025        DO 3 I=1,26       !CALC REMNANT AND FREQ AT ALL I
0026        J=NF(I)+1
      C
0027        FREQ(I)=NF(I)/128.
      C
0028        T3=(FREQ(I)-MU)/SIGL
0029        IF(T3 .LT. 0.) GO TO 4
0031        T3=T3*SIGL/SIGR
0032      4 CONTINUE
0033        REM(I)=KGAIN*EXP(-T3*T3/2.)
0034        IF(T3 .GT. 0.) REM(I)=REM(I)+ALPH*(1.-EXP(-T3))
0036      3 CONTINUE
      C
0037        DO 5 I=1,13       !OUTER FREQ LOOP
0038        I1=2*I
0039        I2=I1-1
0040        J1=NF(I1)+1
0041        J2=NF(I2)+1
      C
      C      CALC UNCORRECTED GAINS AND PHASES
      C
0042        X1G(I1)=(TG(3)/TG(1))*WEELG(J1)/LINKG(J1)
0043        X1P(I1)=WEELP(J1)-LINKP(J1)
0044        X2G(I2)=(TG(3)/TG(2))*WEELG(J2)/FILMG(J2)
0045        X2P(I2)=WEELP(J2)-FILMP(J2)
      C
      C      CALC CORRECTED GAINS
      C
0046        RGAIN=REM(I1)/(TG(1)*LINKG(J1))    !CALC X1GC AT I1 FREQS
0047        NUM=X1G(I1)*X1G(I1)-RGAIN*RGAIN
0048        IF(NUM .LT. EPS) GO TO 7
0050        PGAIN=10.**(PG(I1)/20.)
0051        DENOM=1.-PGAIN*PGAIN*RGAIN*RGAIN
0052        IF(DENOM .LT. EPS) GO TO 7
0054        X1GC(I1)=SQRT(NUM/DENOM)
0055        GO TO 8
0056      7 CONTINUE
0057        X1GC(I1)=0.     !SET TO ZERO SINCE REM BIGGER THAN RESPONSE
0058      8 CONTINUE
      C
      D     WRITE(7,221) I,X1G(I1),X1P(I1),WEELG(J1),LINKG(J1),
      D    1         REM(I1),PGAIN,X1GC(I1)
      D 221 FORMAT(2X,I4,7F15.4)
      C
0059        RGAIN=REM(I2)/(TG(2)*FILMG(J2))    !CALC X2GC AT I2 FREQS
0060        NUM=X2G(I2)*X2G(I2)-RGAIN*RGAIN
0061        IF(NUM .LT. EPS) GO TO 9
0063        PGAIN=10.**(PG(I2)/20.)
0064        DENOM=1.-PGAIN*PGAIN*RGAIN*RGAIN
0065        IF(DENOM .LT. EPS) GO TO 9
0067        X2GC(I2)=SQRT(NUM/DENOM)
0068        GO TO 10

FORTRAN IV      V01C-03A

0069      9 CONTINUE
0070        X2GC(I2)=0.
0071     10 CONTINUE
      C
      D     WRITE(7,221) I,X2G(I2),X2P(I2),WEELG(J2),FILMG(J2),
      D    1         REM(I2),PGAIN,X2GC(I2)
      C
0072      5 CONTINUE
      C
      C
      C     LIMIT PHASE TO BETWEEN ZERO AND 2*PI
      C
0073        CALL AMOD(52,PHASEX)
      C
      D     WRITE(7,222)(I,NF(I),FREQ(I),X1G(I),X1GC(I),X1P(I)*RTD,
      D    1           X2G(I),X2GC(I),X2P(I)*RTD, I=1,26)
      D 222 FORMAT(2X,2I4,F7.3,2F8.4,F8.1,2F8.4,F8.1)
      C
      C     USE ALIN TO INTERPOLATE POINTS NOT ORIGINALLY IN DATA
      C
0074        CALL ALIN(NF,X1G,2,24,0)
0075        CALL ALIN(NF,X1GC,2,24,0)
0076        CALL ALIN(NF,X1P,2,24,1)
0077        CALL ALIN(NF,X2G,1,23,0)
0078        CALL ALIN(NF,X2GC,1,23,0)
0079        CALL ALIN(NF,X2P,1,23,1)
      C
      C     ADDITIONAL CALC FOR END POINTS OF X1 AND X2
      C
0080        TEMP=1.*(NF(1)-NF(2))/(NF(4)-NF(2))
0081        X1G(1)=X1G(2)+TEMP*(X1G(4)-X1G(2))
0082        X1GC(1)=X1GC(2)+TEMP*(X1GC(4)-X1GC(2))
0083        DELP=X1P(4)-X1P(2)
0084        X1P(1)=X1P(2)+TEMP*DELP
0085        IF(ABS(DELP) .GT. PI) X1P(I)=X1P(I)+PI
0087        TEMP=1.*(NF(26)-NF(23))/(NF(25)-NF(23))
0088        X2G(26)=X2G(23)+TEMP*(X2G(25)-X2G(23))
0089        X2GC(26)=X2GC(23)+TEMP*(X2GC(25)-X2GC(23))
0090        DELP=X2P(25)-X2P(23)
0091        X2P(26)=X2P(23)+TEMP*DELP
0092        IF(ABS(DELP) .GT. PI) X2P(26)=X2P(26)+PI
      C
0094        CALL AMOD(52,PHASEX)      !LIMIT PHASE TO 360
      C
0095        DO 11 I=1,26                !MAKE SURE GAINS NOT NEGATIVE
0096        IF(X1G(I) .LT. 0.) X1G(I)=0. !DUE TO EXTRAPOLATION
0098        IF(X2G(I) .LT. 0.) X2G(I)=0.
0100        IF(X1GC(I) .LT. 0.) X2GC(I)=0.
0102        IF(X2GC(I) .LT. 0.) X2GC(I)=0.
0104     11 CONTINUE
      C
      C     DUMP OUT GAIN AND PHASE FOR X1 AND X2
      C
      D     WRITE(7,222)(I,NF(I),FREQ(I),X1G(I),X1GC(I),X1P(I)*RTD,
```

```
     D    1                X2G(I),X2GC(I),X2P(I)*RTD,I=1,26
     C
     C
     C    CONVERT TO COMPLEX VECTORS FOR X1 AND X2 AND P
     C
0105      DO 20 I=1,26
0106      T1=X1G(I)*COS(X1P(I))
0107      T2=X1G(I)*SIN(X1P(I))
0108      X1(I)=CMPLX(T1,T2)
     C
0109      T1=X1GC(I)*COS(X1P(I))
0110      T2=X1GC(I)*SIN(X1P(I))
0111      X1C(I)=CMPLX(T1,T2)
     C
0112      T1=X2G(I)*COS(X2P(I))
0113      T2=X2G(I)*SIN(X2P(I))
0114      X2(I)=CMPLX(T1,T2)
     C
0115      T1=X2GC(I)*COS(X2P(I))
0116      T2=X2GC(I)*SIN(X2P(I))
0117      X2C(I)=CMPLX(T1,T2)
     C
0118      TEMP=10.**(PG(I)/20.)
0119      T1=TEMP*COS(PP(I)/RTD)
0120      T2=TEMP*SIN(PP(I)/RTD)
0121      P(I)=CMPLX(T1,T2)
     C
     C    CALC Y1 AND Y2 (COMPLEX)
     C
0122      TEMPC=P(I)*P(I)*X1(I)*X2(I)+1.
0123      Y1(I)=-X1(I)*(1.+P(I)*X2(I))/TEMPC
0124      Y2(I)=+X2(I)*(1.-P(I)*X1(I))/TEMPC
     C
0125      TEMPC=P(I)*P(I)*X1C(I)*X2C(I)+1.
0126      Y1C(I)=-X1C(I)*(1.+P(I)*X2C(I))/TEMPC
0127      Y2C(I)=+X2C(I)*(1.-P(I)*X1C(I))/TEMPC
     C
     C    CONVERT TO GAIN AND PHASE NOTATION
     C
0128      Y1G(I)=CABS(Y1(I))
0129      Y1P(I)=ATAN2(AIMAG(Y1(I)),REAL(Y1(I)))
0130      Y2G(I)=CABS(Y2(I))
0131      Y2P(I)=ATAN2(AIMAG(Y2(I)),REAL(Y2(I)))
     C
0132      Y1GC(I)=CABS(Y1C(I))
0133      Y1PC(I)=ATAN2(AIMAG(Y1C(I)),REAL(Y1C(I)))
0134      Y2GC(I)=CABS(Y2C(I))
0135      Y2PC(I)=ATAN2(AIMAG(Y2C(I)),REAL(Y2C(I)))
     C
0136   20 CONTINUE
     C
     C    LIMIT PHASE AND CONVERT GAIN TO DB
     C
0137      CALL AMOD(104,PHASEY)
```



```
     C
0138      DO 25 I=1,104
0139      IF(GAIN(I) .LE. 0.) GO TO 24
0141      GAIN(I)=20.*ALOG10(GAIN(I))
0142      GO TO 25
0143   24 CONTINUE
0144   25 CONTINUE
     C
0145      WRITE(7,230)
0146   230 FORMAT(//)
0147      WRITE(7,240)
0148   240 FORMAT(5X,'N',2X,'NF',3X,'FREQ',2X,'Y1GAIN',1X,'Y1PHASE',
         1          1X,'Y1GAINC',1X,'Y1PHASC',2X,'Y2GAIN',1X'Y2PHASE'
,
         1       1X,'Y2GAINC',1X,'Y2PHASC',//)
     C
0149      TEMP=2.*PI
0150      DO 26 I=1,104
0151      PHASEY(I)=RTD*(PHASEY(I)-TEMP)
0152   26 CONTINUE
0153      WRITE(7,220)(I,NF(I),FREQ(I),Y1G(I),Y1P(I),Y1GC(I),Y1PC(I),
         1             Y2G(I),Y2P(I),Y2GC(I),Y2PC(I),I=1,26)
0154   220 FORMAT(2X,2I4,F7.3,F8.2,F8.1,F8.2,F8.1,F8.2,F8.1,F8.2,F8.1)
     C
     C
0155      WRITE(7,250)
0156   250 FORMAT(//,5X,'ENTER OUTPUT FILENAME: '$)
0157      CALL ASSIGN(2,,-1)
0158      WRITE(2,260)(NF(I),FREQ(I),Y1G(I),Y1P(I),Y1GC(I),Y1PC(I),
         1             Y2G(I),Y2P(I),Y2GC(I),Y2PC(I),I=1,26)
0159   260 FORMAT(1X,I3,F5.3,8F8.3)
0160      CALL CLOSE(2)
     C
0161      GO TO 1
     C
0162      STOP
     C
0163      DATA EPS/.001/
0164      DATA RTD,PI/57.294,3.14159/
0165      DATA X1G,X1P,X2G,X2P/104*0./
0166      DATA XIN/1536*0./
0167      DATA NF/2,3,5,7,11,13,17,19,23,29,31,37,41,43,53,61,71,
         1          83,89,97,109,127,137,151,173,229/
     C
     C    PLANT GAIN AND PHASE GIVEN IN DB AND DEG,RESPECTIVELY
     C
0168      DATA PG/8*0.,-.01,-.02,-.02,-.05,-.07,-.08,-.19,-.33,-.58,
         1          -1.04,-1.32,-1.77,-2.56,-3.94,-4.77,-5.97,-7.84,
         1          -12.20/
0169      DATA PP/-1.4,-2.1,-3.5,-4.9,-7.7,-9.2,-12.0,-13.5,-16.4,
         1          -20.8,-22.3,-26.8,-29.9,-31.5,-39.5,-46.1,-54.6,
         1          -64.7,-69.7,-76.2,-85.5,-97.9,-103.8,-111.2,
         1          -120.6,-136.4/
0170      END
*
```

REFERENCES

AFIFI, A.A. and AZEN, S.P., Statistical Analysis: A Computer Oriented Approach, Academic Press, NY, 1972.

ALLNATT, J. "Subjective rating and apparent magnitude", Int J Man-Machine Studies 7:801-816, 1975.

BARON, S., "A model for human control and monitoring based on modern control theory", J Cybernetics and Information Sciences 1(1):3-18, 1976.

BENSON, A.J. and BODIN, M.A., "Interaction of linear and angular accelerations on vestibular receptors in man", Aerospace Med 37:144-154, 1966.

BERGLAND, G.D., "A guided tour of the fast Fourier transform", IEEE Spectrum 6:41-52, 1969.

BERTHOZ, A., PAVARD, B. and YOUNG, L.R. "Perception of linear horizontal motion induced by peripheral vision (linearvection)", Exp Brain Res 23:471-489, 1975.

BRANDT, TH., DICHGANS, J. and KOENIG, E., "Differential effects of central versus peripheral vision on egocentric and exocentric motion perception", Exp Brain Res 16:476-491, 1973.

BRIGHAM, E.O. and MORROW, R.E., "The fast Fourier transform", IEEE Spectrum 4(12), 1967.

CHAPANIS, A., Research Techniques in Human Engineering, The Johns Hopkins Press, Baltimore, 1959.

CHU, W., Dynamic Response of Human Linearvection, S.M. Thesis, Department of Aeronautics and Astronautics, MIT, January, 1976.

CLARK, B., "Thresholds of perception of angular acceleration in man", Aerospace Med 38:443-450, 1967.

CLARK, B. and STEWART, J.D. "Perception of angular acceleration about the yaw axis of a flight simulator", Aerospace Med 33:1426-1432, 1962.

CLARK, B. and STEWART, J.D. "Magnitude estimates of rotational velocity during and following prolonged increasing, constant and zero angular acceleration", J Exp Psychol 78:329-339, 1968.

CLARK, B. and STEWART, J.D. "Thresholds for perception of angular acceleration about the three major body axes", Fourth NASA Symposium on the Role of the Vestibular Organs in Space Exploration, NASA SP-187, 1968.

CLARK, B. and STEWART, J.D. "Effects of angular acceleration on man: Thresholds for the perception of rotation and the oculogyral illusion", Aerospace Med 40:952-956, 1969.

CRAMER, H., Mathematical Methods of Statistics, Princeton University Press, 1966.

DICHGANS, J. and BRANDT, TH., "Optokinetic motion sickness and pseudo-Coriolis effects induced by moving visual stimuli", Acta Otolaryng 76:339-348, 1973.

DICHGANS, J., DIENER, H.C. and BRANDT, TH., "Optokinetic graviceptive interaction in different head positions", Acta Otolaryng 78:391-398, 1974.

DICHGANS, J., HELD, R., YOUNG, L.R. and BRANDT, TH., "Moving visual scenes influence the apparent direction of gravity", Science 178:1217-1219, 1972.

DICHGANS, J., SCHMIDT, C.L. and GRAF, W., "Visual input improves the speedometer function of the vestibular nuclei in goldfish", Exp Brain Res 18:319-322, 1973.

DIGITAL EQUIPMENT CORPORATION, "Lab applications-11: Program Manual", DEC-11-ALPMA-A-D, September 1975.

DIXON, W.J., "BMD-Biomedical Computer Programs", University of California Press, 1973.

DOLEZAL, H. and HELD, R. "Two components of visually-induced tilt during rotary field motion", abstract of paper presented at E.P.A. Meeting, New York, NY, April 3-5, 1975.

FERNANDEZ, C. and GOLDBERG, J.M., "Physiology of peripheral neurons innervating semicircular canals of the squirrel monkey I, II, III", J Neurophysiol 34:661-675, 1971; 35:978-996, 1972.

FERNANDEZ, C. and GOLDBERG, J.M., "Physiology of peripheral neurons innervating otolith organs of the squirrel monkey I, II, III", J Neurophysiol 39:970-1008, 1976.

FINKE, R., "State alterations in the effects induced by a rotating visual field", abstract of presentation made at Eastern Psychological Association (E.P.A.), Boston, April 1977.

FUKUDA, T., "Postural behavior and motion sickness", Acta Otolaryng 81:237-241, 1976.

GELB, A. and VANDERVELDE, W., Multiple-input Describing Function and Nonlinear Systems Design, McGraw Hill Inc., New York, 1968.

GROEN, J.J. and JONGKEES, L.B.W., "The threshold of angular acceleration perception", J Physiol 107:1-7, 1948.

GUEDRY, F.E., "Orientation of the rotation-axis relative to gravity: its influence on nystagmus and the sensation of motion", Acta Otolaryng 60:30-48, 1964.

GUEDRY, F.E., "Relations between vestibular nystagmus and the sensation of motion", Aerospace Med 39:570-579, 1968.

GUEDRY, F.E., "Conflicting sensory orientation cues as a factor in motion sickness", Fourth NASA Symposium on the Role of the Vestibular Organs in Space Exploration, NASA SP-187, 1968.

GUEDRY, F.E., STOCKWELL, C.W. and GILSON, R.D., "Comparison of subjective responses to semicircular canal stimulation produced by rotation about different axes", Acta Otolaryng 72:101-106, 1971.

GUEDRY, F.E., STOCKWELL, C.W., NORMAN, J.W. and OWENS, G.G., "Use of triangular waveforms of angular velocity in the study of vestibular function", Acta Otolaryng 71:439-448, 1971.

HIGGINS, W.T. Jr., "A comparison of complementary and Kalman filtering", IEEE Trans on Aerospace and Electronic Systems, AES-11(3):321-325, 1975.

HELD, R., DICHGANS, J. and BAUER, J., "Characteristics of moving visual scenes influencing spatial orientation", Vision Res 14:1-9, 1974.

HENN, V., YOUNG, L.R. and FINLEY, C., "Vestibular nucleus units in alert monkeys are also influenced by moving visual fields", Brain Res 71:144-149, 1974.

HENN, V. and Young, L.R., "Ernst Mach on the vestibular system 100 years ago", Annals of Oto-Rhinolaryngol 37:138-149, 1975.

HENN, V. and Young, L.R., "Visual influences on vestibular neurons in the brainstem", presented at the Ninth Center for Visual Studies Symposium on Eye Movements and Motion Perception, Rochester, NY, 1975.

HIXSON, W.C., "Frequency response of the oculovestibular system during yaw oscillation", NAMRL MF51,524.005-7016 DEIG, 1974.

HOOD, J.D. and LEECH, J., "The significance of peripheral vision in the perception of movement", Acta Otolaryng 77:72-79, 1974.

HOWARD, I.P. and TEMPLETON, W.B., Human Spatial Orientation, J. Wiley and Sons, London, 1966.

IEEE, Volume AV-15, No. 2, June 1967.

KLEINMAN, D., BARON, S. and LEVISON, W.H., "An optimal control model of human behavior", Fifth Annual NASA University Conference on Manual Control, MIT, Cambridge, MA, 1969.

KLEINMAN, D., BARON, S. and LEVISON, W.H., "A control theoretic approach to manned-vehicle systems analysis", IEEE AC-16(6):824-832, 1971.

KLINKE, R. and SCHMIDT, C.L., "Efferent influence on the vestibular organ during active movements of the body" Pflugers Arch 318:325-332, 1970.

KNOOP, D.E. and FU, K.F., "An adaptive model of the human operator in a control system", Proceedings of the Fifth National Symposium on Human Factors in Electronics, San Diego, CA, pp. 252-265, 1964.

LEDOUX, A.,"Les canaux semi-circulaires: Etude electrophysiologique; contribution a l'effort d'uniformisation des epreuves vestibulaires; essai d'interpretation de la semilogie vestibulaire", Acta Oto-rhinolar Belg 12:111-346, 1958.

LEIBOWITZ, H.W., JOHNSON, C.A. and ISABELLE, E., "Peripheral motion detection and refractive error", Science 177:1207-1208, 1972.

LEVISON, W., BARON, S. and KLEINMAN, D., "A model for human controller remnant", IEEE MMS-10:101-108, 1969.

LOWENSTEIN, O. and SAND, A., "The activity of the horizontal semicircular canal of the dogfish, Scyllium canicula", J Exp Biol 13:416-428, 1936.

LOWENSTEIN, O. and SAND, A., "The mechanism of the semicircular canal", Proc Roy Soc (London) 129:256-275, 1940.

MAGDALENO, R.E., "Serial segments method for measuring remnant", IEEE SMC-2(5):674-678, 1972.

MCRUER, D.T., and GRAHAM, D., "Pilot models for single and multi-loop systems with random forcing functions", Systems Technology, Inc., Technical Report 134-1, 1964.

MCRUER, D.T. and KRENDEL, E.S., "Dynamic response of human operators", WADC Technical Report 56-524, Wright Air Development Center, USAF, Wright Patterson AFB, 1957.

MCRUER, D.T. and KRENDEL, E.S., "The human operator as a servo system element", Journal of the Franklin Institute, 267(5,6), 1959.

MCRUER, D.T. and KRENDEL, E.S., "The man-machine system concept", Proc IRE, 50(5), 1962.

MEIRY, J.L., The Vestibular System and Human Dynamic Space Orientation Sc.D. Thesis, Department of Aeronautics and Astronautics, MIT, 1965.

MELVILL-JONES, G., BARRY, W. and KOWALSKY, N., "Dynamics of the semi-circular canals compared in yaw, pitch and roll", Aerospace Med 35:984-989, 1964.

MELVILL-JONES, G. and MILSUM, J.H., "Spatial and dynamic aspects of visual fixation", IEEE Transactions on Biomedical Engineering, BME-12:54-62, 1965.

MERKER, B. and HELD, R., "Comparison of eye torsion with the apparent horizontal under head tilt and visual field rotation", Abstract of presentation made at Eastern Psychological Association (E.P.A.), Boston, MA, April, 1977.

MORRISON, W., "LINK GAT-1 projector system", Man Vehicle Laboratory Memo, MVL-751, Department of Aeronautics and Astronautics, MIT, 1975.

MURPHY, R.E., A Display System to Induce Self Rotation, S.M. Thesis, Department of Aeronautics and Astronautics, MIT, 1972.

NASHNER, L.M., Sensory Feedback in Human Posture Control, Sc.D. Thesis, Department of Aeronautics and Astronautics, MIT, 1970.

OOSTERVELD, W.J., "Threshold value for stimulation of the horizontal semicircular canals", Aerospace Med 41:386-389, 1970.

ORMSBY, C.C., Model of Human Dynamic Orientation, Ph.D. Thesis, Department of Aeronautics and Astronautics, MIT, 1974.

ORMSBY, C.C. and YOUNG, L.R., "Nonlinear model for the perception of static orientation", Fortschritte fur Zoologie 23:288-294, 1975.

PETERS, R.A., "Dynamics of the vestibular system and their relation to motion perception, spatial disorientation, and illusions", NASA CR-1309, 1969.

POULTON, E.C., "The new psychophysics: Six models for magnitude estimation", Psych Bull 69:1-18, 1968.

ROBINSON, D.A., "Eye movement control in primates", Science 161: 1219-1224, 1968.

RUSSEL, I.J., "The role of the lateral line efferent system in Xenopus laevis", J Exp Biol 54:621-641, 1971.

SCHÖNE, H., "On the role of gravity in human spatial orientation", Aerospace Med 35:764-772, 1964.

SCHMID, R., TAGLIETTI, V., STEFANELLI, M. and CASSELLA, C., "Experimental and theoretical investigation of the semicircular canal dynamics", presented at the Symposium on Physiological Regulation and Control, Rochester, NY, 1973.

SCHMIDT, F. and TIFFEN, J., "Disorientation of driver's estimate of automobile speed as a function of speed adaptation", J Applied Psych 53:536-539, 1969.

SHIRLEY, R., Motion Cues in Man-Vehicle Control, Sc.D. Thesis, Department of Aeronautics and Astronautics, MIT, 1968.

SHIRLEY, R., "A comparison of techniques for measuring human operator frequency response", Sixth Annual Conference on Manual Control, 1970.

STEER, R.W., Jr., The Influence of Angular and Linear Acceleration and Thermal Stimulation on Human Semicircular Canals, Sc.D. Thesis, Department of Aeronautics and Astronautics, MIT, 1967.

STEINHAUSEN, W. "Observations of the cupula in the ampullae of the semicircular canals of the labyrinths of a living pike", Pfluger's Arch ges Physiol 232:500-512, 1933; NASA Technical Translation, NASA TT F-13,665, 1971.

STEVENS, S.S., "Measurement, statistics and the schemapiric view", Science 161:849-856, 1968.

SUGIE, N. and MELVILL-JONES, G., "A model of eye movements induced by head rotation", IEEE Transactions on Systems, Man and Cybernetics, SMC-1:251-260, 1971.

TANG, J., Interaction between Visually Induced Roll and Real Lateral Tilts, S.M. Thesis, Department of Aeronautics and Astronautics, MIT, 1974.

TANG, J., HELD, R. and YOUNG, L.R., "Interaction of visually-induced and labyrinthine-sensed postural tilt", paper presented at meeting of the Psychonomic Society, Boston, MA, November 21-23, 1974.

VAN EGMOND, A.A.J., GROEN, J.J. and JONGKEES, L.B.W., "The mechanics of the semicircular canal", J. Physiol 110:1-17, 1949.

VAN HOUTTE, N.A.J., Display Instrumentation for V/STOL Aircraft Landing, Sc.D. Thesis, Department of Aeronautics and Astronautics, MIT, 1970.

YASUI, S. and YOUNG, L.R., "Perceived visual motion as effective stimulus to pursuit eye movement system", Science 190:906-908, 1975.

YOUNG, L.R., "Dynamic control models of the semicircular canals", ASME Annual Winter Meeting, 1970.

YOUNG, L.R., "The current status of vestibular system models", Automatica 5:369-383, 1969.

YOUNG, L.R., "On visual vestibular interaction", Fifth NASA Symposium on the Role of the Vestibular Organs in Space Exploration, NASA SP-314, 1970.

YOUNG, L.R., "Cross-coupling between effects of linear and angular acceleration on vestibular nystagmus", Biblio Ophthalmol 82: 116-121, 1972.

YOUNG, L.R., "Human control capabilities", in: Bioastronautics Data Book, 2nd edition, NASA SP-3006, 1973.

YOUNG, L.R., "Role of the vestibular system in posture and movement", in: Medical Physiology, 13th edition, V.B. Mountcastle, Ed. C.V. Mosby, Inc. 1974.

YOUNG, L.R., DICHGANS, J., MURPHY, R. and BRANDT, TH., "Interaction of optokinetic and vestibular stimuli in motion perception", Acta Otolaryng 76:24-31, 1973.

YOUNG, L.R. and HENN, V.S., "Selective habituation of vestibular nystagmus by visual stimulation", Acta Otolaryng 77:159-166, 1974.

YOUNG, L.R. and HENN, V.S., "Nystamgus produced by pitch and yaw rotation about non-vertical axes", Fortschritte fur Zool 23:235-246, 1974.

YOUNG, L.R. and MEIRY, J.L., "A revised dynamic otolith model", AMRL-TR-66-209, 1966.

YOUNG, L.R. and OMAN, C.M., "Model for vestibular adaptation to horizontal rotation", Aerospace Med 40:1076-1080, 1969.

YOUNG, L.R. and OMAN, C.M., "Influence of head position and field on visually induced motion effects in three axes of rotation", Proceedings of the Tenth Annual Conference on Manual Control, 1974.

YOUNG, L.R., OMAN, C.M. and DICHGANS, J., "Influence of head orientation on visually induced pitch and roll sensation", Aviat Space Environ Med 46:264-268, 1975.

ZACHARIAS, G.L., "A general purpose simulation library for PDP-11 FORTRAN users", Man-Vehicle Laboratory Memo MVL-771, Department of Aeronautics and Astronautics, MIT, 1977.

anon, "LINK General Aviation Trainer GAT-1: Operation and Maintenance Manual", (LP-1585) Link Group, Systems Division, General Precision Systems, Inc., Binghamton, NY, 1968.

BIOGRAPHICAL SKETCH

Greg L. Zacharias was born in Oakland, California on January 31, 1947. He entered MIT in 1964 as a Sloan Scholar and obtained an S.B. degree in the Department of Aeronautics and Astronautics in 1967. During graduate school at MIT he worked on marine radionavigation systems as a research assistant at the Experimental Astronomy Lab, and later, on aircraft radio-navigation as a staff engineer at Astro Nautical Research, Inc. He was also admitted to the Interdepartmental Instrumentation Doctoral Program at MIT in 1969, and, shortly thereafter, admitted to the service of the United States Air Force.

As a First Lieutenant he was assigned in 1970 to the Johnson Space Center of NASA with the responsibility for preliminary design definition of the entry mission phase autopilot of the SSV. After being released from active duty in 1973, he reentered the Instrumentation Program at MIT and continued to work on SSV autopilot design as a research assistant at Charles Stark Draper Laboratories. He obtained his S.M. in 1974, and continued work at CSDL as a staff engineer on SSV entry control. During this time, he became interested in the manual control of piloted vehicles, and in 1975 reentered graduate school to join the Man Vehicle Laboratory, concentrating on the study of motion sensation dynamics.

Dr. Zacharias is currently a staff scientist in the Control Systems Department at Bolt Beranek and Newman, engaged in modelling pilot behavior in the presence of vehicle motion cues. Dr. Zacharias is married and has no children. He plays a rotten game of squash.